atomic Hydrogen In the local universe

martin zwaan

Atomic Hydrogen in the Local Universe

Cover art:
Zonder titel – Bieke Huls. Reprinted with permission.

RIJKSUNIVERSITEIT GRONINGEN

Atomic Hydrogen in the Local Universe

Proefschrift

ter verkrijging van het doctoraat in de
Wiskunde en Natuurwetenschappen
aan de Rijkuniversiteit Groningen
op gezag van de
Rector Magnificus, dr. D. F. J. Bosscher,
in het openbaar te verdedigen op
maandag 16 oktober 2000
om 14.15 uur

door

MARTIN ALEXANDER ZWAAN
geboren op 28 juni 1971
te Marknesse

Promotor:	Prof. dr. F. H. Briggs
Beoordelingscommissie:	Prof. dr. K. H. Kuijken Prof. dr. R. Sancisi Prof. dr. R. H. Sanders

ISBN 90-367-1305-6

Contents

1

Introduction

ATOMIC HYDROGEN GAS plays a vital role in galaxy evolution. In the widely accepted hierarchical galaxy formation scenario, overdense regions collapse in a hierarchical fashion and structures grow through continuous accretion of smaller mass halos consisting of a mixture of non-baryonic dark matter and gas. The primordial gas dissipates energy when it is confined within a dark halo, allowing it to collapse to become the H I reservoir which forms the fuel for the formation of stars. The density and angular momentum of the H I as it collapses determines much of the properties of the visible part of galaxies as we observe them at the present time. A full assessment of the H I content and distribution of H I in the universe is therefore essential for understanding galaxy evolution.

Most evolutionary studies make use of the optical wave lengths exclusively and therefore concentrate mainly on the stellar component of the galaxies. The obvious reason for this preference is that the H I is much more difficult to chart than the star light. In a typical spiral galaxy the energy output from normal stars is millions of times higher than that from H I in the 21cm line, while the total mass in stars is only four times that of the mass in neutral gas. As a result, 21cm emission line studies have been limited to the very local ($z < 0.1$) universe. Absorption line studies (21cm or Lyman α) can help a great deal, but these are limited to those regions of the universe that are coincidently aligned with the observer and a strong background source that provides the continuum emission against which the gas can be detected.

The physics of radio emission from H I is simple. The mechanism responsible for the 21cm line is the hyperfine splitting of the hydrogen atom. In most situations, the population of the hyperfine levels is fully determined by collisions of H I atoms. The lifetime of the upper level is much higher than the typical time between collisions and the energy difference between the levels is very small. As a result, the efficiency of 21cm emission of an H I cloud is almost independent of its temperature and density. The radiation escapes freely and the H I column density can be readily derived from the brightness of the emission without attenuation by dust, which blocks optical wavelengths.

The aim of this thesis is to present an inventory of the atomic hydrogen gas in the

local universe. Where is the H I? How is it distributed among different types of galaxies? Are there large quantities of H I locked up in dim galaxies that are easily overlooked in optical surveys? How does the amount of H I at the present epoch compare to that at earlier times? This introductory chapter briefly presents a background for the questions addressed in this thesis.

1.1 H I as a tracer of the local galaxy population

The 21cm line has been used extensively as a kinematic tracer of the galactic potential of spiral galaxies. Indeed, one of the main motivations for the theoretical derivation of the 21cm line (van de Hulst 1945) and subsequently measuring it (Ewen & Purcell 1951; Muller & Oort 1951), was to study the structure of the Milky Way Galaxy. Since then, the 21cm line has been used to map the H I distribution and velocity field of many galaxies, leading to the recognition of dark matter and measurements of its distribution (Bosma 1978, van Albada 1985).

Besides providing this indicator of dark matter in galaxies, the 21cm line serves as a useful tracer of the local galaxy population and provides a way to appraise the completeness of optical galaxy catalogs. Optical selection effects have long been known to introduce biases in these catalogs. Soon after Freeman (1970) found that most nearby spiral galaxies have nearly equal optical central surface brightness of 21.65 mag arcsec^{-2}, Disney (1976) realized that this observation could be the result of a selection effect. Disney showed that the brightness of the night sky and conventional selection techniques conspire to disclose only disk galaxies with central surface brightnesses close to Freeman's value[1]. It was speculated that the true dynamic range of central surface brightness is much larger than previously thought, and that a class of galaxies with very low optical surface brightness (LSB galaxies) could have escaped inclusion in conventional galaxy catalogs. These galaxies might contain a significant fraction of the mass content of the universe.

There are several ways to break the surface brightness selection bias. One approach has been the inspection of new photographic survey material to search for galaxies to much lower surface brightness limits. Candidates are followed up with optical or H I spectroscopy to determine distances. This technique was applied by Schombert et al. (1992) to the Second Palomar Sky Survey and by Impey et al. (1996) with the Automated Plate Measuring (APM) technique on UK Schmidt Telescope plates. The analysis of the latter survey by Sprayberry et al. (1997) showed that the space density of LSB galaxies might be comparable to that of normal "Freeman-galaxies". Deep CCD-surveys (Dalcanton et al. 1997, O'Neil, Bothun, & Cornell 1997) yield basically the same conclusion. Despite their selection for low optical surface brightness, the integrated luminosity and H I content for these galaxies is often high.

One of the most famous results of the surveys for LSB galaxies is the detection of Malin 1 (Bothun et al. 1987). With an extrapolated disk central surface brightness of 26.0 B–mag arcsec^{-2}, a disk scale length of $60\,h_{100}^{-1}$ kpc and a total H I mass of $\sim 4 \times 10^{10}\,h_{100}^{-2}\,M_\odot$ (Pickering et al. 1997), this may be one of the most extreme galaxies known. Malin 1 seems to be a spectacular example of the class of galaxies known as "crouching giants", that were predicted by Disney: massive, intrinsically luminous galaxies that are hiding from detection. Note however that its total central surface brightness

[1] A similar effect, known as the Fish-law (Fish 1964) is known to exist for elliptical galaxies. Disney (1976) showed that also this effect could be the result of a selection bias.

(disk plus bulge) is ≈ 20.5 B-mag arcsec^{-2}. This is not a galaxy that would be missed if it were located in the Virgo cluster instead of $240\,h_{100}^{-1}$ Mpc behind it.

Much less conspicuous LSB galaxies do exist. Especially the less luminous dwarf galaxies might easily be missed in optical surveys that select on the basis of stellar content, star-forming regions, or material associated with stellar mass-loss. Among the dimmest galaxies are gas-rich systems that have gas masses well in excess of their stellar mass. Searching for galaxies in the 21cm line can therefore help to develop a fair view of the local galaxy population and might even turn up pristine "proto-galaxies", dark matter potential wells filled with neutral gas that have been unable to convert any of their innate gas into stars. The search for such a new class of galaxies was one of the motivations for this thesis.

1.2 The evolution of $\Omega_{\rm gas}$

The cosmological neutral gas density of the universe is one of the fundamental observational parameters that describes the formation and evolution of stars in galaxies and charts the processes that convert gas into stars. Linked with other indicators that have recently received much attention, such as the cosmic star formation rate (Madau 1996), the luminosity density (Lilly et al. 1996) and the metal enrichment rate (Connolly et al. 1997), it gives strong constraints on galaxy evolution models.

At high z, Lyα absorption lines that are identified in the spectra of background quasars are used to trace the neutral gas content. Most of the observed lines correspond to low column densities and trace the mostly ionized fraction of the gas. The scanty high column density absorbers or damped Lyα (DLA) systems contain by far most of the neutral gas (Turnshek 1997). Most observations point to DLAs at high z being gas-rich disks in the process of contracting to present-day spiral galaxies (Wolfe 1995). The absorption line structures of associated unsaturated metal lines and Lyman series lines in DLA systems are similar to those of sight lines through spiral galaxies at $z = 0$ (Prochaska & Wolfe 1997). The fact that the comoving H I mass density at $z = 3$ is equal to the mass in stars at $z = 0$ (Wolfe 1995, Fukugita, Hogan & Peebles 1998) supports this idea.

The picture emerging from these DLA studies is that $\Omega_{\rm HI}$ was slightly rising at the time corresponding to $z > 3.5$, followed by a nonvariable period from $z \approx 3.5$ to $z \approx 1$ (Storrie-Lombardi & Wolfe 2000). The evolution of $\Omega_{\rm HI}$ in the period from $z \approx 1$ to $z = 0$ is not well determined. Rao & Turnshek's (1999) results indicate that $\Omega_{\rm HI}$ was constant to $z \approx 0.5$, after which it must decline rapidly to $z = 0$. This implies that most of the conversion from gas to stars occurred between $z \approx 0.5$ to $z = 0$. Lane's (2000) measurement based on Mg II-selected absorption systems is in agreement with this, although a more gradual evolution is also consistent with her findings.

To interpret these results, it is crucial to obtain a reliable $z = 0$ anchor point. Just as the optical morphologies of galaxies, their luminosities, and stellar populations at $z = 0$ are fundamental to the study of galaxy evolution, the complete census of H I and its distribution among and within galaxies at present defines the relation between star formation and the raw material from which stars are made.

Determining the current neutral gas content requires a different observational technique than at high z. The small cross-section of DLA absorbers, combined with cosmological expansion, make DLAs very rare along any QSO sightline through the local universe. DLA survey results for the low-z regime must be given in $\Delta z = 0.5$ bins, which are sig-

nificant fractions of a Hubble time. Furthermore, the effects of dust (Pei, Fall & Hauser 1999), and the fact that the Lyα line is not observable from the ground at $z < 1.65$ complicate the measurement at the present epoch. Furthermore, the historical requirement for QSO catalogs that objects be "quasi-stellar" means that only quasars away from foreground galaxies have been selected to search for absorption lines, and it is therefore not surprising to find that at low redshift optical identification of galaxies responsible for DLA absorption is often problematic (cf., Rao & Turnshek 1999).

At $z = 0$, 21cm emission from galaxies and possible intergalactic clouds is the logical indicator for the cosmological mass density of H I. One of the principle results of this thesis is the measurement of an accurate and unbiased value for $\Omega_{\rm HI}(z = 0)$ from a radio survey. The first steps toward 21cm line measurements of $\Omega_{\rm HI}$ as a function of redshift are shown in Chapter 8, where preliminary results on the gas content of galaxies in a cluster at $z = 0.2$ are presented.

1.3 The H I mass function

Quantifying the space density of H I-holding objects is normally done with a tool known as the H I mass function (HIMF). This function is defined analogously to the commonly discussed optical luminosity function and defines the number of galaxies per cubic Mpc as a function of H I mass $M_{\rm HI}$. A reliable measurement of the HIMF contains considerable information: 1) construction of the HIMF yields an alternative view of the local galaxy population based on gas-richness rather than optical brightness; 2) integration over the HIMF readily yields a measurement of $\Omega_{\rm HI}$; 3) the HIMF indicates which types of galaxies currently form the main reservoirs of fuel for star formation; 4) models of galaxy formation require a detailed measurement of the HIMF to test the predictions (e.g., Somerville & Primack 1999; Cole et al. 2000).

A first order computation of the HIMF can be made by using measured H I fluxes of a sample of optically selected galaxies with well-understood selection criteria. For example, Hoffman et al. (1989) conducted a series of pointed observations with the Arecibo telescope of known galaxies in the Virgo cluster. They constructed a preliminary HIMF and concluded that there is no excess of gas rich dwarf galaxies. Briggs (1990) made the first computation of the HIMF for optically selected galaxies and further concluded that there was unlikely to be a significant $z = 0$ population of intergalactic H I clouds of large mass. Briggs & Rao (1993) reappraised the Hoffman et al. Virgo data, supplemented with the Fisher & Tully (1981b) catalog of H I observations of spiral galaxies, and were able to construct the HIMF over the range 10^7 to 10^{10} $M_\odot$. They also concluded that there is no evidence for a sharp rise in the number of gas rich dwarf galaxies toward low masses, and that in clusters the HIMF might even go down.

While these were interesting exercises, they do not solve the surface brightness selection bias. H I clouds that are totally devoid of stars are missed completely if a sample of optically selected galaxies is used to calculate the HIMF. A complete and unbiased view of neutral gas in the local universe can only be obtained using blind 21cm surveys. The computation of the HIMF is a logical step in the analysis of 21cm line surveys, leading to a value for $\Omega_{\rm HI}$. This thesis reports the first HIMF that fully recovers the known galaxy population. This HIMF is valid over three orders of magnitude in H I mass. In the following paragraph I give a brief overview of recent work on H I surveys.

1.4 Extragalactic H I surveys

H I surveys are time-consuming. Blind surveys in the 21cm line take hundreds of hours of observing time to yield only few dozen galaxies, while optical surveys systematically produce catalogs of thousands of galaxies. For illustration, the first published blind H I survey in the field (Shostak 1977) took many days of observing time with the NRAO 300 ft telescope and yielded only one detection which later turned out to be a high velocity cloud gravitationally bound to the Milky Way galaxy. In order to increase the detection efficiency many surveys were pointed toward known overdensities: groups and clusters of galaxies. Surveys in the M81, Sculptor, CVn I and NGC 1023 groups (Lo & Sargent 1979; Haynes & Roberts 1979; Fisher & Tully 1981a; Kraan-Korteweg et al. 1999) yielded several new LSB systems but no H I clouds. Clusters that were surveyed in H I are Hydra (McMahon 1993), Hercules (Dickey 1997), and Centaurus and Fornax (Barnes 1997). No surprises were found there with respect to the HIMF: a similar shape is found in these clusters and in the field.

Empty regions of sky have also been the subject of H I surveys. It is interesting to investigate if the morphology-density relation (Dressler 1980) persists down to the lowest density regions and whether very LSB or dark galaxies might be filling the voids. Krumm & Brosch (1984) performed drift-scan surveys in the Perseus and Hercules voids. Although they covered an enormous volume ($\sim 4500\,h_{100}^{-3}\,\mathrm{Mpc}^3$), their H I mass sensitivity would have allowed them to detect only the most massive of galaxies with $M_{\mathrm{HI}} > 10^{10}\,\mathrm{M}_\odot$. Szomoru et al. (1996) observed selected fields in the Boötes void and found no differences in the properties of void galaxies and field galaxies. No new population of gas rich dwarfs or LSB galaxies was found, although the survey volumes were small and the detection limits not very restrictive.

A fair calculation of the HIMF for H I selected galaxies requires a blind H I survey of the field, with no preference to known over- or underdensities. Henning (1995) conducted a series of pointings on lines of constant declination over a redshift range of 7200 $\mathrm{km\,s^{-1}}$. A total number of 39 significant detections were recorded, of which 50% were previously unknown. While Henning's HIMF seems to be indicative of an increasing number of dwarf galaxies, the overall function lies below the lower limit to the HIMF set by counting the optically selected population. Two large surveys in the 21cm line have been conducted recently, both with the Arecibo telescope. The results from one of these surveys, named AHISS (Arecibo H I Strip Survey) forms the basis for Chapters 2, 3 and 4 of this thesis. The other survey, similar in size, is discussed in Spitzak (1996) and Schneider, Spitzak & Rosenberg (1998). The Arecibo Dual-Beam Survey (Rosenberg & Schneider 2000) covers a larger area on the sky, but is less sensitive to low column density gas and low H I masses than the AHISS. Unfortunately, systematic optical follow-up on this survey does not yet exist. Eventually, the HIPASS survey (Staveley-Smith et al. 1996) with the Parkes Telescope, which covers the entire southern sky out to 12,700 $\mathrm{km\,s^{-1}}$, will yield a sample of thousands of H I selected galaxies.

1.5 The faint tail of the HIMF

The faint tails of the HIMF and the optical luminosity function deserve special attention. The slope of the faint-end is determined by the shape of the distribution function of primordial density fluctuations, a complex interplay of various astrophysical processes during galaxy formation and evolution, and dynamical evolution dependent on the local

galaxy density. The slope of the faint end of the luminosity function is still uncertain; published values range from $\alpha = -2.0$ to $\alpha = -0.7$ (Compare Lin et al. 1996 and Loveday 1997), where α is defined as $N(L)dL \propto L^{\alpha}dL$.

The hierarchical clustering scenario is presently the most widely accepted model for galaxy formation (e.g. Kaufmann 1996). It explains the formation of galaxies by many generations of mergers of dark matter dominated smaller masses. Observational support comes from a increasing merger fraction of field and cluster galaxies with increasing redshift (Lavery et al. 1996, van Dokkum et al. 1999). Numerical models based on the hierarchical scenario generally predict steep slopes of the mass function since large numbers of low mass halos might survive to the present day if the merging and accreting is not fully efficient (Klypin et al. 1999; Moore et al. 1999). On galaxy and galaxy group scales, the predicted halos outnumber optically identified satellites by a factor of 10. If no stars have been found associated with the halos, their baryonic content must consist of primordial gas. Whether the cloud densities are sufficiently high to shield the gas from ionization by the extragalactic uv background determines if most of the baryonic content is neutral or not.

Blitz et al. (1999) have argued that high velocity clouds (HVCs) are either remnants from the formation of the LG or as representatives from an intergalactic population of dark matter dominated mini-halos in which hydrogen has collected and remained stable on cosmological time scales. This scenario gives an appealing solution for the missing satellite problem as it both predicts the right number of dark matter halos (between 500 and 2000) and also shows how the dynamical evolution of the Local Group with infalling gas can reproduce the distribution of the HVCs on the sky.

H I surveys in galaxy groups provide the way to settle the issue of missing satellites. If the flatness of the H I mass function persists down to the lowest masses, current hierarchical clustering models may have to be re-evaluated as this requires severe suppression of the primordial density fluctuation spectrum on small scales (Kamionkowski & Liddle 1999). Self-interacting dark matter (e.g., Spergel & Steinhardt 1999) and other dark-matter flavors (fluid dark matter, repulsive dark matter) have been suggested as possible explanations for a less efficient formation of small mass halos.

It should be noted that the faint tail of the HIMF might also have ramifications for the determination of $\Omega_{\rm HI}$. There might be substantial amounts of H I hiding in very small masses if the faint tail rises to $\alpha = -2$ or steeper. This would have important implications on the interpretation of the evolution of $\Omega_{\rm HI}$. In this thesis we report two surveys of nearby groups and galaxy halos where extragalactic analogs of the HVCs should be detected if they are massive enough to make up the missing satellites.

1.6 Brief thesis outline

The Chapters 2, 3, and 4 of this thesis are devoted to the results of the Arecibo H I Strip Survey, the most sensitive blind H I survey of the extragalactic sky to date. Chapter 2 presents the 21cm and optical follow-up on the 66 detections that were made in this survey. The sample is divided into two subgroups: previously identified galaxies and newly discovered galaxies. It is tested whether the new galaxies have properties that set apart from their optically selected counterparts.

A detailed analysis of the survey sensitivity and possible influence of large scale structure is given in Chapter 3. The HIMF and the cosmological mass density of H I are calcu-

lated and compared to previous determinations. Chapter 4 presents the optical luminosity function and surface brightness distribution of H I selected galaxies. It is tested whether the space density of LSB galaxies is in agreement with previous determinations based on deep CCD surveys. We also calculate the contribution that LSB galaxies make to the local cosmic baryon density and total mass density.

In Chapter 5 a connection is made between QSO absorption line statistics and H I measurements in the local universe. The tool that is used is the column density distribution function, $f(N_{\rm HI})$, which describes the change of finding a certain column density $N_{\rm HI}$ along a normalized path length. A $z = 0$ measurement of $f(N_{\rm HI})$ is calculated from 21cm observations of nearby galaxies.

The next two chapters concentrate on the lowest H I masses. In Chapter 6 we calculate whether the model in which Galactic high velocity clouds (HVCs) are actually distributed throughout the Local Group is in agreement with the results of blind H I surveys. In Chapter 7 a targeted survey for H I clouds in five galaxy groups is discussed.

In Chapter 8 we make a short excursion to higher redshift to present the first results of a program of deep H I imaging of galaxy cluster Abell 2218 at $z = 0.2$

Finally, a summary of the main conclusions and a brief outlook are presented in Chapter 9.

References

Barnes, D. G., Staveley-Smith, L., Webster, R. L., & Walsh, W. 1997, MNRAS, 288, 307
Blitz, L., Spergel, D. N., Teuben, P. J., Hartmann, D., & Burton, W. B. 1999, ApJ, 514, 818
Bosma, A. 1978 Ph.D. thesis, University of Groningen
Briggs, F. H. 1990, AJ, 100, 999
Briggs, F. H., & Rao, S. 1993, ApJ. 417, 494
Cole, S., Lacey, C. G., Baugh, C. M., & Frenk, C. S. 2000, astro-ph/0007281
Connolly, A. J., Szalay, A. S., Dickinson, M., Subbarao, M. U., & Brunner, R. J. 1997, ApJ, 486, L11
Dalcanton, J. J., Spergel, D. N., Gunn, J. E., Schmidt, M., & Schneider, D. 1997, ApJ, 114, 635
Dickey, J. M. 1997, AJ, 113, 1939
Disney, M. J. 1976, Nature, 263, 573
Dressler, A. 1980, ApJ, 236, 351
Driver, S. P., Phillipps, S. 1995, ApJ, 469, 529
Ewen, H. I. & Purcell, E. M. 1951, Nature, 168, 356
Fish, R. A. 1964, ApJ, 139, 284
Fisher, J. R., & Tully, R. B. 1981a, ApJS, 47, 139
Fisher, J. R., & Tully, R. B. 1981b, ApJL, 243, L23
Freeman, K. C. 1970, ApJ, 160, 811
Fukugita, M., Hogan, C. J., & Peebles, P. J. E. 1998, ApJ,
Haynes, M. P., & Roberts, M. S. 1979, ApJ, 227, 767
Henning, P. A. 1995, ApJ, 450, 578
Hoffman, G. L., Lewis, B. M., Helou, G., Salpeter, E. E., & Williams, B. M. 1989, ApJS, 69, 65
Impey, C. D., Sprayberry, D., Irwin, M. J., & Bothun, G. D. 1996, ApJS, 105, 209
Kaufmann, G. 1996, MNRAS, 281, 487
Klypin, A. A., Kravtsov, A. V., Valenzuela, O., & Prada, F. 1999, ApJ, 522, 82
Kraan-Korteweg, R. C., van Driel, W., Briggs, F. H., Binggeli, B., & Mostefaoui, T. I. 1999, A&AS, 135, 255
Krumm, N., & Brosch, N. 1984, AJ, 89, 1461
Lane, W. M. 2000, Ph.D Thesis, University of Groningen
Lavery, R. J., Seitzer, P., Suntzeff, N. B., Walker, A. R., & Da Costa, G. S. 1996, ApJ, 467, L1

Lilly, S. J., Le Fevre, O., Hammer, F., Crampton, D. 1996, ApJ, 460, 1
Lo, K. Y., & Sargent, W. L. W. 1979, ApJ, 227, 756
Loveday, J. 1997, ApJ, 489, 29
Madau, P. 1996, MNRAS, 283, 1388
McMahon, P. M. 1993, Ph.D Thesis, Columbia University
Moore, B., Ghigna, F., Governato, F., Lake, G., Stadel J., Tozzi, P. 1999, ApJ, 524, L19
Muller, C. A. & Oort, J. H. 1951, Nature, 168, 357
O'Neil, K., Bothun, G. D. & Cornell, M. E. 1997, AJ, 113, 1212
Pei, Y. C., Fall, S. M., & Hauser, M. G. 1999, ApJ, 522, 604
Pickering, T. E., Impey, C. D., van Gorkom, J. H., & Bothun, G. D. 1997, AJ, 114, 1858
Prochaska, J. X. & Wolfe, A. M. 1997, ApJ, 487, 73
Rao, S. M. & Turnshek, D. A. 1999, astro-ph/9909164
Rosenberg, J. L. & Schneider, S. E. 2000, astro-ph/0004205
Schneider, S. E., Spitzak, J. G., & Rosenberg, J. L. 1998, ApJ, 507, L9
Schombert, J. M., Bothun, G. D., Schneider, S. E., McGaugh, S. S. 1992 AJ, 103, 1107
Shostak, G. S. 1977, A&A, 54, 919
Somerville, R. S. & Primack, J. R. 1999, MNRAS, 310, 1087
Sprayberry, D., Impey, C. D., Irwin, M. J., & Bothun, G. D. 1997, ApJ, 482, 104
Staveley-Smith, L., Wilson, W. E., Bird, T. S., Disney, M. J., Ekers, R. D., Freeman, K. C., Haynes, R. F., Sinclair, M. W., Vaile, R. A., Webster, R. L., & Wright, A. E. 1996, PASA, 13, 243
Storrie-Lombardi, L. J. & Wolfe, A. M. 2000, astro-ph/0006044
Turnshek, D. A. 1997, in Structure and Evolution of the Intergalactic Medium from QSO Absorption Line Systems, ed. Petitjean & Charlot
van Albada, T. S., Bahcall, J. N., Begeman, K., & Sancisi, R. 1985, ApJ, 295, 305
van de Hulst, H. C. 1945, Ned. Tijd. Natuurk., 11, 210
van Dokkum, P. G., Franx, M., Fabricant, D., Kelson, D. D., & Illingworth, G. D. 1999, ApJ, 520, L95
Wolfe, A. M. 1995, in QSO Absorption Lines, ed. G. Meylan

L2

Properties of H I Selected Galaxies

M. A. Zwaan, D. Sprayberry, & F. H. Briggs

ABSTRACT — A blind extragalactic survey in the 21cm line was undertaken with the Arecibo 300m telescope in order to test the completeness of optical galaxy catalogs. This survey, which covered two strips of sky at constant declination out to a redshift of $cz = 7400$ km s^{-1}, yielded a sample of 66 H I selected galaxies. This sample was studied in more detail in 21cm and in the optical *B*-band. We present the *B*-band images of all galaxies more than 10° away from the Galactic plane, with overlays of the H I distribution. Approximately half of the galaxies in the sample are already listed in existing catalogs of optically selected galaxies. The uncataloged galaxies do not only have high gas fractions, but also low luminosities, low optical surface brightnesses and small exponential disk scale lengths and turn out to be dwarf and irregular galaxies. No large uncataloged low surface brightness galaxies are found within the survey volume. We show that the predominance of small, gas rich galaxies in an H I selected galaxy sample is a natural result of the survey technique. The H I detected galaxies are not anomalously gas rich or underluminous and do not form a separate class of galaxies that has been missed in catalogs of optically selected galaxies. The sample is unique in its dynamic range in galaxy parameters and is therefore very suitable for testing correlations with e.g. surface brightness and gas richness.

2.1 Introduction

OUR PERCEPTION OF galaxy properties, their distribution in the Universe, and their cosmological significance has been shaped primarily by surveys in the optical wavelengths. It is not inconceivable that this selection gives us a biased view of the true population of galaxies. It has become clear in recent years that galaxies exist that easily escape detection in optical surveys since their surface brightness is much lower than that of the night sky: low surface brightness (LSB) galaxies (see Disney 1976). The cosmological significance of these galaxies is still a subject of debate (see Briggs [1997], O'Neil & Bothun [2000], and Schneider & Schombert [2000] for some recent viewpoints).

Deep optical CCD surveys (Dalcanton et al. 1997, O'Neil, Bothun, & Cornell 1997) or automated machine scans of survey plates (Impey et al. 1996), followed up with spectroscopy to determine distances, help to resolve the issue, but a completely different approach would be to select galaxies not by their optical light but by their neutral gas content. Although other biases are introduced this way (gas poor galaxies are clearly discriminated against), this method will certainly help to develop a fairer view of the extragalactic sky. Especially since those galaxies which easily fall below the detection limits in optical surveys are generally found to be rich in neutral gas (Schombert et al. 1992, van der Hulst et al. 1993).

A number of H I surveys have been carried out in the past, but only few of these are truly blind, in the sense that the observations are not pointed towards cataloged galaxies (e.g. Fisher & Tully 1981), groups or clusters of galaxies (e.g. Kraan-Korteweg et al. 1999), or empty regions of sky (e.g. Szomoru et al. 1996). The first blind H I surveys were carried out by Shostak (1977), Kerr & Henning (1987), but large samples of H I selected galaxies are becoming available only recently. The largest published sample to date is that from the Arecibo Dual-Beam Survey (Rosenberg & Schneider 2000), that encompasses 265 galaxies, but unfortunately, systematic optical follow-up on this sample does not yet exist. Eventually, the HIPASS survey, which covers the entire southern sky, will yield a sample of thousands of H I selected galaxies.

In this paper we present optical and 21cm data of a sample of 66 galaxies selected in the Arecibo H I Strip Survey (AHISS) (see also Sorar 1994). The purpose of this survey was to select galaxies independent of their optical properties, over a large enough region of sky to average out the effects of large scale structure and to a low limiting column density to ensure inclusion of the lowest density galaxies. An H I selected sample of similar size is discussed by Spitzak & Schneider (1998).

The AHISS consists of two slices of the extragalactic sky, both slices covering approximately 10 hours of RA at constant declination, one at $\delta = 14\ 14'$ and the second at $\delta = 23\ 09'$. The total area of sky swept out by the Arecibo beam, including the sidelobes, was 65 square degrees. The depth of the survey was $cz = 7400\,\mathrm{km\,s^{-1}}$, the maximum search volume was almost 3000 $h_{100}^{-3}\,\mathrm{Mpc}^3$. Since the same regions of sky were retraced for up to 30 days, the sensitivity of the observations was very low; the limiting column density was 10^{18} cm^{-2} at a 5σ level for 16 km s^{-1} velocity resolution. This sensitivity is unmatched by any other blind H I survey to date.

Follow-up observations, both in 21cm and in the optical, have been performed on all significant signals. In this paper we present B-band images, H I contours and global profiles and tabulate the most important radio and optical parameters. We discuss whether H I selected galaxies form a distinct class of galaxies which have been underrepresented in optically selected galaxy samples. The analysis of the 21cm data and a detailed de-

scription of the survey sensitivity has been presented in Chapter 3. Also the H I mass function and the cosmological mass density of H I were discussed there. Further analysis of the optical data, including the construction of the optical luminosity function and the distribution function of optical surface brightnesses are presented in Chapter 4.

2.2 21cm Follow-up observations

Short 21cm observations of all significant signals were obtained with the NRAO Very Large Array (VLA[2]) in D-Array, the most compact configuration. The data were taken in two IF mode, using 63 channels of each 97.6 kHz, which corresponds to an observable bandwidth of approximately 660 $\mathrm{km\,s^{-1}}$ and a velocity resolution of approximately 10.5 $\mathrm{km\,s^{-1}}$. The typical r.m.s. noise level was 1.2 mJy/beam, while the typical synthesized beam was $60'' \times 60''$. The observing strategy and details of the data reduction have been described in Chapter 3 and will not be repeated here.

The total H I maps were determined by adding the CLEANed spectral channels which contained line emission. If the center of the emission clearly shifted from channel to channel, only the regions with H I emission in each channel were added so as to avoid adding of unwanted noise. The regions with H I emission were determined by smoothing the channel maps to twice the original spatial resolution and clipping the data at 2σ. The resulting maps were used as masks for the original resolution data cubes. Using this method to make H I maps will result in a lower noise level than obtained from a simple sum of velocity channels, but spatially non-uniform noise across the H I map. The H I distributions made in this way are indicated in Figure 2.8 (page 45) by contour levels, overlaid on the optical images. Values for the first three contour levels are shown in one of the lower corners of each image. Total H I masses were determined using $M_{\mathrm{HI}}/\mathrm{M}_\odot = 236\, D^2 \int S dV$, where D is the distance to the source in Mpc and $\int S dV$ is the integrated line flux in $\mathrm{mJy\,km\,s^{-1}}$ corrected for primary beam attenuation.

In order to test the quality of the 21cm fluxes determined by these short observations we compare our measurements with literature values where those are available. Figure 2.1 shows flux values as measured by the VLA plotted against literature flux values of cataloged galaxies. In a few cases more than one measurement of a single galaxy is available, these measurements are connected by a solid line. The dashed line shows the line of equality. The agreement between literature values and new measurements is satisfactory, with no apparent systematic differences. While the scatter around the line of equality is 0.19 dex, the average deviation is only 0.056 ± 0.048 dex, indicating that there is no significant offset.

The global H I profiles are also plotted in Figure 2.8. The horizontal (velocity) scale is equal for each profile to enable comparison of the rotation velocities, the vertical (flux) scale is adjusted to the galaxies' peak flux. The unit of the horizontal axis is $\mathrm{km\,s^{-1}}$, the unit of the vertical axis is Jy. Note that for the sources with H I fluxes lower than 1 $\mathrm{Jy\,km\,s^{-1}}$ the S/N ratios of the global profiles are generally low. Typical 1σ errors on the global profiles are 1 mJy, implying that the apparent structure in the profiles is likely to be a result of poor signal to noise ratio for the galaxies of lowest flux. For most of the inclined galaxies, a normal double horned profile is visible.

Velocity widths were determined from the global H I profiles at 20% of the peak in-

[2]The National Radio Astronomy Observatory is a facility of the National Science Foundation operated under cooperative agreement by Associated Universities, Inc.

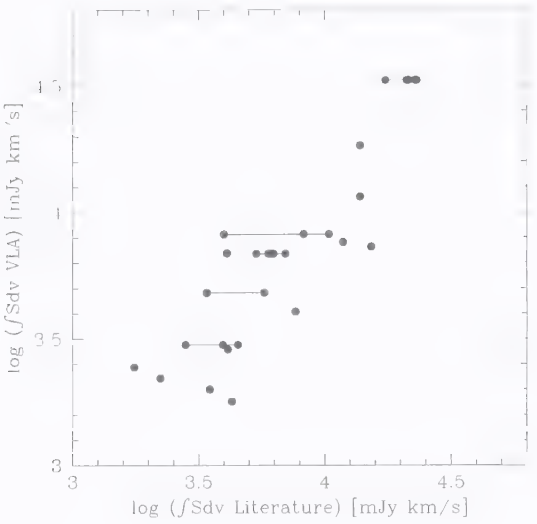

FIGURE 2.1— Comparison between 21cm fluxes as determined from our VLA data and from the literature. The vertical rms scatter around the line of equality (dashed line) is 0.19 dex, while the average deviation is 0.056 ± 0.048 dex.

tensity. The measured velocity widths need to be corrected for instrumental broadening. From a variety of methods available in the literature we choose to apply the recipe proposed by Bottinelli et al. (1990), which consists of subtracting a constant value δW from the measured velocity width to obtain W_{20}. The value of δW is determined by $\delta W = -(0.014 \times 20 - 0.83) \times$ channel separation which results in $\delta W = 5.8 \mathrm{km\,s^{-1}}$. After the correction for instrumental broadening, the widths can be corrected for random and turbulent motion by applying the formalism described by Tully & Fouqué (1985). This procedure subtracts a constant factor from the line width of rapidly rotating galaxies and makes a subtraction in quadrature for slower rotating ones. We adopt the parameters given by Tully & Fouqué, but use the updated value of $W_{t,20} = 22 \mathrm{km\,s^{-1}}$ from Verheijen (1997) which is based on the analysis of high quality WSRT data of 38 spiral galaxies in the Ursa Major cluster.

The distances listed in this paper have been determined from the 21cm radial velocities using a Hubble constant $H_0 = 100 \mathrm{\ km\,s^{-1}Mpc^{-1}}$. The radial velocities have been calculated by taking the mean of the velocities at 20% of the peak flux intensity. The heliocentric distances have been converted to Galactocentric distances by adding the term $\Delta D = 300 \sin l \cos b / H_0$, where l and b are the Galactic longitude and latitude.

2.3 Optical follow-up observations

The optical observations were confined to sources at Galactic latitudes $|b| > 10°$ to avoid severe Galactic extinction and confusion of foreground stars. This reduces the total number of accessible sources to 61. The optical data were obtained at the Isaac Newton Telescope (INT[3]) of the Observatorio del Roqué de los Muchachos on the island of La Palma, Spain. Due to bad weather and equipment problems, the data collection was spread over four observing runs during the period 1995 October through 1997 March. Images were

[3]The Isaac Newton Telescope is operated by the Royal Greenwich Observatory in the Spanish Observatorio del Roque de los Muchachos of the Instituto de Astrofisica de Canarias.

recorded at the Prime Focus camera with a thinned Tektronix 1024^2 pixel CCD. The Tektronix CCD has 24 μm pixels, which give an image scale of 0.59″ per pixel at prime focus. All images were taken through a standard Harris B filter. Flatfields were taken in the twilight, and the residual background variations after flatfielding are typically $< 1\%$ of the sky level. Data reduction steps of bias subtraction and flatfielding were carried out using standard IRAF procedures. Standard stars from the list of Landolt (1992) were observed several times and at several airmasses each night for photometric calibration. Determination of the photometric zeropoints and extinction coefficients was accomplished using the IRAF PHOTCAL routines. The calibration is accurate to 0.13 mag.

2.3.1 Integrated magnitudes and images

Total galaxy magnitudes were determined using aperture photometry on the reduced images. Correct aperture sizes were found using a curve-of-growth algorithm: aperture photometry was performed at a series of aperture radii, increasing in 1 arcsecond steps, until the integrated magnitudes leveled out at an asymptotic maximum. The first radius at which this maximum (brightest) integrated magnitude was reached was then chosen as the correct aperture size. The magnitudes listed in Table 2.1 have been calibrated using the photometric zeropoints and extinction coefficients derived for the relevant night of observation. They have also been corrected for Galactic extinction using the reddening maps of Burstein & Heiles (1982) and assuming that $A(B) = 4.1\,E(B-V)$. For galaxy A44 a accurate magnitude could not be determined since the center of the image was saturated.

Figure 2.8 shows images of the survey galaxies. The orientation is such that north is up and east is to the left. The B-band images are shown as gray-scales. Although the sizes of the images vary, the angular projected scales are all equal. The logarithmic gray-scale levels are chosen in such a way that LSB features are clearly visible, the gray-scale mapping parameters are not the same for all images. If an optical image is not available since the Galactic latitude is less than 10°, this is indicated in the upper right corner of the image. If a galaxy has already been included in a catalog, the standard catalog name has been shown in the top right corner of a panel.

The images clearly illustrate the extremes of the apparent magnitude range covered by the galaxies in our sample and show that the sample is dominated by late type spiral galaxies with irregular morphologies. In all but one case the match between the center of the H I emission and the starlight is excellent. The exception is A44, where the H I emission is centered approximately 80″ east from the center of the nearest galaxy. This galaxy (CGCG 116-001) is clearly of early morphological type (E0) and therefore unlikely to contain H I gas. This bright galaxy is listed in the Zwicky Catalog of Galaxies and Clusters of Galaxies (CGCG), but at the time of our observations there was no redshift listed for it in either the CfA Redshift Survey Catalog or NED[4]. If the galaxy had been at a very different redshift, then the H I cloud would have been the first known instance of a free-floating cloud of extragalactic hydrogen with no associated starlight. We used the IDS at the INT to measured an optical spectrum of the bright galaxy in order to determine its radial velocity . Via cross-correlation against a stellar radial velocity standard star, we determined a radial velocity of 4400 ± 50 km s^{-1}. The radial velocity of the 21cm emission is 4575 km s^{-1} indicating the H I is gravitationally bound to the bright early type galaxy,

[4]The NASA/IPAC Extragalactic Database (NED) is operated by the Jet Propulsion Laboratory, California Institute of Technology, under contract with the National Aeronautics and Space Administration.

similar to the H I ring in Leo (Schneider 1989) and the H I cloud near NGC 4472 (Henning, Sancisi & McNamara 1993).

2.3.2 Central surface brightnesses

Galaxy surface brightnesses were first determined using the area analysis method. The method proceeds along the following steps: (1) estimate the sky background and single-pixel uncertainty in the sky level on the properly flatfielded image; (2) identify all the connected pixels starting at the center of galaxy that are at least 2σ above the sky background; (3) subtract the sky intensity from all these pixels and bin them into an intensity histogram; (4) transpose the axes of the histogram so that intensity increases up the y-axis and area in pixels increases up the x-axis; (5) calibrate the intensity values on the y-axis to magnitudes per square arcsecond using photometric calibrations derived from the standard stars and correct them for Galactic extinction as described above; (6) calibrate the area in pixels on the x-axis to area in square arcseconds using the CCD image scale; (7) take the square root of the values along the x-axis so that the x-axis now has linear units of distance (arcseconds). When these steps are complete, the result is a surface brightness profile of the galaxy showing the amount of the galaxy at each surface brightness level. This profile is not strictly a "radial" profile, in that the "distance" shown on the x-axis does not correspond to "radial distance from the center" but rather to "linear size of the galaxy area within the surface brightness bin."

The advantages of the area analysis are its simplicity and robustness. Unlike isophote fitting, it does not require assumptions that surface brightness monotonically decreases outward from the geometric center or that the isophotal contours can be well-represented by smooth ellipses. These assumptions are not applicable to galaxies that exhibit strong dust lanes, bright off-center H II regions, single or uneven spiral arms, or other non-axisymmetric features. Several of the galaxies in this survey (for example, A4-2, A7, A27, and A38) show such problems. For galaxies like these, a traditional radial profile developed through isophote fitting would probably not be very meaningful since the estimation errors on the individual isophotes would be extremely large (assuming the code produced results at all). Use of area analysis allows us to estimate surface brightness profiles in the same way for all galaxies in the survey, and to have exactly the same quality of information in each profile.

The primary disadvantage of the area analysis technique is that it does not measure out to surface brightness levels as faint as those reachable with isophotal fitting. Because the "area" of the galaxy is analyzed one pixel at a time, the large single-pixel uncertainty in the sky level imposes severe limits on identification of pixels as part of the galaxy in low surface brightness regions. Isophotal fitting routines average over very many pixels in the outer isophotes, so they can take advantage of substantial $\sqrt{N}$ reductions in the single-pixel sky uncertainty to reach much fainter levels. This difference in depth was not a problem for our survey. The single-pixel detection threshold for area analysis (that is, the surface brightness level represented by a single pixel at least 2σ above sky) was for all galaxies at least 2.5 magnitudes per square arcsecond fainter than the projected central surface brightness. In no case was the galaxy identification or measurement hampered by the inability to flag the outermost pixels as being part of the galaxy.

Unlike isophote fitting, area analysis does not return any information about the shape of a galaxy. We have therefore estimated overall ellipticities and position angles by taking intensity-weighted moments of each galaxy within the same apertures used to measure

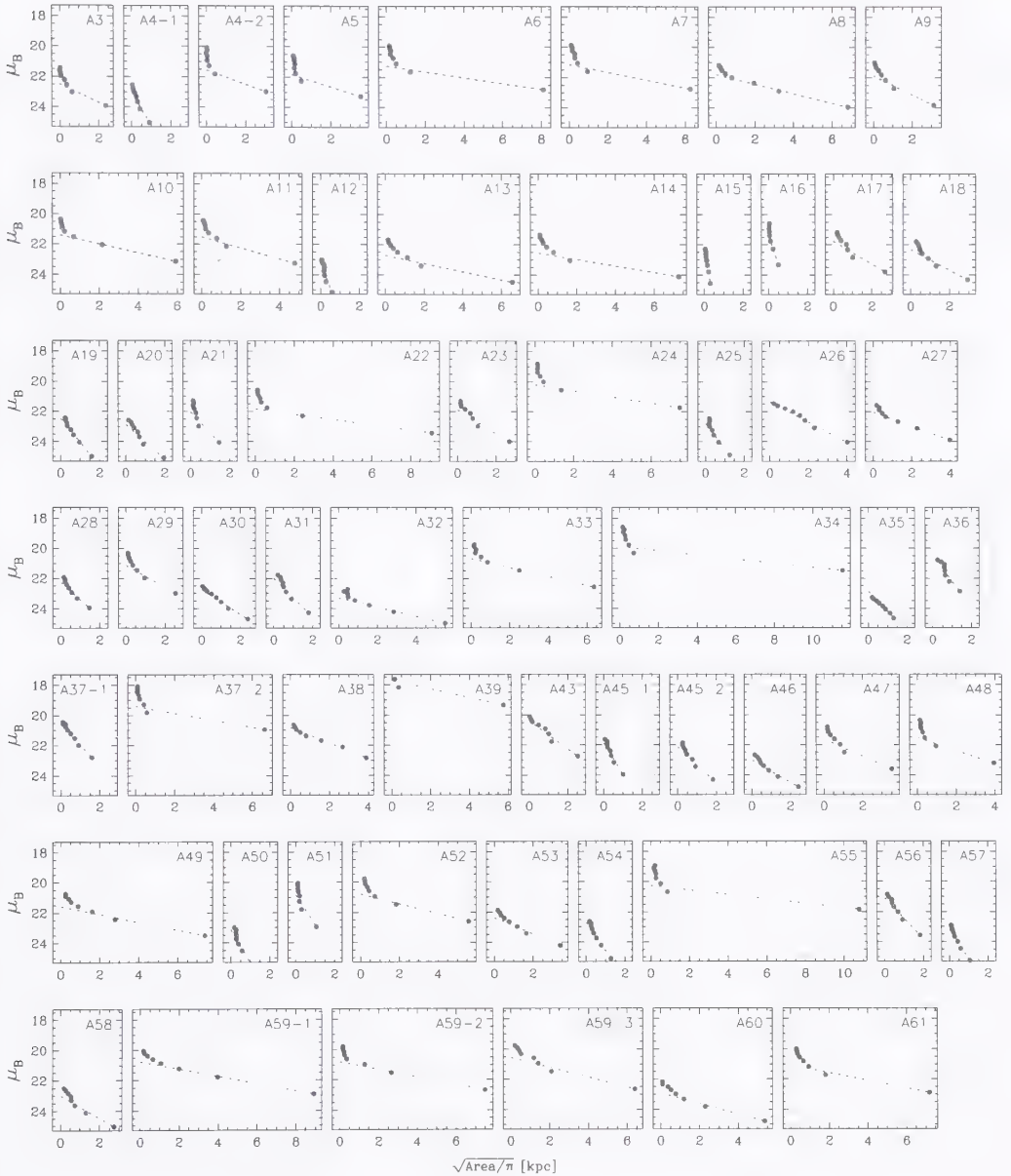

FIGURE 2.2— Area analysis profiles. See text for explanation. All profiles are shown at the same linear scale. The dashed lines are fits to the points, excluding the two bins with the highest surface brightness.

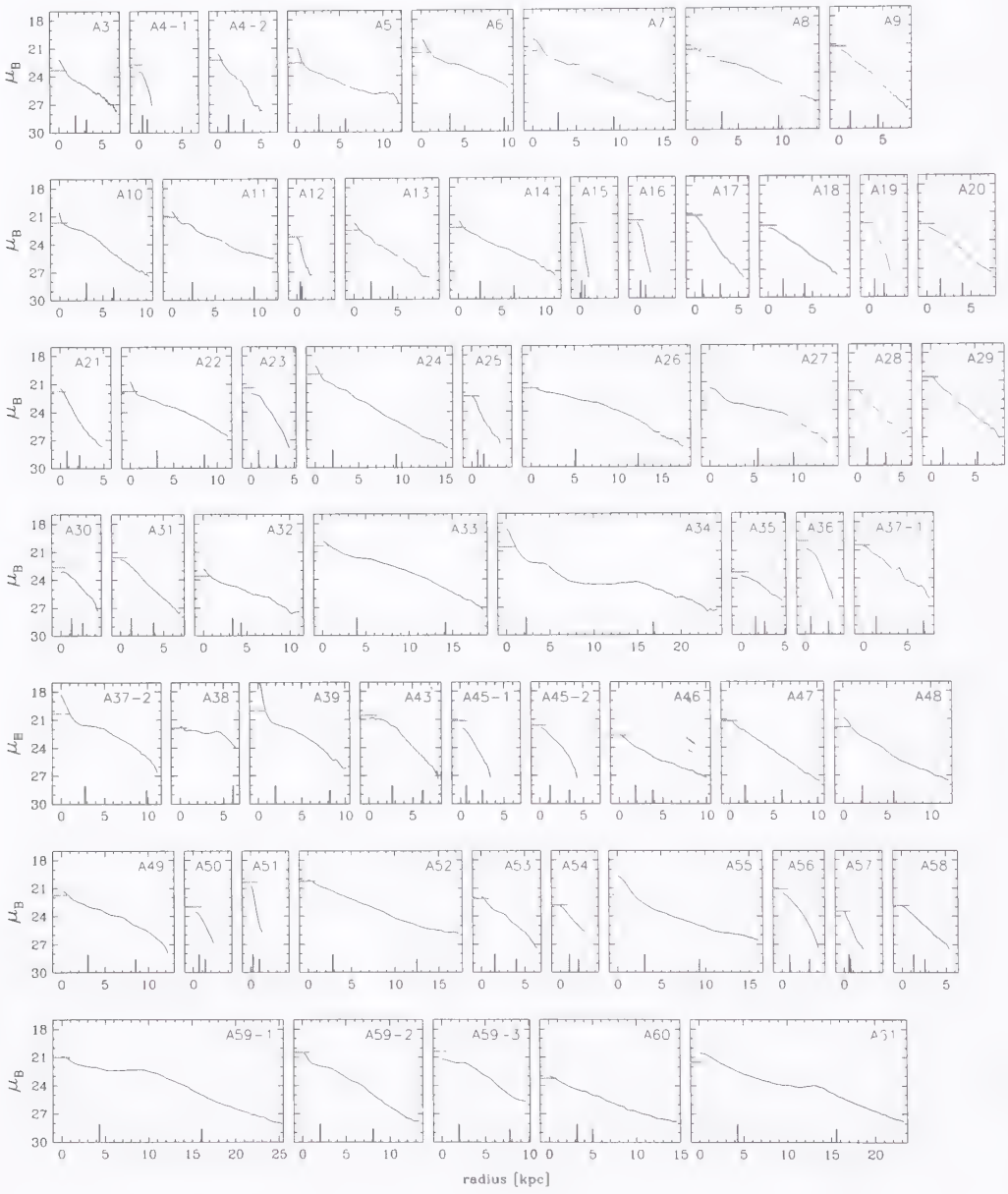

FIGURE 2.3— *B* band radial surface brightness profiles. All profiles are shown at the same linear scale. The small horizontal lines mark the extrapolated central surface brightnesses, vertical lines indicate the exponential scale length and R_{25}.

that galaxy's total magnitude. We have converted these ellipticities into rough estimates of galaxy inclination by assuming that the ellipticity is entirely due to the tilt of a circular disk, where a purely edge-on disk is assumed to have an intrinsic axis ratio of 0.2 due to disk thickness (per Holmberg 1958).

Because Nature conspires to put the brightest parts of spiral galaxy disks at their centers, the area profiles can be used to estimate the disk central surface brightness for spiral galaxies. We have adopted the approach of fitting a straight line to the points on the area profiles, excluding the two bins with the highest surface brightness. The "zero area" intercept of the fit gives a surface brightness level that, for a spiral galaxy, is directly analogous to the projected central surface brightness of the disk, and the slope of the fit gives an estimate of the scale size for the disk. The two highest surface brightness bins are excluded for two reasons: first, if they represent pixels at the center, then they most likely reflect the surface brightness of what is structurally the galaxy bulge and not the disk; and second, these bins often include high surface brightness pixels away from the galaxy center such as bright HII regions. In order to facilitate comparisons with other studies using different surface brightness estimation algorithms, we have taken the additional step of dividing the linear-size values on the x-axis of the area profile by $\sqrt{\pi}$ to make the resulting fitted slope more closely match the radial disk scale length determined from a traditional radial profile where the x-axis represents $\sqrt{ab}$ instead of $\sqrt{\text{Area}}$. In Figure 2.2 we present the area analysis profiles, all shown on the same linear scale.

In addition to the linear fit, the peak surface brightness in the brightest square arcsec is also computed, directly from the pixel intensities. This peak can be compared to the fitted "central" surface brightness as a test of problems with the fit: where the peak surface brightness is fainter than the fitted value, the galaxy image and brightness profile are inspected carefully to see why. This happened with A15, A35, and A36. In all three cases, the anomaly is due to an unusual luminosity distribution in the galaxy (eg., flat in the center, or falling off linearly rather than exponentially) such as is sometimes seen in LSB galaxies. In these three cases, the actual peak value is reported instead of the fitted value.

To test whether the surface brightnesses from the area analysis method show any systematic deviation from surface brightnesses derived via standard techniques, we also determined normal radial profiles via ellipse fitting. The centers of the galaxies were usually taken to be the maximum of the light distribution, but as stated before, in some cases these centers are not well defined. For those galaxies we took the average center of ellipses fitted to isophotes just outside the central region. The pixel values were averaged in ellipses of constant axial ratio and position angle, which were determined by taking intensity weighted moments. The resulting radial surface brightness profiles are presented in Figure 2.3. Next we fitted exponential disk models to the exponential parts of the radial profiles. Any central concentration was excluded from the fits. In many cases it was not exactly clear to which part of the profile a disk should be fitted because there was either a kink in the profile (e.g., A10) or the profile had no exponential part (e.g., A56, A34). In those cases the central extrapolated disk central surface brightness is not a very meaningful number. The correlation between central surface brightnesses derived from the area analysis and those from ellipse fitting is very good, the difference is $\langle \mu_{\text{ellipse}} - \mu_{\text{area}} \rangle = 0.01 \pm 0.06$ mag. There is no apparent systematic offset as a function of surface brightness either way. Nevertheless, the scatter in $\langle \mu_{\text{ellipse}} - \mu_{\text{area}} \rangle$ is quite high, $\sigma = 0.47$ mag, indicating that two independent measurements of the central surface brightness can differ dramatically. This is a probably a problem intrinsic to the population

of galaxies studied here which consists for a large part of dwarf and irregular galaxies. Apparently, central surface brightnesses of dwarf and irregular galaxies should be regarded as rough estimates. From these exponential disk fits we also derived an estimate of the scale lengths of the galaxies. Additionally we derived R_{25}, the radius at which the B-band surface brightness profile reaches 25 mag arcsec^{-2}.

2.3.3 Extinction corrections

It is of course desirable to express the central surface brightnesses as face-on-equivalents. However, it has become clear of late that inclination dependent corrections for extinction are neither straightforward nor without controversy (see for example Valentijn 1994). There have been recent results suggesting that the inclination corrections depend on Hubble type (Valentijn 1994), galaxy luminosity (Giovanelli et al. 1995, Tully et al. 1998), galaxy surface brightness (Tully & Verheijen 1997), and distance from the galaxy center for all galaxy categories (Valentijn 1994; Giovanelli et al. al 1995). The present survey includes galaxies over very broad ranges in luminosity, surface brightness, and Hubble type. Also, many of the galaxies are of very small angular size or irregular morphology which makes applying a radially dependent correction difficult.

In principle, an independent measure of a galaxy's dust content can be obtained from its far infrared flux, since the FIR luminosity is thought to be an indicator of the warm dust content. A cross check of the H I selected sample against the IRAS database suggests that our low luminosity and low surface brightness galaxies suffer much less from dust extinction than luminous or high surface brightness galaxies. Fourteen of the H I selected galaxies turn out out to have counterparts in the IRAS Catalog of Point Sources or in the IRAS Faint Source Catalog. From the IRAS measurements in the 60 and 100 micron bands an FIR flux can be derived via $F_{\rm FIR} = 2.58F_\nu(60) + F_\nu(100)$, where the fluxes are measured in Jy. An FIR luminosity can be calculated using $L_{\rm FIR} = 3.86 \times 10^5 D^2 F_{\rm FIR}$, where D is the distance to the source in Mpc. The galaxies which are found in the IRAS database are preferentially the ones with high luminosity and high surface brightness. Figure 2.4 illustrates this. The left panel shows the distribution of absolute blue magnitudes, the right panel shows the surface brightness distribution, both uncorrected for dust extinction. The galaxies with detected infrared emission are indicated by hatched histograms, those without infrared emission are shown as solid histograms. The probability that galaxies with and without infrared emission are drawn from the same population can be rejected by means of a Kolmogorov-Smirnov (K-S) test at a significance level of 3×10^{-6} for $M_B^{\rm b}$ and 1.3×10^{-4} for μ_B. This result could be (partly) influenced by an incompleteness of IRAS detections of the lowest luminosity spirals. However, there are more indications that the internal dust extinction in LSB galaxies is low: no detection of CO (e.g., Schombert et al. 1990), low H I surface densities (de Blok, McGaugh & van der Hulst 1996), low Balmer decrements towards HII regions (McGaugh 1994) and no strong dust features in optical images (e.g., McGaugh & Bothun 1994).

With this information we now know that using the well known correction from Tully & Fouqué (1985) that assumes the same relation between disk scale height and optical depth for all galaxies, irrespective of surface brightness and luminosity, is probably not accurate. We have chosen to apply the extinction correction proposed by Tully et al. (1998) which is a function of absolute magnitude. The extinction correction can be written as $A^{\rm i} = \gamma \log(a/b)$, where $\gamma = -0.35(15.1 + M_B^{\rm b,i})$. Since for our data set the central surface brightness is well correlated with absolute luminosity, the extinction correction implies

a low correction for LSB galaxies and a higher correction for HSB galaxies. The mean extinction correction for the total sample is only 0.05 mag higher than when the Tully & Fouqué correction is applied.

2.4 The data

Table 2.1 lists all basic parameters of the survey galaxies. Coordinates and names of the galaxies can be found in Table 3.1 on page 54. The following entries are contained: (1) Nr. — Original number of detection in the AHISS. A subscript indicates that the original Arecibo detection was actually caused by the signals of two galaxies stacked up in the same channels; (2) D — Galactocentric distance in Mpc based on the 21cm radial velocity and $H_0 = 100$ km s ^{1}Mpc^{-1}; (3) $M_B^{\rm b}$ — Absolute B-band magnitude corrected for Galactic extinction, not corrected for inclination effects; (4) $\mu_{B,\rm area}(0)$ — Intercept of the straight line fit to the area analysis profile, analogous to the central B-band surface brightness in mag arcsec^{-2}. No correction for inclination has been applied; (5) $\mu_{B,\rm ellipse}(0)$ — Extrapolated disk central surface brightness from ellipse fitting. No correction for inclination has been applied; (6) corr — inclination correction (in magnitudes) to the surface brightness using the extinction correction from Tully et al. (1998). Surface brightnesses can become fainter due to inclination effects and brighter due to dust extinction; (7) i — Inclination in degrees; (8) h — B-band disk scale length in kpc; (9) log $M_{\rm HI}$ — Logarithm of H I mass in solar masses; (10) $W_{\rm R,20}^{\rm i}$ — Velocity width measured at 20% of the peak flux corrected for turbulent motion and inclination; (11) $M_{\rm HI}/L_B^{\rm b,i}$ — Ratio of H I mass to B luminosity in solar units. The luminosity is corrected for inclination effects using Tully's (1998) method; (12) $L_{\rm FIR}$ — Logarithm of FIR luminosity if available. The FIR luminosity in solar units is derived from the FIR flux, $L_{\rm FIR}$, in Jy using $L_{\rm FIR} = 3.86 \times 10^5 D^2 F_{\rm FIR}$, where D is the distance to the source in Mpc. The FIR flux has been calculated from the IRAS flux densities in Jy at 60 and 100 μm via $F_{\rm FIR} = 2.58 F_\nu(60) + F_\nu(100)$.

2.5 Properties of H I selected galaxies

Of the 66 galaxies found in the survey, 32 (48%) are listed in existing catalogs of optically selected galaxies. Most sources (27) are found in the UGC and five of those are also listed in the NGC. The remaining five galaxies are listed in smaller galaxy catalogs. In this discussion we refer to the 34 uncataloged galaxies as "new" galaxies. In the following, a comparison is made between the general properties of cataloged and new galaxies to test whether the Arecibo H I Strip Survey survey has yielded a population of galaxies that

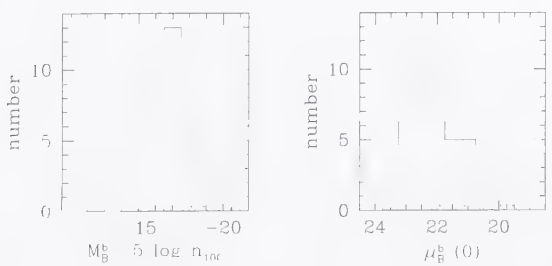

FIGURE 2.4— Histograms of absolute magnitude and central surface brightness both uncorrected for dust extinction. Galaxies with measured FIR fluxes are indicated by hatched histograms.

TABLE 2.1— Optical and 21cm Parameters of Survey Galaxies.

(1) Nr	(2) D	(3) $M_B^{b,i}$	(4) $\mu_{B,\mathrm{area}}(0)$	(5) $\mu_{B,\mathrm{ellipse}}(0)$	(6) corr	(7) i	(8) h	(9) $\log M_{\mathrm{HI}}$	(10) $W^{i}_{R,20}$	(11) $M_{\mathrm{HI}}/L_B^{b,i}$	(12) L_{FIR}
A1	21.5	...	...	...	...	...	...	8.0	...	...	...
A2	41.6	...	...	...	...	...	...	8.3	...	...	...
A3	13.0	-15.8	22.49	23.31	0.37	48	2.29	9.1	179	3.84	..
A4-1	19.1	-13.6	23.02	22.75	0.51	53	0.48	8.0	76	1.99	...
A4-2	18.9	-16.3	21.55	22.24	0.31	46	1.37	9.2	141	2.81	...
A5	46.8	-16.6	21.84	22.62	0.32	48	2.71	9.2	232	1.95	...
A6	56.0	-18.9	21.26	21.59	0.30	62	3.43	9.6	288	0.63	...
A7	50.4	-18.4	21.14	21.46	0.50	72	3.03	9.4	243	0.53	...
A8	53.1	-18.6	21.80	21.49	0.35	63	3.22	9.3	265	0.36	...
A9	18.6	-16.7	21.89	21.20	0.87	74	1.44	8.8	153	0.64	...
A10	22.9	-18.2	21.40	21.66	0.05	24	3.38	8.9	256	0.27	8.8
A11	23.9	-17.5	21.51	21.09	0.83	79	2.56	9.5	234	1.54	8.7
A12	30.2	-12.7	23.22	23.24	0.25	38	0.42	7.9	47	4.21	.
A13	37.7	-17.5	22.71	22.54	0.07	26	2.06	9.3	360	1.31	...
A14	41.3	-17.8	22.54	22.29	0.42	61	2.62	9.7	191	1.94	...
A15	9.5	-12.2	22.10	21.91	0.81	64	0.24	7.3	38	1.57	...
A16	7.6	-12.9	21.44	21.63	1.36	78	0.46	7.7	68	1.43	...
A17	49.2	-16.7	21.76	21.16	0.18	37	0.90	9.2	295	2.02	..
A18	55.3	-16.9	22.31	22.32	0.80	73	1.71	8.5	138	0.26	...
A19	46.8	-15.4	22.45	22.09	0.12	28	0.63	8.9	145	3.48	...
A20	53.8	-15.4	22.86	22.25	1.65	90	1.56	8.6	152	1.16	.
A21	45.0	-15.1	22.04	21.76	1.36	78	0.79	8.3	78	0.83	...
A22	45.8	-18.9	21.83	21.75	0.04	24	3.10	9.4	320	0.39	.
A23	71.9	-16.4	21.87	21.41	0.32	47	0.91	8.8	166	0.99	...
A24	44.9	-19.5	20.21	19.96	0.21	59	2.04	9.6	390	0.31	9.9
A25	38.7	-14.8	22.78	22.39	0.64	58	0.68	8.6	106	2.77	...
A26	38.0	-18.4	21.35	21.58	0.69	90	5.20	9.6	384	0.79	9.1
A27	65.6	-18.0	22.03	22.66	0.70	79	5.49	9.8	384	1.55	9.6
A28	47.9	-16.0	22.23	21.95	0.69	64	1.17	8.9	198	1.56	.
A29	45.3	-17.3	21.12	20.58	0.75	74	1.31	9.0	245	0.55	...
A30	29.7	-15.9	22.74	22.61	0.19	36	1.26	8.7	154	1.36	...
A31	50.6	-15.9	21.98	21.57	1.07	75	1.26	9.0	148	1.93	...
A32	50.9	-17.7	23.30	23.59	0.14	36	3.44	9.1	208	0.67	...
A33	64.8	-18.9	20.69	20.39	0.50	85	3.98	9.5	394	0.33	9.6
A34	62.8	-19.7	19.89	20.57	0.13	48	2.26	9.8	309	0.50	...
A35	54.8	-15.8	22.86	23.34	0.75	65	1.65	9.2	186	4.02	...
A36	50.9	-17.4	20.42	19.99	0.12	33	0.61	8.4	147	0.18	...
A37-1	42.7	-17.5	20.58	20.47	0.87	81	1.47	9.0	153	0.41	...
A37-2	42.5	-20.0	19.41	20.32	0.14	55	2.78	9.0	358	0.05	9.9
A38	44.1	-19.1	20.82	21.86	0.20	53	6.08	9.2	180	0.21	..
A39	63.3	-19.9	17.69	20.05	0.02	17	1.95	9.4	366	0.19	...
A40	57.8	...	...	...	...	...	...	9.1	...	...	...
A41	58.6	...	...	...	...	...	...	9.6	...	...	...
A42	69.6	...	...	...	...	...	...	8.4	...	...	...
A43	22.4	-17.8	20.40	20.51	0.70	76	2.59	8.9	265	0.31	8.9
A44	45.2	...	...	...	...	...	...	8.1	...	...	...
A45-1	44.0	-15.2	21.86	21.13	1.38	79	0.63	8.2	88	0.59	...
A45-2	45.6	-15.6	22.13	21.62	1.06	73	1.14	8.6	150	1.20	...
A46	54.0	-15.7	23.02	22.73	0.86	68	1.82	8.9	151	2.10	...
A47	54.1	-17.4	21.62	21.19	0.93	83	1.69	9.0	184	0.46	...
A48	54.2	-17.2	21.53	21.88	0.98	83	2.14	9.2	144	0.87	...
A49	67.7	-19.0	21.58	21.74	0.19	51	3.01	9.3	262	0.27	9.4
A50	47.2	-14.1	23.12	22.94	1.27	76	0.65	8.4	118	2.68	...
A51	45.9	-15.5	20.84	20.35	0.15	31	0.24	8.0	51	0.41	...
A52	40.3	-18.6	20.80	20.26	0.59	82	2.80	9.3	377	0.32	9.6

TABLE 2.1— Continued.

(1) Nr	(2) D	(3) $M_B^{b,i}$	(4) $\mu_{B,area}(0)$	(5) $\mu_{B,ellipse}(0)$	(6) corr	(7) i	(8) h	(9) log M_{HI}	(10) $W^i_{R,20}$	(11) $M_{HI}/L_B^{b,i}$	(12) L_{FIR}
A53	40.7	-16.8	22.38	22.13	0.04	18	1.50	8.6	310	0.50	.
A54	39.5	-14.8	22.70	22.82	0.88	66	1.02	8.3	87	1.23	...
A55	55.7	-19.4	20.26	21.71	0.28	66	3.03	9.5	464	0.28	...
A56	28.1	-16.8	21.10	21.09	0.72	69	0.87	8.1	169	0.13	.
A57	11.8	-14.0	23.18	23.50	0.09	24	0.52	8.0	154	1.58	...
A58	60.6	-15.9	22.99	22.84	0.71	64	1.28	8.8	137	1.47	...
A59-1	74.3	-20.0	20.77	21.00	0.20	81	4.29	9.7	452	0.22	10.1
A59-2	74.1	-19.5	20.80	20.49	0.16	50	1.98	9.2	426	0.17	9.9
A59-3	73.0	-19.5	20.56	20.35	0.16	51	1.88	9.3	252	0.16	9.9
A60	54.1	-17.3	22.93	23.23	0.56	66	3.13	9.4	204	1.43	...
A61	62.4	-19.0	21.07	21.51	0.48	90	4.25	9.1	482	0.14	9.6

has gone unnoticed in optical surveys. We are especially interested to see whether the newly discovered galaxies can be considered as a new class of galaxies that has distinct properties from optically selected galaxies or is severely under-represented in optically selected catalogs.

2.5.1 Comparison of mean parameters and distributions

In Table 2.2 median values of some basic parameters of total sample, as well as the subsamples of new and cataloged galaxies, are tabulated. The 25th and 75th percentiles are indicated to show the spread of the values among the different samples. K-S tests have been used to test whether the uncataloged and cataloged galaxies have significantly different properties. The probability P that both distributions are drawn from the same parent population is listed in the fifth column of Table 2.2. The same information is presented graphically in Figure 2.5, where solid histograms have been used to represent cataloged galaxies and hatched histograms to represent new galaxies.

TABLE 2.2— Median Properties of Survey Galaxies.

	All	New	Cataloged	P	P'
$M_B^{b,i}$	$-17.51^{1.73}_{1.55}$	$-15.63^{0.86}_{1.08}$	$-19.05^{1.38}_{0.82}$	5.7×10^{-7}	0.99
log M_{HI}	$9.00^{0.31}_{0.38}$	$8.63^{0.35}_{0.34}$	$9.28^{0.25}_{0.16}$	3.6×10^{-6}	0.37
$M_{HI}/L_B^{b,i}$	$0.79^{0.78}_{0.46}$	$1.47^{0.55}_{0.65}$	$0.39^{0.92}_{0.12}$	9.2×10^{-4}	0.74
$\mu_B^{b,i}(0)$	$22.42^{0.77}_{0.86}$	$23.11^{0.42}_{0.95}$	$21.82^{0.97}_{0.86}$	0.016	0.38
h	$1.71^{1.30}_{0.80}$	$1.02^{0.54}_{0.39}$	$2.80^{0.63}_{0.76}$	1.5×10^{-8}	0.38
D	$45.9^{8.3}_{7.9}$	$46.9^{7.1}_{4.1}$	$44.9^{17.5}_{15.2}$	0.269	4.3×10^{-4}

Notes — Subscripts and superscripts denote 25% and 75% percentiles. P indicates the probability that the 'new' and cataloged galaxies are drawn from the same parent population. P' is the same, but then only for subsamples with equal median values of $M_B^{b,i}$.

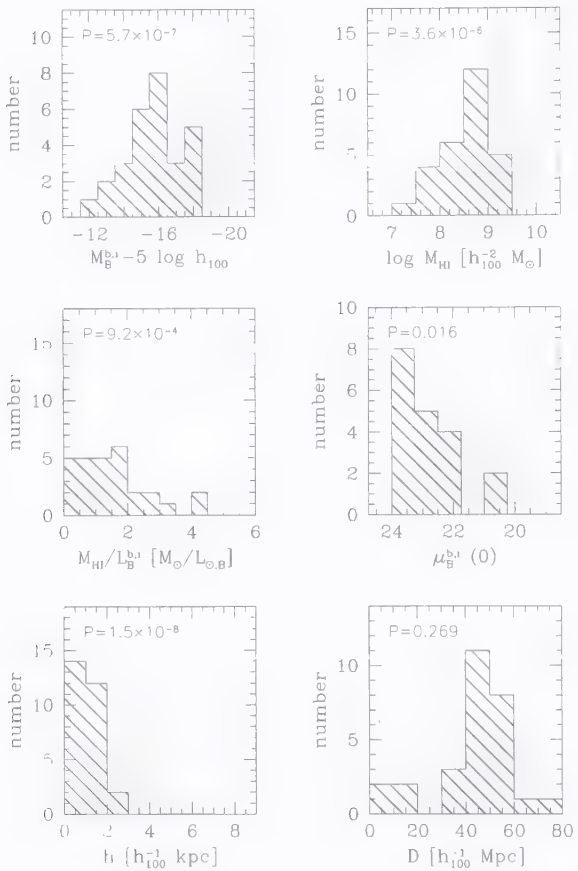

FIGURE 2.5— Comparison between the properties of cataloged galaxies (solid) and new galaxies (hatched). From bottom to top and left to right: absolute B magnitudes, total H I masses, $M_{\rm HI}/L_B^{\rm b,i}$ ratios, B central surface brightnesses, and distances. The probability that the distributions are drawn from the same parent population are indicated in the upper lefts corners of each panel.

Absolute magnitudes and H I masses

The distribution of $M_B^{\rm b,i}$ and $M_{\rm HI}$ are significantly different for the two subsamples. The new galaxies are generally less luminous and have lower total H I masses. Within the survey volume of the AHISS, there are no gas rich galaxies found brighter than $M_B^{\rm b,i} = -18.1\,{\rm mag} \approx \frac{1}{3}{\rm L}^*$ which had not previously been included in optical galaxy catalogs. From this result alone we can conclude that catalogs of optically selected galaxies are remarkably complete. The new H I selected galaxies are all true dwarf galaxies (following the definition of Tammann 1980), no new highly luminous galaxies have been found. The distinction between new and cataloged galaxies is even stronger in the distribution of apparent magnitudes ($P = 2.0 \times 10^{-11}$). All new galaxies have apparent magnitudes $m_B > 15.5\,{\rm mag}$, which agrees well with the limiting magnitudes of optical catalogs. A similar conclusion has been reached by Spitzak & Schneider (1998).

Gas richness

Apart from the distributions of gas mass and optical luminosity, it is also interesting to compare the distributions of the ratio of these quantities, the gas richness $M_{\rm HI}/L_B^{\rm b,i}$. This

quantity is particularly suitable to test whether the new galaxies are anomalously gas rich or under luminous. The distribution of $M_{\rm HI}/L_B^{\rm b,i}$ ratios is given in the third panel of Figure 2.5. Here we have corrected the luminosities for inclination effects using the method described by Tully et al. (1998). The hypothesis that cataloged and new galaxies are drawn from the same population can be excluded with a significance level of 99.91%; uncataloged galaxies are significantly more gas rich. This result may not be surprising since these galaxies are also the less luminous ones and an anti-correlation between gas richness and optical luminosity is known to exist (e.g., Roberts & Haynes 1994; Salpeter & Hoffman 1996) and is also clearly visible in our data set. A fair comparison would be to compare only those galaxies which fall in the absolute magnitude region where the two distribution overlap, that is $-18.5 < M_B^{\rm b,i} < -15.5$. From this bin we select subsamples of new and cataloged galaxies that have equal median values of $M_{I_c}^{\rm b,i}$. If only these subsamples are compared the difference in gas richness between cataloged and new galaxies disappears. The probability that the two distributions are drawn from the same parent distribution is 74%.

When comparing $M_{\rm HI}/L_B^{\rm b,i}$ for different galaxies or galaxy samples one should be aware of the different definitions of L_B used in the literature. Especially the correction for internal absorption can influence the determination of $M_{\rm HI}/L_B^{\rm b,i}$ significantly. If the formalism from Tully & Fouqué (1985) is used to correct for internal absorption, it can be shown that the average correction for a randomly oriented sample of galaxies is 0.54 mag assuming $f = 0.25$ and $\tau_B = 0.55$. This correction causes a decrease of 40% in the $M_{\rm HI}/L_{I_c}^{\rm b,i}$ ratio. However, changing the extinction corrections for different types of galaxies has no influence on the conclusion that cataloged and new galaxies have similar gas richness when compared among comparable luminosities.

The median value of $M_{\rm HI}/L_B^{\rm b,i}$ is 0.79 for our total sample, 1.5 for the new galaxies and 0.39 for the cataloged galaxies. The latter value is typical for late type galaxies as Roberts & Haynes (1994) find that $M_{\rm HI}/L_{I_c}^{\rm b,i}$ ratios span the range from 0.2 for Sa types to 0.7 for types Sm/Im. The gas content of the H I selected cataloged galaxies therefore does not significantly deviate from optically selected galaxies. However, the median $M_{\rm HI}/L_B^{\rm b,i}$ value of the total sample does exceed the nominal value because the uncataloged galaxies contribute significantly higher values. As stated before, the new galaxies are all dwarfs, and these galaxies are known to be ones with the largest gas fractions measured. Typical $M_{\rm HI}/L_B^{\rm b,i}$ ratios for dwarf galaxies are 1.5 (Swaters 1999), but much higher values are not unusual.

For comparative purposes, van Zee, Haynes & Giovanelli (1995) compiled a sample of 513 optically selected, diameter limited, dwarf galaxies from the UGC. These galaxies were all classified as either late morphological type (later than Sd) or as Dwarf or any subclass of dwarf galaxies. They found that the median $M_{\rm HI}/L_{I_c}^{\rm b,i}$ ratio of this sample was 0.9, and 15% have $M_{\rm HI}/L_B$ ratios in excess of 5.0. Furthermore, van Zee et al. (1995) studied a number of isolated, low luminosity galaxies and found a median value of $M_{\rm HI}/L_{I_c}^{\rm b,i}$ of 11.0 for the subsample with extended H I emission and high gas fractions. The most extreme values of $M_{\rm HI}/L_B$ are found by O'Neil, Bothun & Schombert (2000), who report on values up to 50 for red, gas rich, optically selected LSB galaxies. Compare this to the most gas rich galaxies in our sample with $M_{\rm HI}/L_B^{\rm b,i}$ ratios of 3.8 (A3), 4.0 (A35) and 4.2 (A12).

We can conclude that H I selected galaxies have on average truly higher gas fractions

than optically selected galaxies. However, extreme gas rich galaxies, with $M_{\rm HI}/L_B^{\rm b,i} > 5$, are rare. A blind H I survey should be the most successful method of finding these systems, still none such systems are found.

Central surface brightnesses

The fourth panel of Figure 2.5 shows the distribution of central surface brightnesses. Here we choose to plot the surface brightnesses from the area analysis method, and we applied corrections for internal extinction. Essentially the same distribution would appear if the ellipse fitting surface brightnesses would be used. To avoid uncertain extinction corrections we limit the sample here to galaxies with inclination $< 75°$ which reduces the sample size to 44. The new galaxies are preferentially those with lower surface brightness, the median value of the new galaxies is 23.1 mag arcsec^{-2}. It is interesting to note that the median surface brightness of the cataloged galaxies in our sample is $\mu_B^{\rm b,i} = 21.8$ mag arcsec^{-2}, close to the value found by Freeman (1970) for his sample of optically selected galaxies.

An apparent anti-correlation exists between optical surface brightness and luminosity (e.g., de Blok 1997), which might be responsible for the observed discrepancy in central surface brightness between the new and previously cataloged samples. Again we can select only the galaxies with $-18.5 < M_B^{\rm b,i} < -15.5$ to test whether uncataloged galaxies are really of lower surface brightness if equally bright galaxies are compared. The probability that both distributions are drawn from the same parent distribution is now 38%, indicating that uncataloged galaxies are not significantly of lower surface brightness at a particular luminosity.

The distribution of surface brightnesses also shows that none of the H I selected galaxies has a surface brightness fainter than 24.0 B mag arcsec^{-2}. This cut-off is observable both in the area analysis surface brightnesses and in the ellipse fitting surface brightnesses and is independent of the extinction correction that is applied. Even if the galaxies are assumed to be fully transparent, this cut-off remains. Galaxies much fainter then this limit would be easily detectable in the INT observations. Perhaps, we are observing a lower limit to the surface density of stars of gas rich galaxies although galaxies much dimmer than this limit are known to exist from optical surveys (Dalcanton et al. 1997; O'Neil et al. 1997), although it may be possible that they are simply such rare objects compared to normal galaxies that we have not discovered any in our sample. We will return to this fact in Chapter 4.

Scale lengths

The fifth panel in Figure 2.5, which shows the distribution of optical disk scale lengths, indicates that new galaxies seem to be of smaller optical size. But also here the difference between the two subsamples disappears in the $-18.5 < M_B^{\rm b,i} < -15.5$ subsample, were P is only 0.38. The median scale length of the new galaxies is 1.0 kpc, which again illustrates that the H I selected uncataloged galaxies are genuine dwarf galaxies. The median scale length of the sample of optically selected late-type dwarf galaxies defined by Swaters (1999) is also 1.0 kpc. For comparison, the median B-band scale length of the statistically complete diameter limited sample of spiral galaxies studied by de Jong (1996) is 3.0 kpc, the median value of the sample of LSB galaxies of de Blok (1997) is 3.2 kpc.

The question rises whether LSB galaxies studied by de Blok have typical scale lengths for their central surface brightnesses, or are these galaxies the extremes of the LSB galaxies

size distribution? In order to make a representative comparison, we select from our and de Blok's sample those galaxies with central surface brightnesses in the range $22.8 < \mu_B^{\rm b,i} < 24.1$ and compare the median scale lengths. We find that the median scale length of the H I selected LSB galaxies is 1.7 kpc, while the median value for de Blok's sample is 3.2 kpc, a factor of two larger. Moreover, the probability P that both distributions are drawn from the same parent population is 0.9%.

Distances

The last panel shows the distribution of distances, and it is clear that no significant difference between the two distributions exists; new galaxies are found over the total survey volume. The distribution of galaxies in the $-18.5 < M_B^{\rm b,i} < -15.5$ bin appears to be more bimodal; not surprisingly, new galaxies of the same absolute magnitude are found at larger distances (median $D = 51$ Mpc) than cataloged galaxies (median $D = 30$ Mpc).

2.5.2 Tully-Fisher relation

While the comparison of $M_{\rm HI}/L_B^{\rm b,i}$ ratios already has shown that H I selected galaxies are not anomalously faint for their H I masses, there is yet another method to tests whether these galaxies are intrinsically faint and low mass. The Tully-Fisher relation (Tully & Fisher 1977, hereafter T-F relation), the relation between absolute blue magnitude and rotational velocity, provides a tool to test whether H I selected galaxies differ from optically selected galaxies when compared among similar dynamical masses.

Figure 2.6 illustrated the T-F relation for the H I selected sample, with extinction corrected absolute blue magnitudes plotted against inclination corrected H I linewidth measured at 20% of peak flux density. For the extinction correction the Tully & Fouqué (1985) method was used to enable comparison with published relations. Application of the extinction correction advocated by Tully et al. (1998) yields a slightly steeper relation since this correction increases with increasing luminosity. For the line widths we used a relatively optimistic uncertainty in the inclination of ± 5 degrees. Errors in the inclinations are likely to be much higher for the dwarf and irregular galaxies in the sample, where the axis ratios of different isophotes often vary enormously. Cataloged galaxies are represented by open points, uncataloged galaxies by solid points. Only those galaxies for which the inclination exceeds 40° are selected to avoid high inclination corrections in the line width. The difference in luminosity between cataloged and new galaxies is again apparent, but both groups seem to follow the same relation. There is no indication of an offset of uncataloged galaxies from the relation defined by cataloged galaxies. To illustrate this the T-F relation found by Broeils (1992) for his sample of spiral galaxies is shown by a dotted line. A bisector[5] fit to our data points is represented by a dashed line. There are no significant differences in both slope and offset. The scatter in this T-F plot is large, $\sigma_{\rm rms} = 0.85$ mag, a factor two higher than what Verheijen (1997) finds for his sample of Ursa Major galaxies. This is not surprising, given the fact that our data set contains many galaxies with low 21cm fluxes, for which the determinations of the velocity widths are less accurate.

The same T-F data are plotted in the right panel of Figure 2.6, but the galaxies are now divided into bins of different central surface brightness. Although it is obvious that the

[5]The bisector of the direct and the inverse least-squares fit. This is found to be the preferred method when determining an underlying functional relation between two variables which should be treated symmetrically (Isobe et al. 1990).

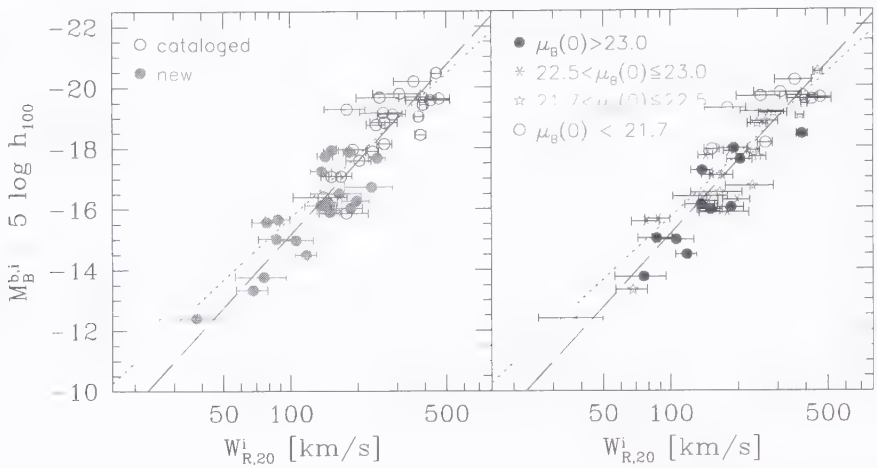

FIGURE 2.6— Tully-Fisher relations for H I selected galaxies. *Left panel:* Solid symbols represent cataloged galaxies, open circles represent new galaxies. Only galaxies that are inclined more than 40° have been plotted. The dotted line is the relation found by Broeils (1992), the dashed line is a bisector fit to the data points. H I selected galaxies follow the same T-F relation as optical selected galaxies. *Right panel:* Same as left panel, but here galaxies are marked according to surface brightness. All galaxies follow the same T-F relation, irrespective of their central surface brightness.

highest surface brightness galaxies generally take their place in the upper right corner and the lowest surface brightness galaxies in the lower left corner of the diagram, galaxies of all surface brightnesses follow the same relation. This is consistent with the findings of Sprayberry et al. (1995), Zwaan et al. (1995), and Verheijen (1997) that all spiral galaxies, regardless of their optical surface brightness, follow the same Tully-Fisher relation. There have been recent claims that a population of massive LSB galaxies exists, that are underluminous for their rotational velocity (O'Neil et al. 2000). The H I selected sample does not provide evidence for such a population, although there are no selection effects discriminating against findings these systems.

2.5.3 Are H I selected galaxies special?

Conclusions drawn from the comparison between cataloged and new galaxies can be summarized as follows: An H I selected galaxy sample is more biased toward galaxies of lower luminosities, lower H I masses, lower surface brightnesses, smaller scale lengths and higher gas fractions than optically selected galaxies. However, these specific properties of H I selected galaxies are a natural result of the survey technique. The AHISS is sensitive to dwarf galaxies at much larger distances than optical surveys usually are. Furthermore, the restricted bandwidth of the receiving system imposes a strict limit on the maximum redshift of detected galaxies which is not present in optical surveys. Luminous, low $M_{HI}/L_B^{b,i}$ galaxies at redshifts higher than that set by the receiving system will never be included in an H I selected sample. Both effects will cause a predominance of sub-L_* galaxies in an H I selected sample. Well established relations between optical luminosity and surface brightness and gas richness certify that an H I selected galaxy sample

is on average gas rich and of low optical surface brightness. Our analysis shows that new H I selected galaxies have no specific properties that separate them from the gas-rich, late type segment of the previously known galaxy population.

2.6 Correlation statistics

The sample of H I selected galaxies spans a dynamic range of 100 in central surface brightness and is therefore ideal to test correlations of galaxy properties with central surface brightness. The leftmost column of panels in Figure 2.7 shows scatter plots of log luminosity, log scale length, and log $M_{\rm HI}/L_I^{\rm b,i}$ against central surface brightness derived from the area analysis. The numbers in the upper left corners show the results of a standard linear correlation (Pearson's r) where surface brightness is the independent variable and the parameters on the vertical axes are the dependent variables. The first number given is the value of the correlation coefficient, and the second number (in parentheses) is the significance of the correlation. The third number is the slope of a bisector fit that is shown by dashed lines.

It is clear that surface brightness is significantly correlated with $M_I^{\rm b,i}$ and $M_{\rm HI}$; the sense is that fainter surface brightness goes with fainter optical luminosity and with lower gas mass. This is an important correlation that is often denied in the literature. Estimates of the contribution of LSB galaxies to the luminosity density of the local Universe often depend on the underlying assumption that luminosity and surface brightness are *uncorrelated*. The correlation can be missed completely when a) samples of only LSB galaxies are plotted so that the dynamic range in surface brightness is too small to see a significant correlation, or b) subsamples of large LSB galaxies are compared with normal spiral galaxies. The sample we discuss here is free from optical selection effects and there is no reason why we should miss luminous LSB galaxies. Apparently, these galaxies are rare.

The strongest correlation is that between surface brightness and gas richness as quantified by $M_{\rm HI}/L_B^{\rm b,i}$. Galaxies with fainter surface brightnesses clearly tend to be the most gas-rich. De Blok et al. (1996) investigated the evolutionary status of LSB galaxies, and found that they appeared to be relatively unevolved, compared to galaxies of higher surface brightness, even for galaxies with similar total luminosities and gas masses. The finding here that gas richness increases with decreasing surface brightness is consistent with their finding that lower surface brightness galaxies are less evolved; the LSB galaxies have turned less of their original H I inheritance into stars, and so retain higher ratios of H I mass to starlight. The evidence from the AHISS suggests that this trend continues more or less evenly across all surface brightnesses; Figure 2.7 shows that there is a fairly even trend of gas richness against surface brightness. Of course, this relation clearly holds only for galaxies with detectable levels of H I. As noted above, optical surveys can detect galaxies with considerably lower surface brightnesses than those found by the AHISS. If, as seems logical, these galaxies are lacking detectable amounts of H I, then they may well be "more evolved" systems that have lost all their neutral gas through previous star formation episodes. This correlation between surface brightness and evolutionary state thus depends for each LSB galaxy on whether low surface brightness reflects late, anemic star formation or early, faded star formation.

The scale length of the H I selected galaxies correlates weakly, but significantly with central surface brightness. McGaugh & de Blok (1997) find no significant correlation over a wide range of surface brightnesses (dynamic range of $\sim$ 100), but the galaxies in their

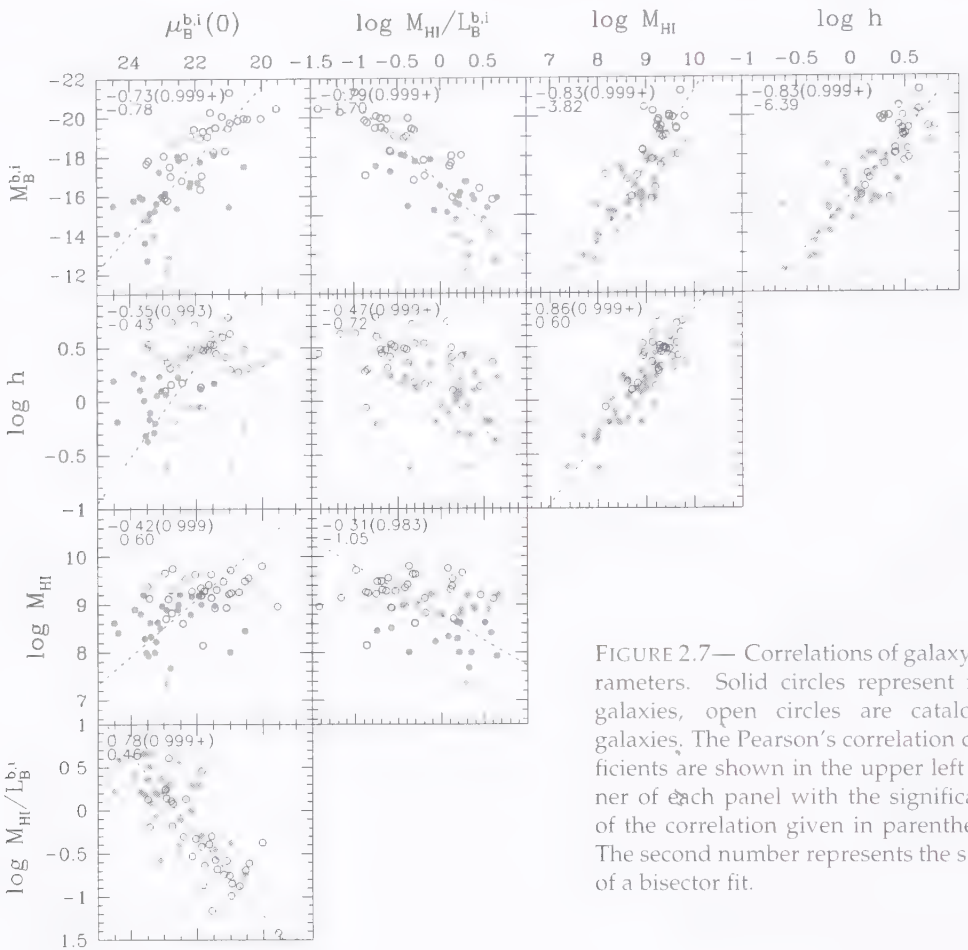

FIGURE 2.7— Correlations of galaxy parameters. Solid circles represent new galaxies, open circles are cataloged galaxies. The Pearson's correlation coefficients are shown in the upper left corner of each panel with the significance of the correlation given in parentheses. The second number represents the slope of a bisector fit.

sample were all first identified optically and were compiled from a variety of data sets. The HSB galaxies in their sample are mostly from the UGC and are therefore diameter limited which implies that HSB galaxies with small scale lengths are likely to be missed. The correlation found here suggests that most LSB galaxies are truly dwarf galaxies; they are both smaller and less luminous than typical HSB spiral galaxies.

Figure 2.7 also shows correlations of other parameters of the AHISS sample. The strongest correlation of all is that between disk scale length and H I mass, with a correlation coefficient of 0.86. An even stronger correlation of $r = 0.89$ is obtained when R_{25} is used instead of the scale length. A similar correlation has been noted by Broeils & Rhee (1997) and Verheijen (1997) for large spiral galaxies and by Salpeter & Hoffman (1996) and Swaters (1999) for dwarf galaxies. The slope of the correlation suggests that the H I density averaged over the optical disk is constant for galaxies of similar size, but decreases mildly for larger galaxies.

Another interesting correlation is that between scale length and $M_{HI}/L_B^{b,i}$. McGaugh

& de Blok (1996) find no such correlation, and therefore pose that the evolutionary state of galaxies is scale free. Our H I selected sample shows that smaller galaxies have preferentially higher gas mass fraction.

Several strong correlations also exist between $M_B^{b,i}$ and all other parameters. These are al well established correlations, and need not be discussed in detail here.

2.7 Conclusions

We have presented *B*-band images, H I contours, global profiles and fundamental parameters of a sample of 66 H I selected galaxies. This sample is the result of the Arecibo H I Strip Survey (AHISS), a blind extragalactic survey in the 21cm line. The H I selected galaxies span a wide range in parameters, from small low surface brightness galaxies to large luminous galaxies. A trivial conclusion is that the H I survey preferentially selects gas rich galaxies, many of which are of low optical surface brightness. However, a fair comparison shows that the properties of the newly identified galaxies are not significantly different from galaxies that are represented in the optical catalogs by late type and extreme late morphological type segment of the galaxy population. Thus, analogs of our H I detected galaxy sample are already included in optical galaxy catalogs.

We have discussed correlation statistics of the fundamental galaxy parameters H I mass, luminosity, gas richness, size and surface brightness, and show that all parameters are significantly correlated. Some of these correlation had previously not been recognized. This shows the importance of a well defined sample with a high dynamic range in galaxy parameters.

Acknowledgments

This project has been supported by the European commission through the Activity "Access to Large-Scale Facilities" within the Programme "Training and Mobility of Researchers", awarded to the Instituto de Astrofisica de Canarias to fund European astronomers' access to its Roque de Los Muchachos and Teide Observatories (European Northern Observatory), in the Canary Islands.

References

Bottinelli, L., Gouguenheim, L., Fouqué, P., & Paturel, G. 1990, A&A, 82, 391
Briggs, F. H. 1997, ApJ, 484, L29
Broeils, A. H. 1992, Ph.D. thesis, Univ. of Groningen
Broeils, A. H.& Rhee, M.-H. 1997, A&A, 324, 877
Burstein, D., & Heiles, C. 1982, AJ, 87, 1165
Dalcanton, J. J., Spergel, D. N., Gunn, J. E., Schmidt, M., Schneider, D. P. 1997, AJ, 114, 635
de Blok, W. J. G., van der Hulst, J. M., & Bothun, G. D. 1995, MNRAS, 274, 235
de Blok, W. J. G. McGaugh, S. S., van der Hulst, J. M. 1996, MNRAS, 283, 18
de Jong, R.S. 1996, A&A, 313, 45
Disney, M. J. 1976, Nature, 263, 573
Fisher, J. R., & Tully, R. B. 1981, ApJS, 47, 139
Freeman, K. C. 1970, ApJ, 160, 811
Giovanelli, R., Haynes, M. P., Salzer, J. J., Wegner, G., Da Costa, L. N., Freudling, W. 1995, AJ, 110, 1059
Henning, P. A. 1992, ApJS, 78, 365
Henning, P. A., Sancisi, R., & McNamara, B. R. 1993, A&A, 268, 536

Holmberg, E. 1958, Medd. Lundl. Astr. Obs. Ser II, No. 136
Impey, C. D., Sprayberry, D., Irwin, M. J., & Bothun, G. D. 1996, ApJS, 105, 209
Impey, C. D., Bothun, G. D. 1997, ARA&A, 35, 267
Isobe, T., Feigelson, E. D., Akritas, M. G., & Babu, G. J. 1990, ApJ, 364, 104
Kerr, F. J., & Henning, P. A. 1987, ApJ, 320, L99
Kraan-Korteweg, R. C., van Driel, W., Briggs, F., Binggeli, B., & Mostefaoui, T. I. 1999, A&AS, 135, 255
Landolt, A. U. 1992, AJ, 104, 340
McGaugh, S. S. 1994, ApJ, 426, 135
McGaugh, S. S. & Bothun, G. D. 1994, AJ, 107, 530
McGaugh, S. S. & de Blok, W. J. G. 1997, ApJ, 481, 689
O'Neil, K., Bothun, G. D., & Cornell, M. E. 1997, AJ, 113, 1212
O'Neil, K., Bothun, G. D., & Schombert, J. 2000, AJ, 119, 136
O'Neil, K. & Bothun, G. D. 2000, ApJ, 529, 811
Roberts, M. S., Haynes, M. P 1994, ARA&A, 32, 115
Rosenberg, J. L. & Schneider, S. E. 2000, astro-ph/0004205
Salpeter, E. E. & Hoffman, G. L. 1996, ApJ, 465, 595
Schneider, S. E. & Schombert, J. M. 2000, ApJ, 530, 286
Schneider, S. E. 1989, ApJ, 343, 94
Schombert, J. M., Bothun, G. D., Impey, C. D., & Mundy, L. G. 1990, AJ, 100, 1523
Schombert, J. M., Bothun, G. D., Schneider, S. E., & McGaugh, S. S. 1992, AJ, 103, 1107
Shostak, G. S. 1977, A&A, 54, 919
Sorar, E. 1994, Ph.D. thesis, Univ. Pittsburgh
Spitzak, J. G. & Schneider, S. E. 1998, ApJS, 119, 159
Sprayberry, D., Bernstein, G. M., Impey, C. D., & Bothun, G. D. 1995, ApJ, 438, 72
Swaters, R. A. 1999, Ph.D. thesis, Univ. of Groningen
Szomoru, A., van Gorkom, J. H., Gregg, M. D., & Strauss, M. A. 1996, AJ, 111, 2150
Tammann, G. A., 1980 in ESO/ESA Workshop on Dwarf Galaxies, ed. Tarenghi, M. & Khar, K., 3
Tully, R. B., Fisher, J. R. 1977, A&A, 54, 661
Tully & Fouqué 1985, ApJS, 58, 67
Tully, R. B., Verheyen, M. A. W. 1997, ApJ, 484, 145
Tully, R. B., Pierce, M. J., Huang, J.-S., Saunders, W., Verheijen, M. A. W., & Witchalls, P. L. 1998, AJ, 115, 2264
Valentijn E. A. 1994, MNRAS, 266, 614
van der Hulst, J. M., Skillman, E. D., Smith, T. R., Bothun, G. D., McGaugh, S. S., & de Blok, W. J. G. 1993, AJ, 106, 548
van Zee, L., Haynes, M. P., & Giovanelli, R. 1995, AJ, 109, 990
Verheijen, M. A. W. 1997, Ph.D. thesis, Univ. of Groningen
Zwaan, M. A., van der Hulst, J. M., de Blok, W.J.G., & McGaugh, S. S. 1995, MNRAS, 273, L35
Zwaan, M. A., Briggs, F. H., Sprayberry, D., & Sorar, E. 1997, ApJ, 490, 173 **[Chapter 3]**

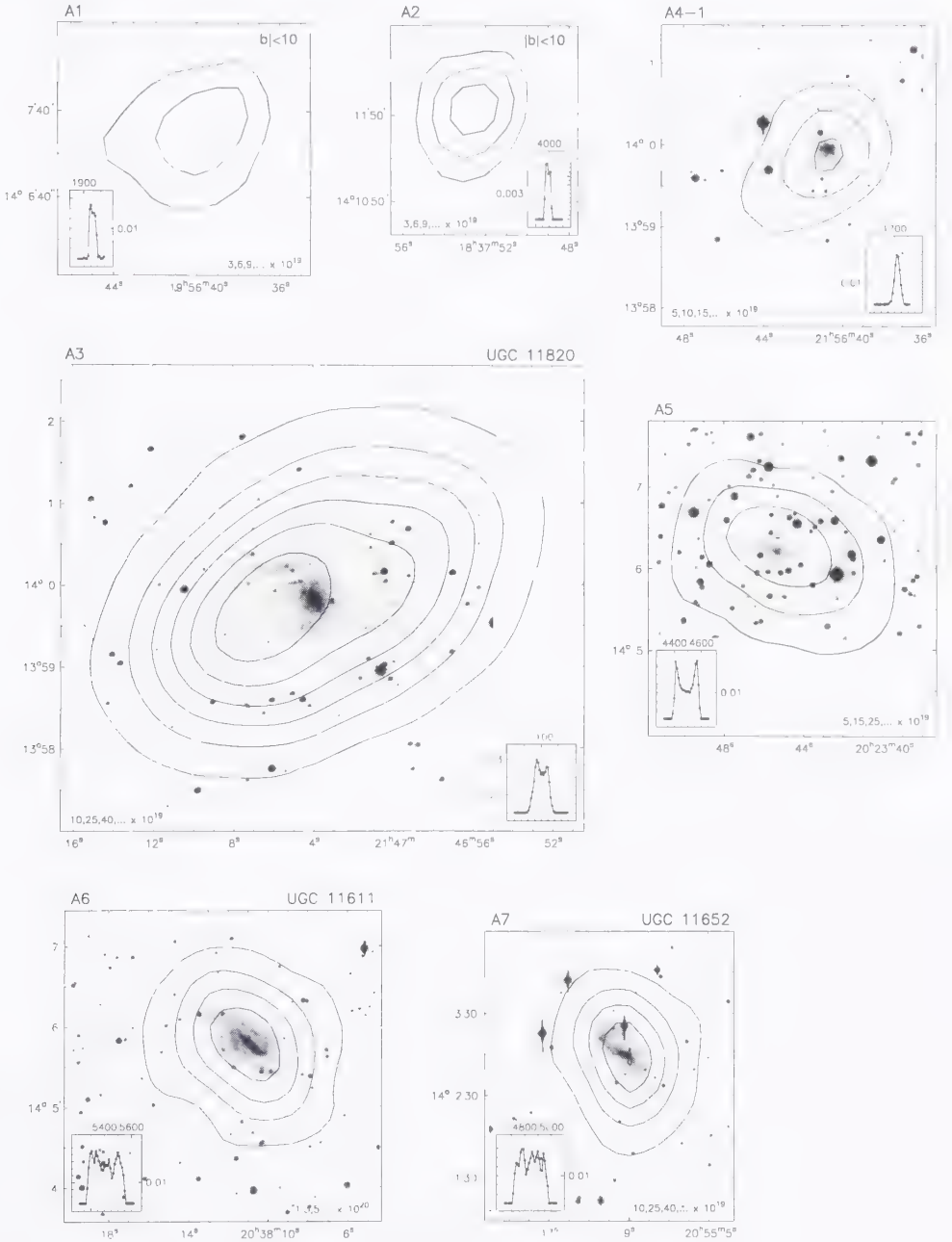

FIGURE 2.8— Contours of H I distribution superposed on optical *B*-band images. The levels of the H I contours are indicated in one of the lower corners of each panel. Global H I profiles are also shown for each galaxy. The units are km s^{-1} on the horizontal axis and Jy on the vertical axis.

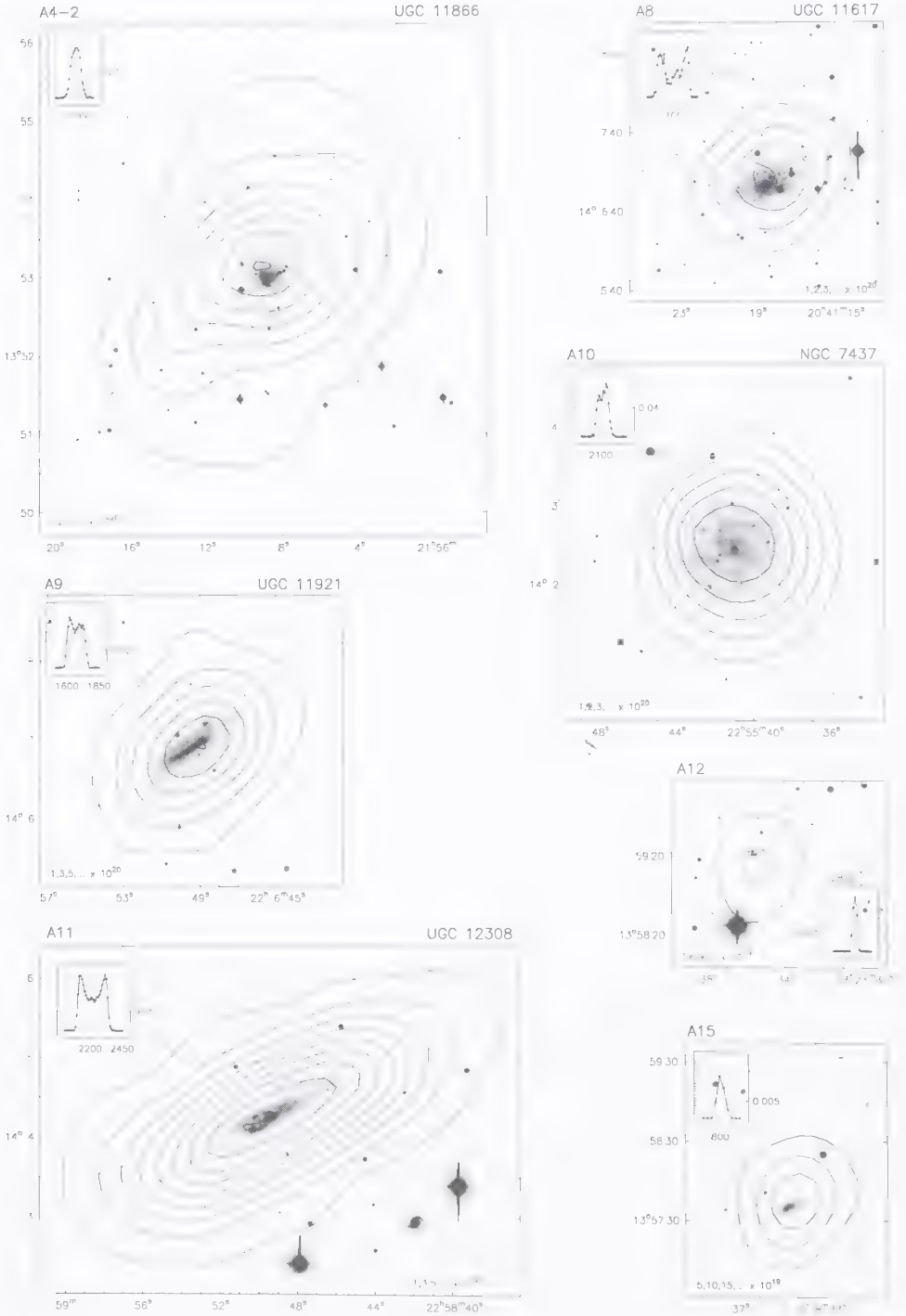

FIGURE 2.8— Continued

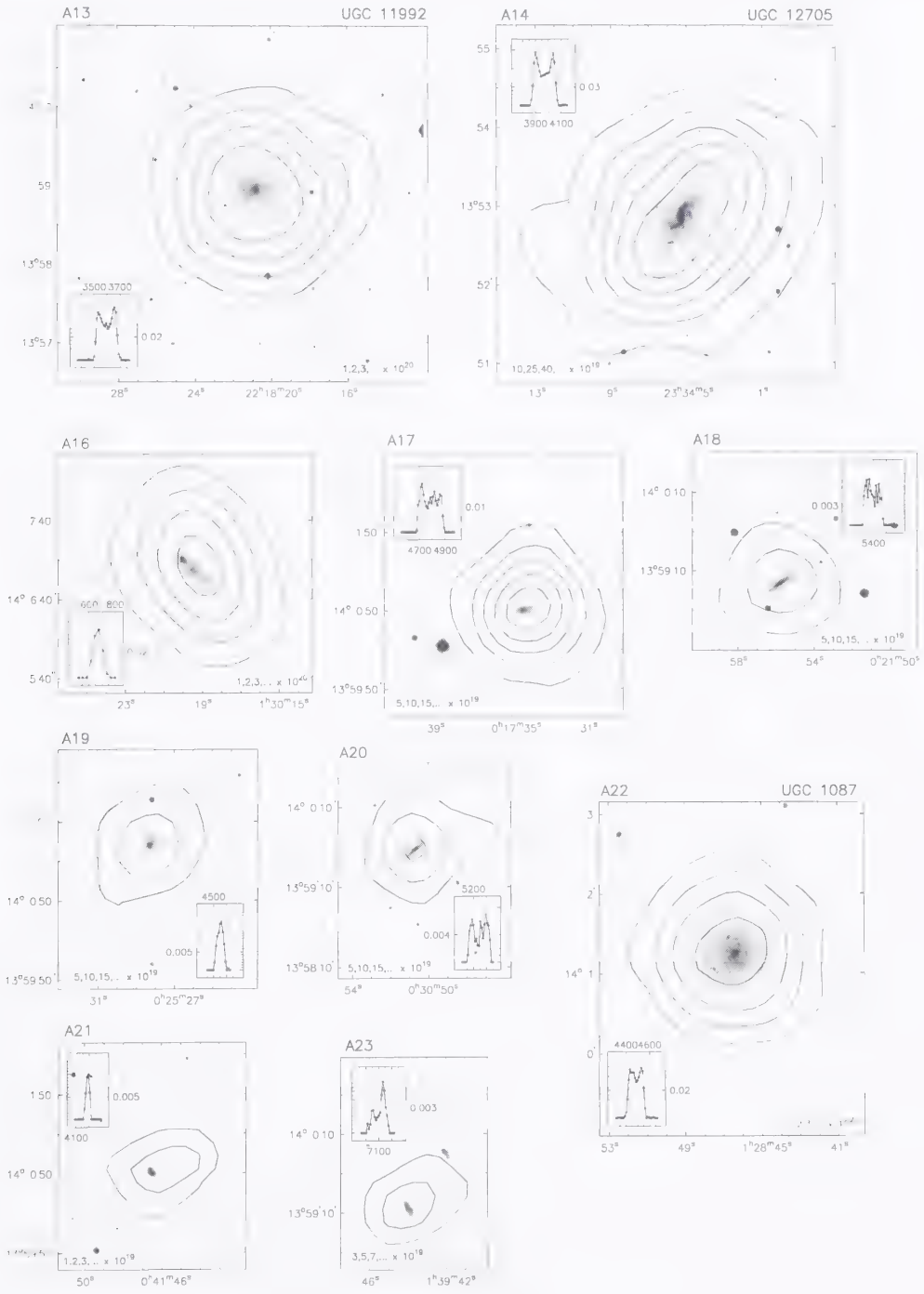

FIGURE 2.8— Continued

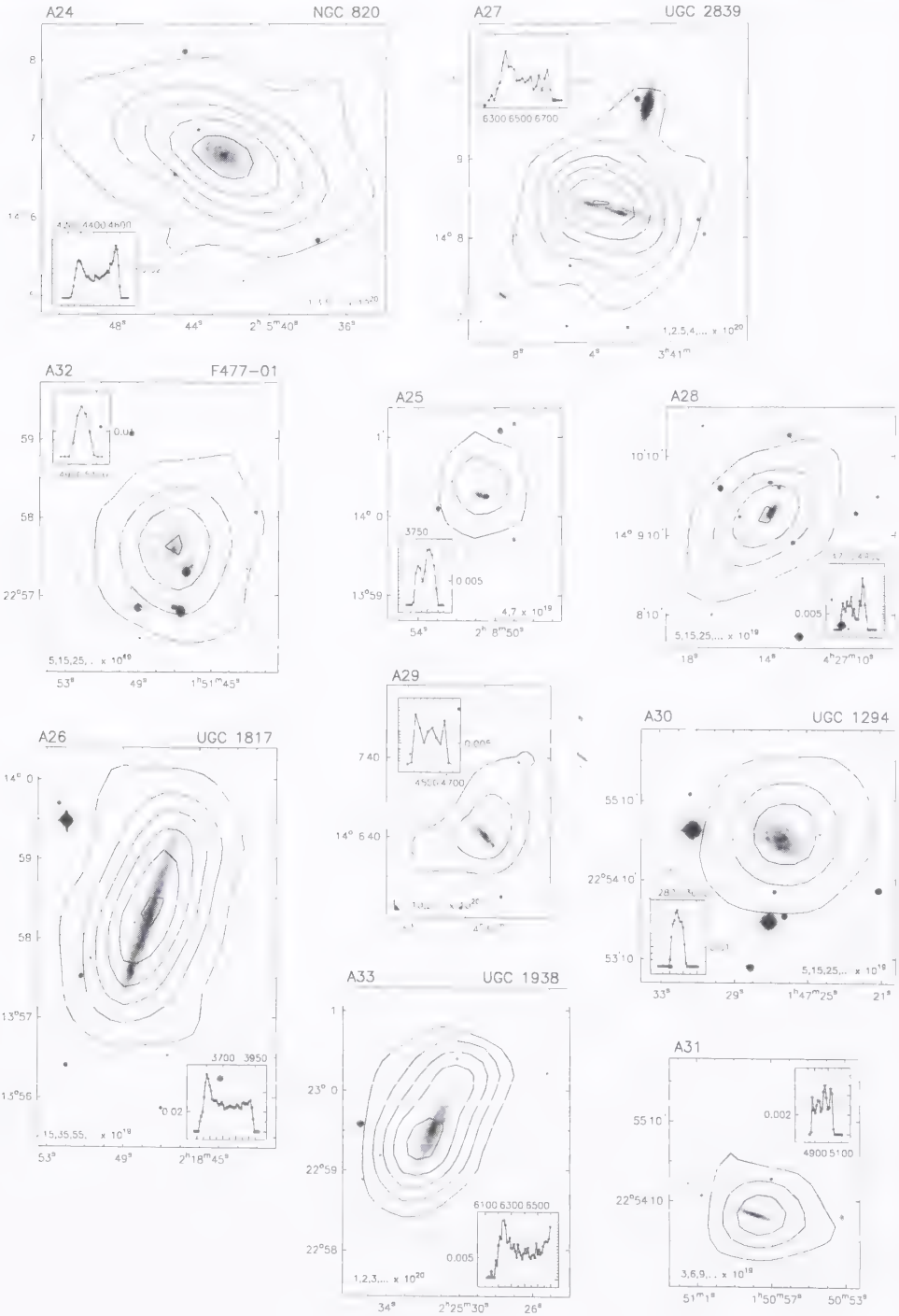

FIGURE 2.8— Continued

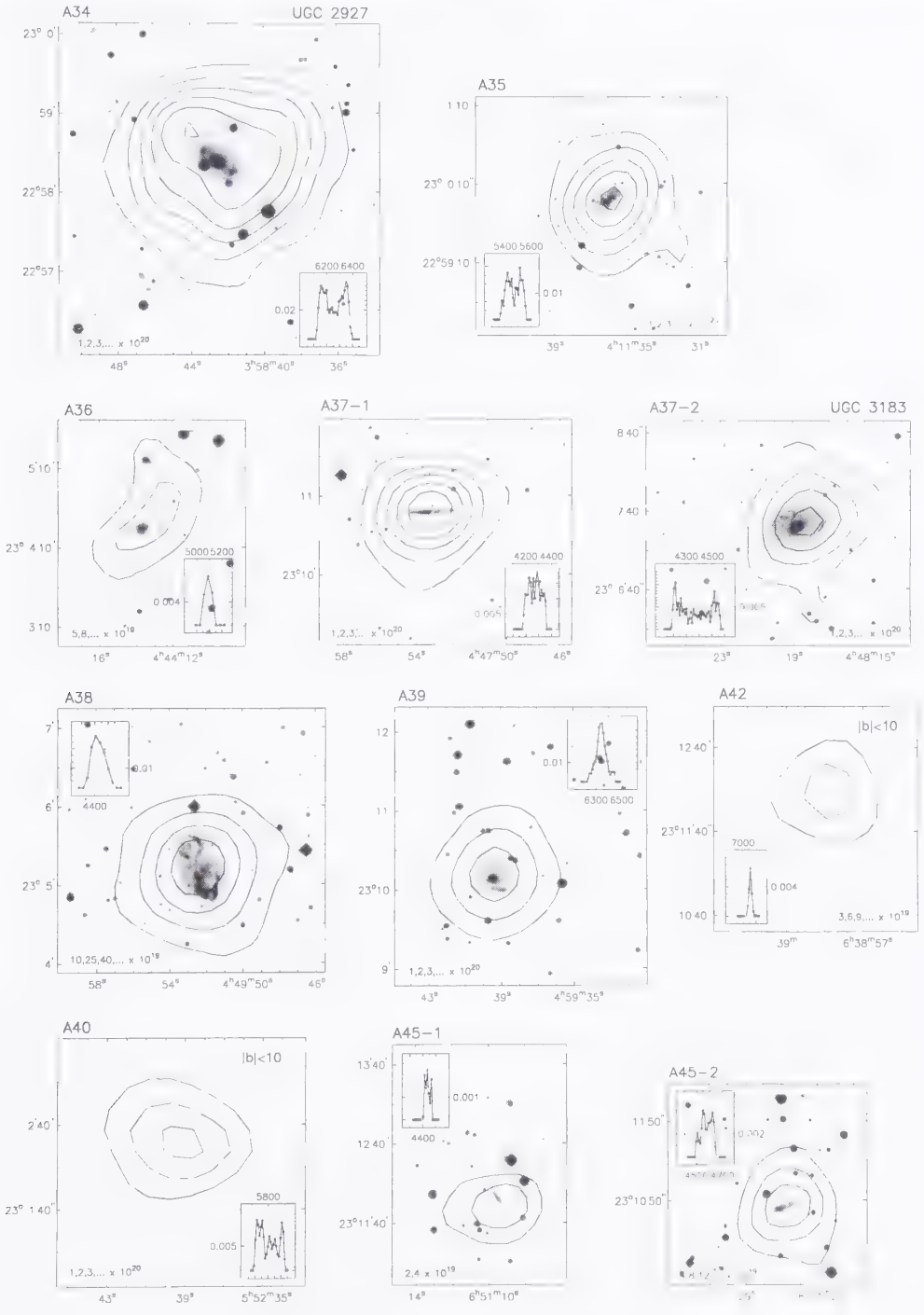

FIGURE 2.8— Continued

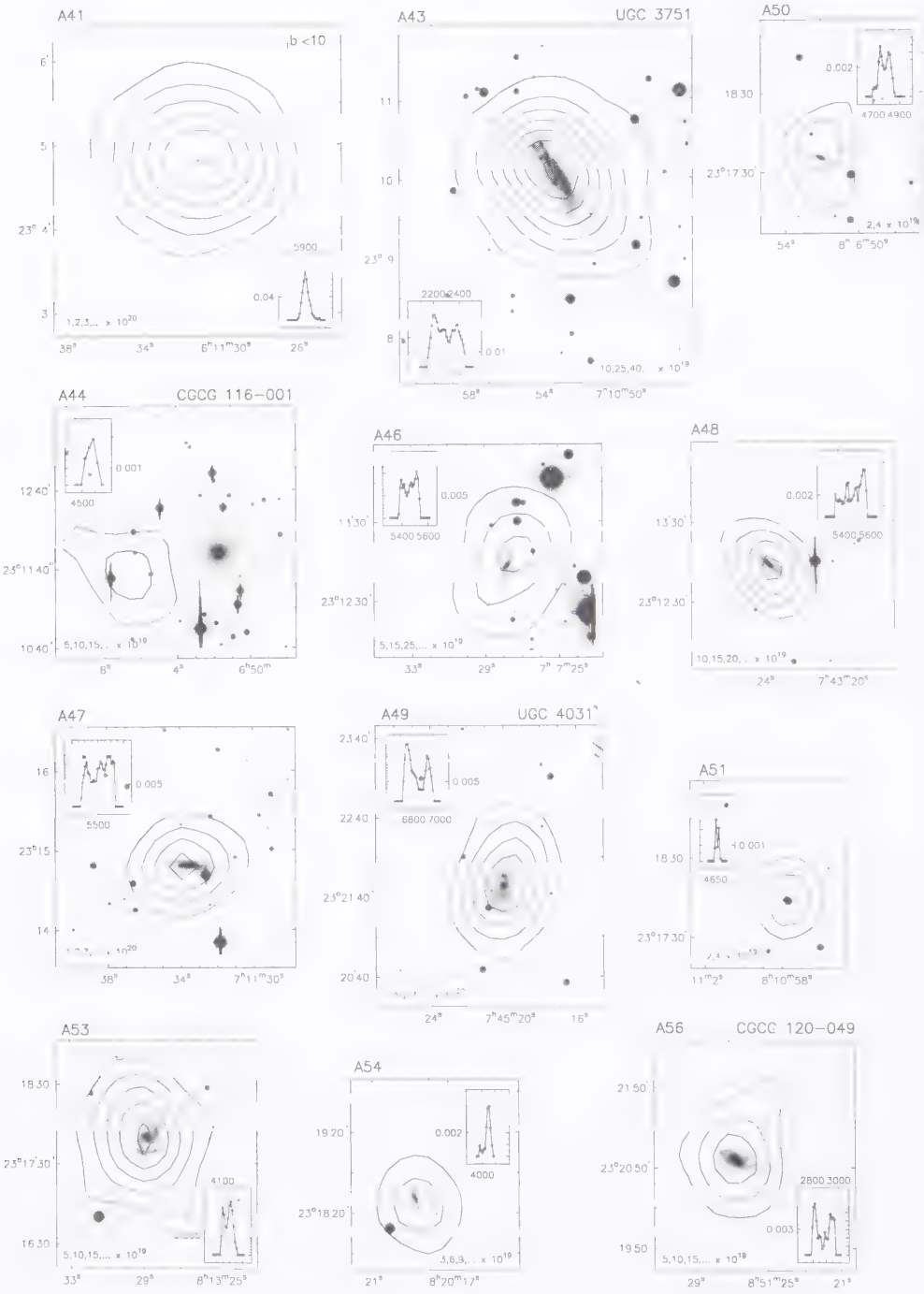

FIGURE 2.8— Continued

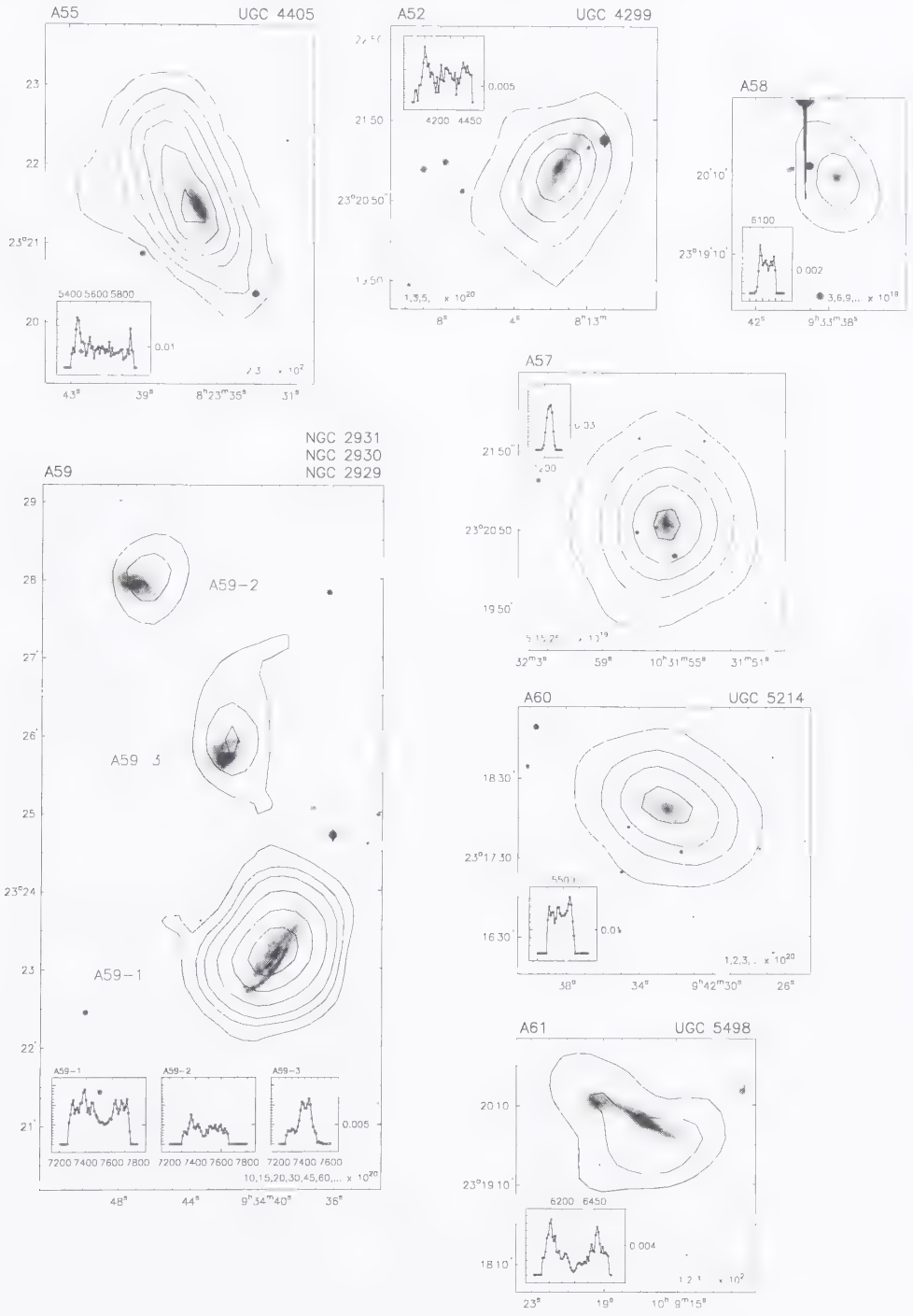

FIGURE 2.8— Continued

L3

The H I Mass Function of Galaxies from a Deep Survey in the 21cm Line[1]

M. A. Zwaan, F. H. Briggs, D. Sprayberry, & E. Sorar

ABSTRACT — The H I mass function (HIMF) for galaxies in the local universe is constructed from the results of the Arecibo H I Strip Survey, a blind extragalactic survey in the 21cm line. The survey consists of two strips covering in total ~ 65 square degrees of sky, with a depth of $cz = 7400$ km s^{-1} and was optimized to detect column densities of neutral gas $N_{\rm HI} > 10^{18}$cm^{-2} (5σ). The survey yielded 66 significant extragalactic signals of which approximately 50% are cataloged galaxies. No free floating H I clouds without stars are found. VLA follow-up observations of all signals have been used to obtain better measurements of the positions and fluxes and allow an alternate determination of the achieved survey sensitivity. The resulting HIMF has a shallow faint end slope ($\alpha \approx -1.2$), and is consistent with earlier estimates computed for the population of optically selected gas rich galaxies. This implies that there is not a large population of gas rich low luminosity or low surface brightness galaxies that has gone unnoticed by optical surveys. The influence of large scale structure on the determination of the HIMF from the Arecibo H I Strip Survey is tested by numerical experiments and was not found to affect the resulting HIMF significantly. The cosmological mass density of H I at the present time determined from the survey, $\Omega_{\rm HI}(z = 0) = (2.1 \pm 0.4) \times 10^{-4} h^{-1}$, is in good agreement with earlier estimates. We determine lower limits to the average column densities $\langle N_{\rm HI} \rangle$ of the galaxies detected in the survey and find that none of the galaxies have $\langle N_{\rm HI} \rangle < 10^{19.7}$cm^{-2}, although there are no observational selection criteria against finding lower density systems. Eight percent of the signals detected in the original survey originated in groups of galaxies, whose signals chanced to coincide in frequency.

[1]published in *Astrophysical Journal* 490, 173 (1997)

3.1 Introduction

THE DISTRIBUTION FUNCTION of neutral hydrogen masses among galaxies and intergalactic clouds (the H I mass function or HIMF), and more generally, the neutral hydrogen density in the nearby universe, Ω_{HI}, are important inputs into models of cosmology and galaxy evolution. Different attempts have been made to construct an HIMF by using optically selected galaxies (Rao & Briggs 1993, Solanes, Giovanelli & Haynes 1996). These studies are based on the assumption that H I is always associated with optically bright galaxies. A major concern is whether the HIMF is complete when it is computed for these galaxies.

For example, the population of low surface brightness (LSB) galaxies might hypothetically constitute a substantial portion of the population of nearby extragalactic objects (Disney 1976, McGaugh 1996, Dalcanton, Spergel & Summers 1997, Sprayberry et al. 1997). The LSB population easily escapes detection optically and would not be included in the samples that are commonly used to evaluate the HIMF. This would be particularly problematic since LSB galaxies are generally found to be rich in neutral gas (Schombert et al. 1992, de Blok, McGaugh & van der Hulst 1996) and could therefore contribute substantially to the neutral gas content. Gas rich dwarf galaxies may also play an important part. For example Tyson & Scalo (1988) have argued that the majority of these dwarf galaxies remain undetected because only the small portion that is currently undergoing a rapid phase of star formation is presently observed with optical telescopes. A final possible population of gas rich systems that would escape inclusion in optical catalogs is a class of intergalactic H I clouds without stars. So far, only a few such systems have been discovered, and they are always found to be gravitationally bound to a galaxy or a group of galaxies (for example the Leo ring, Schneider 1989).

Clearly, the HIMF and the H I content of the local universe should be measured directly, in such a way that they suffer no bias against gas rich galaxies or intergalactic H I clouds which are difficult to detect optically. This is possible by means of surveys in the H I line. Several of these surveys have been carried out over the last two decades. The majority were single dish observations using on/off techniques, since these surveys were done in conjunction with observations targeted on cataloged galaxies (Fisher & Tully 1981b, Giovanelli & Haynes 1985, 1989). Some surveys were concentrated on groups of galaxies (Haynes & Roberts 1979, Lo & Sargent 1979, Fisher & Tully 1981a, Hoffman, Lu & Salpeter 1992) to specifically search for H I clouds in the vicinity of known galaxies. Other surveys were designed to find H I signals in voids (Krumm & Brosch 1984, Szomoru et al 1996), or to compare voids and superclusters (Weinberg et al. 1991, Szomoru et al. 1994). Since these surveys are not pointed at randomly chosen regions of sky, they may not provide fair tests of the shape of the HIMF or an unbiased measure of the average H I density. A few truly blind surveys have been conducted, the first one in driftscan mode (Shostak 1977) and one by observing a series of pointings on lines of constant declination (Kerr & Henning 1987, Henning 1992). It is worrisome that this latter survey could not reproduce the HIMF defined for optically selected galaxies, possibly because the survey was targeted toward large volumes of known voids. Another possibility is that the achieved survey sensitivity is not well understood, leading to an underestimation of the true number density of H I rich galaxies and intergalactic clouds.

More recently, several surveys have been made using the Arecibo telescope (Sorar 1994, Spitzak 1996, Schneider 1997). Surveys are in progress at Dwingeloo (DOGS) and at Parkes, where the survey will cover the entire Southern Sky (Staveley-Smith et al. 1996).

In this chapter we analyze the Arecibo H I Strip Survey (Sorar 1994), a blind survey for extragalactic H I covering ~ 65 square degrees of sky, out to a redshift of 7400 $\mathrm{km\,s^{-1}}$. The analysis of the survey results will concentrate specifically on the understanding of the achieved survey sensitivity and the vulnerability to large scale structure. We describe the details of the survey and the optical and 21cm follow-up observations in section 3.2. Section 3.3 gives a detailed analysis of the achieved survey sensitivity. We present the HIMF in section 3.4, the possible influence of large scale structure on the determination of the HIMF is examined by performing numerical experiments, and the cosmological mass density of H I at the present time is calculated in this section. In section 3.5 we compare our findings with previous estimates of the HIMF based on 21cm surveys and optically selected galaxy samples and discuss the implications of our results. Section 3.6 summarizes the results. The distances used in this chapter are based on a Hubble constant $H_0 = 100\,\mathrm{km\,s^{-1}\,Mpc^{-1}}$.

3.2 Observations

3.2.1 Arecibo H I Strip Survey (AHISS)

The strip survey was carried out on the Arecibo[2] 305m Telescope in the period of August 1993 until February 1994. The survey was designed to take advantage of periods of construction when the telescope pointing was immobilized but the receiving systems were still operational. Therefore, the data were taken in driftscan mode and the telescope beam traced strips of constant declination. The same strips were retraced for as many as 30 days in order to obtain very sensitive observations that are capable of detecting H I of low surface density. The main survey was divided in two sessions: one survey covering 10.5 hours of RA at $\delta = 14°14'$, and the second survey covering 9.7 hours of RA at $\delta = 23°09'$. All observations were made at night. The limiting column density was $10^{18}\mathrm{cm^{-2}}$ (at a 5σ level) for gas filling the telescope beam, which subtends 3 h^{-1} kpc at 3 h^{-1} Mpc and 70 h^{-1} kpc at 74 h^{-1} Mpc. The total sky coverage was approximately 65 square degrees, with a depth of $cz = 7400$ $\mathrm{km\,s^{-1}}$. The survey was capable of detecting H I masses of $6 \times 10^5 h^{-2}\mathrm{M}_\odot$ at 7 h^{-1} Mpc and $1.5 \times 10^8 h^{-2}\mathrm{M}_\odot$ at the full depth of the survey, in the main beam which has a FWHM of 3 arcmin. The first sidelobe of the telescope beam pattern could detect $1.5 \times 10^9 h^{-2}\mathrm{M}_\odot$ at the full depth of the survey, which makes the sidelobes effective in detecting high H I mass galaxies over a 15 arcmin wide strip. The details of the AHISS and the data reduction are described by Sorar (1994). A summary of the reduction path is described by Briggs et al. (1997).

The survey yielded a total of 61 detections, of which approximately half could be associated with cataloged galaxies listed in the NASA Extragalactic Database (NED[3]). Five detections have no obvious counterparts on the Digitized Sky Survey (DSS[4]) although they are more than 10° away from the Galactic plane.

[2]The Arecibo Observatory is part of the National Astronomy and Ionosphere Center, which is operated by Cornell University under cooperative agreement with the National Science Foundation.

[3]The NASA/IPAC Extragalactic Database (NED) is operated by the Jet Propulsion Laboratory, California Institute of Technology, under contract with the National Aeronautics and Space Administration.

[4]Based on photographic data of the National Geographic Society – Palomar Observatory Sky Survey (NGS-POSS) obtained using the Oschin Telescope on Palomar Mountain. The NGS-POSS was funded by a grant from the National Geographic Society to the California Institute of Technology. The plates were processed into the present compressed digital form with their permission. The Digitized Sky Survey was produced at the Space Telescope Science Institute under US Government grant NAG W-2166.

Fig. 3.1 shows slice diagrams of the location of all H I selected objects compared with galaxies in the CfA catalog (Geller & Huchra 1989). Galaxies within a 10° strip centered on the declination of the strip are plotted. Different symbols are used to distinguish between cataloged (circles) and uncataloged (boxes) galaxies. The size of the symbols reflects the H I mass of the galaxies, in the sense that bigger symbols indicate larger H I masses. The Galactic plane intersects the strips at RA $\approx 6^h$ and RA $\approx 19^h$ as indicated by the dashed lines. The CfA catalog is obviously incomplete in these regions of the sky due to Galactic extinction, whereas the H I survey suffers no bias against detection in these regions. It is clear from this figure that H I selected galaxies generally follow the same structures as the optical galaxies. In particular, if we only consider those regions of the sky where the CfA catalog is complete, we find that more than 80% of the H I selected galaxies lie in regions where the average galaxies density is higher than the mean density. This is consistent with the finding that LSB galaxies and gas-rich dwarfs lie on structures delineated by normal, high surface brightness galaxies (Bothun et al. 1986, Thuan, Gott & Schneider 1987, Eder et al. 1989, Thuan et al. 1991, Mo, McGaugh & Bothun 1994). Furthermore, none of the H I selected galaxies in the sections where the CfA is complete are found in regions where the galaxy density is less than one fifth of the cosmic mean. This is in agreement with the results of Szomoru et al. (1994) and Weinberg et al. (1991) that H I selected galaxies are not found in selected void fields. A more detailed analysis of the large scale distribution of the H I selected galaxies will be presented elsewhere.

3.2.2 21cm Follow-up observations

Follow-up 21cm synthesis observations on all signals found in this survey have been performed with the NRAO[5] Very Large Array (VLA) in D-configuration. These follow-up observations are essential for three reasons:
1) As stated before, the survey was capable of detecting signals as far as 7 arcmin from the center of the survey strip. Consequently, the coordinates yielded by the survey have uncertainties on the order of several arcminutes. The association with a cataloged galaxy or a galaxy on the DSS is therefore not always unambiguous, especially in those cases where there are several prominent galaxies visible within a 15 arcmin wide strip. 21cm observations with spatial resolution of ~ 1 arcmin, are sufficient to obtain unique identifications.
2) Flux measurements from the AHISS can be poor if a signal is detected at large distance from the center of the beam. In principle, a correction to the flux could be made since the response function of the telescope is known with reasonable accuracy, but this is only possible if the positional accuracy is sufficient. Furthermore, measurements from the survey spectra might underestimate the integral flux if the source is more extended than the primary beam. Thus, a rough measure of the H I distribution increases confidence in the analysis.
3) Some signals can be caused by pairs or small groups of galaxies, whose line emission might stack up in the same channels. It is not obvious from the Arecibo survey spectra which signals are caused by more than one galaxy. In fact, this situation was found by the VLA observations to occur in five cases.

Short VLA observations ($\sim$ 20 min) of all 61 detected galaxies were performed during the D-configuration sessions in May 1995 and September 1996. The signal of three systems fell below the detection limit of the snap-shot observation. These systems were

[5]The National Radio Astronomy Observatory is a facility of the National Science Foundation operated under cooperative agreement by Associated Universities, Inc.

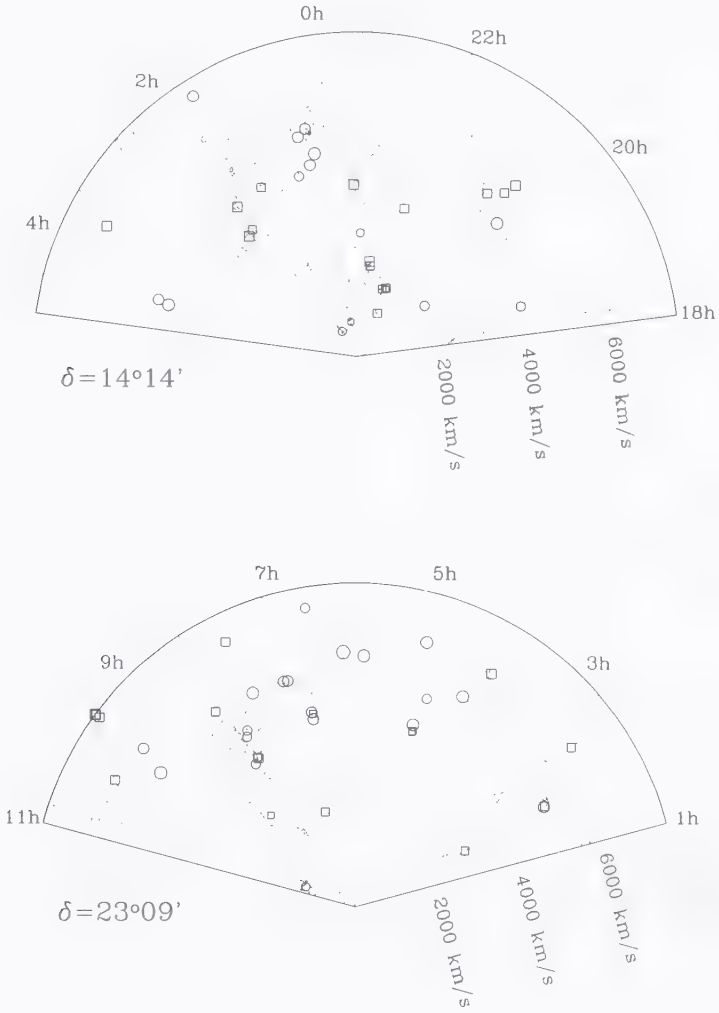

FIGURE 3.1— Slice diagrams of the location of all the H I selected objects from the Arecibo H I Strip Survey. Boxes indicate uncataloged galaxies, circles indicate cataloged galaxies. The size of the symbols reflects the H I mass of the galaxies. Also shown are galaxies from the CfA catalog (Geller & Huchra 1989) within a 10° strip centered on the declination of the surveys. The Galactic plane intersects the strips at RA$\approx 6^h$ and RA$\approx 19^h$ as indicated by the dashed lines.

re-observed in the D-configuration during the second session, but with longer integration times ($\sim$ 3 hours), resulting finally in confirmation of all 61 detections at levels consistent with the AHISS sensitivity. The three weaker signals originated in galaxies whose declinations are at the center of the AHISS.

The VLA observations were performed using 63 channels over a 3.125 MHz bandwidth, corresponding to a velocity range of approximately 660 km s^{-1}. On-line Hanning

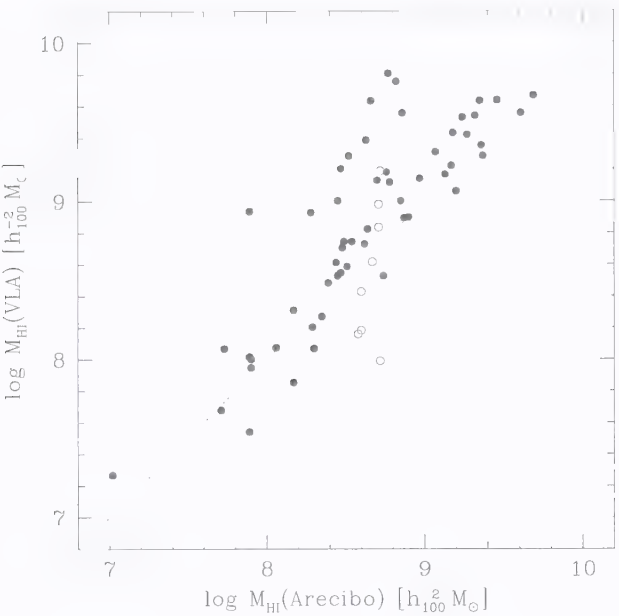

FIGURE 3.2— Comparison of total H I masses as measured with the VLA and H I masses derived from the Arecibo H I Strip Survey spectra. The dashed line is the line of equality. Different symbols distinguish between singe detections (filled circles) and multiple detections (open circles).

smoothing was used, resulting in a velocity resolution of ~ 10.5 km s^{-1}. Phase calibrators were observed once for each source. Only seven different phase calibrators were used. Each time that the phase calibrator was changed, a primary flux calibrator (3C48 or 3C286) was observed in order to tie the flux scales together. Therefore, the primary calibrators were not observed with the same correlator settings as each galaxy, but only with six correlator settings. The overhead time due to slewing of the telescopes and observations of primary calibrators is significantly decreased this way. This technique provided adequate passband calibration for these short observations, where high dynamical range or accurate channel-to-channel flux density calibrations are not needed. There were no strong continuum sources in these fields.

Since the observing conditions were generally quite good, little editing was necessary to remove interference and bad baselines. Continuum was removed from the data in the *uv*-plane, by making linear fits to the real and imaginary components for each visibility in the line-free channels and subtracting the appropriate values from all channels. The *uv* data were calibrated and transformed to datacubes using natural weighting. Using natural weighting rather than uniform weighting results in a slightly lower spatial resolution, but higher sensitivity. The resolution in the transformed datacubes is $\sim 60'' \times 60''$. The final r.m.s noise was approximately 1.2 mJy/beam for each channel (corresponding to a minimal detectable column density of $\sim 1.7 \times 10^{19}$cm^{-2} [5σ]) for the short integrations and 0.8 mJy/beam (limiting column density $\sim 9 \times 10^{18}$cm^{-2} [5σ]) for the longer integrations. Since the observed galaxies were generally barely resolved, CLEANing of the data was not really necessary. Nonetheless, because the synthesized beam of these short observations has strong deviations from a Gaussian shape, we chose to CLEAN the datacubes and restore them with a Gaussian beam in order to make an effective search for companion objects throughout the primary beam.

Total H I masses were calculated using $M_{\rm HI}/{\rm M}_\odot = 236\, d^2 \int S dV$, where d is the distance

to the source in Mpc, and S is the flux density in mJy over profile width ΔV in km s^{-1}. Total H I maps were constructed by adding the regions in the channel maps that contain line emission. Contour maps of H I emission and global profiles are presented in Chapter 2.

Fig. 3.2 shows the H I masses as measured with the VLA plotted against the H I masses that are derived from the AHiSS spectra. Different symbols are used to distinguish between single detections (filled circles) and multiple detections (open circles). Arecibo measurements of these multiple detections are of course always unreliable estimates of the real H I masses. This figure clearly illustrates the fact that the H I masses derived from the Arecibo spectra generally underestimate the true H I masses, and that follow-up observations were essential to determine accurate measurements. In the analysis of the AHiSS results we will use H I masses calculated from the VLA observations, except for galaxies with integrated VLA fluxes less than 1.0 Jy km s^{-1}. Galaxies with these low fluxes are only found at small distances from the center of the Arecibo beam, where the normalized response function is close to unity. Arecibo measurements for these galaxies are therefore reliable estimates of their real fluxes.

Table 3.1 summarizes the global parameters of the detected galaxies which are derived from the VLA observations. The following information is contained: Column 1: Identification number of the Arecibo detection. Indices indicate multiple detections. Column 2: Name of galaxy if already cataloged. Columns 3 and 4: B1950 coordinates. Column 5: Logarithm of H I mass. Column 6: Heliocentric velocity, calculated by taking the mean of the velocities at 20% of peak flux density. Column 7: Declination offset from center of the survey strip. Column 8: Identification code for multiple detections.

3.2.3 Optical follow-up observations

We have also started a program of optical B-band imaging of the H I selected galaxies with the 2.5m Isaac Newton Telescope[6] (INT) on La Palma. During four observing runs in the period between October 1995 and March 1997 we have been able to obtain images of all target galaxies. The first noteworthy result of the follow-up optical observations is that *all* of the H I sources more than 10° away from the Galactic plane are found to be associated with galaxies in the B-band images. We have seen no indication that any of the sources detected in the Arecibo survey are anything other than 'ordinary' galaxies having both gas and stars. Put another way, we have so far failed to find any H I sources that are pure H I clouds without stars. The analysis of the optical observations will be presented in Chapter 4.

3.3 The survey sensitivity

The improved coordinates and H I fluxes derived from the VLA observations help to verify the completeness limit of the survey. The detectability is determined in the following way:

The H I mass in a detected signal can be expressed as $M_{\rm HI}/{\rm M}_\odot = 236 \times S\,\Delta V d^2$, where d is the distance to the source in Mpc, and S is the flux density in mJy that here is considered to be constant over a rectangular profile of width ΔV km/s. The sensitivity of an observation is optimal when the spectra are smoothed to the velocity width of the source. With optimal smoothing the noise becomes $\sigma(\Delta V) = \sigma_0\sqrt{\Delta V_0/\Delta V}$, where ΔV_0 is the spectral reso-

[6] The Isaac Newton Telescope is operated by the Royal Greenwich Observatory in the Spanish Observatorio del Roque de los Muchachos of the Instituto Astrofisica de Canarias.

TABLE 3.1— Basic Parameters of Survey Galaxies.

(1) Nr	(2) Name	(3) α (1950) (h m s)	(4) δ (1950) (° ′ ″)	(5) M_{HI} (log $M_\odot$)	(6) $V_{\odot}$ (km/s)	(7) $\Delta\delta$ (″)	(8) Code
A1		19:56:40.0	14:07:24	8.02	1964	33	
A2		18:37:52.6	14:11:53	8.32	3991	21	
A3	UGC 11820	21:47:06.0	13:59:50	9.12	1107	116	
A4-1		21:56:41.2	13:59:58	7.99	1720	89	A
A4-2	UGC 11866	21:56:09.0	13:53:00	9.20	1705	507	A
A5		20:23:45.0	14:06:12	9.17	4485	49	
A6	UGC 11611	20:38:11.1	14:05:46	9.64	5412	47	
A7	UGC 11652	20:55:09.1	14:02:58	9.42	4843	52	
A8	UGC 11617	20:41:18.4	14:07:03	9.29	5114	152	
A9	UGC 11921	22:06:49.2	14:06:53	8.82	1672	346	
A10	NGC 7437	22:55:40.9	14:02:28	8.93	2117	151	
A11	UGC 12308	22:58:49.2	14:04:16	9.54	2220	261	
A12		23:23:35.4	13:59:09	7.92	2860	27	
A13	UGC 11992	22:18:20.7	13:58:53	9.31	3591	115	
A14	UGC 12705	23:34:05.2	13:52:48	9.67	3968	403	
A15		00:08:34.1	13:57:45	7.35	812	100	
A16		01:30:19.2	14:07:05	7.68	668	392	
A17		00:17:34.1	14:00:50	9.18	4787	82	
A18		00:21:55.2	13:59:05	8.51	5397	25	
A19		00:25:28.8	14:01:30	8.90	4552	119	
A20		00:30:51.3	13:59:30	8.62	5246	3	
A21		00:41:45.9	14:00:51	8.33	4372	71	
A22	UGC 1087	01:28:46.5	14:01:16	9.35	4484	45	
A23		01:39:44.4	13:59:20	8.79	7103	88	
A24	NGC 820	02:05:42.3	14:06:46	9.56	4418	311	
A25		02:08:50.7	14:00:17	8.62	3794	85	
A26	UGC 1817	02:18:47.5	13:58:22	9.63	3735	222	
A27	UGC 2839	03:41:02.0	14:08:30	9.76	6523	156	
A28		04:27:13.5	14:09:45	8.89	4781	68	
A29		04:30:00.0	14:06:40	9.00	4523	118	
A30	UGC 1294	01:47:26.2	22:54:44	8.71	2861	73	
A31		01:50:57.5	22:53:59	8.97	4956	124	
A32	F 477-01	01:51:46.9	22:57:35	9.13	4989	90	
A33	UGC 1938	02:25:32.1	22:59:20	9.48	6383	108	
A34	UGC 2927	03:58:41.5	22:58:20	9.81	6251	180	
A35		04:11:36.0	23:00:00	9.21	5464	148	
A36		04:44:14.3	23:04:19	8.45	5088	1	
A37-1		04:47:54.5	23:10:50	8.98	4272	375	B
A37-2	UGC 3183	04:48:18.6	23:07:29	8.93	4390	192	B
A38		04:49:52.4	23:05:12	9.22	4416	33	
A39		04:59:39.3	23:10:10	9.43	6339	294	
A40		05:52:39.4	23:02:29	9.06	5812	367	
A41		06:11:31.1	23:04:49	9.63	5902	299	
A42		06:38:58.9	23:12:05	8.38	7012	32	
A43	UGC 3751	07:10:53.4	23:10:05	8.94	2300	208	
A44	CGCG116-001	06:50:06.2	23:11:30	8.11	4575	40	
A45-1		06:51:09.6	23:11:52	8.32	4593	28	C

TABLE 3.1— Continued.

(1) Nr	(2) Name	(3) α (1950) (h m s)	(4) δ (1950) (° ′ ″)	(5) M_{HI} (log $M_\odot$)	(6) $V_\odot$ (km/s)	(7) $\Delta\delta$ (″)	(8) Code
A45-2		06:51:26.4	23:10:38	8.63	4562	101	C
A46		07:07:27.5	23:13:02	8.90	5457	18	
A47		07:11:33.6	23:14:49	9.00	5473	74	
A48		07:43:23.7	23:12:56	9.22	5491	151	
A49	UGC 4031	07:45:19.9	23:21:51	9.29	6834	378	
A50		08:06:52.0	23:17:47	8.41	4790	61	
A51		08:10:56.9	23:17:44	8.01	4667	60	
A52	UGC 4299	08:13:00.2	23:21:37	9.31	4107	271	D
A53		08:13:29.0	23:17:51	8.61	4143	44	D
A54		08:20:18.6	23:18:29	8.29	4029	60	
A55	UGC 4405	08:23:36.2	23:21:25	9.49	5617	276	
A56	CGCG120-049	08:51:26.8	23:20:55	8.15	2882	114	
A57		10:31:55.5	23:20:54	8.00	1238	101	
A58		09:33:37.4	23:20:03	8.81	6132	45	
A59-1	NGC 2929	09:34:39.3	23:23:18	9.72	7499	148	E
A59-2	NGC 2931	09:34:46.8	23:28:06	9.45	7478	436	E
A59-3	NGC 2930	09:34:40.8	23:26:12	9.26	7376	321	E
A60	UGC 5214	09:42:32.5	23:18:07	9.39	5480	180	
A61	UGC 5498	10:09:16.4	23:19:42	9.14	6306	138	

lution of the receiving system and σ_0 is the noise level in the unsmoothed spectra. The limiting flux density S_c for a 5σ detection is then given by $S_c(\Delta V) = 5\sigma(\Delta V) = 5\sigma_0\sqrt{\Delta V_0/\Delta V}$. For the AHISS, the average noise level after coadding spectra taken at different days was 0.75 mJy for a velocity resolution of 16 km/s.

The normalized response function of the survey telescope, $I(\theta)$, describes the relative response to a source which is detected at an offset θ from the center of the survey strip. In other words, $I(\theta)$ is the integral of the flux density sensed by the telescope as a source makes a cut through the beam pattern, missing the center of the beam by angle θ, normalized in such a way that $I(0) = 1$. For the Arecibo telescope this function falls off to ~ 0.125 at $\theta = 3.25'$ and reaches a second maximum of ~ 0.2 at $\theta = 4.8'$ due to the high sidelobe level. We define a correction factor $c_r(\theta)$ that accounts for the shape of the response function by $c_r(\theta) = 1/I(\theta)$. The limiting flux density of a galaxy at an offset θ from the center of the survey strip can then be expressed as $S_c c_r(\theta)$. In general, an H I source should be detected by the survey if its flux density exceeds this limiting flux density, that is $S > S_c c_r(\theta)$. This can be rewritten as

$$D \equiv \frac{\int S\,dV\sqrt{(\Delta V_0/\Delta V)}}{5\sigma_0 \Delta V_0 c_f} > c_r(\theta), \tag{3.1}$$

where we define D as the detectability. The factor c_f represents the normalized feed gain of the telescope, which is a function of frequency. c_f can be approximated by an analytical expression of the form $c_f \approx 1 - ([f - f_0]/w)^2$, where f is the frequency in MHz, f_0 is the center of the survey band and w is a parameter which determines the width of the band. During the observations at $\delta = 14°14'$ the shape of the normalized feed gain remained

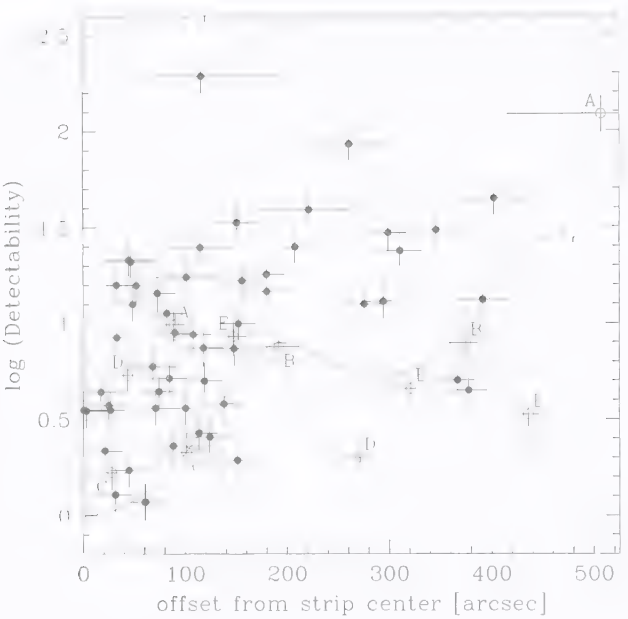

FIGURE 3.3— Detectability, D, of the objects versus the offset from the center of the survey strip. Multiple detections are indicated by open symbols and coded to indicate which galaxies originate from the same Arecibo detection. The solid curve shows the detection limit. Objects below this line should be undetectable if their H I profile widths would be rectangular.

unchanged and could be satisfactorily fit by $f_0 = 1395$ MHz and $w = 40.5$ MHz. During the $\delta = 23°09'$ observations, the gain was retuned a few times to the settings: $f_0 = 1395$ MHz and $w = 37.5$ MHz and $f_0 = 1410$ MHz and $w = 33.8$ MHz. The c_{f} dependence of D leads to a 'distance dependence' for the flux density sensitivity.

The sensitivity can now be verified by plotting the detectability D of the objects against declination offset from the center of the survey strip. This is shown in Fig. 3.3. All signals that were detected are shown in this plot. The horizontal errorbars are the result of a combination of positional accuracy in the VLA maps and the spatial extent of the galaxies in the direction orthogonal to the survey strip. The signals corresponding to pair or group detections are indicated by open circles and letters A to E are used to identify these related or confused signals in Table 3.1. Filled circles mark all single object detections. The solid line represents $c_{\mathrm{r}}(\theta)$, the limit to the detectability. In principle, all filled circles should lie above the solid line, the area below this line is 'undetectable'. The line is a satisfactory limit to the data points, especially if we consider the naive character of Eq.3.1. That is, this equation assumes that the detected profiles are symmetric and featureless. Since the profiles are generally heavily smoothed, this is a reasonable assumption, but lop-sided profiles or strong double horned profiles might exceed the detection limit while they are formally 'undetectable' according to Eq.3.1.

The limiting depth d_{c}, the maximum distance to which the object could be placed and still remain within the sample, can now be expressed as a function of M_{HI}, θ and ΔV:

$$d_{\mathrm{c}}(M_{\mathrm{HI}}, \theta, \Delta V) = \sqrt{\frac{M_{\mathrm{HI}}\, I(\theta)}{236\, S_{\mathrm{c}}(\Delta V)\, \Delta V}}. \tag{3.2}$$

The variation of feed gain with frequency imposes a minor correction to the limiting

depth d_c which can be compensated by solving for d_c in

$$S(d_c)c_f(d_c) = S_c, \tag{3.3}$$

that is, the true flux density $S(d_c)$ of a galaxy located at the distance limit d_c multiplied by the feed gain at a frequency corresponding to that distance has to be equal to the limiting flux density S_c obtained at the center frequency, where the feed gain is optimized and the nominal noise level of the system is normally calculated.

The next step is to calculate the effective search volume of the survey. The volume $d\mathcal{V}$ of a slice of the total survey volume at declination δ and with length l (the total length of the strips in radians, $l = \Delta\mathrm{RA}\, 2\pi \cos\delta/24^{\mathrm{h}}$) and width $d\theta$ is given by

$$d\mathcal{V}(M_{\mathrm{HI}},\theta,\Delta V) = \begin{cases} \frac{1}{3}\, d_c^3(M_{\mathrm{HI}},\theta,\Delta V)\, l\, d\theta, & \text{if } d_c < d_{\mathrm{BW}}, \\ \frac{1}{3}\, d_{\mathrm{BW}}^3\, l\, d\theta, & \text{if } d_c > d_{\mathrm{BW}}, \end{cases} \tag{3.4}$$

where d_{BW} is the limiting depth of the survey imposed by the bandwidth of the receiving system. The total survey volume that is sensitive to a galaxy with H I mass M_{HI} and velocity spread ΔV can then be calculated by taking the integral over θ. For galaxies in the flux limited regime, for which $d_c < d_{\mathrm{BW}}$ for each θ, this integral simply becomes:

$$\mathcal{V}(M_{\mathrm{HI}},\Delta V) = \frac{1}{3}\int_{-\infty}^{\infty} d_c^3 l\, d\theta = \frac{1}{3}\int_{-\infty}^{\infty} \left(\frac{M_{\mathrm{HI}}\, I(\theta)}{236\, S_c\, \Delta V}\right)^{3/2} l\, d\theta. \tag{3.5}$$

For galaxies in the bandwidth limited regime, $d_c > d_{\mathrm{BW}}$ for θ smaller than a certain critical value θ_{BW}. The integral must now be split up in separate parts for the flux limited regimes and the band width limited regime:

$$\begin{aligned} \mathcal{V}(M_{\mathrm{HI}},\Delta V) &= \frac{1}{3}\int_{-\infty}^{-\theta_{\mathrm{BW}}} d_c^3 l\, d\theta + \frac{1}{3}\int_{-\theta_{\mathrm{BW}}}^{\theta_{\mathrm{BW}}} d_{\mathrm{BW}}^3 l\, d\theta + \frac{1}{3}\int_{\theta_{\mathrm{BW}}}^{\infty} d_c^3 l\, d\theta \\ &= \frac{2}{3}\int_{0}^{\theta_{\mathrm{BW}}} d_{\mathrm{BW}}^3 l\, d\theta + \frac{2}{3}\int_{\theta_{\mathrm{BW}}}^{\infty} \left(\frac{M_{\mathrm{HI}}\, I(\theta)}{236\, S_c\, \Delta V}\right)^{3/2} l\, d\theta, \end{aligned} \tag{3.6}$$

where we made use of the symmetry of the beam shape in the last step.

This effective search volume is still dependent on two variables: M_{HI} and ΔV. The most convenient parameterization of $\mathcal{V}$ for computing an HIMF is to express $\mathcal{V}$ as a function of M_{HI} only. This can be achieved by adopting a relation between M_{HI} and ΔV. Such a relation is known to exist since optical luminosity L is related to ΔV via the Tully-Fisher relation (Tully & Fisher 1977), and L is related to M_{HI} as $M_{\mathrm{HI}} \propto L^{0.9}$ (see Briggs 1990). Briggs & Rao (1993) determined the M_{HI}-ΔV relation empirically by plotting ΔV against $\log M_{\mathrm{HI}}$ for 1139 optically selected galaxies from the catalog by Fisher & Tully (1981b). A fit to these points gives $\Delta V = 0.16\, M_{\mathrm{HI}}{}^{1.8}$. Recently, Salpeter & Hoffman (1996) analyzed H I observations of 70 dwarf galaxies and find a similar trend: $\Delta V \propto M_{\mathrm{HI}}{}^{0.36}$. This relation is therefore valid over a wide range in H I mass. Our data are also in good agreement with this relation. Note that the velocity widths in these relations are not the inclination corrected maximum rotational velocities, but just the observed velocity spreads.

The effective survey volume $\mathcal{V}(M_{\mathrm{HI}})$ can now be calculated by substituting the relation between ΔV and M_{HI} found by Briggs & Rao (1993) and $S_c(\Delta V)$ into Eq.3.5 and Eq.3.6. This volume as a function of M_{HI} is shown by the solid line in Fig. 3.4. In the flux limited

regime, for H I masses $< 10^{8.5}$, the search volume is $\mathcal{V} \propto {M_{\rm HI}}^{5/4}$. (A proportionality often used in the literature is $\mathcal{V} \propto {M_{\rm HI}}^{3/2}$ [e.g., Henning 1995, Schneider 1997]. This power 3/2 arises if the dependence of ΔV on $M_{\rm HI}$ is discarded, effectively assuming that all galaxies have the same profile width.) In the high mass region ($M_{\rm HI} > 10^{9.5}$), the limiting depths are no longer determined by the detectability of the signals, but simply by the bandwidth of the receiving system. Therefore, the effective survey volume for high mass systems is not dependent on H I mass or ΔV. The total survey volume in this regime, is $\sim 3000 h^{-3}{\rm Mpc}^3$. For lower H I masses the volume decreases rapidly and is only $\sim 1.0 h^{-3}{\rm Mpc}^3$ for $M_{\rm HI} = 10^7 {\rm M}_\odot$. The dashed and the dotted line show the effective search volume corresponding to the main beam and the sidelobes, respectively. This figure clearly shows that the sidelobes do not add much volume in the low mass range, but are very effective in finding large H I masses.

Since the observed velocity width is related to inclination i and maximum rotational velocity $V_{\rm max}$ as $\Delta V = 2 V_{\rm max} \sin i$, the limiting depth is $d_c \propto (\Delta V)^{-1/4} \propto (\sin i)^{-1/4}$. The limiting depth is therefore weakly dependent on inclination, in the sense that low inclined galaxies can be detected to slightly larger distances. Consequently, an H I survey would in principle preferentially select face-on galaxies. In practice, this effect is negligible, since the expectation for $\langle (\sin i)^{-1/4} \rangle$ of a randomly oriented sample is close to unity:

$$\langle (\sin i)^{-1/4} \rangle = \frac{\int_0^{\pi/2} (\sin i)^{-1/4} \sin i \, di}{\int_0^{\pi/2} \sin i \, di} \approx 1.086. \qquad (3.7)$$

Only the flux limited regime would be hampered by the inclination effect, but most galaxies in this regime are low mass, dwarf galaxies. The velocity spreads are small for these galaxies, and turbulent motions play an important part at establishing the profile width (cf., Lo, Sargent & Young 1993).

A potential hazard in radio surveys is the influence of radio frequency interference (RFI). RFI can in principle cause false negatives (miss a significant signal) in the sample if it affects the spectrum exactly at the frequency of a source, or when a narrow-lined

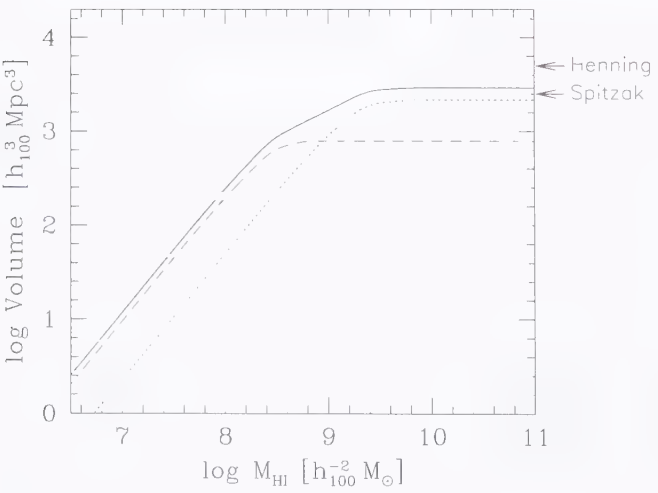

FIGURE 3.4— The effective search volume vs. H I mass. The solid line is the total search volume of the Arecibo H I Strip Survey, the dashed and the dotted line show the effective search volume corresponding to the main beam and the sidelobes, respectively. The arrows indicate the survey volumes of two H I surveys which are comparable in size to the AHISS: Henning (1995) and Spitzak (1996).

source is mistaken for RFI. However, the driftscan method that has been used for the AHISS has proven to provide a very good stability for RFI signals (see Briggs et al. 1997). Repetitive coverage of the same regions of sky makes the survey immune to RFI and unstable baselines. This has been demonstrated by the fact that all signals identified in the Arecibo survey have been confirmed by the VLA follow-up.

3.4 The H I mass function

The H I mass function (HIMF) is defined analogously to optical luminosity functions. The HIMF $\Theta(M_{\rm HI})d(M_{\rm HI})$ gives the total number of galaxies or intergalactic clouds per Mpc^3 in the mass interval $dM_{\rm HI}$ centered on $M_{\rm HI}$. Here, we find it convenient in our analysis and figures to plot the HIMF as the number of galaxies or intergalactic clouds per decade in mass. In order to parameterize the shape of the HIMF, we adopt the conventional Schechter (1976) function,

$$\Theta(M_{\rm HI})d(M_{\rm HI}) = \theta^*(\frac{M_{\rm HI}}{M^*_{\rm HI}})^{\alpha}\ \exp -(\frac{M_{\rm HI}}{M^*_{\rm HI}})d(\frac{M_{\rm HI}}{M^*_{\rm HI}}), \tag{3.8}$$

with free parameters α, the slope of the low-mass end, $M^*_{\rm HI}$ the characteristic mass that the defines the kink in the function and θ^*, a normalization factor. This function must be integrated over decade bins for comparison with the binned data in the figures.

3.4.1 Methods

The classical method (see e.g., Christensen 1975, Schechter 1976) for determining luminosity functions is based on the assumption that galaxies are distributed in a uniform manner. The luminosity function is determined by dividing the number of galaxies in a bin centered on M by $\mathcal{V}(M)$, the effective search volume for that particular M. This method is easily applicable to the AHISS. The search volume can be evaluated with Eq.3.5 and Eq.3.6, using a statistical relation between velocity width and H I mass. The advantages of this method are that it is nonparametric and that it is automatically normalized. The important disadvantage is that it assumes homogeneity and its use might lead to errors in $\Theta(M_{\rm HI})$ if density fluctuations due to large scale structure occur on distance scales comparable to, or greater than the depth d_c at which $M_{\rm HI}$ can be detected.

A slightly modified form of the 'classical' method is the $\sum(1/\mathcal{V}_{\rm max})$ method, first used by Schmidt (1968), which is also applicable to H I surveys. Instead of calculating a mean survey volume for each mass bin, this method consists of summing the reciprocals of the volumes corresponding to the maximum distances to which the objects could be placed and still remain within the sample. The values of $\mathcal{V}_{\rm max}$ can be calculated directly using Eq.3.5 and Eq.3.6, using now the measured velocity spread instead of the statistical value. The two procedures give similar results when the number of galaxies per bin is large. For the less densely populated bins the two procedures can give different results because $\mathcal{V}_{\rm max}$ of a particular galaxy can strongly deviate from the average $\mathcal{V}$ of the mass bin it falls in. In section 3.4.2 the HIMF is calculated using Schmidt's method. Like the classical method, Schmidt's method is also vulnerable to errors caused by large scale structure. The possible effects of large scale structure are discussed in section 3.4.3.

3.4.2 Results

Fig. 3.5 shows the principal results of this analysis. The lower panel shows the observed distribution of H I masses binned per half decade, with errorbars given by Poisson statistics. This histogram shows that the survey has detected galaxies with H I masses in the range from 10^7 to 10^{10}M$_\odot$ and therefore enables us to determine the HIMF over three orders of magnitudes in H I mass.

The solid dots in the upper panel of Fig. 3.5 show the HIMF determined by the $\sum(1/\mathcal{V}_{max})$ method. The errorbars are given by Poisson statistics. Also drawn in this figure are analytical curves given by the Schechter function of Eq 3.8. A satisfactory fit to the points is obtained with $\alpha = -1.20$, $\theta^* = 0.014$ Mpc^{-3} and $\log(M^*_{HI}/M_\odot) = 9.55$. Mass functions with faint end slopes of -1.10 and -1.30 are shown to indicate the uncertainty in the value of α. We note that in the present analysis the parameterization of the HIMF in the form of a Schechter function is only used to enable comparison with other H I survey results and results based on the optically selected galaxy population. The $\sum(1/\mathcal{V}_{max})$ method recovers the shape and amplitude of the HIMF simultaneously without using a Schechter function (or any other parameterization) as an assumption about the intrinsic shape of the HIMF.

The observational limits to the determination of the HIMF are also illustrated in Fig. 3.5 by the thin line. This line represents the sensitivity function of the survey to objects of H I mass M_{HI}, defined as $\phi(M_{HI}) = 1/\mathcal{V}(M_{HI})$, where $\mathcal{V}(M_{HI})$ is the effective search volume. In the range 10^7M$_\odot$ $< M_{HI} < 10^{10}$M$_\odot$ this function defines an upper limit to the space density of intergalactic H I clouds without stars. It also shows that this survey is not capable of measuring the HIMF directly in the regions $M_{HI} < 10^7$M$_\odot$ and $M_{HI} > 10^{10}$M$_\odot$ if the extrapolation of the analytical form for $\Theta(M_{HI})$ holds. The sensitivity function does allow us to define upper limits in these ranges as indicated by arrows. The upper limit at $M_{HI} = 10^{10.75}$M$_\odot$ is from the complementary survey with the Arecibo telescope over the range 19,000 to 28,000 km s^{-1}, which is only sensitive to high mass galaxies (See Sorar (1994) for details).

3.4.3 Influence of large scale structure

The slice diagrams in Fig 3.1 show that the survey strips sample a wide range of large scale structure, as the combined RA range extends nearly 2/3 of the way around the sky. On the other hand, the limited depth of the survey for small H I masses might cause the low mass end of the HIMF to be affected by local density fluctuations. Therefore, a major concern in the determination of the mass function following Schmidt's method, is whether homogeneity is a fair assumption. For instance, a local density enhancement would overestimate the number of low mass galaxies or clouds and would give rise to an overestimate of the faint end slope of the mass function. The biases in the shape of the mass function due to large scale structure can be avoided by making use of a maximum likelihood estimator (cf., Efstathiou, Ellis & Peterson 1988, Saunders et al. 1990). If the spatial density distribution of galaxies and intergalactic clouds is given by $N(M_{HI}, \vec{r})$, then the overall density $\rho(\vec{r})$ and the mass function $\Theta(M_{HI})$ can be separated as $N(M_{HI}, \vec{r}) = \rho(\vec{r})\Theta(M_{HI})$. Maximum likelihood estimators can then be used to solve either for $\Theta(M_{HI})$ without knowledge of $\rho(\vec{r})$ or solve for $\rho(\vec{r})$ without knowledge of $\Theta(M_{HI})$.

Although the maximum likelihood method is a powerful procedure for determining optical luminosity functions (Marzke, Geller & Huchra 1994, Lin et al. 1996, Saunders et al. 1990), we chose not to apply it to the AHISS. The most important problem is that

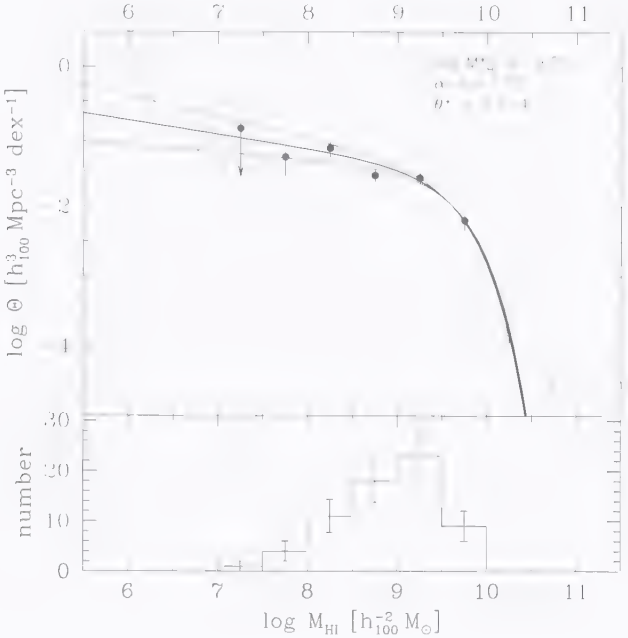

FIGURE 3.5— *Lower panel*: The distribution of H I masses of the detected galaxies from VLA follow-up measurements. The errorbars are given by Poisson statistics. *Upper panel*: The thin line is the sensitivity of the survey defined by $\phi = 1/\mathcal{V}$, where $\mathcal{V}$ is the effective search volume. In the region $10^7 M_\odot < M_{HI} < 10^{10} M_\odot$ this function defines an upper limit to the space density of intergalactic H I clouds without stars. The measured H I mass function per decade is shown by the points. The fat line is a Schechter luminosity function with parameters as given in the upper right corner. Also Schechter functions with $\alpha = -1.1$ and $\alpha = -1.3$ are shown. The arrows show upper limits to the space density of H I rich galaxies or intergalactic H I clouds. The two arrows on the right are from a complementary survey with the Arecibo telescope over the range 19,000 to 28,000 km s^{-1}.

we have to deal with small number statistics. Especially the faint end slope of the mass function is defined by very few galaxies or clouds per bin. Some experimentation with application of the algorithm to small samples such as ours showed that maximum likelihood methods can produce erratic results in these situations. Another complication arises because maximum likelihood methods assume that the shape of the H I mass function is independent of the space density $\rho(\vec{r})$. In practice, high mass galaxies will have a higher statistical weight in the determination of $\rho(\vec{r})$ since they are simply more numerous in our sample. It is questionable whether this space density defined by the high mass galaxies is a fair estimate for the galaxies at the faint end side of the mass function, in the region that is dominated by dwarf and LSB galaxies. Although these galaxies are found to follow the same general large scale structures as the normal HSB galaxies, they preferentially avoid the highest density regions (Mo et al. 1994, Taylor 1997). In principle, the spatial density ρ could be separated into different functions for individual morphological types or different ranges in H I mass, but the limited number of galaxies in our sample does not allow this differentiation.

In order to investigate the effect of large scale structure we have performed numerical experiments. These tests consisted of randomly placing artificial galaxies in a volume with weights given by the HIMF given in Eq.3.8. A range of HIMF parameters were investigated. The results are illustrated using the derived HIMF parameters from Fig 3.5: $\theta = 0.014$ Mpc^{-3}, $\log(M^*_{\rm HI}/{\rm M}_\odot) = 9.55$ and $\alpha = -1.20$. The galaxies have random inclination, and rotational velocity related to H I mass as determined by Briggs & Rao (1993). Galaxies were selected from these volumes in the same manner as the Arecibo H I Strip Survey selects galaxies from the sky.

Fig. 3.6 shows the results of three experiments, labeled as A, B and C. The presented results are each the average of 100 independent simulations. The left upper panels show the assumed normalized density fluctuations ρ. The left lower panels show the redshift distribution of the simulated data as thick-lined histograms, thin solid lines show 1σ uncertainties. Overlaid on these histograms is the measured redshift distribution of our survey sample, indicated by solid circles and dashed histograms. The right panels show the averaged HIMFs of the simulated catalogs as open squares, with 1σ errorbars computed as the standard deviations of the 100 simulations. The $\sum 1/\mathcal{V}'_{\rm max}$ method has been used.

In case A a homogeneous density distribution is assumed. It is not surprising to see that the input HIMF and the measured HIMF agree with high accuracy. The $\sum 1/\mathcal{V}_{\rm max}$ method should give reliable results in this situation. It is however apparent that the survey observations have several distance bins that are overdense or underdense compared to the uncertainty band of the 'uniform density' simulation. The comparison implies that we may be observing underdensities at $D \approx 30$ Mpc and $D \approx 70$ Mpc and an overdensity at $D \approx 50$ Mpc. To test this hypothesis we constructed catalogs with a density fluctuation as indicated by the top panel in case B. The precise functional form of this fluctuation is not important, the condition is that is should produce consecutive under and overdensities at $D \approx 30$, 50 and 70 Mpc. The central panel shows that the imposed density fluctuation reproduces the observed redshift distribution satisfactorily. It is surprising however that if the $\sum 1/\mathcal{V}'_{\rm max}$ method is applied to these simulated data the resulting HIMF is still indistinguishable from the input HIMF. In other words, the $\sum 1/\mathcal{V}_{\rm max}$ method appears to be a robust method, and not very sensitive to the effects of large scale structure. This is even true for case C, where a more severe density fluctuation is imposed, and where the resulting HIMF is still in good agreement with the input HIMF. We can conclude from these simulations that although we see a hint of the effects of large scale structure in our data, the observed deviations from uniformity have no significant influence on our determination of the HIMF.

3.5 Discussion

3.5.1 Previous estimates of the HIMFs from H I surveys

The first H I surveys could only be used to set upper limits to the space density of intergalactic H I clouds without stars, and did not yield enough detections to allow the determination of the shape of the HIMF. Shostak (1977) was to first to define these limits by means of blind driftscan emission and absorption searches in the 21cm line with the NRAO 91m telescope. Due to the relatively poor sensitivity (12 - 40 mJy) and the small total effective search volume ($\sim 300h^{-3}$Mpc^3), these limits were not very strict. In the region $M_{\rm HI} < 10^{8.5}$M$_\odot$ the limits set by the Arecibo H I Strip Survey are at least two orders of magnitude lower (99% confidence) than those set by Shostak. Haynes & Roberts (1979),

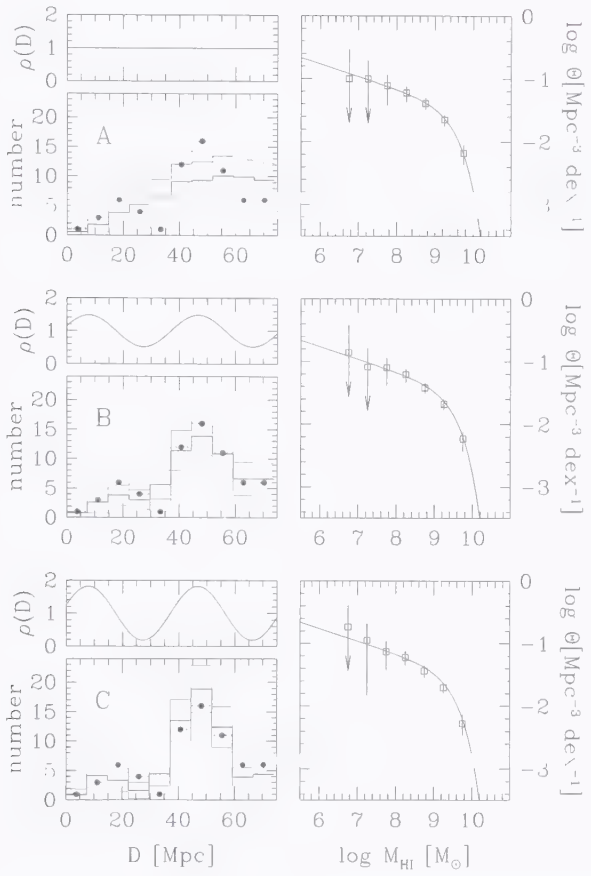

FIGURE 3.6— Numerical tests of the influence of large scale structure on the determination of the HIMF. The left panels show the imposed normalized density fluctuations in artificial catalogs. The histograms show the redshift distributions of the simulated data as solid lines, with 1σ uncertainties as thin lines. The measured redshift distribution of our survey sample is represented by solid circles and a dashed line. The right panels show the $\sum(1/V_{max})$ HIMF of the simulated data as open squares, with 1σ errorbars. The input HIMF is indicated by the solid curves.

Lo & Sargent (1979) and Fisher & Tully (1981a) search for invisible galaxies in groups of galaxies. Haynes & Roberts conclude from observations in the direction of the Sculptor group that intergalactic H I clouds with $M_{HI} > 10^5 M_\odot$ do not exist. Lo & Sargent find four previously uncataloged LSB dwarf galaxies but their upper limits to the space density of unseen objects do not improve Shostak's. Fisher & Tully used the NRAO 91m telescope to search for invisible galaxies in the M81 group. Their null result allowed them to push the upper limits to the space density 0.6 dex lower than those set by Shostak. Also Krumm & Brosch (1984) find no H I sources in their driftscan searches of void regions and are only able to define upper limits. These limits are not very strict since their survey is only sensitive in the redshift range above 5300 km s^{-1}, and is consequently only capable of finding

H I masses $> 10^{10}$M$_\odot$.

A series of papers by Kerr & Henning (1987) and Henning (1992, 1995) describes blind surveys which consisted of observing a series of pointings along lines of constant declination in the zone of avoidance and at high galactic latitude. These surveys yielded 39 detections (of which half were previously unknown) and were the first to put serious constraints on the shape of the HIMF. For comparison, the HIMF calculated by Henning (1995) is reproduced in Fig. 3.7 as solid squares, together with the AHISS HIMF represented as a solid line. Henning's points are significantly lower than our measured curve. According to Henning's calculations objects with $10^{8.5}$M$_\odot$ $< M_{\rm HI} < 10^{9.5}$M$_\odot$ are deficient by a one order of magnitude compared to the AHISS HIMF. The presence of the Local Void in Henning's survey could explain a part of this discrepancy, but even if the void is omitted the points are still beneath our HIMF. The most reasonable explanation for the discrepancy is that the sensitivity of Henning's survey is not well understood, leading to a serious underestimate of the HIMF.

The most recent determination of the HIMF is the one by Schneider (1997) who used both the uncorrected Arecibo data from Sorar's (1994) survey and the data from Spitzak's (1996) survey with the Arecibo telescope. Schneider assessed the completeness limits of the surveys with the use of $\mathcal{V}/\mathcal{V}_{\rm max}$ tests. He calculated the average value of $\mathcal{V}/\mathcal{V}_{\rm max}$ and scaled that to the correct value of 0.5 by increasing the limiting flux density S_c. Schneider noted the vulnerability of this method to the influence of large scale structure. Despite this different approach, the resulting HIMF is in good agreement with our estimate, as can be seen in Fig. 3.7. Only the low mass end deviates significantly. The statistics in the bins with $M_{\rm HI} \leq 7.25$ are poor, and Schneider could not rule out a slope as high as $\alpha = -1.7$. The differences in the slopes can be partly explained by the fact that *uncorrected* H I masses are used in Schneider's estimate of the HIMF from Sorar's data. The effect that the flux is underestimated when the Arecibo beam misses a galaxy by a certain angle θ was not taken into account. The VLA H I masses that are used in our HIMF are on average 50% higher, leading to a shift of galaxies to higher H I mass bins. As an alternate approach, Schneider also applied a maximum likelihood fit to all the signals brighter that 20σ. The resulting HIMF had a faint end slope $\alpha = -1.32$. This result is also drawn in Fig. 3.7 and is in very good agreement with our function over the whole range in H I mass.

In addition to making comparisons with surveys that are equally blind as the AHISS, it is also interesting to compare our results with surveys that cover comparable volumes in underdense and overdense regions. It is noteworthy that the HIMF determined from HI observations in clusters (McMahon 1993), as well as that determined in cosmic voids (Szomoru et al. 1996) are both well fit by a Schechter function, with approximately the same shape as as our HIMF. The scaling θ^*, however, differs by a factor of ten or more between these different regions.

Since the AHISS crosses the Galactic plane twice, and consequently a large fraction of the total survey volume lies in regions which are not complete in optical catalogs, it is difficult to calculate the exact void filling factor of our survey. If we limit the calculation to the regions where $|b| > 30^\circ$, we estimate that approximately 50% of the survey volume consists of regions where the average galaxy density is less than one third of the cosmic mean, and approximately 10% of the volume consists of structures where the galaxy density takes on more than three times the cosmic mean. The same percentages are obtained if random slices through the Universe are taken. If voids would be omitted from the survey, the scaling θ^* of the HIMF would increase by a factor of two.

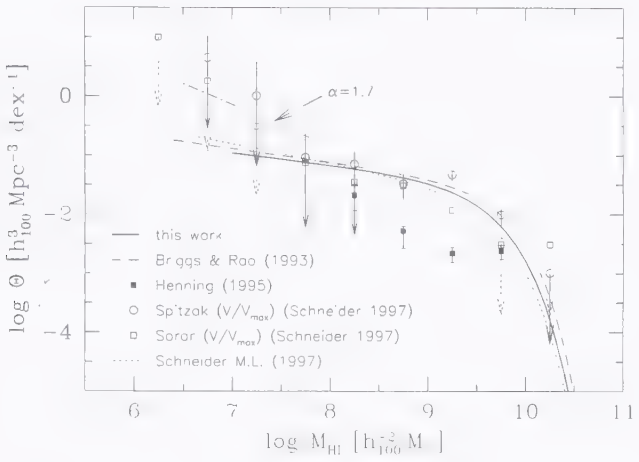

FIGURE 3.7— Comparison of H I mass functions of different surveys. The fat solid line shows the HIMF presented in this paper, using VLA observations of galaxies found in the Arecibo H I Strip Survey. Briggs & Rao's (1993) HIMF based on the Fisher & Tully catalog is indicated by dashed curve. The solid squares are from Henning (1995). The open symbols result from Schneider's (1997) $\mathcal{V}/\mathcal{V}_{\rm max}$ method applied to the data of Spitzak (1995) (circles) and the uncorrected Arecibo data from Sorar (1994) (squares). Schneider's (1997) maximum likelihood solution is indicated by the dotted curve. The dash-dot line shows a faint end slope of $\alpha = -1.7$.

3.5.2 Comparison with HIMFs based on optically selected galaxies

The construction of an HIMFs from a sample of optically selected galaxies can either be done statistically, by studying optical luminosity functions and the dependence of H I mass on on optical luminosity, or directly by using 21cm data of optically selected galaxies. The first method was used by Rao & Briggs (1993), who reviewed the literature that describes luminosity functions and H I richness for individual morphological types. Combining these data enabled them to construct an HIMF over three orders of magnitude in H I mass. Their result is in good agreement with our estimate of the HIMF in the range of H I mass where our survey is sensitive.

The second method is discussed by Briggs & Rao (1993) who analyzed H I observations drawn from the catalogs of Fisher & Tully (1981b) and Hoffman et al. (1989), and recently by Solanes et al. (1996) who use 21cm data of an optical magnitude-limited sample of galaxies in the direction of the Pisces-Perseus supercluster. Both authors arrive at the same values for the normalization and $M^*_{\rm HI}$, but their values of the faint end slope differ significantly. Briggs & Rao (1993) find $\alpha \sim -1.25$ while Solanes et al. find a declining slope. The Solanes et al. result may not be relevant to the discussion here since their sample excluded all dwarf irregular galaxies and contained no galaxies with $M_{\rm HI} < 10^{8.5} \sim \frac{1}{10} M^*_{\rm HI}$. The HIMF determined by Briggs & Rao (1993) is reasonably consistent with with our estimate of the HIMF as shown in Fig. 3.7.

3.5.3 Implications: A new H I selected galaxy population?

The comparison between our result and the HIMFs based on optically selected galaxy samples provides a direct test of the existence of a new population of gas rich galaxies that has gone unnoticed by optical surveys. In a way, this comparison appraises the completeness of optically selected catalogs for gas rich galaxies. Any contribution of uncataloged gas rich dwarf or gas rich LSB galaxies would yield an difference between HIMFs computed from optically selected and HI-selected galaxy catalogs. Fig 3.7 shows that the HIMF derived from the results of the AHISS is in very good agreement with previous estimates based on optically selected galaxy catalogs. This implies that the optically selected samples that have been used to evaluate the HIMF are remarkably complete. There is no evidence for a large number of neutral gas rich objects that have escaped inclusion in these catalogs. To the extent that optically selected catalogs are incomplete for LSB galaxies, the excluded galaxies must be predominantly gas poor, consistent with the finding by Spray berry et al. (1997) that these excluded LSB galaxies are predominantly of low optical luminosity.

Several authors have speculated about the existence of a large class of gas rich dwarf galaxies (e.g., Dekel & Silk 1986, Tyson & Scalo 1988). These galaxies would yield a steep rise in the HIMF below $M_{\rm HI} \approx 10^8 {\rm M}_\odot$. We find no observational support for the existence of this class of galaxies. Based on the counting statistics in the mass bins $10^{6.5}$ to $10^8 {\rm M}_\odot$ we can exclude a faint end slope of $\alpha = -1.7$ or steeper with a 99% confidence level.

3.5.4 Neutral gas density

Our knowledge of $\Omega_{\rm g}$ at high redshift is determined by the statistics of Damped Ly-α systems, seen in absorption against background quasars (e.g., Lanzetta, Wolfe & Turnshek 1995, Storrie-Lombardi, Irwin & McMahon 1996). The picture emerging from these studies is that $\Omega_{\rm g}$ reaches a maximum at $z \approx 3$ and has been declining since then. At low redshifts different effects complicate the determination of $\Omega_{\rm g}$. Firstly, at redshifts $z < 1.6$, the Ly-α line is not redshifted to optical wavelengths and has to be observed from space (Lanzetta et al. 1995, Rao, Turnshek & Briggs 1995). Secondly, the evaluation of $\Omega_{\rm g}$ may depend on the selection effects in the sample of quasars that has been used. Especially at these low redshifts, it is very difficult to compile a unbiased sample of quasars since QSOs would need to be observed within the optical images of galaxies. At the one hand, gravitational lensing can bring faint quasars into the sample which should otherwise be below the detection limit (Smette, Claeskens & Surdej 1997). But on the other hand, dust in Ly-α systems might obscure the background objects to a level where they are undetected (Fall & Pei 1993).

The Arecibo H I Strip Survey can be used to evaluate the gas density differently. The mentioned problems are circumvented since $\Omega_{\rm g}$ is not measured by using the Ly-α line, but the 21cm line in emission.

The space density of H I contained in objects of different H I masses is plotted in Fig. 3.8. The solid line indicates an analytical expression of this function, determined from the product $M_{\rm HI}\Theta(M_{\rm HI})$. The thin line represents the sensitivity limits and the arrows mark upper limits determined analogously to the upper limits in Fig 3.5.

The integral H I mass density at the present epoch can be determined by taking the integral over the solid line in Fig. 3.8. This yields: $\rho_{\rm HI} = \Gamma(2+\alpha)\theta^* M^*_{\rm HI}$, where Γ is the Euler gamma function. Using the best fit Schechter parameters, we derive that

$\rho_{\rm HI}(z=0) = 5.8 \times 10^7\, h\, {\rm M}_\odot\ {\rm Mpc}^{-3}$ or $3.9 \times 10^{-33}\, h\, {\rm g\,cm}^{-3}$, with a statistical error of 20%. A summation over all survey galaxies $\rho_{\rm HI} = \sum M_{\rm HI}/\mathcal{V}_{\rm max}$ yields a slightly smaller value: $\rho_{\rm HI}(z=0) = 5.4 \times 10^7\, h\, {\rm M}_\odot\ {\rm Mpc}^{-3}$ since this calculation does not include the contribution to $\rho_{\rm HI}$ of the density function below $M_{\rm HI} = 10^7 {\rm M}_\odot$ or above $M_{\rm HI} = 10^{10} {\rm M}_\odot$. The cosmological mass density of H I at $z = 0$ is $\Omega_{\rm HI}(z=0) = (2.1 \pm 0.4) \times 10^{-4} h^{-1}$. The total cosmological mass density of neutral gas at the present epoch is $\Omega_g(z=0) = (2.7 \pm 0.5) \times 10^{-4} h^{-1}$, assuming that the mass percentage of He is 25% of the total gas density.

This value agrees surprisingly well with earlier estimates by Rao & Briggs (1993), who find $\rho_{\rm HI}(z=0) = (4.8 \pm 1.1) \times 10^7\, h\, {\rm M}_\odot\ {\rm Mpc}^{-3}$ by using optically selected galaxies. Fall & Pei (1993) arrive at approximately the same value of $\Omega_{\rm HI}$ by simply computing the average $M_{\rm HI}/L_b$ of the Huchtmeier & Richter (1989) catalog and multiplying that by the mean luminosity density in the local universe as estimated by Efstathiou et al. (1988). The agreement between the cosmological mass density based on optically selected galaxies and that based on H I selected galaxies illustrates once more that there is not much neutral gas hidden in objects like LSB galaxies, dwarfs or intergalactic H I clouds that are missed by optical surveys.

The contribution of dwarf galaxies to the H I content of the nearby universe is modest, galaxies with H I masses $< 10^8 {\rm M}_\odot$ make up only $\sim 17\%$ of the integral H I density. The density function in Fig. 3.8 clearly illustrates that the integral H I mass density is dominated by high mass galaxies with H I masses in the range $10^9 {\rm M}_\odot < M_{\rm HI} < 10^{10} {\rm M}_\odot$, which are L^* galaxies. At $M_{\rm HI} \sim 10^{10} {\rm M}_\odot$ the density function drops off sharply, indicating that Malin 1 type galaxies make no significant contribution to $\Omega_{\rm HI}$. This sharp cutoff was al-

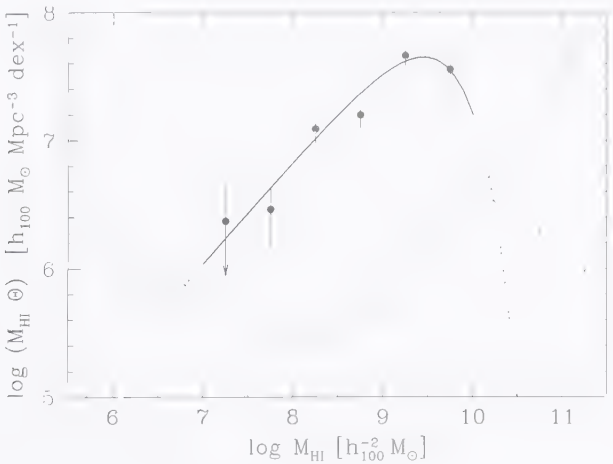

FIGURE 3.8— Space density of H I mass contained in objects of different masses per decade. The fat line shows the converted analytical H I mass function calculated by multiplying $\Theta \times M_{\rm HI}$, where Θ is the HIMF plotted in Fig. 3.5. The dashed regions of the curve indicate that the sample contains no galaxies with $M_{\rm HI} < 10^7 {\rm M}_\odot$ or $M_{\rm HI} > 10^{10} {\rm M}_\odot$. The thin line indicates the sensitivity of the survey. The arrows mark upper limits to the space density of H I mass. The three arrows on the right are from a complementary survey with the Arecibo telescope over the range 19,000 to 28,000 km s^{-1}. Note that galaxies with $10^9 {\rm M}_\odot < M_{\rm HI} < 10^{10} {\rm M}_\odot$ contribute most to the integral H I density.

ready noted by Bothun (1985). Much stronger upper limits to the contribution of galaxies with $M_{\rm HI} > 10^{10}{\rm M}_{\odot}$ will be set in the near future by the results of the Parkes Multibeam Survey (Staveley-Smith et al. 1996).

The estimate of the integral gas density from the AHISS is a robust result. Two effects cause a relatively low uncertainty in the determination of $\Omega_{\rm HI}$. Firstly, the peak in the H I gas density function is conveniently caused by the galaxies that dominate the counting statistics. Galaxies in the lower mass bins, where the Poisson errors are large, contribute not much to the total density and therefore also not much to the uncertainty in $\Omega_{\rm HI}$. Secondly, the effective search volume in the mass region that dominates the density function is mostly band width limited. Uncertainties in $M_{\rm HI}$ and velocity width do not influence the search volume in this regime.

3.5.5 What could be missed?

The question arises which gas rich systems could be missed by the survey and could still contribute significantly to the integral gas mass density in the local universe. The only possible candidates that might escape detection are extremely low gas density systems with H I column densities below $10^{18}{\rm cm}^{-2}$, the detection limit of the AHISS.

It has been shown that the gas density of spiral galaxies is correlated with the optical surface brightness in such a way that lower optical surface brightness implies lower gas densities. De Blok et al. (1996) observed a sample of LSB galaxies and showed that the neutral gas densities are generally a factor of two lower than those of late type high surface brightness galaxies. Furthermore, van der Hulst et al. (1993) has shown that the gas densities of LSB galaxies are often just below or equal to the critical density for star formation. If the relation between optical surface brightness and gas density extends to still lower surface brightnesses this implies that galaxies that most easily escape detection in optical surveys are also the ones that might be missed in 21cm surveys.

Until recently, blind H I surveys were not able to reach column densities much lower than $10^{20}{\rm cm}^{-2}$. These surveys would therefore still miss low density systems, and would not be capable to set strict constraints on the number density of LSB galaxies. However, the AHISS is sensitive to column densities $\sim 10^{18}{\rm cm}^{-2}$ at a 5σ level for gas filling the beam. Using an extrapolation of the scaling of Disney & Banks (1997), $N_{\rm HI} = 10^{20}(M_{\rm HI}/L_B)10^{0.4(27-\mu_B)}$, where μ_B is the surface brightness averaged over the H I disk, and a typical value of $M_{\rm HI}/L_B = 1$ for LSB galaxies, the AHISS would be capable of finding galaxies with $\mu_B = 32$ mag arcsec^{-2}. Even if a ten times lower value of $M_{\rm HI}/L_B$ is used, and if the area of the galaxy were ten times smaller than the area covered by the Arecibo beam, still galaxies as faint as $\mu_B = 27$ mag arcsec^{-2} would be detectable.

The VLA observations of the AHISS galaxies can be used to set lower limits to average column densities for the sample. Due to the low spatial resolution of the observations ($\sim 1'$), the measured column density is in many cases an average $\langle N_{\rm HI}\rangle$ over the entire projected surface of the H I layer of the galaxy. If the galaxy is spatially unresolved, an upper limit to the extent $D_{\rm HI}$ of the H I layer can be determined, leading to a lower limit of the average column density $\langle N_{\rm HI}\rangle \propto M_{\rm HI}D_{\rm HI}^{-2}$. Although many of the galaxies in the sample are unresolved, and many of the true values of $\langle N_{\rm HI}\rangle$ may be higher, we find no values of $\langle N_{\rm HI}\rangle$ below $10^{19.7}{\rm cm}^{-2}$. Hence, all galaxies in the sample have normal H I column densities, even though there are no observational selection effects against finding extreme low density systems. There is no indication of the existence of a group of extreme low column density galaxies that has been missed by previous H I surveys, simply because

they were not capable of reaching the same low column densities as the AHISS. Because we seem to be observing a lower limit to $\langle N_{\rm HI} \rangle$, much higher than our detection limit, it is very unlikely that galaxies with even lower column densities are missed by the AHISS.

Theoretical predictions of the ionization of gas layers by the extragalactic UV background (Corbelli & Salpeter 1993, Maloney 1993, Charlton, Salpeter & Linder 1994) demonstrate physical mechanisms that can explain the possible non-existence of low column density neutral gas layers. These models predict photoionization by the extragalactic UV background of low column density regions, below $10^{19.5}{\rm cm}^{-2}$. Furthermore, models by Quinn, Katz & Efstathiou (1996) show that the ionization only moderately suppresses the formation of galaxies with rotational speeds larger than 50 km s^{-1}, but that it seriously affects the low density regions around these systems. The models are verified by very deep VLA observations on one galaxy which appears to have a sharp truncation of the HI disk below a column density of $10^{19.5}{\rm cm}^{-2}$ (van Gorkom et al. 1993). Further confirmation of ionization of low density HI comes from recent observations by Bland-Hawthorn et al. (1997) who have detected ionized gas beyond the truncated HI disk in NGC 253.

3.5.6 H I self absorption

The calculation of the total H I masses in this chapter is based on the assumption that the optical depth of the H I layer is close to zero. Any possible influence of H I self absorption, which will cause an underestimation of the true H I mass, is ignored. In this paragraph we will make a rough estimate of the influence of H I self absorption on the determination of the cosmological mass density $\Omega_{\rm HI}$ and the HIMF. The possible effect of self absorption could apply to all HIMFs compared in this paper (see Section 3.5.1, 3.5.2 and Fig. 3.7), since none of these have addressed this possibility.

The problem of self absorption for galaxies can be assessed statistically by plotting the 21cm flux of different Hubble types as a function of inclination i to the line of sight. The line of sight through a inclined galaxy will be larger, generally causing a higher fraction of self absorption. Haynes & Giovanelli (1984) use data of a sample of 1500 galaxies with 21cm fluxes measured with Arecibo. They define a correction factor $f_{\rm HI}$ which is defined by the corrected flux divided by the measured flux and find a general trend: $f_{\rm HI} = (\cos i)^{-c}$ where c is a constant dependent on morphological type. The values of c are found to be 0.04 for Sa and Sab, 0.16 for Sb and 0.14 for Sbc and Sc galaxies. No correlations are found for morphological types earlier than Sa or later than Sc, indicating that self absorption is negligible in these types. Higher self absorption in types Sb to Sc can be explained by the fact that these galaxies generally have the highest H I surface densities (Cayatte et al. 1994). Furthermore, rotation curves of early type spiral galaxies show the strongest deviations from solid body rotation implying large velocity spreads per line of sight, which further decreases self absorption.

Mean self absorption factors per morphological type can be obtained by averaging $f_{\rm HI}$ over a random distribution of inclinations. This yields

$$\langle f_{\rm HI} \rangle = \frac{\int_0^{\pi/2} (\cos i)^{-c} \sin i \, di}{\int_0^{\pi/2} \sin i \, di} = 1/(1-c). \qquad (3.9)$$

The mean correction factors then become 1.04 for Sa and Sab, 1.19 for Sb and 1.16 for Sbc and Sc galaxies.

The cosmological H I mass density is dominated by high mass galaxies, which are statistically most likely to be late type spirals. The correction to $\Omega_{\rm HI}$ due to H I self absorption will therefore probably not be more than the value of $\langle f_{\rm HI} \rangle$ averaged over morphological types Sb to Sd. Assuming that all types Sb to Sd contribute equally to $\Omega_{\rm HI}$, we derive that the mean value of $\langle f_{\rm HI} \rangle$ is 1.10. Even in the most pessimistic approach, the correction factor can not be more than 1.19.

What will be the effect of H I self absorption on the shape of the HIMF? Using the same arguments as above, we conclude that the effect on the high mass range will be marginal. The normalization factor θ^* and the value which determines the kink, $M^*_{\rm HI}$, will probably increase by no more than 10%. Galaxies that determine the faint end slope α are mostly dwarf and LSB galaxies. On the one hand, self absorption may be unimportant because the gas density in these galaxies is usually low (van der Hulst 1993) and the dust content is presumably low (McGaugh 1994) which implies scarcity of clumped gas (Haynes & Giovanelli 1984). On the other hand, the rotation curves of dwarf and LSB galaxies often show solid body rotation (de Blok et al. 1996, Swaters 1997) which causes a low velocity spread along a line of sight, leading to high fractions of self absorption. These two counteracting effects make the value of $\langle f_{\rm HI} \rangle$ for low mass galaxies uncertain, but probably higher than that for high mass galaxies. After applying the correction factor to the low mass galaxies, some galaxies will shift to higher mass bins, eventually leading to a slightly shallower faint end slope of the mass function. The conclusion that the faint end slope of the mass function is shallow will therefore not be altered by the effects of H I self absorption.

3.6 Conclusions

We have used the Arecibo H I Strip Survey in combination with 21cm follow-up observations with the VLA to determine the H I mass function of gas rich galaxies in the local universe. The resulting HIMF is in good agreement with earlier estimates based on samples of optically selected galaxies. This implies that there is not a large population of gas rich dwarfs or low surface brightness galaxies, previously undetected by optical surveys. The observed faint end slope of the HIMF is flat ($\alpha \sim -1.2$) leaving no room for a large class of gas rich dwarfs. The cosmological mass density of H I in the local universe is $\Omega_{\rm HI}(z=0) = (2.1 \pm 0.4) \times 10^{-4} h^{-1}$, also consistent with earlier estimates. The neutral gas content is dominated by high mass galaxies with $10^9 {\rm M}_\odot < M_{\rm HI} < 10^{10} {\rm M}_\odot$. The observations indicate the existence of a lower limit to the average H I column density of 19.7 cm^{-2}, consistent with theoretical predictions concerning the ionizing extragalactic UV background.

Acknowledgments

We thank G. Bothun, E. de Blok, P. Sackett, A. Szomoru, M. Verheijen, and the referee J. van Gorkom for useful comments.

References

Bland-Hawthorn, J., Freeman, K. C., Quinn, P. J. 1997, ApJ, 490, 143
Bothun, G. B. 1985, 90, 1982
Bothun, G. B., Beers, T., Mould, J., & Huchra, J. 1986, ApJ, 308, 510
Briggs, F. H. 1990, AJ, 100, 999
Briggs, F. H., & Rao, S. 1993, ApJ, 417, 494

Briggs, F. H., Sorar, E., Kraan-Korteweg, R. C., & van Driel, W. 1997, PASA, 14, 37
Cayatte, V., Kotanyl, C., Balkowski, C., & van Gorkom, J. H. 1994, AJ, 107, 1003
Charlton, J. C., Salpeter, E. E., & Linder, S. M. 1994, ApJ, 430, L29
Christensen, C. G. 1975, AJ, 80, 282
Corbelli, E., Salpeter, E. E. 1993, ApJ, 419, 104
Dalcanton J. J., Spergel, D. N., & Summers, F. J. 1997, ApJ, 482, 659
de Blok, W. J. G., McGaugh, S. S., & van der Hulst, J. M. 1996, MNRAS, 283, 18
Dekel, A. & Silk, J. 1986, ApJ, 303, 39
Disney, M. J. 1976, Nature, 263, 573
Disney M. J. & Banks, G. 1997, PASA, 14, 69
Eder, J. A., Oemler, A. Jr., Schombert, J. M., & Dekel, A. 1989, ApJ, 340, 29
Efstathiou, G., Ellis, R. S., & Peterson, B. A. 1988, MNRAS, 231, 479
Fall, S. M. & Pei, Y. C. 1993, ApJ, 402, 479
Fisher, J. R. & Tully, R. B. 1981a, ApJS, 47, 139
Fisher, J. R. & Tully, R. B. 1981b, ApJ, 243, L23
Geller, M. J. & Huchra, J. P. 1989, Science, 246, 897
Giovanelli, R. & Haynes, M. P. 1989, ApJ, 346, L5
Giovanelli, R. & Haynes, M. P. 1985, AJ, 90, 2445
Haynes, M. P. & Roberts, M. S. 1979, ApJ, 227, 767
Haynes, M. P. & Giovanelli, R. 1984, AJ, 89, 758
Henning, P. A. 1992, ApJS, 78, 365
Henning, P. A. 1995, ApJ, 450, 578
Hoffman, G. L., Lewis, B. M., Helou, G., Salpeter, E. E., & Williams, B. M. 1989, ApJS, 69, 65
Hoffman, G. L., Lu, N. Y., & Salpeter, E. E. 1992, AJ, 104, 2086
Huchtmeier, W. K., & Richter, O. -G. 1989, A General Catalog of H I Observations of Galaxies: The Reference Catalog (New York: Springer-Verlag)
Kerr, F. J., & Henning, P. A. 1987, ApJ, 320, L99
Krumm, N., & Brosch, N. 1984, AJ, 89, 1461
Lanzetta, K. M., Wolfe, A. M., & Turnshek, A. M. 1995, ApJ, 440, 435
Lin, H., Kirshner, R. P., Shectman, S. A., Landy, S. D., Oemler, A., Tucker, D. L., & Schechter, P. L. 1996, ApJ, 464, 60
Lo, K. Y. & Sargent, W. L. W. 1979, ApJ, 227, 756
Lo, K. Y., & Sargent, W. L. W., & Young, K. 1993, AJ, 106, 507
Maloney, P. 1993, ApJ, 414, 41
Marzke, R. O., Geller, M. J., & Huchra, J. P. 1994, AJ, 108, 437
McGaugh, S. S. 1994, ApJ, 426, 135
McGaugh, S. S. 1996, MNRAS, 280, 337
McMahon, P. M. 1993, Ph.D. Thesis, Columbia University
Mo, H. J., McGaugh, S. S., & Bothun, G. D. 1994, MNRAS, 267, 129
Quinn, T., Katz, N., & Efstathiou, G. 1996, MNRAS, 278, L49
Rao, S. & Briggs, F. H. 1993, ApJ, 419, 515
Rao, S., Turnshek, A. M., & Briggs, F. H. 1995, ApJ, 449, 488
Salpeter, E. E. & Hoffmann, G. L. 1996, ApJ, 465, 595
Saunders, W., Rowan-Robinson, M., Lawrence, A., Efstathiou, G., Kaiser, N., Ellis, R. S., & Frenk, C. S. 1990, MNRAS, 242, 318
Schechter, P. 1976, ApJ, 203, 297
Schmidt, M. 1968, ApJ, 151, 393
Schneider, S. E. 1989, ApJ, 343, 94
Schneider, S. E. 1997, PASA, 14, 99
Schombert, J. M., Bothun, G. D., Schneider, S. E., & McGaugh, S. S. 1992, AJ, 103, 1107
Shostak, G. S. 1977, A&A, 54, 919

Smette, A., Claeskens, J. -F., & Surdej, J. 1997, NewA, 2, 53
Solanes, J. M., Giovanelli, R., & Haynes, M. 1996, ApJ, 461, 609
Sorar, E. 1994, Ph.D. Thesis, University of Pittsburgh
Spitzak, J. G. 1996, Ph.D. Thesis, University of Massachusetts
Sprayberry, D., Impey, C. D., Irwin, M. J., & Bothun, G. D. 1997, ApJ, 482, 104
Staveley-Smith, L., Wilson, W. E., Bird, T. S., Disney, M. J., Ekers, R. D., Freeman, K. C., Haynes, R. F., Sinclair, M. W., Vaile, R. A., Webster, R. L., & Wright, A. E. 1996, PASA, 13, 243
Storrie-Lombardi, L. J., Irwin, M. J., & McMahon, R. G. 1996, MNRAS, 282, 1330
Swaters, R. A., 1997, in preparation
Szomoru, A., Guhathakurta, P., van Gorkom, J. H., Knapen, J. H., Weinberg, D. H., & Fruchter, A. S. 1994, AJ, 108, 491
Szomoru, A., van Gorkom, J. H., Gregg, M. D., & Strauss, M. A. 1996, AJ, 111, 2150
Taylor, C. L. 1997, ApJ, 480, 524
Thuan, T. X., Gott, J. R., & Schneider, S. E. 1987, ApJ, 315, L93
Thuan, T. X., Alimi, J.-M., Gott, J. R., & Schneider, S. E. 1991, ApJ, 370, 25
Tully, R. B., & Fisher, J. R., 1977, A&A, 54, 661
Tyson, N. D., & Scalo, J. M. 1988, ApJ, 329, 618
van der Hulst, J. M., Skillman, E. D., Smith, T. R., Bothun, G. D., McGaugh, S. S., & de Blok, W. J. G. 1993, AJ, 106, 548
van Gorkom, J. H., et al. 1993, in The Environment and Evolution of Galaxies, ed. J. M. Shull and H. A. Thronson (Dordrecht: Kluwer), 345
Weinberg, D. H., Szomoru, A., Guhathakurta, P., & van Gorkom, J. H. 1991, ApJ, 372, L13

4

The Luminosity Function and Surface Brightness Distribution of Galaxies from a Deep Survey in the 21cm Line

M. A. Zwaan, F. H. Briggs, & D. Sprayberry

ABSTRACT — We measure the $z = 0$ luminosity function for galaxies selected in a blind H I survey. The LF is flat and in good agreement with LFs of optically selected late-type galaxies. The Schechter parameters are $\alpha = -1.03^{+0.25}_{-0.15}$ and $M^* = -19.38^{+1.02}_{-0.62} + 5\log h_{100}$ mag. Gas rich galaxies constitute 50% of the integral luminosity density of the local Universe. The number density of very low surface brightness (> 24.0 mag arcsec^{-2}) gas rich galaxies is considerably lower than what is found in optical surveys designed to detect dim galaxies. This implies that the population of LSB galaxies is only partly gas rich and an additional population of gas poor LSB galaxies must exist. However, we show that this gas poor population must be cosmologically insignificant in baryon content. The contribution of gas rich LSB galaxies (> 23.0 mag arcsec^{-2}) to the local cosmological gas and luminosity density is modest (18% and 5%), their contribution to $\Omega_{\rm matter}$ is not well-determined, but probably < 11%. These values are in excellent agreement with the results from the Hubble Deep Field. Bivariate distribution functions of several galaxy parameters show that the H I density in the local Universe is more widely spread over galaxies with different size, surface brightness, and luminosity than the luminosity density.

4.1 Introduction

UNDERSTANDING GALAXY EVOLUTION requires well-determined local benchmarks. One of the most fundamental of these is the field galaxy luminosity function, the shape of which should be predicted by any reliable galaxy formation theory. In principle, the shape of the luminosity function is related to the power spectrum of primordial density fluctuations and complex processes such as gas cooling, star formation and feedback to the interstellar medium as well as the behaviour of dark matter as it undergoes gravitational collapse and merging in galaxy halos (see e.g., Cole et al. 2000 for a recent review). Reference points in the local Universe will help in developing a full understanding of these processes. Another motive for determination of the local luminosity function, is the problem of the faint blue galaxies. The normalization of the $z = 0$ luminosity function seems to be too low to be reconciled with no-evolution predictions based on intermediate redshift ($z \sim 1$) surveys (Ellis 1997; Broadhurst, Ellis & Shanks 1988; Koo & Kron 1992), but to quantify this problem a reliable measurement of the faint end slope is essential.

The last few years have seen a proliferation of published luminosity functions from optical redshift surveys of the local ($z < 0.2$) Universe (see e.g., Zucca et al. 1997; Ratcliffe et al. 1998; and Folkes et al. 1999 for some recent examples). These surveys systematically produce samples of 10^4 galaxies and are able to determine the luminosity function down to absolute magnitude limits of $M_B = -14$. However, considerable uncertainty remains about the exact shape and normalization of the luminosity function. Especially the faint-end slope for the dwarf galaxies ($M_B > -18$) is practically unconstrained (see discussion in Driver & Phillipps 1996).

A potential cause of the uncertainty in low z galaxy counts is the surface brightness selection effect (Disney 1976; Disney & Phillips 1987). Sprayberry et al. (1997) specifically searched for the low surface brightness (LSB) galaxies in the APM survey (Impey et al. 1996), and concluded that including LSB galaxies in the low z census steepens the field luminosity function, but still does not close the gap between number counts at moderate redshift and $z = 0$.

The discussion on LSB galaxies ties in directly with another important benchmark at $z = 0$: the distribution function of optical surface brightnesses. Based on photometry of 36 nearby spiral and S0 galaxies, Freeman (1970) concluded that $\sim 80\%$ have a B band central surface brightness $\mu_B(0)$ in the range 21.65 ± 0.30 mag arcsec^{-2}. The eight deviant galaxies consisted of one dwarf irregular LSB galaxy ($\mu_B(0) = 23.7$ mag arcsec^{-2}) and seven brighter galaxies of various morphological type. The consensus at the present moment seems to be that the distribution function is flat (McGaugh 1996; de Jong 1996; Dalcanton et al. 1997b; O'Neil & Bothun 2000). However, Tully & Verheijen (1997) have a dissenting view and present evidence for bimodality in the distribution of near-infrared surface brightnesses in the Ursa Major Cluster. This view has been contested by Bell & de Blok (2000) who claim that the data set is insufficient to establish the presence of a bimodal surface brightness distribution.

New insight in both issues can be obtained by selecting galaxies via a method that is free from optical selection effects. In this paper we measure for the first time the optical luminosity function and surface brightness distribution function of H I selected galaxies. This sample is the result of the Arecibo H I Strip Survey, a blind strip survey in the 21cm line. We stress that this sample is small (60 members) compared to those produced by modern redshift surveys, and large statistical errors are therefore unavoidable. This work

should be regarded as the first step toward measuring these functions for H I selected galaxy samples. Much larger galaxy samples will be available in the near future, and the measurements of optical luminosity functions, surface brightness functions and bivariate distributions will greatly improve.

We organize this chapter as follows. First, in section 4.2, we briefly describe the sample. In section 4.3 we present the optical luminosity function of this H I selected galaxy sample, and discuss the distribution of luminosity density and H I gas density among different galaxies. In section 4.4 the surface brightness distribution function and the contribution of LSB galaxies to the mass density of the local Universe are discussed. Bivariate distribution functions of various galaxy parameters are presented in section 4.5. Finally, in section 4.6 we summarize the conclusions. Throughout this chapter we use $H_0 = 100\,h_{100}\,\mathrm{km\,s^{-1}\,Mpc^{-1}}$ for calculating distance dependent quantities.

4.2 The data

The sample of galaxies used here to measure distribution functions of optical luminosity and central surface brightness is selected in the 21cm line, and it is therefore free from selection effects related to optical surface brightness. The sample is the result of the Arecibo H I Strip Survey (AHISS), a blind extragalactic H I survey consisting of two strips of constant declination, together covering approximately 65 square degrees of sky over a depth of $cz = 7500$ km s^{-1}. The limiting column density was $\approx 10^{18}\mathrm{cm}^{-2}$ (5σ) for gas filling the telescope beam. Details of the survey and the reduction are described by Sorar (1994) and Chapter 3. In total 66 galaxies have been detected, 61 of which are observed in the optical B-band with the 2.5m Isaac Newton Telescope (INT) on the island of La Palma. Low resolution 21cm aperture synthesis observations have been obtained with the Very Large Array. In Chapter 2 we presented the optical and 21cm data, and discussed the properties of these H I selected galaxies.

4.3 Luminosity functions

The luminosity function (LF) of galaxies is defined as the number of galaxies per cubic Mpc in a luminosity interval dM centered at magnitude M. The interval dM is generally taken to be 1 mag. The most used parameterization of the luminosity function is the Schechter (1976) function defined by

$$\phi(M)dM = 0.4 \ln 10\, \phi^* \,[10^{0.4(M^*-M)}]^{1+\alpha} \exp[-10^{0.4(M^*-M)}]\, dM, \qquad (4.1)$$

where α is the faint-end slope, ϕ^* is the normalization factor and M^* is the characteristic absolute magnitude at that define the boundary between the exponential and power-law part.

4.3.1 Methods

Many different galaxy luminosity function estimators can be found in the literature. In Chapter 3 we discuss different luminosity function estimators and conclude that the $\Sigma(1/V_{\mathrm{max}})$ method is the preferred way to determine mass functions and luminosity functions for our sample. We demonstrated that the determination of H I mass function with this method is not sensitive to density fluctuations due to large scale structure. The $\Sigma(1/V_{\mathrm{max}})$ method consists of summing the reciprocals of the volumes corresponding

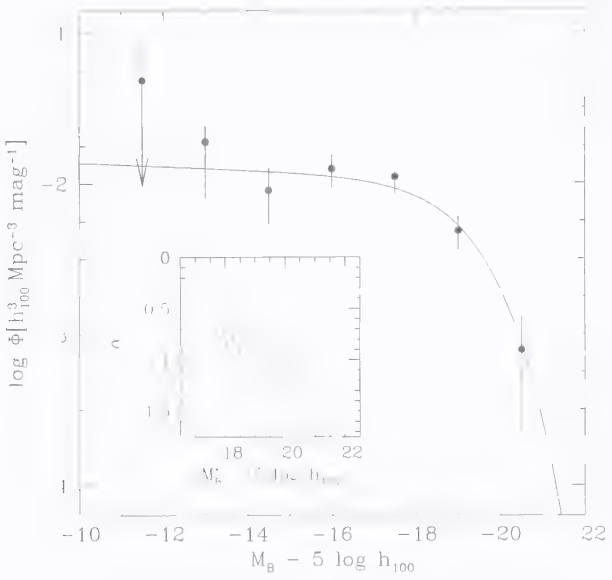

FIGURE 4.1— Luminosity function for H I selected galaxies. The points were determined using the V_{max} method, the errorbars are 1σ uncertainties from Poisson statistics. The line is the best fit Schechter function with parameters: $\alpha = -1.03^{+0.25}_{-0.15}$, $M^* = -19.38^{+1.02}_{-0.62} + 5\log h_{100}$ mag and $\phi^* = (1.15 \pm 0.40) \times 10^{-2} h_{100}^{-3}\mathrm{Mpc}^{-3}$. The inset shows the 1σ and 2σ joint two-parameter confidence levels for α and M^*.

to the maximum distances at which galaxies could be seen and still remain within the sample. Summing these values per bin in H I mass or absolute magnitude immediately gives the binned H I mass function or optical luminosity function. The advantages of the $\Sigma(1/V_{max})$ method are that it is automatically normalized and non-parametric; it recovers the amplitude and the shape of the luminosity function simultaneously, without using the Schechter function as an assumption about the intrinsic shape. An overview of the different galaxy luminosity function estimators is given by Willmer (1997), who tests the validity of different methods by means of Monte-Carlo simulations. Careful examination of his tables shows that the $\Sigma(1/V_{max})$ method (with binning in magnitudes) recovers the input luminosity function satisfactorily, and equally well as the more conventional parameterized maximum likelihood method (Sandage, Tammann & Yahil 1979) or the Stepwise Maximum Likelihood Method (SWLM, Efstathiou, Ellis & Peterson 1988). Supported by this, we choose to apply the $\Sigma(1/V_{max})$ method to evaluate the optical luminosity function. The details of the determination of the values of V_{max} are described in Chapter 3 and will not be repeated here.

4.3.2 Results

The resulting luminosity function $\phi(M_B)$ is shown in Figure 4.1 as solid dots with 1σ errorbars. The data are binned per 1.5 mag in order to obtain a reasonable number of galaxies per bin, but scaled in such a way that ϕ represents number densities per magnitude bins. Furthermore, the data are multiplied by a factor 66/60 to account for the galaxies for which no optical information is available. To enable direct comparison with published luminosity functions, we choose to use the absolute magnitudes uncorrected for opacity effects in the galactic disk (see Leroy & Portilla [1998] for a discussion on the influence of optical depth effects on the shape of the luminosity function). The line indicates the best fit Schechter function which is determined by minimizing χ^2 for the expected number of galaxies per bin. The uncertainties in the best fit are indicated

in the inset that shows the 1σ and 2σ error contours of the χ^2 fit for α and M^* fitted jointly. As is usually the case in these fits, the parameters α and M^* are strongly correlated in the sense that steeper faint end slopes imply brighter values of M^*. The best fit Schechter parameters are found to be $\alpha = -1.03^{+0.25}_{-0.15}$, $M^* = -19.38^{+1.02}_{-0.62} + 5\log h_{100}$ mag and $\phi^* = (1.15 \pm 0.40) \times 10^{-2}\, h_{100}^{3}\mathrm{Mpc}^{-3}$, where the quoted errors are 1σ one-parameter uncertainties. The uncertainties given here are solely the result of counting statistics, and therefore may understate the true uncertainties. Measurement errors in the parameters that define $V_{\max}$ and measurement errors in M_B also contribute to the uncertainties, but these are relatively small compared to the Poisson errors for this small sample.

The parameterization in the form of a Schechter function is a satisfactory representation of luminosity function of the AHISS galaxies. However, due to the small number of galaxies in the low luminosity bins, the value of the faint end slope α is poorly constrained. Especially for magnitudes fainter than $M_B = -14$, the slope of the LF is almost unconstrained. There is no need for a modification of the LF, such as the Schechter function plus a power law, proposed by Sprayberry et al. (1997) for his sample of LSB galaxies, although our present sample does not rule out this extra component.

4.3.3 Comparison with optical determinations of the LF

It is interesting to compare the luminosity function for H I selected galaxies to luminosity functions of optically selected galaxies. Recently, there has been much interest in steep faint-end slopes of the luminosity function, and the galaxies responsible for this steep part 1) are found to be of late morphological type (e.g., Marzke et al. 1998), 2) show strong emission lines indicative of star active formation (e.g., Zucca et al. 1997), and 3) have blue colors (Lin et al. 1999). These are the types of galaxies that are expected to contain high fractions of H I, and therefore should be included in the AHISS sample.

A vast number of luminosity functions based on optical redshift redshift surveys, is available in the literature. All these surveys contain typically a few thousand galaxies. When making a comparison with our luminosity function for H I selected galaxies, we will concentrate on those studies which have made a specific distinction between late and early type galaxies, or star forming and quiescent galaxies. We consider: the Stromlo-APM redshift survey (APM, Loveday et al. 1992), the Center for Astrophysics redshift survey (CfA, Marzke et al. 1994), the ESO Slice Project (ESP, Zucca at al. 1997), the Las Campanas Redshift Survey (LCRS, Lin et al. 1996), the Autofib Redshift Survey (ARS, Heyl et al. 1997), the Second Southern Sky Redshift Survey (SSRS2, Marzke et al. 1998), the CNOC Field Galaxy Redshift Survey (CNOC2, Lin et al. 1999) and preliminary results from the 2dF survey (Folkes et al. 1999).

Table 4.1 summarizes the Schechter parameters of "late type" luminosity functions of these surveys. In Figure 4.2 these functions are represented, together with our measured points and the best fit Schechter function. The functions have been transformed to the B filter using the conversions $M_B = M_Z - 0.45$ for the CfA, $b - r = 1.1$ for the LCRS, and $M_B - M_{bJ} = 0.24$, and all functions are recalculated for $H_0 = 100\, h_{100}\,\mathrm{km\,s^{-1}\,Mpc^{-1}}$.

The direct comparison of these luminosity functions is rather naive for a number of reasons. Firstly, different optical wave bands have been used in the selection of these galaxies. This effect can be corrected for by applying a magnitude correction, but this is most certainly a oversimplification of the problem. The use of different wave bands does not only have an influence on the luminosity of the selected galaxies but surely also on the morphological classifications. Secondly, the separation between late and early type galaxies

TABLE 4.1— Comparison of Luminosity Functions for Late Type Galaxies

Sample	Selection	α	$M^* - 5\log h_{100}$	$\phi^{*\,a}$	$\rho_L{}^b$
AHISS	H I selected	−1.03	19.38	11.5	10.3 ± 2.0
APM (Loveday 1992)	Sp/Irr	−0.80	−19.16	10	6.7
CfA (Marzke 1994)	Sa-Sb	−0.58	−18.93[c]	8.7	8.9
	Sc-Sd	−0.96	−19.02[c]	4.4	
	Sm-Im	−1.87	−19.00[c]	0.6	
ESP (Zucca 1997)	Emission lines	−1.40	−19.23	10	11.4
LCRS (Lin 1997)	3727 $W_\lambda \geq 5$ A	−0.90	−18.93[d]	13	7.7
Autofib (Heyl 1997)	Sab	−0.99	−19.76	2.19	8.4
	Sbc	−1.25	19.16	2.80	
	Scd	−1.37	−18.96	3.01	
	Sdm	−1.36	−18.76	0.50	
SSRS2 (Marzke 1998)	Spirals	−1.11	−19.43	8.0	9.2
	Irr/Pec	−1.81	−19.78	0.2	
CNOC2 (Lin 1999)[e]	Intermediate type	−0.53	18.97	9.0	11.1
	Late type	−1.23	−19.07	7.2	
2dF (Folkes 1999)	Sab	−0.86	−19.44	3.9	14.0
	Sbc	−0.99	−19.14	5.3	
	Scd	−1.21	−18.76	6.5	
	Sdm-Im	−1.73	−18.78	2.1	

[a] Units are $10^{-3}\,h_{100}^3\,\mathrm{Mpc}^{-3}$
[b] Units are $10^7\,h_{100}\,\mathrm{L}_\odot^B\,\mathrm{Mpc}^{-3}$
[c] $B - M_Z = -0.21$
[d] $B - R = 1.1$
[e] Values extrapolated to $z = 0$

has been made in different ways for each sample. In the CfA sample a detailed separation between morphological types has been made on the basis of the galaxies' appearances on Palomar Sky Survey. Also the SSRS2 and the APM samples have been classified by visual inspection. The CNOC2 data is split into different populations using color information of the galaxies. For the 2dF and Autofib surveys spectral information has been used to make the classifications. The selection criteria for the ESP and the LCRS samples has been the occurrence of emission lines in the spectra. In the LCRS sample a distinction has been made on basis of the criterion of OII 3727 $W_\lambda \geq 5$ Å, in the EPS sample the selection was simply based on the detection the OII line.

With these restrictions in mind, we can compare the different luminosity functions for optically selected galaxies with H I selected galaxies. What is particularly striking is that the values of the faint-end slope span a wide range from −0.80 for the APM survey to ~ -1.50 for the ESP and 2dF surveys. Even for surveys that use comparable methods for classifying their different galaxy population, the differences in faint-end slope can be large. Evidently, the shape of the luminosity distribution of late type galaxies is still ill-constrained. On the other hand, the normalization and the value that defines the knee are quite similar for all surveys; all functions cross approximately the same point at $M_B \approx -19 + 5\log h_{100}$. The luminosity function for the AHISS falls in between those of the optical samples. We therefore conclude that our estimate of the luminosity function is in good agreement with that of optically selected samples.

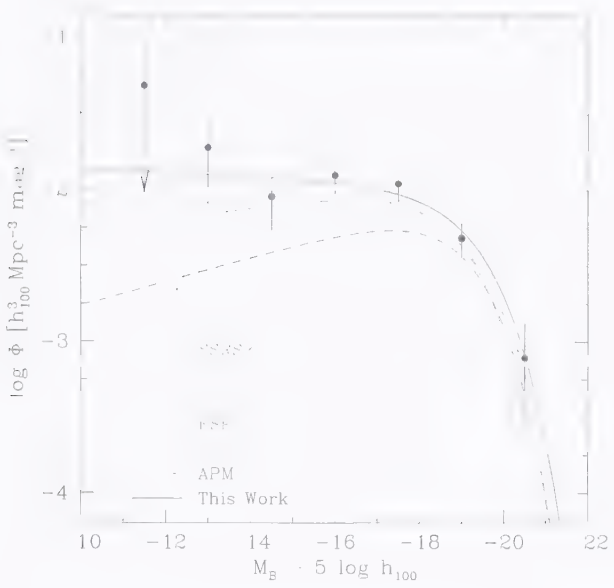

FIGURE 4.2— Luminosity functions for late type galaxies. The points are the same as in Figure 4.1. The lines show the luminosity functions from several recent redshift surveys. The details are given in Table 4.1. Some of these are the summations of several luminosity functions for different types.

4.3.4 Luminosity density of gas rich galaxies

A more fundamental parameter is the luminosity density, the integrated light from the whole population of galaxies. As is discussed by Lilly et al. (1996), this parameter is in principle less dependent on the details of galaxy evolution than the luminosity function. The integral luminosity density of late type galaxies can be determined by integrating the luminosity function weighted by luminosity, which gives $\rho_{L_B} = \phi^* L_B^* \Gamma(2+\alpha)$, where Γ is the Euler gamma function. The values of ρ_{L_B} for late-type galaxies as determined by the different optical surveys is given in the last column of Table 4.1. It is remarkable that all values of ρ_{L_B} are within $\sim 1.5\sigma$ from the value determined from the AHISS. A notable exception is the 2dF survey that finds a value 60% higher than the mean of the other surveys. Folkes et al. (1999) note that the 2dF results are preliminary, and that corrections for completeness, clustering, and Malmquist-bias have not been applied yet. It remains to be seen whether the final 2dF results will remain in excess of the AHISS estimate of ρ_{L_B}.

The mean value of ρ_{L_B} of all optically selected galaxy samples is $9.7 \times 10^7\, h_{100}\, L_\odot^\prime\, \mathrm{Mpc}^{-3}$, while that for the AHISS sample is $(10.3 \pm 2.0) \times 10^7\, h_{100}\, L_\odot^\prime\, \mathrm{Mpc}^{-3}$. This latter value translates to $\rho_{L_B} = (3.4 \pm 0.7) \times 10^{19}\, h_{100}^{-2}\, \mathrm{W\,Hz^{-1}\,Mpc^{-3}}$, using the conversion of Lilly et al. (1996). This is approximately 50% of the integral luminosity density of the local Universe (see Lilly et al. 1996).

4.3.5 Intermezzo: Luminosity and H I mass distributions for different morphological types

A more detailed view of the relative importance of different morphological types to the H I and luminosity density can be made be transforming luminosity functions into H I mass functions, assuming correlations between H I mass and optical luminosity. Rao & Briggs (1993) used this method to determine the H I mass function and $\Omega_{\rm HI}$ based on at that time available luminosity functions. They showed that by adopting the relation $\log M_{\rm HI} = a - bM_B$ between H I mass and optical luminosity, the H I mass function can be

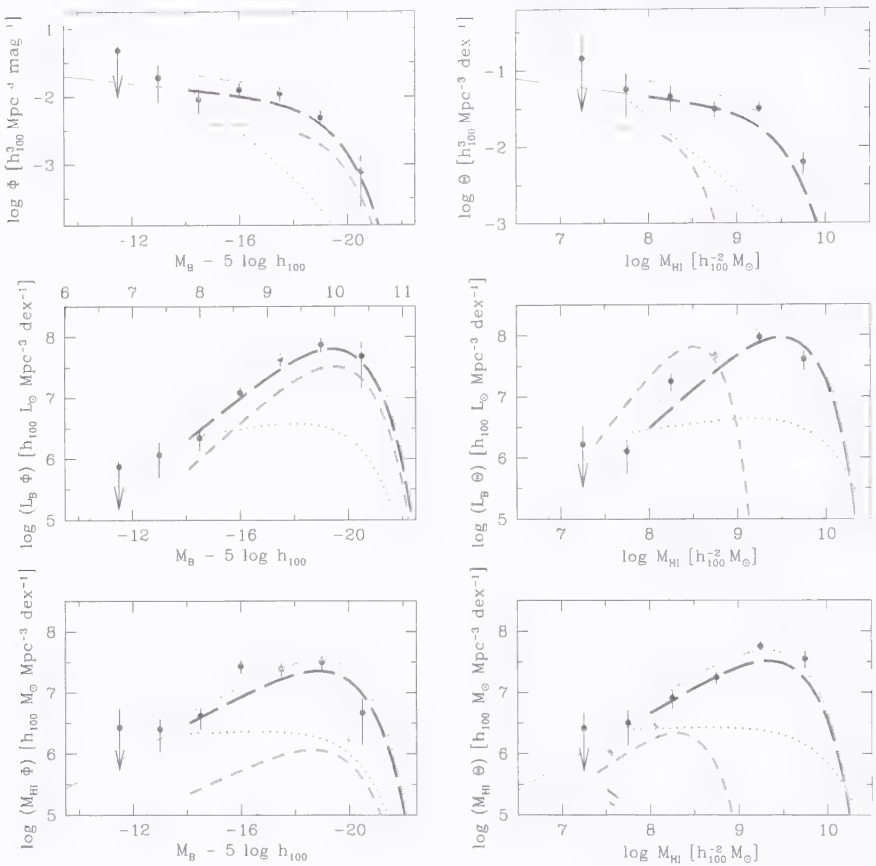

FIGURE 4.3— Luminosity and H I density functions for different morphological types. The points are from the AHISS and are the result of the $1/V_{max}$ method. The lines are converted functions for different morphological types, using Marzke et al. (1998) luminosity functions, and H I to M_B relations from the Nearby Galaxy Catalog (Tully 1988). The solid grey lines are for all galaxy types, the black dashed lines for spirals, the grey dashed lines for E and S0, and the grey dotted lines for Irr/Pec. The thin parts of each line are extrapolations beyond the confidence levels set by Marzke et al. (1998). *Upper left panel*: Luminosity function. *Upper right panel*: H I mass function. *Middle left panel*: Luminosity density as a function of M_B. *Middle right panel*: Luminosity density as a function of M_{HI}. *Lower left panel*: H I density as a function of M_B. *Lower right panel*: H I density as a function of M_{HI}.

written as

$$\Theta(M_{\rm HI})d(M_{\rm HI}) = \frac{0.4}{b}\,\phi^*\,(\frac{M_{\rm HI}}{M^*_{\rm HI}})^{(\alpha+1)\frac{0.4}{b}-1}\,\exp-(\frac{M_{\rm HI}}{M^*_{\rm HI}})^{\frac{0.4}{b}}\,d(\frac{M_{\rm HI}}{M^*_{\rm HI}}), \qquad (4.2)$$

where $\log M^*_{\rm HI} = a - bM^*_B$, and α and ϕ^* are the Schechter parameters of the luminosity functions.

Here we update the calculations by Rao & Briggs (1993) with more recent luminosity function parameters, and test if the results are in agreement with our measurements. For

completeness, we present all possible ways of plotting the number density, the H I density, and the luminosity density as a function of absolute magnitude and H I mass. We adopt the Marzke et al. (1998) luminosity functions for different morphological types, and we fit linear regression lines to $M_{\rm HI}$ vs. M_B taken from the Nearby Galaxy Catalog (Tully 1988) to find the values of a and b.

Figure 4.3 shows the results. The solid grey lines are for all galaxy types, the black dashed lines are for spirals, the grey dashed lines for E and S0 types, and the grey dotted line for Irr/Pec types. The thin parts of each line are extrapolations beyond the confidence levels set by Marzke et al. (1998). The solid points plus errorbars are different representations of the AHISS data. The results are basically the same as what Rao & Briggs (1993) found. We show here that the optical luminosity functions, combined with conversion factors from M_B to $M_{\rm HI}$, give excellent fits to our data. The H I density distribution matches the converted luminosity functions for all galaxy types summed, and the luminosity distribution is fitted satisfactorily with spiral and irregular population. It is no surprise that the luminosity density from ellipticals exceeds the measured values from the AHISS, since these objects are not selected by H I surveys. This is especially clear in the middle right panel.

The integral H I density can be determined from a optical luminosity functions via

$$\rho_{\rm HI} = \int_{\searrow}^{+\infty} \Phi(L)\, M_{\rm HI}\, dL = \phi^*\, 10^{a-b\,M^*}\, \Gamma(1+\alpha+2.5\,b). \qquad (4.3)$$

If we apply this to our adopted luminosity functions we find that spirals make up 62% of the H I gas density, Irr and Pec types contribute 35%, and E and S0 types only 3%. Natarajan & Pettini (1997) apply this same method to measurements of the luminosity function at higher redshift in order to chart the evolution of the cosmic gas content between $z = 1$ and $z = 0$. The viability of this result is unclear since the amount of evolution of the $M_{\rm HI}/L$ ratio of galaxies is presently unknown. Future deep H I surveys at redshifts $z > 0$ are required to constrain the $M_{\rm HI}/L$ evolution.

4.4 Contribution of LSB galaxies to the cosmic mass budget

More than two decades after the seminal paper by Disney (1976) who defined the potential selection effects against LSB galaxies, the debate on the cosmological significance of LSB galaxies is still open. The AHISS sample, which is not biased by the sky background, can make a valuable contribution to the discussion of the cosmological significance of LSB galaxies.

4.4.1 The surface brightness distribution function

The bottom panel of Figure 4.4 shows a histogram of the distribution of B-band surface brightnesses for the AHISS galaxies. These surface brightnesses are the results of an area analysis described in Chapter 2 and are corrected for dust extinction following the formalism described by Tully et al. (1998). The unshaded histogram shows the distribution for the full set of AHISS galaxies, and the grey histograms show the distribution for the subset of AHISS galaxies with inclinations $i \leq 75°$ for which the corrections to face-on values are modest. The galaxies with high inclinations ($i > 75°$) do not appear from their optical images to be very low surface brightness: they often exhibit bright central condensations and strong dust lanes, both features not normally found in extreme LSB galaxies

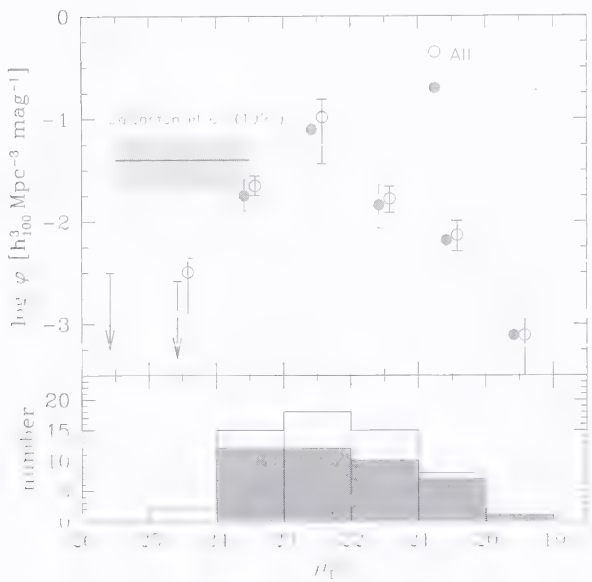

FIGURE 4.4— *Bottom panel*: Distribution of surface brightnesses in the AHISS sample. The grey histogram is for those galaxies with $i \leq 75°$ and is embedded in the histogram for all galaxies. *Top panel*: Volume corrected distribution of surface brightnesses. The open and solid symbols have the same meaning as in the bottom panel. For clarity, the points are slightly offset horizontally. Errorbars indicate 68% confidence levels. Arrows denote 95% confidence upper limits. The space density of optically selected LSB galaxies determined by Dalcanton et al. (1997b) is indicated by a light grey box, and corresponds to 90% confidence levels.

(see McGaugh, Schombert, & Bothun 1995). It therefore seems possible that the true face-on surface brightness of these disks is brighter than those given by either Tully's (1998) prescription or the assumption that the disk are fully transparent.

The top panel of Figure 4.4 shows the volume-corrected surface brightness distribution function of AHISS galaxies. This function is determined by summing values of $1/V_{\rm max}$ per 1 mag bins of surface brightness. The errorbars indicate 68% confidence levels and are determined from 100 bootstrap resample realizations of the data. The hollow symbols show the distribution for the complete set of AHISS galaxies, and the solid symbols are limited to those AHISS galaxies with $i \leq 75°$.

4.4.2 A cutoff in surface brightness?

As Figure 4.4 shows, the AHISS detected no galaxies with reliably determined face-on central surface brightnesses fainter than $\mu_B^{\rm b,i} = 24$ mag arcsec^{-2}. Even among the highly inclined galaxies with large (and possibly unreliable) corrections to face-on values, there are no galaxies with $\mu_B \gtrsim 25$ mag arcsec^{-2}. This conclusion is not dependent on the method of determining central surface brightnesses; the central surface brightnesses from ellipse fitting show exactly the same result. The statistical significance of this results depends on the assumptions we make about the detectability of very LSB systems. We can make an estimate by calculating the average value of $V_{\rm max}$ for the different surface brightness bins. We find that $V_{\rm max}$ is mildly correlated with $\mu_B^{\rm b,i}$: dimmer galaxies can on average be detected over smaller volumes. This correlation arises because decreasing surface brightness correlates with decreasing total H I mass, and the sample selection is based on H I flux. If we extrapolate the $\mu_B^{\rm b,i} - V_{\rm max}$ correlation to the surface brightness bins in which we have no detections, we find that $\langle V_{\rm max} \rangle$ would be $1150 h_{100}^{-3}$ Mpc^3 for the $24 - 25$ mag arcsec^{-2} bin, and $950 h_{100}^{-3}$ Mpc^3 for the $25 - 26$ mag arcsec^{-2} bin. The probability p_k of finding k

objects when the mean is n, is given by the Poisson distribution: $p_k = e^{-n} n^k / k!$. The mean number of detected objects per mag is given by $\varphi(\mu) V_{\max}(\mu)$, where $\varphi(\mu)$ is the space density of objects as a function of surface brightness. Hence, the probability of finding zero sources in one bin is $p_0 = e^{-\varphi(\mu) V_{\max}(\mu)}$. A 95% confidence upper limit to $\varphi(\mu)$ can now be expressed as $\varphi(\mu) = -\ln(0.05)/V_{\max}(\mu)$. This equation is used for the upper limits that are indicated by arrows in Figure 4.4.

This absence of extreme LSB galaxies suggests two things. First, the space density of massive, gas-rich, extremely LSB disks such as Malin 1 (Bothun et al. 1987) must be low. Such a disk would have been easily detectable to the limit of 7500 km s^{-1} of the AHISS, so they must be intrinsically less common on average than 1 per $1000 h_{100}^{-3}$ Mpc^3 (95% confidence level, using the Poisson statistics). Second, optical surveys for LSB galaxies (Sprayberry et al. 1996; Dalcanton et al. 1997b; O'Neil et al. 1997) systematically find galaxies at lower surface brightnesses than $\mu(0) = 24$ mag arcsec^{-2}, so there must be some reason why the present H I survey fails to detect any.

One possibility is that such galaxies have detectable amounts of neutral hydrogen but are extremely rare, so that it would not be expected to find one in the AHISS search volume. Apart from a few special objects like Malin 1, this seems unlikely because optical surveys find these objects in significant numbers despite the relatively small volume limits imposed by optical surface brightness selection effects (McGaugh 1996). Specifically, Dalcanton et al. (1997b) find that the number density of galaxies with V-band central surface brightnesses in the range $23 < \mu < 25$ mag arcsec^{-2} is $0.08^{+0.05}_{-0.04} h_{100}^3$ Mpc^{-3} comparable to the number density of normal galaxies. For reference, we have indicated this estimated with a shaded box in Figure 4.4, where we have adopted $B - V = 0.5$, a typical value for LSB galaxies (de Blok, van der Hulst & Bothun 1995).

The other possibility is that a significant number of galaxies exist in the AHISS search volume with optical surface brightnesses $\mu(0) > 24$ mag arcsec^{-2}, but that they do not contain enough H I to be detected by the AHISS. This seems considerably more likely, as there are two ways such a population could come to exist: First, these very low density systems could have formed a first generation of stars and then either lost most of their remaining gas through supernova-driven winds (Babul & Rees 1992; Babul & Ferguson 1996) or consumed all their gas in vigorous star formation and since then faded to become LSB disks (Bell et al. 1999). Second, like the outskirts of normal spiral galaxies, LSB disks have low H I surface densities (de Blok, McGaugh & van der Hulst 1996), and as such, they are subject to ionization by the extragalactic UV background that produces the sharp cutoffs seen at the edges of normal spirals, for column densities below $10^{19.5}$ cm^{-2} (e.g., Maloney 1993; Corbelli & Salpeter 1994; Dove & Shull 1994). Thus, much of the gas in LSB disks should become ionized, and thus be undetectable in 21cm surveys. This is consistent with the finding that no AHISS galaxies were found with average H I column densities lower than $\langle N_{\rm HI} \rangle > 10^{19.7}$ cm^{-2} (Chapter 3), at least an order of magnitude above the sensitivity limit of the survey.

At present there is insufficient data to distinguish between these two hypotheses. Currently available studies of the stellar compositions of LSB galaxies (McGaugh & Bothun 1994; de Blok et al. 1995; Bell et al. 1999 and 2000) have concluded that gas-rich LSBs form stars slowly and continuously and have fairly young stellar populations. Judging from their colors, the newly identified class of red LSB galaxies (O'Neil, Bothun & Schombert 2000) are consistent with a scenario in which they are simply a fading, passively evolving population (Bell et al. 1999). However, O'Neil et al. (2000) report that some of these

galaxies have high values of M_{HI}/L, but also note that 60% of their LSB galaxy sample that was followed-up with Arecibo is *undetected* in H I, in sharp contrast to the high succes rate in earlier LSB samples (e.g., Schneider et al. 1990). Moreover, a cross-correlation of the tables in O'Neil et al. (1997) and O'Neil et al. (2000) shows that the global $V - I$ colors of the undetected galaxies are on average 0.3 mag redder than the galaxies in which H I was found.

Multicolor photometry of galaxies with $\mu_B > 24.0$ mag arcsec^{-2}, in combination with deep H-α imaging and deep 21cm observations should show whether the lowest surface brightness galaxies are consistent with a fading, passively evolving population.

4.4.3 The LSB contribution to the neutral gas density

To address the problem of the cosmological significance of gas rich LSB galaxies in a meaningful way, an LSB galaxy should be well-defined. In the literature, the definitions of the surface brightness that divides galaxies into the classes 'normal' and LSB varies from 21.65 mag arcsec^{-2} (the "Freeman value") to 23.5 mag arcsec^{-2}. In the remainder of this chapter we define a LSB galaxy as a galaxy with deprojected B-band central surface brightness > 23.0 mag arcsec^{-2}. This limits the LSB galaxies to those that are $\sim 4\sigma$ dimmer than the Freeman value.

The cumulative distribution of H I density among AHISS galaxies of different surface brightness is presented in the top panel of Figure 4.5. The H I density distribution can be fit satisfactorily with a Gaussian distribution. There is no fundamental physical motivation for using a Gaussian to parameterize the distribution function, but Dalcanton, Spergel & Summers (1997a) note that a galaxy formation scenario based on a log-normal distribution of the spin parameter λ, produces a (nearly) Gaussian function of luminosity density vs. surface brightness (see also de Jong & Lacey 2000). The inset in Figure 4.5 gives 1σ and 2σ confidence ellipses for the Gaussian fits, the horizontal axis shows the center of the distribution, the vertical axis the dispersion (1σ). The actual fitting was done on the binned data, not on the cumulative distribution.

The H I mass density of the local Universe is dominated by galaxies dimmer than the Freeman (1970) value of 21.7 mag arcsec^{-2}. The peak of the distribution is at 22.0 mag arcsec^{-2}, the width is 1.0 mag arcsec^{-2}. Low surface brightness galaxies contribute a minor fraction to the H I density, galaxies fainter than 23.0 mag arcsec^{-2} make up $18^{+6.0}_{-5}$% of the H I mass density in the local Universe (the quoted errors have been determined using bootstrap resampling and mark the 68% confidence levels).

4.4.4 The LSB contribution to the luminosity density

The lower panel of Figure 4.5 shows the cumulative distribution of luminosity density against surface brightnesses. The peak of the distribution is at 21.2 mag arcsec^{-2}, the 1σ dispersion is 1.0 mag arcsec^{-2}. This implies that while most of the H I resides in galaxies dimmer than the Freeman value, most of the light in gas-holding galaxies in the local Universe is in galaxies 0.5 mag brighter than the Freeman value. The contribution of LSB galaxies is insignificant; galaxies with $\mu_B^{b,o} > 23$ mag arcsec^{-2} constitute no more than 5 ± 2% to the luminosity density.

We stress that this result only holds for gas rich LSB galaxies. The contribution of gas free LSB galaxies is unconstrained by our survey. Sprayberry et al. (1997) conclude that optically selected LSB galaxies contribute about 30% to the field galaxy lu-

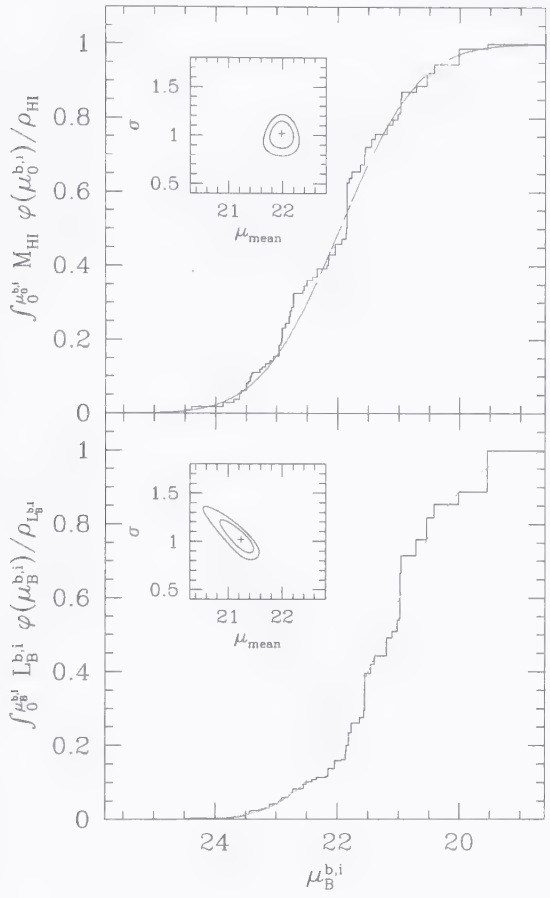

FIGURE 4.5— Cumulative distributions of H I mass density (top panel) and luminosity density (bottom panel) as a function of central surface brightness for the AHISS sample. The lines show Gaussian fits. The 1σ and 2σ confidence levels on the two jointly fitted parameters μ and σ, the mean and the width of the Gaussian, are shown in the inset. The H I density of the local Universe is dominated by galaxies with B-band central surface brightness of 22.0 mag arcsec^{-2}, the luminosity density by 21.2 mag arcsec^{-2}.

minosity density. A result very consistent with ours, since their definition of a LSB galaxy is $\mu_B > 22.0$ mag arcsec^{-2}. De Jong & Lacey (2000) find that the luminosity density of optically selected galaxies is dominated by $\mu_I \sim 19.3$ mag arcsec^{-2}, which compares to 21.0 mag arcsec^{-2} in the B-band (using their value of $B - I = 1.7$). They estimate that approximately 4% of the luminosity density is provided by galaxies with $\mu_B^{b,i} > 22.75$ mag arcsec^{-2}. Driver (1999) defines a volume limited subsample of 47 galaxies at $0.3 < z < 0.5$ from the Hubble Deep Field and derives that LSB galaxies (mean surface brightness within the effective radius > 21.7 mag arcsec^{-2}) contribute 7 ± 4% to the luminosity density. All these results are very much in agreement with our estimates. This fact implies that if a population of very LSB, gas free LSB galaxies exists (as was discussed in Section 4.4.2), their contribution to the luminosity density must be negligible.

4.4.5 The LSB contribution to Ω_{matter}

The contribution of LSB galaxies to the total mass budget of the local Universe is a long-standing question. The calculation critically depends on the assumptions one makes on the dependence of the dynamical M/L on central surface brightness. A zeroth order approximation is to assume that M/L is equal for all galaxies, independent of central surface

brightness. This assumption follows naturally from the observation that surface brightness is not a parameter in the Tully-Fisher relation (Sprayberry et al. 1995; Zwaan et al. 1995; Verheijen 1997). Moreover, Verheijen (1997) shows that it is possible to use one model for the dark matter halo to fit the rotation curves of three galaxies, all at equal position in the Tully-Fisher relation, but with different surface brightness. In the terminology of McGaugh & de Blok (1998) this invariant M/L would the "same halo hypothesis." It is consistent with the idea that all galaxies of equal luminosity form in the same mass halo, but the angular momentum of an LSB disk is higher, which causes the disk to be less centrally concentrated (Dalcanton et al. 1997a). Combined with the result on the luminosity density from section 4.4.4, this assumption leads to the conclusion that ρ_M(LSB) is 5% of the total ρ_M (i.e., equal to the contribution to the luminosity density).

Van den Bosch & Dalcanton (2000) show that their semi-analytical galaxy models are consistent with $M/L \propto \Sigma^{-1/2}$ (Zwaan et al. 1995), where Σ is the central surface brightness in linear units. M/L ratios are calculated via $M \propto DV^2$, where V is the maximum rotational velocity and D is a characteristic size of the dark halo, which is assumed to be directly proportional to the scale length of the optical disk. If we, like Driver (1999), adopt this relation for M/L we find that the LSB contribution to ρ_M rises to 11^{+4}_{-3}%. If we apply the calculations of $M \propto DV^2$ directly to our AHISS data set, we find ρ_M(LSB) $= 10^{+4}_{-3}$%. Both values are in excellent agreement with the 12 ± 6% that Driver finds.

At present it is unclear what the true dependence of the dynamical M/L on optical surface brightness is. Clearly, high precision measurements of rotation curves of LSB systems are needed (see Swaters, Madore & Trewhella 2000; van den Bosch & Swaters 2000; van den Bosch et al. 2000). At the moment we adopt as a conservative estimate that gas rich LSB galaxies contribute no more than 11% to ρ_M, the dynamical mass contained in galaxies.

4.5 Bivariate distributions

A more detailed view of the distribution of baryons among galaxies of different size and brightness can be obtained by calculating bivariate distribution functions. The importance of this way of looking at galaxy parameters is stressed by van der Kruit (1989), de Jong (1996), and most recently by de Jong & Lacey (2000) who study 10^5 galaxies with types Sb to Sdm. First, the bivariate distribution function is a important constraint for galaxy formation theories, as any theory should not only produce the integrated luminosity function (and integrated distribution functions of other structural parameters), but also higher dimensional distribution functions. Second, bivariate distribution functions help to clarify the selection effects that influence the determination of (e.g.) the luminosity function.

The aim of the present work is 1) to test whether an H I selected galaxy sample yields qualitatively the same bivariate distribution function, and, 2) extend the bivariate distribution functions to the distribution of H I properties. The sample we study here is small, and, as is discussed by de Jong & Lacey (1999) and Minchin (1999), at least $500 - 1000$ galaxies are required to avoid problems with small number statistics. We only intend to make qualitative comparisons and care should be taken with the interpretation of the results.

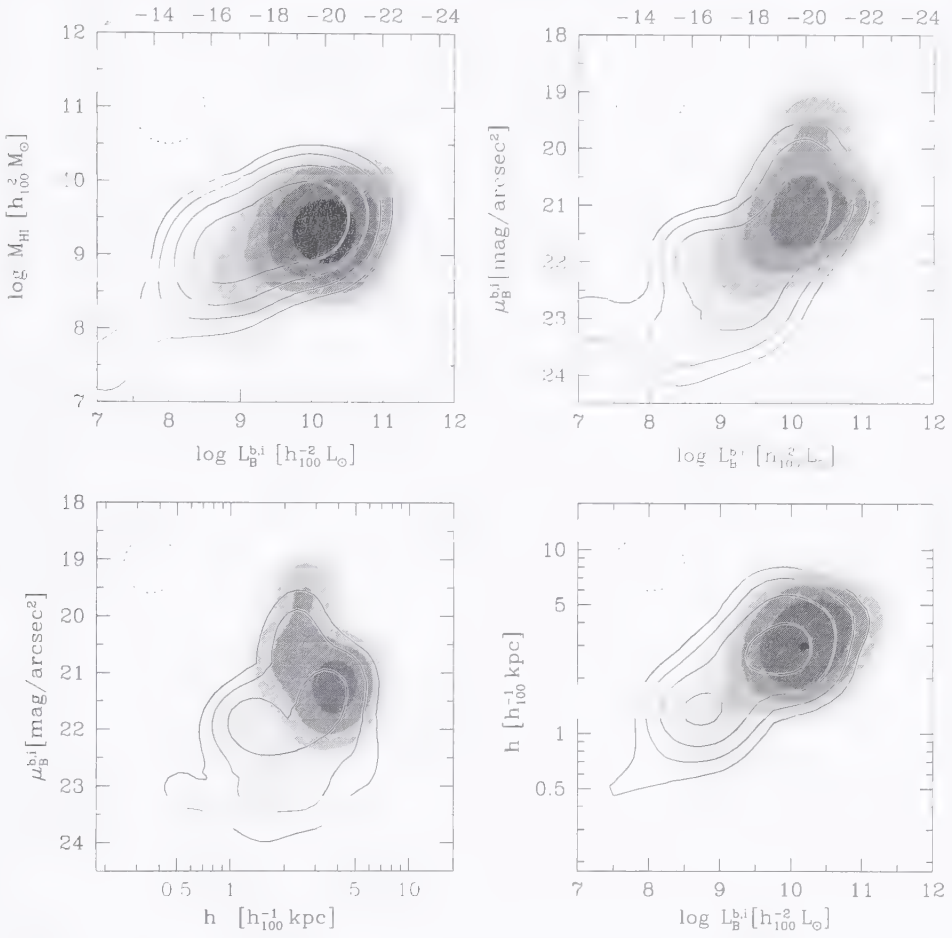

FIGURE 4.6— Bivariate distribution of luminosity density (greyscales) and H I density (contours) in the ($L_B^{b,i}$, M_{HI})-plane (*top left*), the ($L_B^{b,i}$, $\mu_B^{b,i}$)-plane (*top right*), the (h, $\mu_B^{b,i}$)-plane (*lower left*), and the ($L_B^{b,i}$, h)-plane (*lower right*). Greyscales correspond to ($10^{6.5}$, $10^{6.75}$, $10^{7.0}$, ...) × h_{100} $L_\odot$ Mpc^{-3}, contours to ($10^{6.25}$, $10^{6.5}$, $10^{6.75}$, ...) × h_{100} $M_\odot$ Mpc^{-3}. The densities are per decade for $L_B^{b,i}$ and M_{HI}, per 0.3 dex for h and per mag for $\mu_B^{b,i}$. The dashed ellipses in the upper right corners of each panel indicate the FWHM of the Gaussian smoothing filter that has been applied to the data.

4.5.1 Results

In Figure 4.6 we present bivariate distributions of several fundamental parameters. Our aim is to show the distribution of H I mass density and luminosity density as a function of galaxy luminosity, gas mass, size, and surface brightness.

The figures are calculated by distributing values of M_{HI}/V_{max} and $L_B^{b,i}/V_{max}$ over a fine grid with 0.1 dex resolution for M_{HI} and $L_B^{b,i}$, 0.1 mag resolution for central surface brightness $\mu_B^{b,i}$, and 0.05 dex resolution for disk scale length h. Next, the images were smoothed with a Gaussian filter, of which the FWHM values are indicated by the dashed

ellipses in the upper left corners of each panel. The H I density distributions are shown as contours, the luminosity density distribution as greyscales. Steps in intensity are in logarithmic intervals of 0.25 dex.

The first thing to notice is that the general trends are the same for the gas density and the luminosity density, but the maximum of the gas density is shifted towards less luminous, lower surface brightness galaxies. The second point is that the luminosity density is more strongly concentrated towards large, luminous HSB galaxies, whereas the H I density is more widely distributed.

What is obvious from the top right panel is that both the luminosity and the H I mass distribution are strongly dependent on optical surface brightness in the sense that both functions are shifted towards fainter absolute magnitudes for lower surface brightness galaxies. This fact was also observed by de Jong (1996), and the peak of the distribution, at $M_B^{b,i} = -20 + 5\log h_{100}$ and $\mu_B^{b,i} = 21$ mag arcsec^{-2} agrees well with his determination. A similar effect can be seen in the lower right panel: the luminosity and the H I mass distribution are shifted towards fainter absolute magnitudes for smaller galaxies. This correlation has been studied in detail by de Jong & Lacey (2000), who discuss the predictions of hierarchical galaxy formation theories and conclude that the observed distribution is in qualitative agreement with theory, but the distribution in disk size is narrower than predicted.

4.6 Conclusions

We have presented several volume corrected distribution functions for galaxies that have been selected in the H I 21cm line. The conclusions are the following:

1. The luminosity function of the H I selected galaxies is in agreement with other determinations based on late-type, or star-forming galaxies. The integral luminosity density of gas rich, late-type, or star-forming galaxies is well determined and equals $\rho_{L_i} = (3.4 \pm 0.7) \times 10^{19} h_{100}^{-2}$ W Hz^{-1} Mpc^{-3}. This is approximately 50% of the integral luminosity density of the local Universe.

2. The contribution of low surface brightness (LSB) galaxies to the integral luminosity density and H I density is modest, 5% and 18%, respectively. This in in good agreement with calculation based on optically selected galaxies. The fraction of $\Omega_{\rm matter}$ that resides in LSB galaxies is at present not well determined, but probably less than 11%.

3. We observe a lower limit to the surface brightness of gas rich galaxies: no galaxies were found with deprojected central surface brightness > 24.0 mag arcsec^{-2} in the B-band. It will be interesting to test whether this result stands up with future large H I surveys, such as the HIPASS survey (Staveley-Smith et al. 1996).

4. Bivariate distributions of various fundamental galaxy parameters show that the H I density in the local Universe is more diffusely spread over galaxies with different size, surface brightness, and luminosity than the luminosity density. The luminosity density is concentrated towards bright, large, high surface brightness disks.

References

Babul, A. & Ferguson, H. C. 1996, ApJ, 458, 100
Babul, A. & Rees, M. J. 1992, MNRAS, 255, 346
Bell, E. F., Bower, R. G., de Jong, R. S., Hereld, M., & Rauscher, B. J. 1999, MNRAS, 302, L55
Bell, E. F., Barnaby, D., Bower, R. G., de Jong, R. S., Harper, D. A., Hereld, M., Loewenstein, R. F. & Rauscher, B. J. 2000, MNRAS, 312

Bell, E. F. & de Blok, W. J. G. 2000, 311, 668
Bothun, G. D., Impey, C. D., Malin, D. F., Mould, J. R. 1987, AJ, 94, 23
Broadhurst, T. J., Ellis, R. S., Shanks, T. 1988, MNRAS, 235, 827
Cole, S., Lacey, C. G., Baugh, C. M., & Frenk, C. S. 2000, astro-ph/0007281
Corbelli, E. & Salpeter, E. E. 1993, ApJ, 419, 104
Dalcanton, J. J., Spergel, D. N., Gunn, J. E., Schmidt, M., & Schneider, D. P. 1997b, AJ, 114, 635
Dalcanton, J. J., Spergel, D. N., & Summers, F. J. 1997a, ApJ, 482, 659
de Blok, W. J. G., van der Hulst, J. M., & Bothun, G. D. 1995, MNRAS, 274, 235
de Blok, W. J. G., McGaugh, S. S., & van der Hulst, J. M. 1996, MNRAS, 283, 18
de Jong, R. S. 1996, A&A, 313, 45
de Jong, R. S. & Lacey, C. 1999, ASP Conf. Ser. 170: The Low Surface Brightness Universe, eds. Davies, Impey & Phillipps
de Jong, R. S. & Lacey, C. 2000, ApJ, in press, astro-ph/0008071
Disney, M. J. 1976, Nature, 263, 573
Disney, M. J. & Phillipps, S. 1987, Nature, 329, 203
Dove, J. B. & Shull, J. M. 1994, ApJ, 423, 196
Driver, S. P. & Phillipps, S. 1996, ApJ, 469, 529
Driver, S. P. 1999, ApJ, 526, L69
Efstathiou, G., Ellis, R. S., Peterson, B. A. 1988, MNRAS, 231, 479
Ellis, R. S. 1997, ARA&A, 35, 389
Fisher, J. R., Tully, R. B. 1975, A&A, 44, 151
Folkes, S. et al. 1999, MNRAS, 308, 159
Freeman, K. C. 1970, ApJ, 160, 811
Heyl, J., Colless, M., Ellis, R. S., Broadhurst, T. 1997, ApJ, 489, 67
Impey, C. D., Sprayberry, D., Irwin, M. J., Bothun, G. D. 1996, ApJS, 105, 209
Koo, D. C. & Kron, R. G. 1992, ARA&A, 30, 613
Leroy, P. & Portilla, M. 1998 A&A, 329, 840
Lilly, S. J., Le Fevre, O., Hammer, F., Crampton, D. 1996, ApJ, 460, 1
Lin, H., Kirshner, R. P., Shectman, S. A., Landy, S. D, Oemler, A., Tucker, D. L., Schechter, P. L. 1996, ApJ, 464, 60
Lin, H., Yee, H. K. C., Carlberg, R. G., Morris, S. L., Sawicki, M., Patton, D. R., Wirth, G. & Shepherd, C. W. 1999, ApJ, 518, 533
Loveday, J., Peterson, B. A., Efstathiou, G., Maddox, S. J. 1992, ApJ, 390, 338
Maloney, P. 1993, ApJ, 414, 41
Marzke, R. O., Geller, M. J., Huchra, J. P., Corwin, H. G. 1994, AJ, 108, 437
Marzke, R. O., da Costa, L. N., Pellegrini, P. S., Willmer, C. N. A. & Geller, M. J. 1998, ApJ, 503, 617
McGaugh, S. S. 1996, MNRAS, 280, 337
McGaugh, S. S. & Bothun, G. D. 1994, AJ, 107, 530
McGaugh, S. S. & de Blok, W. J. G. 1998, 499, 41
McGaugh, S. S., Schombert, J. M. & Bothun, G. D. 1995, AJ, 109, 2019
Minchin, R. F. 1999, PASA, 16, 12
Natarajan, P. & Pettini, M. 1997, MNRAS, 291, 28
O'Neil, K., Bothun, G. D., Schombert, J., Cornell, M. E., & Impey, C. D. 1997, AJ, 114, 2448
O'Neil, K. & Bothun, G. D. 2000, ApJ, 529, 811
O'Neil, K., Bothun, G. D. & Schombert, J. 2000, AJ, 119, 136
Rao, S. & Briggs, F. H. 1993, ApJ, 419, 515
Ratcliffe, A., Shanks, T., Parker, Q. A., & Fong, R. 1998, MNRAS, 293, 197
Sandage, A., Tammann, G. A., & Yahil, A. 1979, ApJ, 232, 352
Schechter, P. 1976, ApJ, 203, 297
Schneider, S. E., Thuan, T. X., Magri, C., & Wadiak, J. E. 1990, ApJS, 72, 245
Sprayberry, D., Bernstein, G. M., Impey, C. D., & Bothun, G. D. 1995, ApJ, 438, 72

Sprayberry, D., Impey, C. D., & Irwin, M. J., 1996, ApJ, 463, 535
Sprayberry, D., Impey, C. D., Irwin, M. J., & Bothun, G. D. 1997, ApJ, 482, 104
Staveley-Smith, L., Wilson, W. E., Bird, T. S., Disney, M. J., Ekers, R. D., Freeman, K. C., Haynes, R. F., Sinclair, M. W., Vaile, R. A., Webster, R. L., & Wright, A. E. 1996, PASA, 13, 243
Swaters, R. A., Madore, B. F., & Trewhella, M. 2000, ApJ, 531, L107
Tully, R. B. 1988, Nearby Galaxies Catalog, Cambridge and New York, Cambridge University Press, 1988
Tully, R. B. & Verheijen, M. A. W. 1997 ApJ, 484, 145
Tully, R. B., Pierce, M. J., Huang, J., Saunders, W., Verheijen, M. A. W. & Witchalls, P. L. 1998, AJ, 115, 2264
van den Bosch, F. C. & Dalcanton, J. J. 2000 ApJ, 534, 146
van den Bosch, F. C., Robertson, B. E., Dalcanton, J. J., & de Blok, W. J. G. 2000, AJ, 119, 1579
van den Bosch, F. C. & Swaters, R. A. 2000, astro-ph/0006048
van der Kruit, P. C. 1989, in Gilmore, G., King, I. & van der Kruit, P.: The Milky Way as a Galaxy, (Geneva Observatory, Switzerland)
Verheijen, M. A. W. 1997, Ph.D. Thesis, University of Groningen
Willmer, C. N. A. 1997, AJ, 114, 898
Zucca, E.et al. 1997, A&A 326, 477
Zwaan, M. A., van der Hulst, J. M., de Blok, W.J.G., & McGaugh, S. S. 1995, MNRAS, 273, L35
Zwaan, M. A., Briggs, F. H., Sprayberry, D. & Sorar, E. 1997, ApJ, 490, 173 **[Chapter 3]**

5

The H I Column Density Distribution Function at $z = 0$: the Connection to Damped Lyα Statistics[1]

M. A. Zwaan, M. A. W. Verheijen, & F. H. Briggs

ABSTRACT — We present a measurement of the H I column density distribution function [$f(N_{\rm HI})$] at the present epoch for column densities $> 10^{20}$ cm^{-2}. These high column densities compare to those measured in damped Lyα lines seen in absorption against background quasars. Although observationally rare, it appears that the bulk of the neutral gas in the Universe is associated with these damped Lyα systems. In order to obtain a good anchor point at $z = 0$ we determine $f(N_{\rm HI})$ in the local Universe by using 21cm synthesis observations of a complete sample of spiral galaxies. We show that $f(N_{\rm HI})$ for damped Lyα systems has changed significantly from high z to the present and that change is greatest for the highest column densities. The measurements indicate that low surface brightness galaxies make a minor contribution to the cross section for H I, especially for $N_{\rm HI} > 10^{21}$ cm $^{-2}$.

[1]A concise version of this chapter is published in *Publ. Astron. Soc. Aust.* 16, 100 (1999)

5.1 Introduction

HIGH COLUMN DENSITY absorbers seen in the spectra of background QSOs are referred to as Damped Lyα (DLα) systems if the observed H I column density exceeds the value of $N_{\rm HI} = 2 \times 10^{20}$ cm^{-2}. The DLα absorption lines are on the square-root part of the curve of growth where damping wings dominate the profile and column densities can be determined accurately by fitting the line profiles. Wolfe (1995) argues that these systems at high redshifts are gas-rich disks in the process of contracting to present-day spiral galaxies. This idea is supported by the fact that the characteristic velocity profiles of metal lines and Lyman series lines in DLα systems are similar to those of sightlines through spiral galaxies at $z = 0$. More recently, detailed modeling of DLα absorption profiles by Prochaska & Wolfe (1998) has shown that the DLα systems are consistent with rapidly rotating, thick disks. Note however that alternative models, like protogalactic clumps coalescing into dark matter halos (Haehnelt et al. 1997; Khersonsky & Turnshek 1996), can also explain the kinematics. The cosmological mass density of neutral gas in DLα systems at high redshift is comparable to the mass density of luminous matter in galaxies at $z = 0$ (e.g. Lanzetta, Wolfe & Turnshek 1995).

One of the best known statistical results of the study of QSO absorption line systems is the column density distribution function (CDDF) of neutral hydrogen. The function describes the chance of finding an absorber of a certain H I column density along a random line of sight per unit distance. An observational fact from high-z Lyα studies is that the differential CDDF [$f(N_{\rm HI})$] can be described by a single power law of the form $f(N_{\rm HI}) \propto {N_{\rm HI}}^{\alpha}$, where $\alpha \approx -1.5$ over ten orders of magnitude in column density (e.g. Tytler 1987; Hu et al. 1995) from 10^{12} cm^{-2} (Lyα forest) to 10^{22} cm^{-2} (DLα).

An integration over the distribution function gives the total cosmological neutral gas density as a function of redshift. The H I gas density relates to $f(N_{\rm HI})$ as $\Omega_{\rm HI} \propto \int_{N_1}^{N_2} N_{\rm HI} f(N_{\rm HI}) dN_{\rm HI}$ and it is readily seen that $\Omega_{\rm HI}(N_{\rm HI}) \propto N_2^{0.5}$ if $\alpha = -1.5$ and $N_2 \gg N_1$. This implies that although the high column density systems are observationally rare, they contain the bulk of the neutral gas mass in the Universe. Because so few DLα systems are known (≈ 80), the uncertainties on $\Omega_{\rm HI}$ and the CDDF for high column densities are large, especially if the measurements are split up into different redshift bins. But following the CDDF as a function of redshift is certainly very important in constraining models of complicated physical processes like star formation or gas feedback to the interstellar medium.

There are several reasons why the determination of $f(N_{\rm HI})$ at the present epoch using QSO absorption lines is difficult. Firstly, there is a cosmological effect: due to the expansion of the Universe the expected number of absorbers along a line of sight decreases with decreasing redshift. Secondly, gravitational lensing may play a role as it can bring faint quasars into the sample of background objects if these quasars are behind DLα systems, and the light of the quasar is amplified by the intervening DLα system (e.g. Smette et al. 1997). Thirdly, if DLα lines arise in normal galaxies, then starlight and dust in these absorbing foreground galaxies may hinder the identification of the background quasars. Finally, the Lyα line is not observable from the ground for redshifts smaller than 1.65. The two lowest redshift DLα systems currently known are at $z = 0.09$ and $z = 0.19$ (Rao & Turnshek 2000), illustrating that a $z = 0$ point can not yet reliably be derived from DLα observations.

At the present epoch the largest repositories of neutral gas are clearly galaxies. No instance of a free-floating H I cloud not confined to the gravitational potential of a galaxy

has yet been identified. It is therefore justified to use our knowledge of the local galaxy population to estimate the shape and normalization of the CDDF.

5.2 Theoretical expectations for $f(N)$ from simple galaxy models

A simple but illustrative and instructive method is to take the analytical approach. This is illustrated in Figure 5.1. Here we represent the radial distribution of the neutral hydrogen gas in galaxies by both an exponential and a Gaussian model. The differential cross sectional area of an inclined ring with a column density in the range N to $N + dN$ is given by $d\Sigma(N, i) = 2\pi r(N) dr \cos i$, where $r(N)$ is the radius at which a column density N is seen, and i is the inclination of the ring. We assume that the luminosity function $\phi(M)$ of the local galaxy population can be described by a Schechter function as indicated in the upper right panel of figure 5.1. The local $f(N)$ can be derived from $\phi(M)$ and the area function $d\Sigma(N)$ by taking the integral

$$f(N) = \frac{c}{H_0} \frac{\int_{M_{\rm min}}^{M_{\rm max}} \phi(M) \langle d\Sigma(N) \rangle_i dM}{dN}, \tag{5.1}$$

where the subscript i indicates an average over all inclinations. To evaluate this integral, the area function, or more generally the radial H I distribution, needs to be related to M. Here we adopt the relation $\log M_{\rm HI} = A + BM_B$ (following Rao & Briggs 1993) and assume that the central gas surface density in disks is not dependent on morphological type or luminosity. The resulting $f(N)$ for both models is shown in the lower left panel. The integral H I gas density in $h_{100}\,{\rm g\,cm^{-3}}$ as a function of column density is shown in the lower right panel. This function can be calculated with $\rho_{\rm HI}(N) = m_{\rm H} N \frac{H_0}{c} f(N) dN$, where $m_{\rm H}$ is the mass of the hydrogen atom. More details on the calculation of $f(N)$ are presented in section 5.A.

The Gaussian models yield a CDDF of the form $f(N) \propto N^{\alpha}$, where $\alpha = -1$ for N smaller than the maximum column density seen in a face-on disk ($N_{\rm max}$) and $\alpha = -3$ for the higher values of N. The exponential model gives a smoother function. The logarithmic slope is approximately -1.2 around $N = 10^{20}$ cm^{-2}, slowly changing to -3 at higher column densities. In fact, it was shown already by Milgrom (1988) that $f(N) \propto N^{-3}$ for $N > N_{\rm max}$ for any radial surface density distribution. The lower right panel clearly illustrates that an overwhelming fraction of the total H I mass in the local Universe is expected to be associated with column densities close to $N_{\rm max}$.

In addition to these simple models we also show the effect of disk truncation on the CDDF. The thin dashed line illustrates a Gaussian disk truncated at $N_{\rm HI} = 10^{19.5}$ cm^{-2}, the level below which photo-ionization by the extragalactic UV-background is normally assumed to be important (e.g. Corbelli & Salpeter 1993; Maloney 1993). It appears that this truncation only seriously affects the CDDF below $N_{\rm HI} = 10^{19.5}$ cm^{-2}. No significant changes occur at higher column densities.

5.3 Direct measurement of the $f(N)$ distribution at $z = 0$

Maps of nearby galaxies in the 21cm line routinely reach sensitivity limits comparable to column densities that typify DLα absorbers. It is therefore natural to calculate $f(N_{\rm HI})(z = 0)$, simply by adding cross sectional areas as a function of $N_{\rm HI}$ for a large sample of galaxies for which 21cm synthesis observations are available. However, application

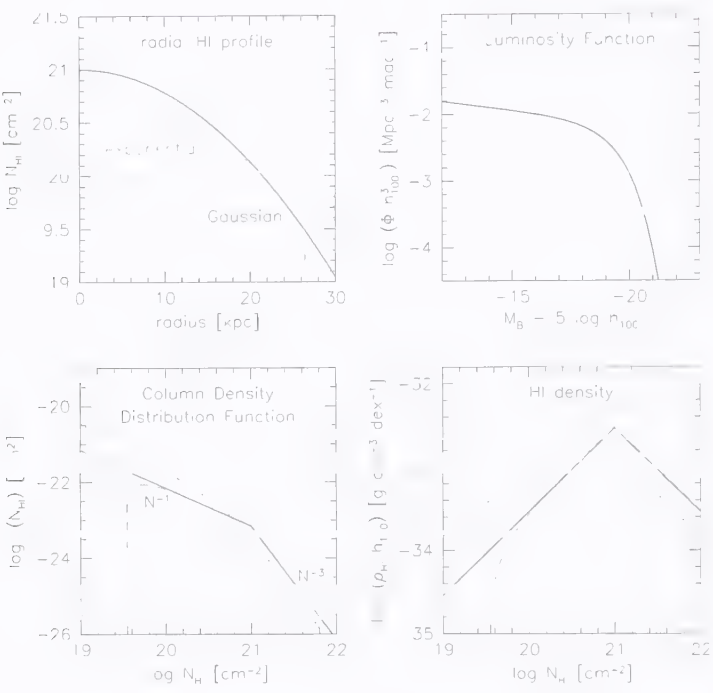

FIGURE 5.1— Illustration of simple models for the CDDF. *Upper left*: Gaussian and exponential models for the radial distribution of neutral gas density in galactic disks. *Upper right*: Schechter function describing the local luminosity function. *Lower left*: Resulting CDDFs for the Gaussian and exponential radial profiles. *Lower right*: Integral neutral gas density in the local Universe as a function of column density for both models. The effect of disk truncation is indicated by the dashed line.

of this approach to the large number of maps in the literature would complicated by the fact that there is an enormous variation in sensitivity and angular resolution of the 21cm maps. Furthermore, it would be difficult to chose a fair and complete sample of galaxies. Most galaxies that have been studied extensively in the 21cm line were selected on having either a large H I diameter, so that the rotation curve can be sampled out to large galactocentric radii, or on having peculiarities such as polar rings or warps. Until recently, only those galaxies showing strong HI signal in single-dish observations were granted time at synthesis telescopes. Thus, most samples for which 21cm synthesis data exist are not representative of the galaxy population of the local Universe and would likely be biased against dwarf and low surface brightness galaxies.

5.4 The Ursa Major cluster

The Ursa Major cluster of galaxies, studied extensively by Verheijen (1997), forms an ideal sample for an unbiased study of the column density distribution function. The Ursa Major cluster, at a distance of 15 Mpc, is different in many respects from famous, equally

distant clusters like Virgo and Fornax. Ursa Major's member galaxies show no concentration towards a central condensation and their velocity dispersion is exceptionally low, approximately 150 km s^{-1}. The estimated crossing time is half a Hubble time and hence the galaxies do not seem to be seriously affected by tidal interactions. In addition to this, there is a predominance of late type galaxies and the morphological mix of galaxies is indistinguishable from that in the field. This combination of properties implies that the Ursa Major cluster is merely an overdensity of galaxies and not a "cluster of galaxies" in the usual sense. This means that the Ursa Major sample is a reasonable representation of the galaxy population for use in studying the shape of the CDDF of neutral hydrogen in the local Universe.

The Ursa Major cluster as defined by Tully et al. (1996) comprises a volume of 80 Mpc^3, within which 80 galaxies are identified to date. For a complete sample of 62 galaxies intrinsically brighter than the Small Magellanic Cloud ($M_B = -16.5^m$) 21cm synthesis observations have been performed with the WSRT[2]. H I has been detected by the WSRT in 49 galaxies. Details on observations and data reduction are described in Verheijen (1997).

An obvious advantage of using the UMa sample for this study is that all the member galaxies are at approximately the same distance. Therefore, the spatial resolution of the synthesis observations are constant for the whole sample. This simplifies the problem of assessing the influence of resolution on the determination of the CDDF and the comparison with the CDDF at high redshift.

The shape of the column density distribution function is determined by counting in each H I map the number of pixels per logarithmic bin of 0.1 dex in column density. The solid angle covered by pixels of a certain column density is then determined by multiplying the number of pixels with the angular pixel size which varies slightly from galaxy to galaxy.

The disadvantage of using a galaxy sample taken from a clear cosmic overdensity is that the CDDF is not automatically normalized. If we would naively assume that the Ursa Major cluster is a representative part of the nearby Universe, we would overestimate the normalization of the CDDF by roughly a factor of 12. This factor is obtained by comparing the H I mass function of the cluster (Verheijen et al. 2000) with that of the field galaxy population (Zwaan et al. 1997). The shape of the Ursa Major mass function is indistinguishable from that of the field, but the normalization, θ^*, is larger by a factor of ~ 12. Ideally, one would use a sample of galaxies with well understood selection criteria so that the normalization would occur automatically. Unfortunately, there are no such samples available for which H I synthesis observations with sufficient angular resolution have been performed. The HIPASS survey, a blind 21cm survey of the whole southern sky, will eventually yield a suitable galaxy sample for this purpose, provided a representative subsample is followed up with the ATCA to obtain high spatial resolution maps.

There are several methods for normalizing the UMa CDDF. By assuming a local luminosity function (LF) or H I mass function (HIMF), each galaxy could be given a weight according to its absolute magnitude or H I mass. However, this method introduces extra uncertainty in the derived CDDF, due to uncertainties in the exact shape and normalization of the LF and the HIMF. Our preferred method of normalizing the CDDF is to scale the complete function, not the individual contributors to it. This can be achieved by scaling

[2]The Westerbork Synthesis Radio Telescope is operated by the Netherlands Foundation for Research in Astronomy (NFRA/ASTRON), with financial support by the Netherlands Organization for Scientific Research (NWO).

the integral H I mass density that is contained under the CDDF:

$$\rho_{\rm HI} = \int_{N_{\rm min}}^{N_{\rm max}} m_{\rm H} N \frac{H_0}{c} f(N) dN. \qquad (5.2)$$

By means of a blind 21cm survey Zwaan et al. (1997) determined $\rho_{\rm HI} = 5.8 \times 10^7 h_{100}\,{\rm M}_\odot{\rm Mpc}^{-3}$, a result that is in excellent agreement with earlier estimates based on optically selected galaxies. Note that dependencies on H_0 disappear in the final specification of the CDDF.

5.5 The column density distribution function

Figure 5.2 shows the CDDF determined from the 21cm observations of the Ursa Major sample. From left to right the function is shown for three different resolutions of the H I maps: 15″, 30″, and 60″. The solid line is the determined CDDF; the dashed lines indicate the quality of the measured column densities. Each pixel in the H I maps has an estimate of the signal to noise level assigned to it. In the determination of the CDDF we calculated an average S/N level for each bin in column density by averaging the S/N ratios for the individual pixels. The dashed lines show the average 1σ errors on the column densities and should be interpreted as horizontal errorbars. Nonetheless, they clearly overestimate the real uncertainties on the CDDF as many pixels are used in each bin (as many as 2500 independent beams for full resolution). The lines merely serve as an indicator of the quality of the measurements at each resolution. The thin solid line represents the CDDF for a Gaussian model, where $f(N_{\rm HI}) \propto {N_{\rm HI}}^{-1}$ for $N_{\rm HI} < 10^{21}$ cm^{-2} and $f(N_{\rm HI}) \propto {N_{\rm HI}}^{-3}$ for higher column densities.

When comparing the CDDFs at different resolution, it appears that the highest resolution maps yield the smoothest CDDF. This occurs because there the measurements of column density have the lowest S/N ratios. The low resolution (but high S/N) CDDF is in excellent agreement with the Gaussian model for $10^{20} < N < 10^{21.5}$, but for higher column densities, the measured curve drops below the model since high column density peaks are smeared away. Going to higher resolutions leads to better agreement between the measured curve and the model for the highest $N_{\rm HI}$, and at 15″ resolution the CDDF follows the ${N_{\rm HI}}^{-3}$ distribution up to $10^{21.9}$ cm^{-2}.

Besides beam smearing two other effects can cause a deviation from the ${N_{\rm HI}}^{-3}$ function. Firstly, the calculations assume that the gaseous disks are infinitely thin. Observations show that the bulk of the H I indeed resides in a thin layer with axis ratio < 0.1 (Rupen 1991). The thin disk approximation is therefore valid for moderately inclined disks. However, the highest column densities in the models arise in highly inclined thin disks. A small degree of puffiness will prevent these high column densities from being observed. The second effect is H I self absorption. The theoretical calculation of the CDDF is based on the assumption that the optical depth of the neutral gas layer is negligible. Column densities much higher than the maximum column density in a face-on galaxy can only be seen in a highly inclined disk when the gas is optically thin. It is remarkable that the full resolution CDDF follows the $f(N) \propto {N_{\rm HI}}^{-3}$ line up to $N_{\rm HI} = 10^{21.9}$, well above the value where H I self absorption is normally assumed to set in. For example, Dickey & Lockman (1990) calculate that an H I cloud with $T = 50$ K and an FWHM velocity dispersion of 10 km s^{-1} becomes optically thick ($\tau = 1$) at column densities $N = 10^{21}$ cm^{-2}.

Also shown in Figure 5.2 are the measurements of $f(N_{\rm HI})$ at high redshifts as determined by Storrie-Lombardi et al. (1997). We choose not to split up their high-z sample in

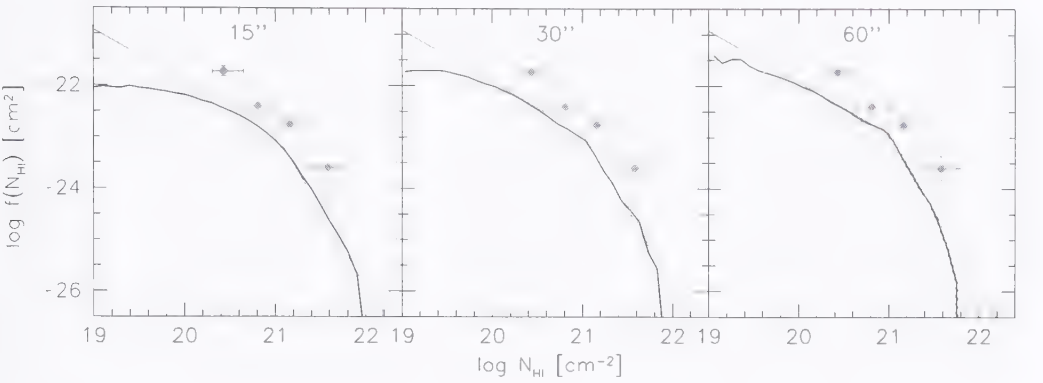

FIGURE 5.2— The column density distribution function at $z = 0$. From left to right the function is shown for three different resolutions of the H I maps: 15″, 30″, and 60″. The thick solid line is the CDDF as measured in the Ursa Major cluster. The dashed lines indicate the average 1σ uncertainties in the column density determinations. For reference, a Gaussian model with $N_{max} = 10^{21}$ cm^{-2} is also shown as a thin solid line. The points indicate the H I CDDF for damped Lyα systems at high redshift ($\langle z \rangle \approx 2.5$) taken from Storrie-Lombardi et al. (1997). Note the strong evolution, especially at the highest column densities.

different redshift bins in order to get reasonable signal to noise. The median redshift of the total DLα sample is $z = 2.5$. A value of $q_0 = 0.5$ has been used here. Lower values of q_0 would not significantly change the slope of $f(N_{HI})$ but would decrease the normalization by approximately a factor of 2. Strong redshift evolution of the CDDF from $z = 2.5$ to the present is apparent. The intersection cross-section for H I column density $< 10^{21.2}$ cm^{-2} has decreased by a factor of 6 (factor 3 for $q_0 = 0$) from $z = 2.5$ to $z = 0$. Higher column densities show a larger decrease, the evolution accounting for a factor of 10 (5 for $q_0 = 0$). Lanzetta et al. (1995) report still stronger evolution of the higher column densities for higher redshift, although the highest column densities suffer from small number statistics and the effect is hardly seen by Storrie-Lombardi et al. (1997). The strong evolution of the higher column densities can be understood if gas consumption by star formation occurs most rapidly in regions of high neutral gas density (Kennicutt et al. 1994).

Rao & Briggs (1993) evaluated the CDDF at the present epoch by analyzing Arecibo observations of a sample of 27 galaxies with optical diameters in excess of 7′. They made double-Gaussian fits to the observed radial H I distribution in order to describe $N_{HI}(r)$, the radial column density dependence for each galaxy. The disadvantage of this method is that the Gaussian fits automatically introduce the N_{HI}^{-1} for low N_{HI} and N_{HI}^{-3} for high N_{HI}. In the present study no modeling has been applied. However, the location of the change of the slope and the normalization show excellent agreement between Rao & Briggs' work and the Ursa Major determination.

5.6 Contribution of low surface brightness galaxies

It has been argued in the literature that low surface brightness (LSB) galaxies might contribute a considerable H I cross section. In particular, Linder (1998) explores a scenario in which the outskirts of galaxies are responsible for most of the cross section for low column density neutral gas ($N_{\rm HI} < 10^{20.3}$ cm^{-2}). She concludes that Lyα absorber counts at low redshifts can be explained if LSB galaxies of moderate absolute luminosity with extended low density gas disks are included in the analysis. Contrary to this view, Chen et al. (1998) claim that extended disks of luminous galaxies can account for most of the observed Lyα lines below $N_{\rm HI} = 10^{20.3}$ cm^{-2}. The contribution of dwarf and LSB galaxies to the cross section for high column density H I is also unclear. For instance, Rao & Turnshek (1998) show that there are no luminous spiral galaxies in the vicinity of the quasar OI 363 in which spectrum they identify two low-z DLα systems.

Here we evaluate the contribution of LSB galaxies to the cross section for high column density gas at $z = 0$. First we have to address the problem of completeness. The Ursa Major sample is essentially a magnitude limited sample. Selection effects against LSB galaxies are therefore to be expected. Tully & Verheijen (1997) discuss the completeness of the sample by plotting the observed central surface brightness against the exponential disk scale length. Theoretical approximations of the visibility limits seem to describe the boundaries of the observed sample satisfactorily. We apply the same visibility limits to the H I selected galaxy sample of Zwaan et al. (1997) to estimate what fraction of the H I mass density in the Ursa Major cluster could be missed in the present study. It appears that galaxies below the optical detection limits of our Ursa Major sample probably contain 10% of the total H I density of the cluster. Not surprisingly, most of this missed H I density must reside in LSB galaxies. Following Tully & Verheijen (1997), the separation between LSB and HSB galaxies is made at an extrapolated central surface brightness of 18.5 mag arcsec^{-2} in the K'-band, which roughly compares to 22.0 mag arcsec^{-2} in the B-band.

Figure 5.3 illustrates the contribution of LSB galaxies to the cross section for high column density gas, relative to the total galaxy population. We have corrected for the incompleteness by adding extra cross section for the LSB galaxies, equally over all column densities, in such a way that the mass density in these galaxies increases by an amount equal to 10% of the total H I density. The left panel shows the CDDF, the right panel shows the cosmological mass density of H I as a function of column density. The full resolution data are used. LSB galaxies do not make a significant contribution to the cross section for column densities higher than $N_{\rm HI} = 10^{21.3}$ cm^{-2}. Below that value they are responsible for approximately 25% of the cross section. The right panel shows that LSB galaxies make a minor contribution to the local neutral gas density, a conclusion very much in concordance with the results of Briggs (1997), Zwaan et al. (1997), and Côté et al. (1998).

5.7 Conclusions

We have used the present knowledge of the nearby galaxy population to estimate the H I column density distribution function at $z = 0$. It is shown that $f(N_{\rm HI})$ undergoes strong redshift evolution from $z \sim 2.5$ to the present, especially at the high column densities. The observed evolution in $f(N_{\rm HI})$ critically depends on whether the census of H I in the local Universe is complete. Surveys in H I and the optical indicate that the density of visible light and neutral gas is dominated by luminous, high surface brightness galaxies. The H I surveys routinely reach column density limits much lower than what is required to

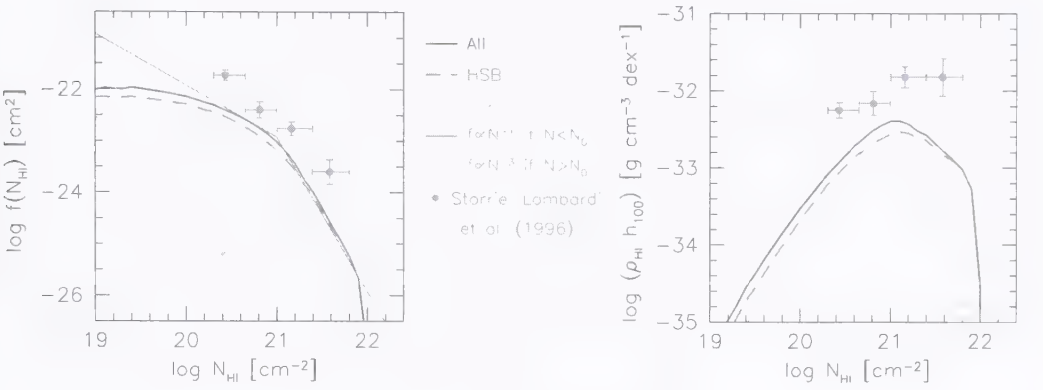

FIGURE 5.3— The column density distribution function (*left*) and H I mass density (*right*) for high and low surface brightness galaxies. High surface brightness galaxies dominate the H I cross section, especially for column densities $> 10^{21.3}$ cm^{-2}.

detect the $z = 0$ counterparts of DLA systems. Since H I mass functions published to date typically lose sensitivity below $M_{HI} = 10^7$ M$_\odot$, the region of parameter space still open to hide a large amount of high column density gas is that of low H I masses. Observations to measure the space density of these small H I masses (H I clouds and extreme LSB dwarf galaxies) and to evaluate to what extent they contribute to the H I density and the CDDF of the local Universe are important next steps.

References

Briggs, F. H. 1997, ApJ, 484, 618
Chen, H. -W. Lanzetta, K. M., Webb, J. K., & Barcons, X. 1998, ApJ, 498, 77
Corbelli, E.& Salpeter, E. E. 1993, ApJ, 419, 104
Côté, S, Broadhurst, T., Loveday, J., & Kolind, S. 1998, in 'The Low Surface Brightness Universe', Ed. Davies, J. I., Impey, C., & Phillipps, S.
Dickey, J. M. & Lockman, F. J. 1990, ARA&A, 28, 215
Haehnelt, M. G., Steinmetz, M., & Rauch, M. 1998, ApJ, 495, 647
Hu, E. M., Kim, T. -S., Cowie, L. L., Songaila, A., & Rauch, M. 1995, AJ, 110, 1526
Kennicutt, R. C. 1998, ApJ, 498, 541
Khersonsky, V. K. & Turnshek, D. A. 1996, ApJ, 471, 657
Lanzetta, K. M., Wolfe, A. M., & Turnshek, D. A 1995, ApJ, 440, 435
Linder, S. M. 1998, ApJ, 495, 637
Maloney, P. 1993, ApJ, 414, 41
Milgrom, M. 1988, A&A, 202, L9
Prochaska, J. X. & Wolfe, A. M. 1997, ApJ, 487, 73
Rao, S. M. & Briggs, F. H. 1993, ApJ, 419, 515
Rao, S. M. & Turnshek, D. A. 1999, astroph/9909164
Rupen, M. P. 1991, AJ, 102, 48
Smette, A., Claeskens, J. F., & Surdej, J. 1997, NewA, 2, 53
Storrie-Lombardi, L. J., Irwin, M. J., & McMahon, R. G. 1996, MNRAS, 282, 1330

Tully, R. B., Verheijen, M. A. W., Pierce, M. J., Huang, J. S., & Wainscoat, R. J. 1996, AJ, 112, 2471
Tully, R. B. & Verheijen, M. A. W. 1997, ApJ, 484, 145
Tytler, D. 1987, ApJ, 321, 49
Verheijen, M. A. W. 1997, Ph.D. thesis, Univ. Groningen
Verheijen, M. A. W., Trentham, N., Tully, R. B., & Zwaan, M. A. 2000, astro-ph/0006122
Wolfe, A. M. 1995, in QSO Absorption Lines, ed. G. Meylan
Zwaan, M. A., Briggs, F. H., Sprayberry, D., & Sorar, E. 1997, ApJ, 490, 173 **[Chapter 3]**

5.A Modeling the $z = 0$ column density distribution function

The column density distribution function $f(N)$ is defined such that $f(N)dNdX$ is the number of absorbers with column densities between N and $N + dN$ over a distance dX. The local $f(N)$ can be derived from the local luminosity function $\phi(M)$ and the area function $d\Sigma(N)$:

$$f(N) = \frac{c}{H_0} \frac{\int_{M_{min}}^{M_{max}} \Phi(M) \langle d\Sigma(N) \rangle_i \, dM}{dN}, \tag{5.3}$$

where $d\Sigma(N)$ should be expressed in Mpc^{-2}. The luminosity function is defined as

$$\phi(M)dM = 0.4 \ln 10 \, \phi^* \, [10^{0.4(M^* - M)}]^{1+\alpha} \exp[-10^{0.4(M^* - M)}] \, dM, \tag{5.4}$$

where α is the faint-end slope, ϕ^* is the normalization factor and M^* is the characteristic absolute magnitude that defines the knee.

In the following the mathematical details of the calculation of $d\Sigma(N)$ are given for various models of the H I disk.

Exponential Disk

The H I column density N_{HI} in an exponential gas disk, inclined by an angle i is

$$N(r, i) = N_0 \, e^{-r/h} / \cos i, \tag{5.5}$$

where r is distance along the major axis, h is the scale length of the gas disk and N_0 is the face-on central column density of the disk. The differential cross-sectional area of an inclined ring with a column density in the range N to $N + dN$ is given by

$$d\Sigma(N, i) = 2\pi r(N) dr \cos i, \tag{5.6}$$

where $r(N)$ is the radius at which a column density N is seen. Relations for r and dr can be found by inverting Eq.5.5:

$$r(N, i) = h \ln[N_0/(N \cos i)], \tag{5.7}$$

$$dr(N, i) = -h \, dN/N. \tag{5.8}$$

The cross-sectional area can now be expressed as

$$d\Sigma(N, i) = -\frac{2\pi h^2}{N} \ln\left(\frac{N_0}{N \cos i}\right) \cos i \, dN. \tag{5.9}$$

The calculation of the differential cross-sectional area averaged over all possible inclinations, $\langle d\Sigma(N)\rangle_i$, should be split up in two parts. First, for $N < N_0$, we derive

$$\begin{aligned}\langle d\Sigma(N)\rangle_i &= \frac{\int_0^{\pi/2} d\Sigma(N,i)\sin i\, di}{\int_0^{\pi/2}\sin i\, di} \\ &= -\frac{2\pi h^2}{N}\int_0^{\pi/2}\ln\left(\frac{N_0}{N\cos i}\right)\cos i\sin i\, dN di \\ &= -\frac{\pi h^2}{2N}[1+2\ln\left(\frac{N_0}{N}\right)]\, dN. \end{aligned} \tag{5.10}$$

Column densities $> N_0$ can only be seen for for disks with inclination $i > \arccos(N_0/N)$. There, the averaged differential cross-sectional area becomes

$$\begin{aligned}\langle d\Sigma(N)\rangle_i &= \frac{\int_{\arccos(N_0/N)}^{\pi/2} d\Sigma(N,i)\sin i\, di}{\int_0^{\pi/2}\sin i\, di} \\ &= -\frac{2\pi h^2}{N}\int_{\arccos(N_0/N)}^{\pi/2}\ln\left(\frac{N_0}{N\cos i}\right)\cos i\sin i\, dN di \\ &= -\frac{\pi h^2}{4N}\left[1+\cos\left[2\arccos(N_0/N)\right]\right] dN \\ &= -\frac{\pi h^2}{2N}\left(\frac{N_0}{N}\right)^2 dN. \end{aligned} \tag{5.11}$$

Note that in this regime $\langle d\Sigma(N)\rangle_i \propto N^{-3}$.

Gaussian disk

For a Gaussian disk with distribution

$$N(r,i) = N_0\, e^{-\frac{1}{2}\left(\frac{r}{\sigma}\right)^2}/\cos i, \tag{5.12}$$

we can perform the same exercize:

$$r(N,i) = \sigma\sqrt{-2\ln(N\cos i/N_0)} \tag{5.13}$$

$$dr(N,i) = -\frac{\sigma\, dN}{N\sqrt{-2\ln(N\cos i/N_0)}} \tag{5.14}$$

$$d\Sigma(N,i) = -\frac{2\pi\sigma^2\cos i}{N}\, dN. \tag{5.15}$$

For $N < N_0$:

$$\begin{aligned}\langle d\Sigma(N)\rangle_i &= -\frac{2\pi\sigma^2}{N}\frac{\int_0^{\pi/2}\cos i\sin i\, dN di}{\int_0^{\pi/2}\sin i\, di} \\ &= -\frac{\pi\sigma^2}{N}\, dN. \end{aligned} \tag{5.16}$$

For $N > N_0$:

$$\begin{aligned}\langle d\Sigma(N)\rangle_i &= \frac{\int_{\arccos(N_0/N)}^{\pi/2} d\Sigma(N,i)\sin i\, di}{\int_0^{\pi/2}\sin i\, di} \\ &= -\frac{2\pi\sigma^2}{N}\int_{\arccos(N_0/N)}^{\pi/2}\cos i\sin i\, dN di \\ &= -\frac{\pi\sigma^2}{N}\left(\frac{N_0}{N}\right)^2 dN. \end{aligned} \tag{5.17}$$

Truncated Exponential Disk

It is interesting to study the effects of ionization of the outer H I disks of galaxies on the shape of $f(N)$. Here we calculate the area functions of truncated disks, where N_c is the column density below which the gaseous disk becomes ionized. The observed column density N is always larger than $N_c/\cos i$. Therefore, the upper limit in the integrals is $\arccos(N_c/N)$.

For $N_c < N < N_0$:

$$\begin{aligned}\langle d\Sigma(N)\rangle_i &= -\frac{2\pi h^2}{N}\int_0^{\arccos(N_c/N)}\ln\left(\frac{N_0}{N\cos i}\right)\cos i\sin i\, dN di \\ &= -\frac{\pi h^2}{4N}\left\{1+2\ln(\frac{N_c}{N})+2\ln(\frac{N_0}{N})- \right. \\ &\quad \left. \cos(2\arccos(\frac{N_c}{N}))\left(1+2\ln(\frac{N_0}{N_c})\right)\right\} dN. \end{aligned} \tag{5.18}$$

For $N > N_0$

$$\begin{aligned}\langle d\Sigma(N)\rangle_i &= -\frac{2\pi h^2}{N}\int_{\arccos(N_c/N)}^{\arccos(N_0/N)}\ln\left(\frac{N_0}{N\cos i}\right)\cos i\sin i\, dN di \\ &= -\frac{\pi h^2}{4N}\left\{\cos(2\arccos(\frac{N_0}{N}))+2\ln(\frac{N_c}{N})-2\ln(\frac{N_0}{N})- \right. \\ &\quad \left. \cos(2\arccos(\frac{N_c}{N}))\left(1+2\ln(\frac{N_0}{N_c})\right)\right\} dN. \end{aligned} \tag{5.19}$$

This can be approximated by

$$\langle d\Sigma(N)\rangle_i \approx -\frac{\pi h^2}{2N}\left[\left(\frac{N_0}{N}\right)^2-\left(\frac{N_c}{N}\right)^2\right] dN. \tag{5.20}$$

Truncated Gaussian Disk

For $N_c < N < N_0$:

$$\begin{aligned}\langle d\Sigma(N)\rangle &= -\frac{2\pi\sigma^2}{N}\int_0^{\arccos(N_c/N)}\cos i\sin i\, dN di \\ &= -\frac{\pi\sigma^2}{N}\left[1-\left(\frac{N_c}{N}\right)^2\right] dN. \end{aligned} \tag{5.21}$$

For $N > N_0$:

$$\begin{aligned} \langle d\Sigma(N) \rangle_i &= \frac{2\pi\sigma^2}{N} \int_{\arccos(\ldots)}^{\arccos(\ldots)} \cos i \sin i \, dN di \\ &= -\frac{\pi\sigma^2}{N} \left[\left(\frac{N_0}{N} \right)^2 - \left(\frac{N_c}{N} \right)^2 \right] dN. \end{aligned} \tag{5.22}$$

6

The Space Density of Primordial Gas Clouds near Galaxies and Groups and their Relation to Galactic HVCs[1]

M. A. Zwaan & F. H. Briggs

ABSTRACT — High Velocity Clouds (HVCs) have recently attracted renewed attention as being long lived, massive dark matter dominated clouds of primordial composition distributed throughout the Local Group. In this picture the HVCs would contain a few $\times 10^7$ $M_\odot$ of H I and would be at distances of a few hundred kpc to 1.5 Mpc from the Local Group barycenter. If this extragalactic interpretation of HVCs is true, similar clouds are expected in other galaxy groups and around galaxies. We discuss the limits blind H I surveys and QSO absorption line studies put on this proposed population of clouds. We conclude that HVCs are deployed at typical distances of $\leq$200 kpc from the galaxies or group barycenters. If the each cloud is in gravitationally bound, virial equilibrium, their average dark matter fraction must be 98% or higher.

[1]based on Zwaan, M. A. & Briggs, F. H., *Astrophysical Journal Letters* 530, L61 (2000) and Zwaan, M. A., *Science* 288, 822 (2000)

6.1 Introduction

AFTER AN EXTENSIVE review of the High Velocity Cloud (HVC) literature, Wakker & van Woerden (1997) concluded that no single origin can account for the properties of the HVC population of neutral hydrogen clouds that surround the Milky Way Galaxy. Instead, several mechanisms, including infalling extragalactic clouds, cloud circulation within the Galactic halo driven by a galactic fountain, and a warped outer arm extension to the Galaxy must be invoked. Well established is the explanation for the Magellanic Stream, the largest H I structure observed in the sky, except for the gaseous disk of the Milky Way itself. This HVC is likely the result of tidal interaction between the Milky Way and the Magellanic Clouds, where LMC gas is stripped away and spread along an orbit around the Milky Way (see Putman et al. 1998). However, this HVC is not typical for the large number of clouds presented by Wakker & van Woerden (1991), the standard catalog of HVCs.

A defining property for the HVCs has been the lack of associated stellar emission. This also means that spectroscopic parallax methods cannot be used to measure distances to the clouds, and the lack of known distances, in turn, hinders the calculation of the clouds' physical properties. Some distance brackets have been specified with the absorption line method where spectra of stars with known distances are checked for the presence of (e.g.) Ca, Fe, and Mg absorption features (van Woerden et al. 1999). Recently, Balmer recombination line emission driven by reprocessing of the UV ionizing radiation originating from hot, young stars in the Galactic disk has been used to specify distances to a few clouds (Bland-Hawthorn et al. 1998; Bland-Hawthorn & Maloney 1999), indicating a range of distances from within the Galactic halo to greater than 50 kpc. These measurements require an accurate model for the Galactic ionizing field, and work best for clouds with large perpendicular distances from the Galactic disk. Braun & Burton (2000) present yet another distance estimator. For a cool HVC core they use the measured H I column density and the angular size to calculate an H I volume density which depends on the distance to the cloud. Assumptions about the thermodynamics of the H I gas yields a likely density and hence a distance.

Oort (1966) was the first to consider HVCs in an extragalactic context. His distance estimation assumed that the clouds are self-gravitating, stable entities. By comparing their solid angle on the sky, brightness temperature, and velocity dispersion Hulsbosch (1975) found that the typical distance would be approximately 10 Mpc, which places the clouds outside the Local Group (LG) and implies that their neutral hydrogen mass would be $\sim 10^9 M_\odot$, comparable to that of normal spiral galaxies. At these distances, the clouds should be participating in the Hubble expansion, rather than approaching the Milky Way.

Blitz et al. (1999, hereafter BSTHB) and Braun & Burton (1999, hereafter BB) have recently revived the idea that HVCs are extragalactic. These authors show that the clouds' distribution on the sky, as well as their kinematics as an ensemble are consistent with a model in which HVCs are distributed throughout the LG, at typical distances of a few hundred kpc (BB) to 1 Mpc (BSTHB). In order to make the total mass of the HVCs consistent with the assumption of self-gravity, the authors suggest that, like galaxies, HVCs are dominated by dark matter. This dark matter provides the binding potential that keeps the clouds from falling apart; the only directly observable constituent, H I, is only 10% of the total mass. In this scenario, the HVCs are either remnants from the formation of the LG or representatives from an intergalactic population of dark matter dominated mini-halos in which hydrogen has collected and remained stable on cosmological time scales. This

segment of the HVC population (1) inhabits the LG rather than the Galactic halo, (2) has typical H I mass per cloud greater than $\sim 10^7$ M$_\odot$, and (3) increases the LG H I mass budget by contributing $\sim 4 \times 10^{[11]}$ M$_\odot$ in the case of the BSTHB sample. For the BB sample, which is restricted to 65 confirmed "compact HVCs", the integral H I content adds $\sim 10^9$ M$_\odot$ to the LG.

Further impetus to search for a primordial population of low mass objects comes from hierarchical clustering scenarios that explain the formation of galaxies by many generations of mergers of smaller masses. Large numbers of proto-galactic gas clouds might survive to the present day if the mergers are not fully efficient. However, only about ten percent of the predicted number of halos have been identified as dwarf galaxies (Klypin et al. 1999; Moore et al. 1999). The association of HVCs with this missing population, as well as arguments based on the kinematics of the cloud population (BSTHB and BB), makes an appealing picture for the extragalactic/LG explanation.

Similar concerns motivated the extragalactic 21cm line survey by Weinberg et al. (1991), whose study of several representative environments (clusters and voids) found only gas-rich galaxies containing stars. Several extragalactic H I surveys of substantially larger volumes and more sensitive H I mass limits have also found no objects with HVC properties (i.e. H I detections without associated starlight; Zwaan et al. 1997; Spitzak & Schneider 1999; Kilborn, Webster, & Staveley-Smith 1999). This evidence does not rule out the existence of a population of dark matter mini-halos, but instead simply argues that whenever hydrogen is confined in a gravitational potential to sufficient density that it can remain neutral in the face of the ionizing background radiation, it is apparently also unstable to collapse and the formation of stars.

Clearly, if the HVC phenomenon is a common feature of galaxy formation and evolution, then extragalactic surveys of the halos and group environments of nearby galaxies should show evidence for this population. We take three approaches to the problem of placing the local HVC population in an extragalactic context. The first (in sections 6.3 and 6.4) is to compute the H I mass function for the LG, both for optically selected group members and for group members plus HVC populations as modeled by BSTHB and BB. The second, separate approach (section 6.4) is to calculate the probability that the narrow strip that the Arecibo[2] H I Strip Survey (AHISS; Sorar 1994; Zwaan et al. 1997) makes through the halos of $\sim$200 galaxy halos and $\sim$14 groups would detect members of HVC populations in those systems. The third approach (section 6.5) is to calculate the expected influence of HVCs on the the incidence of QSO absorption line systems.

6.2 The Local Group H I mass function

The H I mass function (HIMF) is used in extragalactic astronomy to quantify the space density of gas-rich galaxies and possible intergalactic clouds as a function of H I mass. For the field galaxy population, the HIMF has been determined accurately for $M_{\rm HI} > 10^{7.5}\ h_{65}^{-2}$ M$_\odot$ and can be fit satisfactorily with a faint end slope $\alpha \approx -1.2$ (Briggs & Rao 1993; Zwaan et al. 1997; Kilborn et al. 1999). At lower $M_{\rm HI} < 10^{7.5}\ h_{65}^{-2}$ M$_\odot$, where there is considerable uncertainty due to the small number of detections, Schneider, Spitzak, & Rosenberg (1998) have found evidence for a steep upturn in the tail of the HIMF. Although this steep tail has a tantalizing similarity to the signature of massive HVCs, it appears that

[2]The Arecibo Observatory is part of the National Astronomy and Ionosphere Center, which is operated by Cornell University under a cooperative agreement with the National Science Foundation.

FIGURE 6.1— Cumulative distribution of Local Group member galaxies with H I deletections as a function of $1 - \sin|b|$. Form measuring the number of galaxies within 50% and 67% (the two vertical lines) of the Local Group volume, we estimate that 4 to 7 galaxies with $M_{HI} > 10^8 M_\odot$ are probably missing at low $|b|$.

at least one of the two H I signals responsible for the rise comes from a normal galaxy, and the other is too close to a bright star to exclude faint optical emission (Spitzak & Schneider 1999).

We construct the HIMF for the LG from H I measurements of all known LG members as compiled recently by Mateo (1998). Within the LG volume, a total of 22 galaxies are known in which H I has been detected. The statistics are therefore poor, and consequently the HIMF is noisy. The LG HIMF is in one sense the best measured HIMF, with data over six orders of magnitude, compared to three or four orders of magnitude for determination for the field galaxy population. On the other hand, the LG HIMF may suffer from severe selection effects due to obscuration by dust in the disk of the Milky Way galaxy. In order to estimate how many galaxies might have escaped detection so far, Mateo (1998) plotted the cumulative number of galaxies as a function of $1 - \sin|b|$, for the total sample of LG galaxies. If LG galaxies were distributed equally over the sky, the resulting histogram should be a straight line. We applied the same method to the sample of galaxies with H I detections and found that 4 to 7 galaxies with H I masses $> 10^8$ $M_\odot$ are likely to be missing at low Galactic latitude. The missing galaxies would be predominantly the ones with low optical surface brightness, but since there is no clear correlation between surface brightness and H I mass, it is not possible to make a more refined correction to the HIMF than just adding one galaxy to each half decade mass bin below $M_{HI} = 10^8$ $M_\odot$. For larger galaxies with $M_{HI} > 10^8$ $M_\odot$, we assume that the census of the LG galaxy population is complete (see Henning et al. 1998).

The result is presented in the top panel of Figure 6.2, where the points represent the LG HIMF and the line is the field HIMF derived by Zwaan et al. (1997) scaled vertically so as to fit the points in the region around $M_{HI} = 10^9$ $M_\odot$ where the curve has been measured accurately. This scaling is justified given the fact that the HIMF for optically selected and H I selected galaxies is identical (see Briggs & Rao 1993; Zwaan et al. 1997). The scaling accounts for the overdensity of the LG, which amounts to a factor of 25, assuming that the LG volume is 15 Mpc^3. Also shown is a HIMF with a steep upturn proposed by Schneider et al. (1998). The large divergence between the extrapolated curves from Zwaan et al (1997) and Schneider et al. (1998) illustrates the uncertainty in HIMF below $M_{HI} = 10^{7.5}$ $M_\odot$. The LG HIMF for optically selected galaxies is remarkably flat, with the

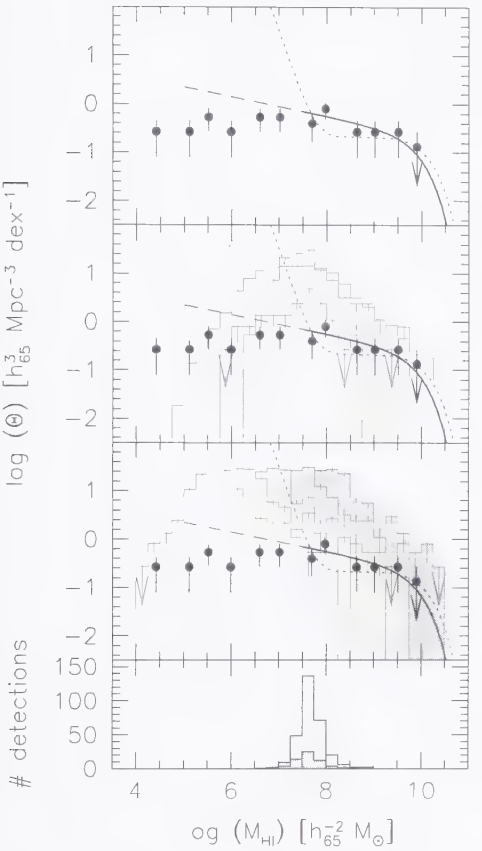

FIGURE 6.2— *Top panel:* H I mass function of the Local Group (LG). The points show the space density of LG members containing H I, after correcting for incompleteness. The solid line shows the field HIMF from Zwaan et al. (1997), scaled vertically so as to fit the points at the knee of the curve. The dotted line is a HIMF with a steep upturn at the low mass end, recently proposed by Schneider et al. (1998) *Second panel:* H I mass functions for extragalactic HVCs. The dark histogram shows the space density of BSTHB HVCs if they are put at the critical radii for gravitational stability. The unshaded histogram shows the effect of a baryon to total mass ratio f_B varying from cloud to cloud. The lighter shaded histogram corresponds to BB HVCs, all at the same distance of 1 Mpc. Lines are as in top panel. *Third panel:* H I mass function for BSTHB HVCs for different values f_B (from right to left: f_B=0.2, 0.1, 0.05, 0.025, 0.0125). The HVC HIMF is consistent with the field HIMF if $f_B \leq 0.02$ and the median distance $\leq$ 200 kpc. *Bottom panel:* Distribution of the expected H I detections in the AHISS for the BSTHB population. The light grey histogram corresponds to clouds surrounding galaxies, the dark grey histogram represents clouds in galaxy groups. See section 6.4 for explanation.

faint-end slope of a Schechter function fit of $\alpha \approx -1.0$. Dwarf galaxies with $M_{HI} < 10^8 M_\odot$ contribute only $\sim 2.5\%$ to the total H I budget of the LG.

Studies of the H I content of galaxies in different environments (including voids [Szomoru et al. 1996], clusters [McMahon 1993] and groups [Kraan-Korteweg et al. 1999]) have shown that the shape of the HIMF for $M_{HI} > 10^8$ $M_\odot$ is independent of cosmic density. The fact that we find here that the HIMF of optically selected LG members is flat down to H I masses of a few times 10^4 $M_\odot$ does not, however, insure that the field HIMF is also flat to these low masses. Although the crossing time of the LG is approximately equal to a Hubble time, there are clear indications of interactions (Mateo 1998 and references therein). The H I distributions in the lowest luminosity LG dwarfs are often highly asymmetric, perhaps indicative of tidal distortions. It is quite possible that low mass systems are destroyed or merged, which could cause the LG HIMF to be flatter than that of the field.

6.3 H I mass functions for extragalactic HVCs

We now derive HIMFs for the population of extragalactic HVCs as proposed by BSTHB and BB. For the compact, isolated HVCs identified by BB, we estimate H I masses by using

their measurements of the integrated fluxes and the assumption that all clouds are at the same 1 Mpc distance, suggested by BB. Typical H I masses are then 10^7 M$_\odot$ and the sizes are approximately 10 kpc. The resulting HIMF is indicated by the light shaded histogram in the second panel of Figure 6.2. For the BSTHB sample we use the compilation of HVCs by Wakker & van Woerden (1991; hereafter WW), which forms the main source for the BSTHB analysis. For each cloud the distance r_g at which the cloud is gravitationally stable is calculated. Adopting BHTHB's value of $f_B = 0.1$ for the ratio of baryonic mass to total mass leads to typical distances of self-gravitating HVCs of ~ 1 Mpc.

The dark shaded histogram represents the HIMF for the BSTHB clouds, assuming that all clouds are at their distance r_g. The resulting HIMF shows a clear peak at approximately 3×10^7 M$_\odot$, equal to the typical H I mass estimated by BSTHB. The largest uncertainty in the determination of M_{HI} is f_B, which might vary from cloud to cloud. We tested the effect of a varying f_B on the HIMF by applying to each individual cloud a random value of f_B in the range 0.03 to 0.3. The resulting HIMF (shown by the unshaded histogram) is not significantly different from the HIMF based on a fixed f_B in the region of interest greater than 10^7M$_\odot$.

The space density of the BB HVC population is comparable to the HIMF for optically selected LG galaxies, but it is obvious that the BSTHB HVCs outnumber normal galaxies by a factor 5 to 10 in the range $10^{7.5} < M_{HI} < 10^9$ M$_\odot$. This implies that if the BSTHB cloud population is typical for galaxy groups, H I surveys in groups should have encountered 5 to 10 dark H I clouds for every detected galaxy. This is clearly at variance with the observations.

At what distances from the Milky Way must the HVCs be located so that their HIMF is not in conflict with the observed field HIMF? Since the virial distance r_g is directly proportional to f_B, we can test this by varying f_B from 0.2 to 0.025 and then calculating the resulting HIMF. The results are shown in the third panel of Figure 6.2. The space density of HVCs in the LG can only be brought into agreement with the observed field HIMF if the median value of f_B is lowered to $\sim$ 0.02. This ratio of baryonic to dark matter of only 2% is much lower than the 10% – 15% that is normally observed in galaxies and clusters (Fukugita, Hogan & Peebles 1998). For this value of f_B, the median distance of such clouds must be smaller than ~ 200 kpc.

6.4 Expected number of extragalactic HVC detections

The Arecibo H I Strip Survey (AHISS), which is discussed in detail in Sorar (1994) and Zwaan et al. (1997), puts limits on the space density of primordial gas clouds in external galaxy groups and around galaxies. The survey was taken in drift-scan mode and consists of two strips at constant declinations, together covering 20^h of RA over a redshift range from 0 to 7500 km s^{-1}. The limiting column density was 10^{18} cm^{-2}, which is lower than that of most of the HVCs in the WW compilation and those presented in BB. The sky coverage is small (15 deg^2 excluding the side lobes) but the survey strip passes through the halo regions of many groups and galaxies as shown in Figure 6.4. These unique characteristics of this survey make it more suitable than other surveys of equal size for assessing the HVC problem. From the Lyon-Meudon Extragalactic Database[3] we selected all known galaxies with projected distances $< 1/h_{50}$ Mpc from the two AHISS strips. The circles in Figure 6.4

[3]We have made use of the Lyon-Meudon Extragalactic Database (LEDA) supplied by the LEDA team at the CRAL-Observatoire de Lyon (France).

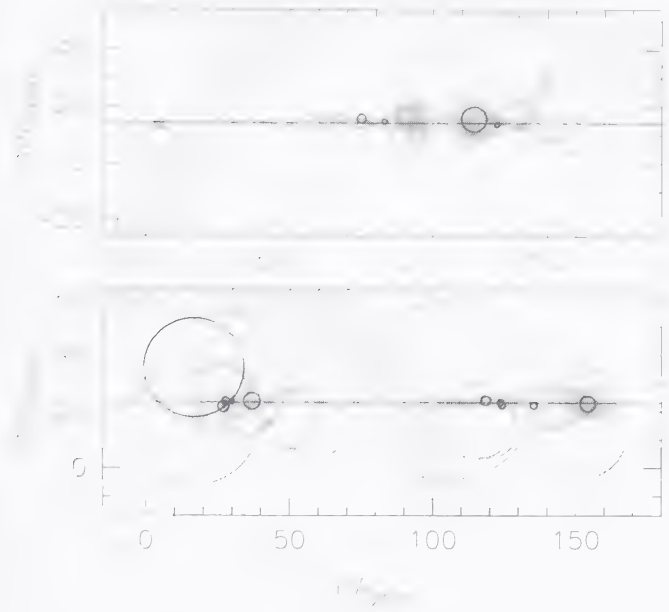

FIGURE 6.3— Illustration of the two survey strips and the distribution of spheres with radii of 1 Mpc around known galaxies (thin circles) and galaxy groups (thick circles). The grey areas indicate the Zone of Avoidance where $|b| < 10°$. The solid horizontal lines show the paths of the Arecibo beam.

indicate shells with 1 Mpc radii around the galaxies. Since the discussion in BSTHB is primarily focussed on galaxy groups, we also selected all cataloged groups within 1 Mpc of the strips. Galaxy groups were drawn from the lists of Willick et al. (1997), who used the the Mark III catalog, and Garcia (1993) who selected groups from the LEDA galaxy sample.

To compute the expected detection rate for different models, we fill the volumes around the selected groups and galaxies with a synthetic population of HVCs similar to the one proposed in BSTHB. In constructing such an ensemble we make use of the compilation of HVCs by WW as discussed in section 6.3. Although BSTHB put particular emphasis on galaxy groups, we choose to consider clouds around individual galaxies as well. Hierarchical formation scenarios do not distinguish between galaxies and groups in the relative number of satellites (Klypin et al. 1999). Further motivation comes from the fact that in the LG, strong subclustering of dwarfs is observed around the Milky Way and M31 (Mateo 1998).

The 3′ beam of the Arecibo telescope subtends $d_{\rm beam} = 0.87D$ kpc at a distance D Mpc. The typical size of an HVC discussed in BSTHB is 28 kpc, and therefore the lowest column density clouds could be detected out to distances of 32 Mpc, beyond which the average HVC would no longer fill the beam. HVCs with column densities in excess of the limiting value of 10^{18} cm^{-2} could be detected to larger distances. The limiting column density for clouds at large distances for which $d_{\rm cloud} < d_{\rm beam}$ is $N_{\rm lim} = 10^{18} \times (d_{\rm beam}/d_{\rm cloud})^2$. For each group and galaxy, a fraction of the volume of the surrounding sphere is scanned by the Arecibo beam. The number of clouds within that volume is calculated, taking into account the column densities, velocity widths and sizes of the individual clouds.

Table 6.1 lists the number of clouds that would have been detected in the Arecibo H I strip survey if a population of extragalactic HVCs existed with the BSTHB properties. We calculate the numbers of clouds differently for groups and for galaxies. Since BSTHB do

TABLE 6.1— Expected extragalactic HVCs detections.

	BSTHB				
	uniform	shell	Gaussian	BB	selected
groups	70(52)	72(54)	70(52)	9(8)	14
galaxies	248(167)	256(173)	260(177)	39(28)	347

NOTES — The number of expected HVC detections are calculated assuming a 5σ detection threshold. The numbers in parentheses indicate the expected number if the threshold is raised to 7σ. The last column shows the number of groups and galaxies that are included in the analysis. For the Gaussian distributions a selection radius of 2 Mpc has been used for inclusion in the sample.

not specify the exact radial distribution of clouds, we tested three different radial distribution functions to fill the volumes with clouds: 1) a spherical volume of radius R, 2) a thin spherical shell of radius R, and 3) a thick spherical shell with clouds distributed according to a Gaussian about the radius R with dispersion $\sigma = R/3$. The latter distribution most closely resembles the derived distribution of r_g given in BSTHB. The numbers in the table are based on $R = 1$ Mpc, the value preferred by both BSTHB and BB. The group halos are filled with 450 clouds, the number of HVCs identified by WW, excluding complexes A, C, M, the Outer Arm and the Magellanic Stream. To calculate the expected number of clouds around galaxies, the number of clouds associated with each galaxy is scaled in direct proportion to the ratio of the galaxy luminosity compared to the integral luminosity of the LG. This leads to a median number of clouds per galaxy of 40.

Table 6.1 shows that the expected number of detections is essentially independent of how the clouds are distributed around the groups and galaxies. For these samples we should detect approximately 250 clouds around galaxies and 70 around groups if the HVC population of BSHTB is a common feature of nearby galaxies. Restricting our analysis to the compact clouds of BB, reduces these numbers to 39 and 9. For a uniformly filled spherical distribution of BSTHB clouds, the distribution of H I masses of the expected detections is shown in the lowest panel in Figure 6.2. This figure illustrates that our analysis is sensitive to typical H I clouds (compare second panel of Figure 6.2), and not only to the most massive ones.

The robustness of the result is demonstrated in Table 6.1, where the numbers in parentheses indicate the expected number of detections if the detection threshold is increased from 5σ to 7σ. The average decrease is 25%. A 50% decrease occurs if the detection threshold is set at 10σ. This extremely conservative threshold would still predict more than 100 detections.

These predictions are in sharp contrast with the results of the AHISS analysis: all H I detections away from the Zone of Avoidance could be optically identified with galaxies containing stars. Other surveys have turned up a few instances of dark H I clouds, but these are all found to be confined to the gravitational potential of a bright optical galaxy, and are much too scanty to agree with the numbers calculated above. Kilborn et al. (2000) report on the first discovery of an isolated extragalactic H I cloud without optical identification, but this cloud too might be explained as a very high velocity cloud in the outskirts of the Milky Way-LMC system.

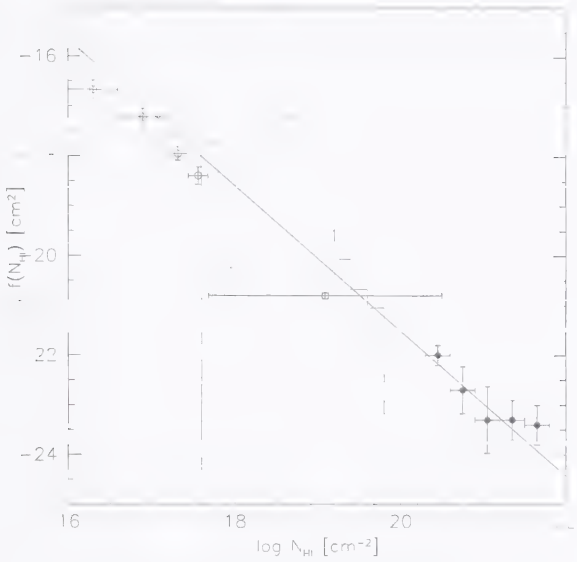

FIGURE 6.4— The simulated column density distribution function ($f(N_{\rm HI})$) for HVCs *a)* if they were at typical distances of 1 Mpc distributed throughout all galaxy groups (dashed histogram); *b)* if they existed around all galaxies in the local Universe (solid histogram). The points are measured values of $f(N_{\rm HI})$ from QSO absorption line studies.

6.5 QSO absorption line statistics

A completely independent way of investigating the idea of extragalactic HVCs is provided by QSO absorption line statistics. Charlton, Churchill & Rigby (2000) showed that the incidence of Mg II and Lyman limit absorption systems is in conflict with the idea that extragalactic groups contain several hundreds of clouds with typical H I masses of 10^7 M$_\odot$. We illustrate this same point here by plotting the column density distribution function of H I ($f(N_{\rm HI})$) for the proposed HVC population. This function describes the chance of finding an absorber of a certain H I column density along a random line of sight per unit distance.

For the HVCs, we again use the Wakker & van Woerden catalog. The area covered by each cloud is calculated from its measured solid angle Ω on the sky, and its distance based on the assumption of virial equilibrium. An area function $\Sigma(N_{\rm HI})$ that describes the total area in Mpc^2 that is covered by the ensemble of clouds as a function of $N_{\rm HI}$ is calculated by binning the clouds in column density, and adding the areas. The column density distribution function can be calculated from

$$f(N_{\rm HI}) = \frac{c}{H_0} \frac{\phi^* \Sigma(N_{\rm HI})}{dN_{\rm HI}}, \qquad (6.1)$$

where ϕ^* is the space density of groups. Charlton et al. (2000) derive ϕ^* from the CfA redshift survey by dividing the number of identified groups by the total survey volume and find $\phi^* = 3 \times 10^{-4}$. This is a conservative estimate since it does not incorporate a correction for incompleteness of the survey at higher redshifts. Ramella et al. (1999) compose a catalog of groups from the ESO Slice Project (ESP) redshift survey. Within the volume of $1.9 \times 10^5 h_{100}^{-3}$ Mpc^3 at the effective depth of $z = 0.16$ they identify 231 groups with at least three members. The space density of groups within that volume is therefore at least $1.2 \times 10^{-3} h_{100}^3$ Mpc^{-3}. If we limit the calculation to the volume at the sensitivity peak of the survey at $z = 0.1$ the value of ϕ^* rises to $2.0 \times 10^{-3} h_{100}^3$ Mpc^{-3}, which illustrates the ef-

fect of incompleteness. As a conservative estimate we adopt $\phi^* = 1.2 \times 10^{-3}\mathrm{Mpc}^{-3}$ for the calculation of $f(N_{\mathrm{HI}})$. The resulting $f(N_{\mathrm{HI}})$ is shown in Figure 6.4 as a dashed histogram.

The same calculation can be performed for individual galaxies. In this case we have to integrate over the luminosity function of galaxies, and the number of clouds associated with each galaxy is again scaled with the galaxy luminosity compared to the integral luminosity of the LG. For the luminosity function we adopt the average values from different large galaxy redshift surveys (see Fukugita et al. 1998): $M_B^* = 19.5$ mag, $\alpha = -1.1$ and $\phi^* = 0.020\ \mathrm{Mpc}^{-3}$. The resulting $f(N_{\mathrm{HI}})$ is shown as the solid histogram in Figure 6.4.

For comparison, the measured values of $f(N_{\mathrm{HI}})$ are shown as points with errorbars. The leftmost points represent the high N_{HI} part of the Lyman α forest measured by Hu et al. (1995). The typical HVC column densities $10^{17.7} - 10^{20.5}\ \mathrm{cm}^{-2}$ fall in the "Lyman limit" regime, the point here is taken from Petitjean et al. (1991). The forest and Lyman limit points are all derived from high z (> 2) data, since a low z $f(N_{\mathrm{HI}})$ distribution determined from QSO absorption line methods is not available in this regime. The points for damped Lyman α systems at the highest N_{HI} part are taken from Rao & Turnshek (2000) and are for $z \approx 0.8$. The straight line is the canonical fit to $f(N_{\mathrm{HI}})$ at $z = 0$ with a slope -1.5. As was noted by BSTHB, the *shape* of $f(N_{\mathrm{HI}})$ for HVCs agrees reasonably with the general observed trend. However, this plot clearly illustrates that the simulated $f(N_{\mathrm{HI}})$ for clouds exceeds the measured one by a large factor of one to two orders of magnitude.

This point can be made more quantitatively by calculating dN/dz, the number of absorbers per unit redshift, by integrating over $f(N_{\mathrm{HI}})$. For the groups we derive $dN/dz = 6$ and for clouds around individual galaxies we find $dN/dz = 27$. Extrapolating the results of Stengler-Larrea et al. (1995) on Lyman limit systems to $z = 0$ yields $dN/dz = 0.25 \pm 0.15$. The conclusions that we can draw from this exercise are similar to those of Charlton et al. (2000): QSO absorption line statistics are inconsistent with the hypothesis that galaxies and galaxy groups are surrounded by a large population of $M_{\mathrm{HI}} = 10^7 \mathrm{M}_\odot$ gas clouds.

Again we can limit the calculations to a subsample of some 65 compact HVCs as defined by BB, and place them at a median distance of 1 Mpc from the galaxies or groups' barycenters, at which the H I mass would be $\sim 10^7 \mathrm{M}_\odot$. For such a population, we derive $dN/dz = 0.6$ for groups and $dN/dz = 2.5$ for clouds around individual galaxies. Again these limits are much weaker than for the BSTHB samples of HVCs, but also in the BB scenario the QSO absorption line statistics can not be reconciled with the proposed population of clouds.

6.6 Conclusions

The hypothesis that most HVCs are primordial gas clouds with typical H I masses of a few $\times 10^7$ M$_\odot$ at distances of ~ 1 Mpc from the Galaxy is not in agreement with observations of nearby galaxies and groups and with QSO absorption line statistics. Blind H I surveys of the extragalactic sky would have detected these clouds if they exist around all galaxies or galaxy groups in numbers equal to those suggested for the Local Group. These results are highly significant: the Arecibo H I strip survey would have detected approximately 250 clouds around individual galaxies and 70 in galaxy groups. Furthermore, the measured incidence of QSO absorption line systems dN/dz is at least a factor 20 lower than what would be expected if all groups and galaxies were surrounded by a collection of H I clouds similar to what is proposed for the Local Group.

Several additional observations could help identifying the true nature of HVCs. Mea-

suring the Hα flux in HVCs can yield accurate distances, provided that the UV ionizing field around the Milky Way is accurately known (Bland-Hawthorn et al. 1998; Bland-Hawthorn & Maloney 1999). Also, determining metal abundances in HVCs is a useful method to distinguish between different HVC scenarios. If the clouds are primordial remnants of the formation of the Local Group they would not have been contaminated with these heavier elements and would retain a composition closer to the pristine environment of the early Universe.

Results to date have been confusing, since different teams report different measured metallicities, even in the same cloud. HST spectra of Complex C taken in the direction of background source Mrk 290 yield a sulphur abundance ten times lower than that of the gas layer of the Milky Way (Wakker et al. 2000). On the other hand, very recent data from FUSE, probing a different position in the same cloud, show an abundance of iron approximately half that found in the solar neighborhood (Murphy et al. 2000). Furthermore, Sembach et al. (2000) report on FUSE observations that show the first detection in a HVC of O VI, a high ionization level probably produced in interactions between the HVC and the halo gas of the Galaxy.

A viable view at this moment is that HVCs are a mixture of several species with different origins. This conclusion was reached by Wakker & van Woerden (1997). Some HVCs are clearly the result of gravitational interactions. Some might be produced in a Galactic fountain where hot gas is blown out of the Galactic disk, into the halo, where it cools and precipitates on the Galaxy. Some fraction might be primordial gas clouds distributed throughout the Local Group. Future deep 21cm surveys that are capable of detecting H I masses of 10^6 $M_\odot$ in nearby groups will certainly provide the tighter constraints on the significance of an intra-group population.

Acknowledgments

We are grateful to B. Wakker for discussions and for providing the list of HVC parameters. J. Bland-Hawthorn, L. Blitz, R. Braun, J. van Gorkom, and H. van Woerden are thanked for useful comments. We thank E. Murphy for communicating some of the early FUSE results.

References

Bland-Hawthorn, J., Veilleux, S., Cecil, G. N., Putman, M. E., Gibson, B. K., & Maloney, P. R. 1998, MNRAS, 299, 611

Bland-Hawthorn, J., & Maloney, P. R. 1999, ApJ, 510, L33

Blitz, L., Spergel, D. N., Teuben, P. J., Hartmann, D., & Burton, W. B. 1999, ApJ, 514, 818

Braun, R., & Burton, W. B 1999, A&A, 341, 437

Braun, R., & Burton, W. B. 2000, astro-ph/0004033

Briggs, F. H., & Rao, S. 1993, ApJ, 417, 494

Charlton, J. C., Churchill, C. W., & Rigby, J. R. 2000, astro-ph/0002001

Fukugita, M., Hogan, C. J., & Peebles, P. J. E. 1998, ApJ, 503, 518

Garcia, A. M. 1993, A&AS, 100, 47

Henning, P. A., Kraan-Korteweg, R. C., Rivers, A. J., Loan, A. J., Lahav, O., & Burton, W. B 1998, AJ, 115, 584

Hu, E. M., Kim, T., Cowie, L. L., Songaila, A. & Rauch, M. 1995, AJ, 110, 1526

Hulsbosch, A. N. M. 1975, A&A, 40, 1

Kilborn, V., Webster, R. L., & Staveley-Smith 1999, PASA, 16, 8

Klypin, A. A., Kravtsov, A. V., Valenzuela, O., & Prada, F. 1999, ApJ, 522, 82

Kraan-Korteweg, R. C., van Driel, W., Briggs, F. H., Binggeli, B., & Mostefaoui, T. I. 1999, A&AS, 135, 255
Mateo, M. L. 1998, ARA&A, 36, 435
McMahon, P. M. 1993, Ph.D Thesis, Columbia University
Moore, B., Ghigna, F., Governato, F., Lake, G., Stadel J., Tozzi, P. 1999, ApJ, 524, L19
Oort, J. H., Bull. Astr. Inst. Neth. 1966, 18, 421
Petitjean, P., Webb, J. K., Rauch, M., Carswell, R. F. & Lanzetta, K. 1993, MNRAS, 262, 499
Putman, M. E. et al. 1998, Nature, 394, 752
Ramella, M. et al. 1999, A&A, 342, 1
Schneider, S. E., Spitzak, & J. G., Rosenberg, J. L. 1998, ApJ, 507, L9
Sorar, E. 1994, Ph.D. Thesis, University of Pittsburgh
Spitzak, J. G., & Schneider, S. S. 1999, ApJS, 119, 159
Stengler-Larrea, E. A., et al. 1995, ApJ, 444, 64
Szomoru, A., van Gorkom, J. H., Gregg, M. D., & Strauss, M. A. 1996, AJ, 111, 2150
van Woerden, H., Schwarz, U. J., Peletier, R. F., Wakker, B. P., & Kalberla, P. M. W. 1999, Nature, 400, L138
Wakker, B. P., & van Woerden, H. 1991, A&A, 250, 509
Wakker, B. P., & van Woerden, H. 1997, ARA&A, 35, 217
Weinberg, D. H., Szomoru, A., Guhathakurta, P., & van Gorkom, J. H. 1991, ApJ, 372, L13
Willick J. A., Courteau S., Faber S. M., Burstein D., Dekel A., & Strauss M. A. 1997, ApJS, 109, 333
Zwaan, M. A., Briggs, F. H., Sprayberry, D., & Sorar, E. 1997, ApJ, 490, 173 **[Chapter 3]**

7

A Targeted Survey for H I Clouds in Galaxy Groups

M. A. Zwaan

ABSTRACT — Five galaxy groups with properties similar to those of the Local Group have been surveyed for H I clouds with the Arecibo Telescope. In total 300 pointings have been observed on grids of approximately 2.5 × 1.5 Mpc centered on the groups. The 5σ detection limit on the minimal detectable H I masses is approximately 6×10^6 $M_\odot$. No significant detections have been made that could not unambiguously attributed to optical galaxies. This null result leads to the conclusion that the total H I mass of intragroup clouds must be less than 10% of the total H I mass of galaxy groups and less than 0.05% of the dynamical mass. The hypothesis that Galactic high velocity clouds are Local Group satellites is highly inconsistent with the observations.

7.1 Introduction

GROUPS OF GALAXIES have been the subject of many H I studies. Famous H I maps of, for example, the M81 group (Yun, Ho & Lo 1994) show that these groups often host tidal H I features (see e.g., Li & Seaquist 1994). This was quantified by Haynes (1981) who found that six galaxy groups from a sample of 15 show H I appendages from at least one member galaxy. These data might suggest that H I filaments and intragroup clouds are commonplace in galaxy groups. Such a conclusion could be misleading since H I surveys are normally concentrated on the inner parts of galaxy groups and often on interacting pairs within the groups. Systematic searches throughout the volumes occupied by the groups are rare because the projected sizes of groups on the sky are too large to be covered by aperture synthesis instruments. A notable exception is the survey described by Lo & Sargent (1979) who systematically searched for H I clouds throughout the volumes around the M81, CVnI and NGC 1023 groups. No clouds were detected to the H I mass limit of 4×10^7 $M_\odot$, although several new dwarf galaxies were discovered.

Lo & Sargent (1979) already discussed their null-result in the context of Galactic High Velocity Clouds (HVCs). They concluded that HVCs are unlikely to be intergalactic gas clouds in the Local Group (LG) because they should have detected equivalents in the external groups. However, the idea that the HVCs instead of being small clouds close to the Milky Way galaxy, are clouds of primordial composition at LG distances has recently seen a revival. Originally proposed by Oort (1966), subsequently discussed by Verschuur (1969) and Hulsbosch (1975), the idea has been refined by Blitz et al. (1999, hereafter BSTHB), who added a dark matter component to the clouds. The problem with earlier contemplations on the extragalactic origin of HVCs was their derived distance. Hulsbosch (1975) concluded on the basis of the virial theorem that typical distances would be approximately 10 Mpc, which places the clouds outside the LG. BSTHB show that if the HVCs are built from the same material that galaxies are made of (typical baryon content f_B of 10%), their distances would reduce to ~ 1 Mpc. Moreover, they show that the clouds' distribution on the sky resembles that of LG dwarfs, and their kinematics as an ensemble can be well modeled if they are distributed throughout the LG. Braun & Burton (1999, hereafter BB) define a subsample of 65 compact HVCs and come to basically the same conclusions about their subsample.

Placed at LG distances, the HVCs have H I masses of $\sim 3 \times 10^7$ $M_\odot$ and typical diameters of 30 kpc. Approximately 500 to 1000 clouds are distributed throughout the LG, together adding approximately 4×10^{10} $M_\odot$ to the LG H I mass. Interestingly, the number of HVCs is in reasonable agreement with the number of mini halos that are predicted by numerical simulations of the hierarchical LG formation (Klypin et al. 1999; Moore et al. 1999). Corrected for incompleteness, the BB sample comprises ~ 100 clouds. Using the updated average distance of 650 kpc (Braun & Burton 2000), the total H I mass in their clouds would be approximately 10^9 $M_\odot$.

Charlton, Churchill & Rigby (2000) claim that the statistics of MgII and Lyman limit absorbers is in conflict with the hypothesis that the HVCs are intragroup material (see also Chapter 6). The typical distances must be less than 200 kpc from the LG barycenter. A very similar conclusion has been reached by Zwaan & Briggs (1999) who show that existing H I surveys impose strong constraints on the existence extragalactic HVCs. If H I clouds exist in other groups or around galaxies, with properties similar to those proposed for the LG, several instances should already have been detected in large H I surveys such as the Arecibo survey discussed by Zwaan et al. (1997).

In this chapter we present additional evidence by means of a targeted survey of five galaxy groups with the Arecibo telescope. The selection of the targets is discussed in § 7.2 and the data acquisition and analysis is summarized in § 7.3. In § 7.4 the detections are presented, and in § 7.5 we discuss the implications on the existence of intragroup H I clouds. To enable direct comparison between the surveyed groups and the LG, we adopt a realistic value of $H_0 = 65 h_{65}\,\mathrm{km\,s^{-1}\,Mpc^{-1}}$.

7.2 Sample selection

In order to make the targeted survey for H I clouds most efficient, we have selected the galaxy groups according to the following criteria: 1) The distance to the groups must be such that the expected H I cloud diameters match the projected extent of the Arecibo beam. BSTHB estimate that the cloud diameters are approximately 30 kpc. The 3′ beam of the Arecibo Telescope subtends $d_{\mathrm{beam}} = 0.87 D$kpc at a distance D Mpc. The optimal group distance at which the clouds fill the beam is therefore 30 Mpc. We have selected groups with radial velocities in the range $\sim 1800\,\mathrm{km\,s^{-1}}$ to $3000\,\mathrm{km\,s^{-1}}$. 2) The declination must be in the range 10° to 30° so that the groups are accessible with the Arecibo Telescope and can be tracked for at least one hour. 3) To enable comparison with the LG, the global properties of the groups, such as the integral H I mass, luminosity, and dynamical mass, must be comparable to those of the LG.

The list of galaxy groups compiled by Garcia (1993) was found to be the most successful in meeting the above listed criteria. This catalog was compiled from the LEDA[2] galaxy sample, and is basically a cross section of groups found via a percolation method (Huchra & Geller 1982) and groups identified via the hierarchical clustering method (Materne 1978). Table 7.1 lists the data of the member galaxies of the six selected groups. Table 7.2 gives the measured and derived properties of the groups. The groups are named after their brightest member.

We have made crude estimates of the groups' dynamical masses by applying the "projected mass estimator" which is discussed by Heisler, Tremaine & Bahcall (1985) and is defined as

$$M_{\mathrm{PM}} = \frac{32/\pi}{G(N_{\mathrm{m}} - 1.5)\Sigma_i V_i^2 R_i},$$

where N_{m} is the number of members, V_i is the radial velocity of member i with respect to the group mean velocity, and R_i is the projected distance of member i from the center of the group. Since the groups have only 3 to 6 identified members, the errors on the mass estimates are large (approximately $M_{\mathrm{PM}}/\sqrt{N_{\mathrm{m}}}$). The radius of the zero-velocity surface, R_0, beyond which galaxies participate in the Hubble expansion, can be calculated via (Sandage 1986)

$$R_0 = \left(\frac{8GT^2}{\pi^2} M_{\mathrm{dyn}}\right)^{1/3},$$

where T is the age of the group. We take the ages of all groups to be 14 Gyr.

For comparison, we also give in Table 7.2 the most recent published properties of the LG, taken from Mateo (1998), Courteau & van den Bergh (1999), and van den Bergh (2000). For the LG, the dynamical mass is estimated using the virial theorem, but it has

[2]We have made use of the Lyon-Meudon Extragalactic Database (LEDA) supplied by the LEDA team at the CRAL-Observatoire de Lyon (France).

TABLE 7.1— Properties of Member Galaxies

(1) Name	(2) $\alpha(2000)$ (h m s)	(3) $\delta(2000)$ (° ′ ″)	(4) v (km s^{-1})	(5) M_B^b ($5\log h_{65}$ + mag)	(6) $\log M_{\rm HI}$ ($h_{65}^{-2} M_\odot$)
NGC 5798	14 57 38.4	29 58 07	1788	-18.7	9.1
NGC 5789	14 56 35.8	30 14 01	1803	-18.2	9.1
UGC 9597	14 54 54.3	30 49 53	1727	...	8.9
NGC 5962	15 36 31.7	16 36 32	1956	-20.7	9.4
NGC 5951	15 33 43.1	15 00 27	1779	-19.9	9.6
NGC 5953	15 34 32.3	15 11 42	1965	-19.2	9.2
NGC 5954	15 34 34.8	15 12 12	1961	-19.7	9.1
UGC 9902	15 34 32.4	15 07 42	1696	...	8.8
NGC 5970	15 38 30.1	12 11 09	1960	-20.6	9.6
NGC 5957	15 35 23.1	12 02 56	1827	-19.9	9.6
NGC 5956	15 34 58.4	11 45 03	1902	-19.4	9.2
UGC 9941	15 38 21.2	12 57 15	1859	-18.1	9.3
NGC 6278	17 00 50.1	23 00 41	2791	-20.0	8.9
NGC 6267	16 58 08.5	22 59 06	2978	-19.8	9.5
UGC 10650	17 00 13.9	23 06 07	2964	-19.0	...
NGC 6500	17 55 58.9	18 20 26	2999	-20.9	9.8
NGC 6501	17 56 03.8	18 22 26	2858	-20.7	9.3
NGC 6467	17 50 40.1	17 32 20	3037	-20.5	9.3
UGC 10966	17 45 14.9	18 08 18	3061	-20.0	9.6
UGC 11044	17 55 34.9	18 55 36	2882	-18.6	...
UGC 11037	17 54 59.7	18 16 33	3127	...	...
NGC 6574	18 11 50.6	14 58 50	2292	-20.9	9.2
NGC 6570	18 11 07.5	14 05 35	2282	-20.4	9.5
UGC 11168	18 13 59.4	13 16 38	2303	-20.0	9.8
UGC 11141	18 11 49.2	12 05 16	2240	-19.7	9.6

NOTES — (1) Galaxy Name, (2) and (3) RA and Dec, (4) Radial velocity, (5) Absolute B-band magnitude corrected for Galactic extinction, (6) H I mass.

been shown by Heisler et al. (1985) that the virial theorem and the "projected mass estimator" give very similar results. It is evident from the table that the selected groups have properties not very dissimilar from those of the LG: the selected groups are on average equally gas rich, luminous, and massive and have a similar radial extent as the LG. Note that the centers of the NGC 5962 and NGC 5970 groups are only $1.6 h_{65}^{-1}$ Mpc apart and that their formal zero velocity radii are overlapping. Their difference in $v_{\rm hel}$ is only 15 km s^{-1}. It is suggestive that these two groups actually form one gravitationally bound system. If we assume that they form one group, its dynamical mass would become $\log M_{\rm dyn} = 13.2 - \log h_{65}$, and its zero velocity radius would be $2.3 h_{65}^{-1}$ Mpc. In the remainder of this chapter we regard the NGC 5962/5970 group as one group.

7.3 Observational strategy

Observations were carried out with the refurbished Arecibo[3] Telescope during five nights in the period from April 18 until 24, 1999 and on June 8 and 9, 1999. The data were taken with the L-narrow Gregorian receiver which has a measured system temperature of 32 K,

[3]The Arecibo Observatory is part of the National Astronomy and Ionosphere Center, which is operated by Cornell University under a cooperative agreement with the National Science Foundation.

TABLE 7.2— Properties of Surveyed Groups

(1) Name	(2) α_{2000} (h m)	(3) δ_{2000} (° ′)	(4) N_m	(5) $\langle v \rangle$ (km s^{-1})	(6) σ_r (km s^{-1})	(7) $\log L_B$ ($h_{65}^{-2} L_\odot$)	(8) $\log M_{HI}$ ($h_{65}^{-2} M_\odot$)	(9) $\log M_{dyn}$ ($h_{65}^{-1} M_\odot$)	(10) R_0 (h_{65}^{-1} Mpc)
NGC 5798	14 56	30 21	3	1773	40	9.9	9.5	12.0	0.9
NGC 5962	15 35	15 26	5	1872	126	10.8	10.0	13.0	1.9
NGC 5970	15 37	12 14	4	1887	58	10.7	10.1	12.3	1.2
NGC 6278	17 00	23 02	3	2911	104	10.5	9.6	12.8	1.7
NGC 6500	17 53	18 16	6	2994	105	11.0	10.2	13.3	2.3
NGC 6574	18 12	13 37	4	2279	28	10.9	10.2	12.2	1.1
Local Group					61[a]	10.6[b]	10.1[c]	12.4[a]	1.2[a]

NOTES — (1) Most luminous member, (2) and (3) Unweighted average RA and declination, (4) Number of known member with measured redshifts, (5) Unweighted average radial velocity, (6) Radial velocity dispersion. The uncertainty on this is approximately $\sigma_r/\sqrt{N_m}$, (7) Integral B-band luminosity, (8) Integral H I mass, (9) Rough estimate of dynamical projected mass (see text), (10) Estimate of the "zero-velocity radius" (see text).

[a] Taken from Courteau & van den Bergh (1999)

[b] Taken from van den Bergh (2000)

[c] Dwarfs from Mateo (1998) and gaints from van den Bergh (2000)

and a gain of 10 K/Jy. Spectra were recorded for two polarizations with each 2048 channels over a bandwidth of 12.5 MHz, centered on the frequency of the 21cm line redshifted to the mean velocity of each galaxy group. This setting results in a total velocity coverage of ~ 2600 km s^{-1} and a velocity resolution of 1.3 km s^{-1} before Hanning smoothing. Spectra were dumped every 60 seconds.

The pointings were arranged in rectangular grids centered on the galaxy groups. The grids were built from several series of five pointings on lines of constant declination, where each pointing was separated by 5 minutes in hour angle. The integration time per pointing was 4 minutes and integrations were separated exactly 5 minutes in time. The remaining minute was used to slew the telescope back. This strategy insures that the same path on the telescope dish was traced during each of the five pointing in a series. No separate OFF scans were taken, but for each scan a synthetic OFF scan was computed by averaging the other four scans in the same series. This synthetic OFF scan y_j can be written as

$$y_j = \frac{N\bar{x} - x_j}{N-1},$$

where N is the number of pointings in an array, x_j is an individual scan and $\bar{x}$ is the average of all scans in one series.

For this type of observations, this observing technique is superior in its efficiency compared to a traditional observing scheme where separate ON/OFF pairs are taken for each pointing. For this ON/OFF scheme the total noise depends on integration time as $\sigma \propto \sqrt{1/T_{ON} + 1/T_{OFF}}$. Normally, the integration times for the ON and the OFF scans are taken to be equal so that $\sigma \propto 2/\sqrt{T_{tot}}$, where $T_{tot} = T_{ON} + T_{OFF}$ is the total integration time needed for each pointing. For our strategy, where we make composite OFF scans from other scans in the array, the noise $\sigma' \propto \sqrt{1/T'_{tot} + 1/([N-1]T'_{tot})}$, where N is the number of pointings in one series and T'_{tot} is the time spend on each pointing. From this we can

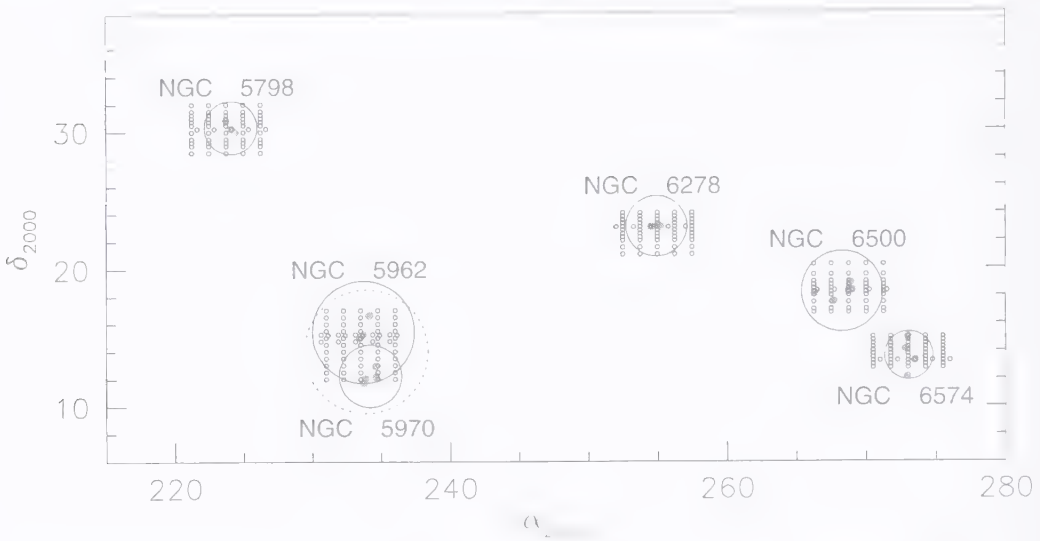

FIGURE 7.1— Positions of groups and pointings on the sky. The grey dots represent the individual galaxies in the groups, the big circles show the surfaces of zero-gravity. These are typically 1.5 Mpc. For the NGC 5962 and NGC 5970 groups their joint surface of zero-gravity is also indicated. The groups are named after their brightest members.

derive

$$\frac{T_{\rm tot}}{T'_{\rm tot}} = \frac{4(N-1)}{N}\frac{\sigma'^2}{\sigma^2}.$$

This shows that in our case, where $N = 5$, the technique is a factor of 3.2 faster than traditional ON/OFF procedures. In other words, in the same amount of time a factor 1.8 higher signal to noise can be achieved.

Figure 7.1 shows a schematic view of the pointings that were observed, together with the positions of the group galaxies. The circles indicate the sizes of the groups characterized by the zero-gravity radius R_0. The grids of pointings sparsely sample rectangular areas of approximately 2.5×1.5 Mpc.

Calibration of the data was performed by observing continuum sources with known flux densities. Separate scans and polarizations were averaged and Hanning smoothed. Polynomials were fitted to regions free from apparent signals, and subtracted from the spectra in order to obtain flat baselines. A first order polynomial was generally found to be sufficient. Each spectrum was then Gaussian smoothed to resolutions 5, 10, 25 and 50 km s^{-1}. The resulting noise level was on average 0.75 mJy per 10 km s^{-1}, which corresponds to a minimal detectable H I column density level of 1.2×10^{18} cm^{-2} (4.5σ). The lowest detectable H I mass at 30 Mpc was 7.1×10^6 M$_\odot$ for a 10 km s^{-1} broad signal. The H I mass limit increases to 1.6×10^7 M$_\odot$ for signals 50 km s^{-1} wide.

All spectra were checked for 4.5σ peaks in the full resolution and the smoothed spectra. The list of 4.5σ peaks was first checked for false positives due to RFI by re-analyzing the separate 60 second scans for both polarizations. All peaks that could not unambiguously attributed to RFI were re-observed for confirmation on 8 and 9 June 1999. The new observations were conducted following an ON-OFF fashion, spending 8 minutes ON and

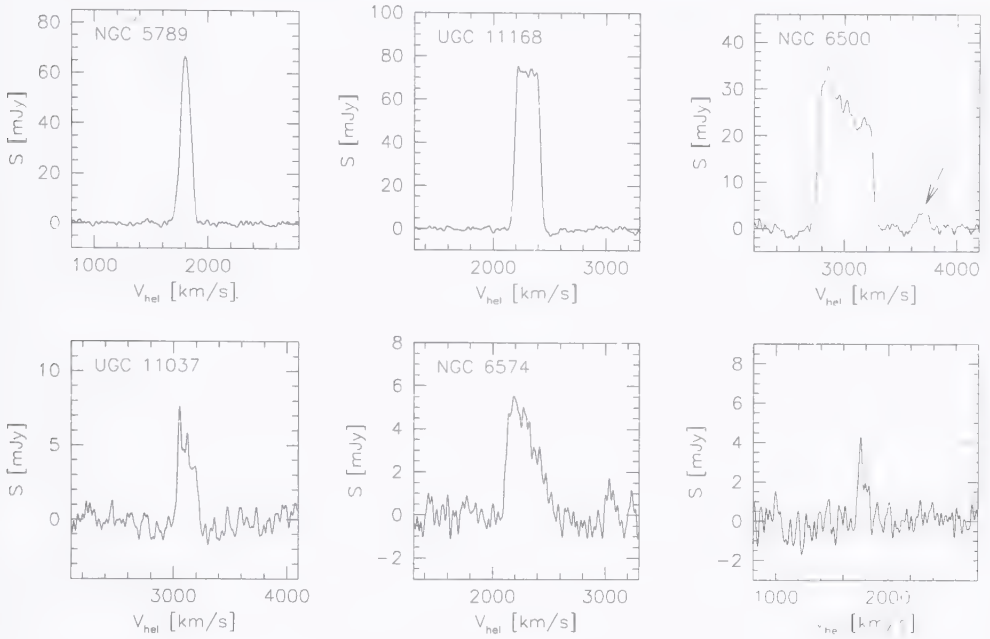

FIGURE 7.2— "Detections" in the Arecibo group survey. The top three spectra are the result of pointings aimed at known galaxies. The secondary peak in the spectrum of NGC 6500 is caused by a known filamentary H I structure in the NGC 6500/6501 pair. The lower left and middle left are serendipitous detections of known galaxies. The lower right spectrum is probably the result of a nearby optical galaxy. All spectra are smoothed to an effective resolution of 15 km s^{-1}.

8 minutes OFF on each position. The resulting noise level for these observations was therefore a factor 0.89 lower than for the original observations carried out in April 1999.

7.4 The detections

Three pointings were deliberately aimed at the positions of known galaxies. This was done to check the positional accuracy of the pointing method, and to obtain a confirmation of the flux calibration. The top three panels of Figure 7.2 shows the spectra of NGC 5789, UGC 11168 and NGC 6500. The latter one shows a secondary peak at ~ 3500 km s^{-1}. This turns out to be part of the H I filament in the galaxy pair NGC 6500/6501, that has been mapped with the WSRT by van Driel, Davies & Appleton (1988). The authors describe the H I structure as a "classical bridge and tail configuration of a double galaxy interaction". This is obviously of tidal origin, and not a primordial H I cloud.

The bottom panels of Figure 7.2 show the three other confirmed detections. The first one is due to UGC 11037. This galaxy was not intentionally pointed at, but one of the pointings happened to fall very close ($\sim 1.3'$) to this galaxy. There is a similar explanation for the detection in the spectrum in the central bottom panel. This pointing was only 2.6′ separated from the center of NGC 6574. The redshift of the signal agrees very well with the measured redshift of NGC 6574.

Finally, the lower right spectrum shows a detection at $15^{\rm h}39^{\rm m}00^{\rm s}$, $12°30'00''$ (α, δ).

There is no cataloged galaxy at this position, but there is an obvious optical galaxy visible on the DSS, only 3′ to the north. From the DSS we estimate the brightness of the galaxy to be $m_B = 17$ (assuming $B - V = 0.5$). The number density of galaxies brighter that $m_B = 17$ is approximately 4.0 per square degree (Metcalfe et al. 1995). The probability of encountering a galaxy of such brightness within a 3′ radius is therefore approximately 3%. Furthermore, the velocity width of the signal is 150 ± 15 km s^{-1}, a factor of ~ 7 larger than the typical width of the HVCs in the Wakker & van Woerden (1991) catalog, and broader that any known HVC. We therefore conclude that this H I signal is very likely associated with the optical galaxy. Additional 21cm observations on this field are required to confirm this.

In summary, no H I clouds of the type predicted by the BSTHB scenario have been found. Two detections were made that could not unambiguously identified as known optical galaxies. One is a known tidal H I filament in the NGC 6500/6501 pair, similar to the Magellanic Stream seen in the Local Group (Putman et al. 1998). The other detection is very likely the result of a uncataloged member of the NGC 5970 group.

7.5 Space density of H I clouds

We now use the null-result of the Arecibo group survey to derive upper limits to the space density of H I clouds in galaxy groups and discuss the cosmological significance of intragroup H I clouds.

7.5.1 HVCs as intragroup clouds

An explanation for Galactic HVCs that is of widespread current interest is provided by BSTHB who suggest that most of the HVCs are actually distributed throughout the LG and each cloud contains a few $\times 10^7$ $M_\odot$ of H I. We test this scenario by filling the five observed galaxy groups with synthetic populations of clouds following a recipe outlined by BSTHB. For the cloud properties we use the measured solid angles Ω, velocity widths ΔV, and average brightness temperatures T_B for Galactic HVCs from Wakker & van Woerden (1991). Virial distances r_g are calculated for each cloud individually. The values of r_g are directly proportional to the assumed ratio of baryon to total mass f_B. If f_B is 0.1, the virial distances r_g are found to be approximately 1 Mpc. At those distances, the distribution of HVCs is in agreement with the kinematics of the LG, which was one of the main motivations of BSTHB to propose the extragalactic HVC scenario.

Within the groups, the clouds are placed at r_g from the group's barycenter, in a random direction. This situation would resemble that in the LG, albeit that all the substructure that BSTHB attribute to LG dynamics is not simulated in the models of the external groups. The radial column density distribution for each cloud is first assumed to be flat. The

TABLE 7.3— Expected Detections

N_{LG}	no scaling	M_{dyn}-scaling
100	7 ± 3	23 ± 8
500	34 ± 9	116 ± 29
1000	66 ± 11	229 ± 65

average column density is calculated by taking $\langle N_{\rm HI} \rangle = M_{\rm HI}/(\pi r_{\rm cloud}^2)$, where $M_{\rm HI}$ is the cloud H I mass based on its value of $r_{\rm g}$ and its observed flux, and $r_{\rm cloud}$ is the cloud radius, calculated from its measured solid angle and $r_{\rm cloud}$. The number of clouds per group N is varied by drawing randomly N clouds from the Galactic HVC parent population.

The synthetic cloud ensembles are 'observed' with patterns of beams following the observational strategy of our survey. A detection is counted if the fraction of the flux of a cloud within the beam exceeds the detection threshold. The velocity spread of the signals is taken into account. The same simulation is run 100 times for each group in order to obtain reliable error estimates on the expected number of detections.

Table 7.3 shows the expected number of detections for two scenarios of filling the groups with clouds. The quoted errors indicate the 1σ variations around the mean. In the first column of Table 7.3 the number of clouds per group, N, is taken to be invariant over the different groups. If $N = 100$, substantially lower than the number of HVCs observed around the Milky Way Galaxy, the expected number of detections is still 6 ± 3. Note that $N \approx 1000$ in the BSTHB scenario and $N \approx 100$ in the BB scenario. In the second column of Table 7.3 we drop the restriction that all groups contain an equal number of clouds and instead scale N with the dynamical mass of the group. This seems like a more logical thing to do since the H I mass and luminosity are also observed to scale in direct proportion to the dynamical mass. However, N could of course be dependent on the dynamical state of the groups. In groups that have formed more recently, the primordial clouds are likely to have been less efficient in merging than in older groups. We have no detailed information on the dynamical state of the groups, and therefore simply assume that N scales proportional to $M_{\rm dyn}$. We find that the expected number of detections rises under this assumption. The reason for this is that the average $M_{\rm dyn}$ for the external groups is slightly higher than that for the LG.

The conclusion from Table 7.3 is that the hypothesis set forward by BSTHB that HVCs are infalling gas clouds in the LG is highly inconsistent with the observations. If the LG is not unique and the five surveyed external groups are representative of the LG, our survey should have detected at least 30 clouds.

7.5.2 Constraints on intragroup H I cloud properties

A graphical representation of the constraints on intragroup H I clouds is presented in Figure 7.3. This figure shows the combined constraints on the mean H I mass of clouds, and the number of clouds in each group. The lines show 68%, 90%, 95%, and 99% confidence levels at which the existence of a cloud population can be excluded. Again we have made use of the observed parameters of Galactic HVCs to model cloud populations in the external groups and the number of clouds N is again scaled with $M_{\rm dyn}$. For reference, the cloud populations proposed by BSTHB and BB are indicated by hatched boxes, the size of which reflects the uncertainty in the number and average H I mass. The horizontal arrow indicates the effect of changing the mean distance of the BB clouds from 1 Mpc to 650 kpc from the Local Group barycenter. This latter value is preferred by Braun & Burton (2000) after they have estimated the distance to one HVC by comparing the measured H I column density and the angular size of the cool core. Both the BSTHB and the BB populations are inconsistent with the observations at the $> 99\%$ confidence level.

The distribution of H I column densities in HVCs often show a core-halo structure (Wakker & van Woerden 1997). Braun & Burton (2000) present high resolution WSRT imaging of six compact HVCs and show that the morphology can be described by a dif-

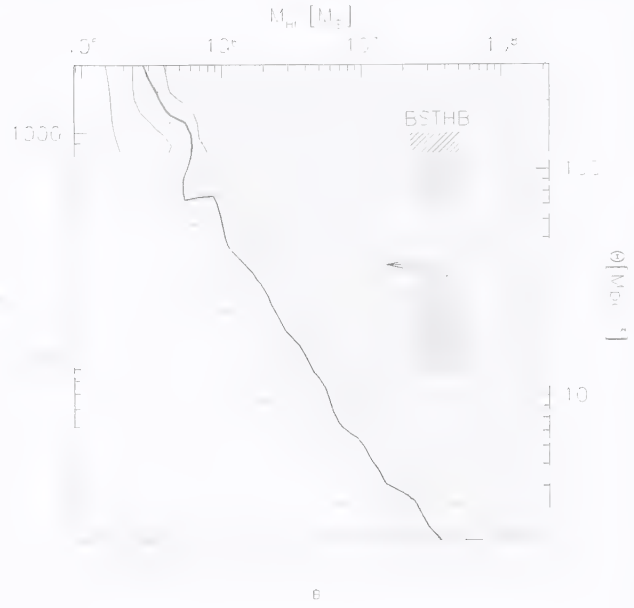

FIGURE 7.3— Combined constraint on the baryon fraction f_B and the number of clouds N per group. The number of clouds in each group normalized using the dynamical mass estimates, the number on the vertical axis is the assumed number in the Local Group. The average H I masses of the cloud populations are indicated on the top axis. The contours represent 68, 90, 95 (fat line), and 99% confidence levels on the hypothesis that the existence of a group population can be rejected. The dashed line is the 95% confidence level assuming that the clouds can be described by a core-halo model in which 50% of the flux is in a core with radius $R_{cloud}/5$.

fuse halo that encompasses one or more compact cores. We test the influence of this morphology on the detection efficiency in our survey by designing clouds with cores which account for 50% of the total flux and have a radius $R_{core} = R_{cloud}/5$. The remaining 50% of the flux is distributed over a halo with a flat H I column density distribution. The 95% confidence level on this population is indicated by a dashed line. It is clear that the detection efficiency is not significantly changed by this modification of the cloud structure.

Figure 7.4 is similar to Figure 7.3, but here the number of clouds per group is nonvariant. Also in this case, both proposed populations of clouds can not be reconciled with our observations.

7.5.3 Significance of intragroup clouds

How do these upper limits compare to the hierarchical formation scenarios of galaxy groups? Klypin et al. (1999) and Moore et al. (1999) show that in numerical simulations of a hierarchical universe the relative amount of dark matter substructure halos is scale-invariant. The predicted relative amount of dark matter halos is similar in clusters, groups and galaxies. However, only in clusters does the predicted number of clumps agree with observed luminosity functions; on galaxy and group scale the simulations predict an excess over the observed number of satellites by a factor of 10, especially for halos with circular velocities < 50 km s^{-1}.

One of the proposed solutions for this problem of missing satellites is provided by the BSTHB hypothesis. However, the evidence presented in this paper, by Charlton et al. (2000) and by Zwaan & Briggs (2000) seem to rule out this solution. Only a very limited number of clouds with $M_{H\,I} \sim 10^7$ M$_\odot$ could exist in galaxy groups. A similar conclusion has been reached by Verheijen et al. (2000), who systematically survey a region of the Ursa Major cluster of galaxies and find no H I clouds to a limit of 10^7 M$_\odot$.

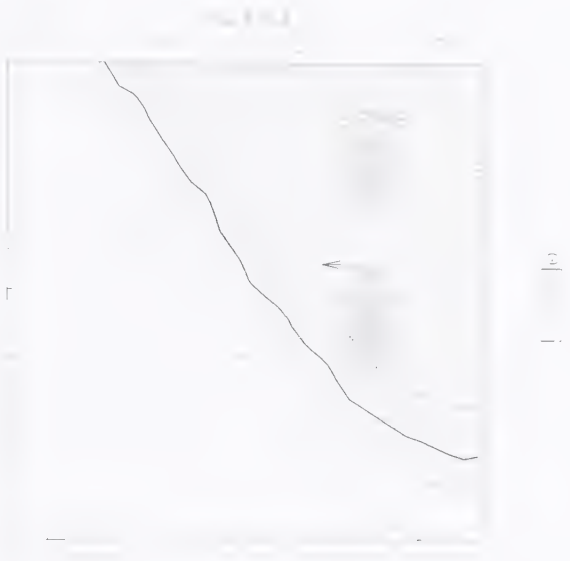

FIGURE 7.4— Same as Figure 7.3, but here the number of clouds per group, N, is equal for all galaxy groups.

From Figure 7.3 we conclude that the intragroup H I clouds contribute a maximum of 1.0×10^9 $M_\odot$ of H I to the total group mass. This implies that no more than 10% of all the H I in groups can reside in clouds with masses greater than $M_{HI} = 6 \times 10^6$ $M_\odot$. The H I mass in clouds must be less than 0.05% of the total dynamical mass of the groups. In the nonvariant N case, these numbers rise to 20% and 0.1%. The dynamical mass of a cloud population that is still permitted by the observations is more difficult to constrain. If we assume that the cold gas (H I and He I) is the only baryonic component in the clouds, and the baryon fraction is 10% (a factor normally observed in galaxies and clusters, Fukugita, Hogan & Peebles 1998), then the total contribution of the clouds to the dynamical mass of the groups must be less than 1 %. Note that Klypin et al. (1999) estimate that mass fraction in the predicted dark matter satellites is approximately 5%. This predicted high mass fraction in satellites can only be brought into agreement with our survey results if the baryon fraction of the clouds is lowered to 2%. However, the median distance of the clouds from the groups' barycenters would then reduce to ~ 200 kpc. It is not clear whether this is still consistent with the hierarchical model predictions in which the dark matter sattelites are distributed throughout the groups.

A solution to the problem of missing satellites might be that the cold neutral gas is only a minor contributor to the total baryonic content of the clouds making the H I so insignificant that it can not be detected in 21cm surveys. This situation could occur if a large fraction of the gas reservoirs in the satellites are ionized by the intergalactic background. Klypin et al. (1999) and Moore et al. (1999) discuss gas ejection by early generation supernova-driven winds and inhibiting gas cooling and star formation by photoevaporation as possible explanation of the absence of cold gas and stars in the satellites.

Solutions of a different kind can be found in changing the predicted number of clouds instead of modifying the baryons within the clouds. This can be achieved by either sup-

pressing the primordial density fluctuation spectrum on small scales, which makes the formation of small masses less efficient (Kamionkowski & Liddle 1999) or by modifying the standard cold dark matter theory. This can be done by introducing collisional or self-interacting dark matter (see e.g., Spergel & Steinhardt 1999).

7.6 Summary

The conclusion reached by Lo & Sargent (1979) that Galactic HVCs are unlikely to be intergalactic gas in the Local Group (LG) remains sound and intact under scrutiny of a new 21cm survey with the refurbished Arecibo Telescope. This new survey consists of 300 pointings in five nearby galaxy groups and is sensitive to H I masses of approximately 6×10^6 $M_\odot$, depending on the velocity spread and distance of the signals. Two detections have been made that are not unambiguously caused by known optically selected galaxies. One is a known tidal H I filament in the NGC 6500/6501 pair, comparable to the Magellanic Stream (Putman et al. 1998). The other detection very likely originates in an uncataloged member of the NGC 5970 group. We therefore conclude that we have made no significant detections of H I clouds in galaxy groups.

We use this null-result to estimate constraints on the proposed population of H I clouds in groups, suggested by Blitz et al. (1999) and Braun & Burton (1999). These authors present a scenario in which the Galactic high velocity clouds (HVCs) are actually distributed throughout the LG at typical distances of a few hundred kpc to 1.5 Mpc. Figure 7.3 shows the combined upper limits on the number of clouds per galaxy group, and the average H I mass on such clouds. The Blitz et al. (1998) scenario can be ruled out with $> 99\%$ confidence levels, assuming that the LG is typical of the five groups studied here. The integral amount of H I in intragroup clouds is typically less than 10% of the groups total H I mass, and less than 0.05% of the total dynamical mass of the groups.

The absence of clouds in groups seems to present a problem for hierarchical structure formation scenarios that predict many satellites within groups. At present it remains unclear whether the solution to this problem lies in modifying the descriptions of hierarchical formation so that the predicted number of satellites drops, or that the baryons in the clouds are simply hiding from detection.

Acknowledgments

I thank Karen O'Neil for doing part of the observing for this project and Frank Briggs for useful discussion.

References

Blitz, L., Spergel, D. N., Teuben, P. J., Hartmann, D., & Burton, W. B. 1999, ApJ, 514, 818
Braun, R., & Burton, W. B 1999, A&A, 341, 437
Braun, R., & Burton, W. B. 2000, astro-ph/0004033
Charlton, J. C., Churchill, C. W., & Rigby, J. R. 2000, astro-ph/0002001
Courteau, S. & van den Bergh, S. 1999, AJ, 118, 337
Fukugita, M., Hogan, C. J., & Peebles, P. J. E. 1998, ApJ, 503, 518
Garcia, A. M. 1993, A&AS, 100, 47
Haynes, M. P. 1981, AJ, 86, 1126
Heisler, J., Tremaine, S.,& Bahcall, J. N. 1985, ApJ, 298, 8
Huchra, J. P., & Geller, M. J. 1982, ApJ, 257, 423
Hulsbosch, A. N. M. 1975, A&A, 40, 1

Kamionkowski, M. & Liddle, A. R. 1999, astro-ph/9911103
Klypin, A. A., Kravtsov, A. V., Valenzuela, O., & Prada, F. 1999, ApJ, 522, 82
Li, J. G. & Seaquist, E. R. 1994, AJ, 107, 1953
Lo, K. Y. & Sargent, W. L. W. 1979, ApJ, 227, 756
Metcalfe, N., Shanks, T., Fong, R., & Roche, N. 1995, MNRAS, 273, 257
Mateo, M. L. 1998, ARA&A, 36, 435
Materne, J. 1978, A&A, 63, 401
Moore, B., Ghigna, F., Governato, F., Lake, G., Stadel J., Tozzi, P. 1999, ApJ, 524, L19
Oort, J. H., Bull. Astr. Inst. Neth. 1966, 18, 421
Putman, M. E. et al. 1998, Nature, 394, 752
Sandage, A. 1986, ApJ, 307, 1
Spergel, D. N. & Steinhardt, P. J. 1999, astro-ph/9909386
van den Bergh, S. 2000, PASP, 112, 529
van Driel, W., Davies, R. D., & Appleton, P. N. 1988, A&A, 199, 41
Verschuur, G. L. 1969, ApJ, 156, 771
Wakker, B. P., & van Woerden, H. 1991, A&A, 250, 509
Wakker, B. P., & van Woerden, H. 1997, ARA&A, 35, 217
Yun, M. S., Ho, P. T.P., & Lo, K. Y. 1994, Nature, 372, 530
Zwaan, M. A., Briggs, F. H. 2000, ApJ, 530, L61 **[Chapter 6]**
Zwaan, M. A., Briggs, F. H., Sprayberry, D., & Sorar, E. 1997, ApJ, 490, 173 **[Chapter 3]**

8

Deep HI Imaging of Galaxy Cluster Abell 2218 at $z = 0.2$

M. A. Zwaan, P. G. van Dokkum, M. A. W. Verheijen, & F. H. Briggs

ABSTRACT — Deep H I imaging with the Westerbork Synthesis Radio Telescope in the direction of Abell 2218 has resulted in the first detection of H I 21cm emission at cosmological distance. The H I signal originates in a galaxy in the outskirts of the cluster and has an H I mass of $(2.3 \pm 0.8) \times 10^9 \, h_{100}^{-2} \, \mathrm{M}_\odot$. The coincidence of the H I signal and the optical galaxy is confirmed by optical spectroscopy. The galaxy, at a projected distance of $1.5 \, h_{100}^{-1}$ Mpc from the cluster core, could be a merger system and is probably in the process of being accreted onto the cluster. These processes are thought to yield enhanced star-formation in such gas rich systems. However, the spectrum suggests that the galaxy has an evolved stellar population and a low star-formation rate. This suggests that star-formation in infalling galaxies is suppressed at large distances from the cluster. The detection of this galaxy demonstrates that H I 21cm emission line surveys at cosmological distances are feasible with present-day radio telescopes. We show that stacking H I spectra of optically identified galaxies is a useful method of measuring the mean H I content of cluster galaxies. This same technique may prove useful in the future for measuring the H I content of Lyman break galaxies at high z.

8.1 Introduction

CLUSTERS OF GALAXIES accrete a significant amount of mass after their initial collapse (e.g., Gunn & Gott 1972; Frenk et al. 1996). This accretion enhances the density contrast between cluster and 'field' regions, leading to the development of the large-scale structure we observe at $z = 0$. Theoretical modeling shows that a large fraction of the galaxy population in clusters must have been accreted after $z = 1$ through infall of galaxies and groups that originally formed in much lower density 'field' regions. The galaxy population of the field has a very different morphological composition from that in nearby rich clusters (e.g. Dressler 1980), implying that the accretion process must alter the properties of the infalling galaxies in fundamental ways. To understand the formation and evolution of clusters and cluster galaxies, it is necessary to learn what happens during the infall process.

Optical studies of clusters at $0 < z < 1$ have provided many clues to the nature of the infalling galaxies. An important observational result is that clusters at higher redshifts ($z \geq 0.2$) have a much larger fraction of blue galaxies than clusters at low redshift (the Butcher & Oemler [1984] effect). Some of the blue galaxies have the characteristics of present day (field) spirals, and some have "E+A" spectra, indicating recent truncation of star formation. The blue galaxies are tentatively identified as the galaxies that have recently entered the cluster environment (e.g., Butcher & Oemler 1984; Moore et al. 1996). Detailed optical studies of clusters at $0.2 < z < 0.3$ have shown that accretion is probably a continuous process, and that a large fraction of the present day cluster population experienced a "blue phase" at relatively low redshift ($z < 0.3$) (Abraham et al. 1996; van Dokkum et al. 1998). Strong evidence for morphological evolution in cluster environments is provided by HST studies of clusters at $z \approx 0.5$. The fraction of spirals in these distant clusters appears to be roughly twice that in nearby clusters. This trend is accompanied by a marked decrease in the S0 fraction with increasing redshift (Dressler et al. 1997). Similarly, the number fraction of early-type galaxies decreases by a factor two from $z = 0$ to $z = 1$ (van Dokkum et al. 2000), and the fraction of interacting and merging systems in clusters increases with redshift (Lavery & Henry 1989; Couch et al. 1998; van Dokkum et al. 1999). Rather surprisingly, spectra and colors of most of the mergers and a large fraction of the spiral galaxies indicate that they have evolved stellar populations and low star formation rates (Poggianti et al. 1999; van Dokkum et al. 1999). The usual interpretation is that the galaxies somehow suddenly lost their gas, and hence their fuel for star formation. It is unclear which processes are responsible for removal of the gas of infalling galaxies. It can be stripped by the ram-pressure (Gunn & Gott 1972) or viscous stripping (Nulsen 1982) in interactions with the hot intracluster gas (ICM) or exhausted in a vigorous star burst. Violent interactions between galaxies known as "galaxy harassment" (Moore et al. 1996) might also help in removing the cool gas. Finally, a completely different option is that the cocoon of hot diffuse gas that surrounds an infalling galaxy is stripped before it can condense into cool clouds that replenish the gas reservoir (e.g., Mori & Burkert 2000). This latter process will cause a slow decrease in the star formation rate.

A key observation to understand the morphological transitions is the gas content of galaxies in various stages of the infall process. There has been much progress in measuring the gas content of cluster galaxies at redshifts $z < 0.1$ (see van Gorkom 1996 for an extensive review). There is now direct observational evidence that the accretion process alters the gas disks. For example, Cayatte et al. (1990) showed that galaxies in the center of the Virgo cluster have lost the outer parts of their H I disk, while galaxies in the outer

parts appear undisturbed. However, the accretion rate of $z < 0.1$ clusters has become very low: the fraction of blue galaxies is $< 3\%$, and the blue galaxies have low luminosities (e.g., Butcher & Oemler 1984). The accretion rate was much higher in the past, and the gas content of infalling galaxies at higher z is expected to be significantly greater than that of infalling galaxies at $z = 0$.

We have initiated a program of deep H I imaging of clusters at $z \sim 0.2$ to study the gas content of cluster galaxies at intermediate z. Here we report on first results from WSRT observations of Abell 2218 at $z = 0.176$. Abell 2218 is one of the best studied clusters at $z \sim 0.2$. The cluster is extremely rich and massive, with an Abell richness class of 4 (Abell, Corwin & Olowin 1989) and a measured velocity dispersion of 1370 $\mathrm{km\,s^{-1}}$(Le Borgne et al. 1992). An azimuthally symmetric x-ray distribution is observed with a core radius of approximately 1 arcmin, but the x-rays are detected out to at least 9 arcmin ($1.3h_{100}^{-1}$ Mpc) from the cluster center (Squires et al. 1996). Abell 2218 has become widely known for the HST imaging that revealed a rich structure of strong gravitational arcs (Kneib et al. 1996). The blue fraction is $\sim 10\%$ (Butcher & Oemler 1984), significantly higher than what is typically found in rich $z = 0$ clusters. Throughout this chapter we adopt $H_0 = 100h_{100}\,\mathrm{km\,s^{-1}\,Mpc^{-1}}$ and $q_0 = 0.15$.

8.2 Data acquisition and analysis

Observations were performed with the Westerbork Synthesis Radio Telescope (WSRT[1]) during commissioning of the upgraded system in the period from July to September 1999. Data were taken with the cooled 21cm receivers in two adjacent bands of 10 MHz each, thus producing 2×128 channels of each 78.1 kHz corresponding to a velocity spacing of 19.5 km/s at the redshift of the cluster and a resolution of 38.9 km/s after Hanning smoothing. Each frequency band was observed for 18x12 hours, with varying positions of the four movable telescopes. Optimal uv coverage was obtained with baselines from 36 to 2700m in steps of 9m. Table 8.1 gives a summary of the observing parameters.

We stress that these data were taking during commissioning of the WSRT after the upgrade. Some hard- and software problems were encountered which resulted in a higher noise level than expected. The results reported in this paper are based on a preliminary analysis of 60% the data.

The data were taken around 1200 MHz, which is well outside the protected bands for radio astronomy. As a results, a large fraction of the data was affected by interfering signals and careful inspection and editing of the data was essential. We have experimented with different methods to assess this problem. Editing all data by eyeball inspection is a very time consuming enterprise, so we were motivated to test the automatic flagging routine FLGIT in the reduction package AIPS. This task fits and subtracts linear fits to the real and imaginary spectra and flags channels that exceed a specified cut-off. Alternatively, it can flag strongly polarized signals. After experimenting with different input values of FLGIT we concluded that high S/N RFI is flagged satisfactorily, but extended spurious low-level emission was not filtered out. Also wings of strong interfering signals were not recognized. Eventually, all data were flagged by eyeball inspection. In total, taking into account dead antennas, baselines with obvious errors and RFI, approximately 30% of the data was flagged. This is high compared to 21cm observations at $z = 0$, where generally

[1]The WSRT is operated by the Netherlands Foundation for Research in Astronomy (NFRA/ASTRON), with financial support by the Netherlands Organization for Scientific Research (NWO)

TABLE 8.1— Observing Parameters.

Length of observation	(h)	18 ×12
Dates of observation		July, August 1999
Field center α (1950)		16:35:42.1
δ (1950)		66:18:60
Central Frequency	(MHz)	1204.61; 1213.20
Bandwidth	(MHz)	2 × 10
Primary beam FWHM	(arcmin)	44.0
Baselines (min, max, incr)	(m)	36, 2700, 9
Nr. of interferometers		91
Synthesized beam ($\alpha \times \delta$)	(arcsec)	18.04 × 19.67
Number of channels		2 × 128
Channel separation	(kHz)	78.1
	(km/s)	19.5
rms noise per channel	(mJy/beam)	0.11; 0.10
Equivalent of 1 mJy/beam	(K)	2.35

only a few percent is excised.

The data were externally calibrated using observations of 3C48 and 3C286 which were observed before and after each 12 hour run. However, despite the generally assumed stability of the WSRT it was necessary to apply self-calibration to the data. The peak flux in the field of interest is $\sim$ 200 mJy, sufficiently high to determine complex gain solutions every 15 minutes. These solutions were determined for a pseudo-continuum data set which is formed by averaging the channels over the inner 75% of the passband. The gain solutions were later copied to the line data. In approximately 50% of the data sets, the phases and amplitudes were found to be stable within a few percent, but in many cases phase excursions up to several tens of degrees were found.

Continuum emission was removed from the UV line data by subtracting the Fourier transform of the CLEAN components from the self-calibration model from the visibility data set. Subsequently, linear fits to the real and imaginary components were made and subtracted from all channels to remove any remaining continuum emission. In principle, fits should be made to only the line-free channels, but the expected level of H I line emission is too low on a single spatial baseline to have a significant influence on the determination of its spectral baseline.

The *uv* data were transformed to datacubes using a robustness parameter[2] of 1. This results in a spatial resolution of 18.0″ × 19.7″ and a r.m.s. noise level of 0.11 mJy/beam in the lower band and 0.10 mJy/beam in the higher frequency band. Higher values of the robustness parameter give slightly lower noise levels, but give more structure in the noise which is harmful to a detection experiment like this. The measured r.m.s. noise is approximately 40% higher than what would be obtained under ideal circumstances, that is assuming no RFI, no dead antennas, no phase drifts, no noise added by continuum subtraction etc.

[2] AIPS allows the user to adjust the relative weightings so that hybrid weighting schemes can be applied. ROBUST= 5 is close to classical natural weighting and ROBUST= −5 is virtually pure uniform weighting.

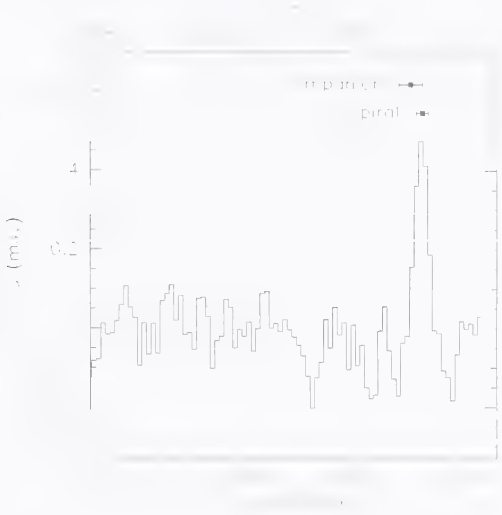

FIGURE 8.1— Global H I profile of the first H I selected galaxy at $z = 0.18$. The profile is Hanning smoothed which results in a spectral resolution of 38.9 $\mathrm{km\,s^{-1}}$. The flux scale has not been corrected for primary beam attenuation. The optical redshifts of the spiral galaxy and its companion are also indicated, with 1σ uncertainties.

8.3 First H I selected galaxy at $z = 0.2$

We first searched the data cube for H I emission disregarding coincidence with the positions and/or redshifts of known galaxies. The most prominent signal adds up to 7σ, with optimal smoothing, both spatially and in frequency domain. The integrated flux in this detection is 33 mJy km s^{-1}, corrected for primary beam attenuation. This is equivalent to an H I mass of $(2.3 \pm 0.8) \times 10^9\, h_{100}^{-2}\, M_\odot$, which is slightly less than the typical H I mass of a field galaxy ($M^*_{HI} = 3.5 \times 10^9\, h_{100}^{-2}\, M_\odot$, Zwaan et al. 1997). The velocity width of the detection is very small, 60 ± 20 km s^{-1} at 50% of the peak flux. This suggests that the signal is from a galaxy with low inclination with respect to the plane of the sky. The narrowness of the signal explains why this modest H I mass stands out from the noise so clearly. Fig. 8.1 shows the global H I profile of the detection. Here, for each channel we have added the flux in a $25'' \times 25''$ box centered on the detection.

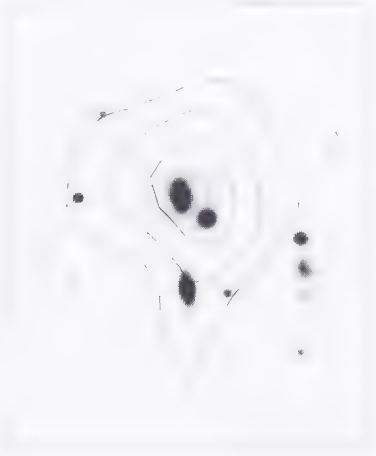

FIGURE 8.2— Overlay of H I contours on a greyscale representation of the optical R-band Keck image. The contours correspond to 1.2, 1.9, and 2.5×10^{19} cm^{-2}. The size of the image is $60'' \times 67''$ which corresponds to $140 \times 156\, h_{100}^{-1}$ kpc at the redshift of Abell 2218.

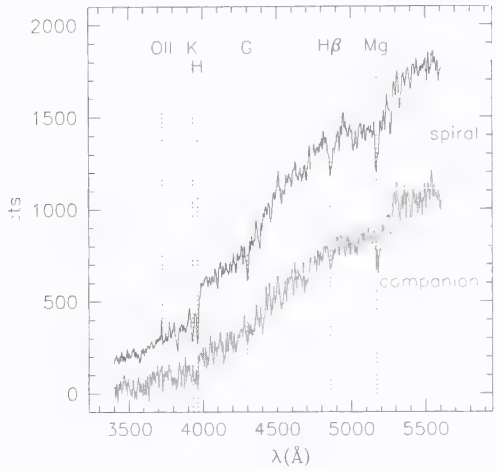

FIGURE 8.3— Keck spectra of the spiral galaxy A2218-H1 and its companion. Spectra have been shifted to their rest-wavelengths. For comparison, several identified lines are indicated. The redshift of the spiral is $z = 0.1766 \pm 0.0001$ and that of the companion is $z = 0.1768 \pm 0.0002$. For clarity, the top spectrum is offset vertically.

The position of the H I signal is approximately 11 arcmin west from the central cD galaxy that also marks the peak of the x-ray profile and dark matter distribution (Squires et al. 1996). This separation translates to a projected distance of $1.5 h_{100}^{-1}$ Mpc from the cluster core. The detected galaxy therefore resides in the outskirts of the cluster, beyond the point where the bright x-ray halo has been measured. The redshift of the H I line is $z = 0.1766$, coincident with the peak in the redshift distribution of the confirmed cluster members.

We obtained optical imaging and spectroscopic observations of the galaxy responsible for the H I emission, to confirm the signal and to investigate the properties of the galaxy. Imaging observations of the field centered on the H I detection were obtained with the ESI on the 10m W. M. Keck II Telescope on April 4, 2000. The field was observed for 600s in the *R*-band. The seeing was 0.9″. Fig. 8.2 shows an overlay of the H I contours on a greyscale representation of the optical image. The H I position coincides with a spiral galaxy with two well developed spiral arms, one of which connects to a smaller companion $\sim 12 h_{100}^{-1}$ kpc to the south-west. The H I distribution is just resolved with the 20″ beam; there seems to be an extension in the direction of a lenticular galaxy $\sim 40 h_{100}^{-1}$ kpc south. We christen the H I selected spiral galaxy A2218-H1.

We obtained spectroscopic data with LRIS spectrograph (Oke et al. 1995) on the W. M. Keck II Telescope on March 31, 2000. Spectra were obtained for both the spiral galaxy A2218-H1 and its companion using the 300 lines mm^{-1} grating and a 1″ slit. A2218-H1 was observed for 800 seconds, and its companion for 300 seconds, both during twilight. The redshift of A2218-H1 is $z = 0.1766 \pm 0.0001$ and that of the companion is $z = 0.1768 \pm 0.0002$, thus giving a velocity separation of $60 \pm 70\,\mathrm{km\,s^{-1}}$. Both redshifts are within 1σ of the redshift of the H I detection. This confirms the identification and suggests that the spiral and its companion are interacting. Further spectroscopy is required to investigate whether the lenticular galaxy to the south is also associated with A2218-H1. Fig. 8.3 shows the optical spectra of A2218-H1 and the companion. Both are typical of early type galaxies with evolved stellar populations. Despite their gas reservoir, the galaxies show no signs of star formation in the spectra.

A2218-H1 is at present the highest redshift galaxy in which H I has been detected in the 21cm line in emission. To the best of our knowledge, the previous record holder was Malin 1 at a redshift of $z = 0.083$, of which the spectrum was recorded with the Arecibo Telescope (Bothun et al. 1987). The highest redshift cluster to date in which H I has been detected in emission is Abell 2670 at $z = 0.0767$ with the Very Large Array (van Gorkom 1996).

8.4 Average H I mass of confirmed members

A2218-H1 is currently the only detection in our preliminary H I data cube that is significant without requiring an optical identification or a measured redshift. However, the sensitivity of the H I survey can be increased by cross-correlating optical redshifts of cataloged galaxies with the H I data cube. At present, optical redshift measurements are limited to the very central region of Abell 2218. The spectroscopic survey of Le Borgne et al. (1992) covers the central $4' \times 4'$ ($560 \times 560 h_{100}^{-1}$ kpc), which corresponds to only 1.3% of the total area covered by the primary beam of the WSRT. We extract spectra from the H I cube at the positions of 45 galaxies for which the measured redshift falls within the boundaries set by the bandwidth of the 21cm observations. There are no significant ($> 3\sigma$) detections of H I in this sample.

Limits to the mean H I mass of Abell 2218 members can be derived by stacking up the 45 extracted 21cm spectra of the optically identified galaxies. In Fig. 8.4 we show the resulting composite spectrum that is derived by 1) concatenating each spectrum with itself to insure that at each position in the composite spectrum the same number of measurements are added; 2) normalizing the redshift axis of each spectrum by subtracting the corresponding optical redshift; 3) co-adding the spectra. A reference spectrum has been constructed by extracting spectra at 40″ north of each galaxy and assuming the same redshift distribution. We find a positive signal in the upper spectrum at $\Delta V = 0$ of $(10 \pm 4)\,\mu$Jy, where the 1σ error has been determined by bootstrap resampling. From this we calculate that the average H I mass of galaxies with measured redshifts in the core of Abell 2218 is $(3 \pm 1.2) \times 10^8 h_{100}^{-2}\,M_\odot$.

FIGURE 8.4— Statistical detection of H I in optically identified galaxies in the central $4' \times 4'$ of Abell 2218. The lower spectrum is constructed from random spectra through the 21cm cube. The dashed lines are smoothed with a Gaussian with FWHM = 300 $\mathrm{km\,s^{-1}}$, the solid lines are boxcar smoothed with a 450 $\mathrm{km\,s^{-1}}$ filter. The top spectrum is offset by 0.04 mJy.

8.5 Discussion

The main result of this preliminary analysis is that the volume surrounding Abell 2218 is very H I deficient. The most prominent detection is a galaxy slightly less massive than a field $M^*_{\rm HI}$ galaxy. No large H I rich spiral galaxies have been detected although the survey covers a large volume around the cluster. The survey volume is defined by the WSRT primary beam which extends to a radius of 2.5 Mpc, and the velocity range of 4000 km s^{-1} set by the bandwidth. Together, these define a total survey volume of $\sim 750 {\rm Mpc}^3$.

We can make a crude estimate of the expected detections if this survey were targeted on a random field region instead of this clear overdensity. We adopt the Schechter parameters for the H I mass function from Zwaan et al. (1997). The detection of A2218-H1 proves that the survey is at least sensitive to H I masses of $2.3 \times 10^9 h_{100}^{-2}$ M$_\odot$. If we integrate the H I mass function from 2.3×10^9 M$_\odot$ to infinity we find that should have made 4 ± 2 detections. This is a very conservative estimate because measurements of the cosmic H I density indicate that $\Omega_{\rm HI}$ decreases significantly from $z = 0.18$ to $z = 0$. From an interpolation of the results from Mg II-selected systems (Lane 2000), damped Lyα systems (Rao & Turnshek 1999) and field galaxy redshift surveys (Natarajan & Pettini 1997) we estimate that $\Omega_{\rm HI}(z = 0.18)$ is twice the value at $z = 0$. Under this assumption, the number of expected detections would rise to 8 ± 3. This is almost independent on whether $\Omega_{\rm HI}$ evolves through a rise in $M^*_{\rm HI}$ or through an increase in mean galaxy density.

The very low average H I mass of galaxies in the core of Abell 2218 is in qualitative agreement with a recent H I study of the Coma cluster by Bravo-Alfaro et al. (2000). Strong H I deficiency was found in Coma in the inner 0.6 Mpc, which roughly coincides with the extent of the x-ray halo. Galaxies in that volume show reduced gas masses as compared to field galaxies of similar morphological type, and show asymmetric H I distributions. The largest H I mass found in the inner 0.6 Mpc of Coma is 9×10^8 M$_\odot$, while approximately 50% of the galaxies in this region are undetected to limits of $M_{\rm HI} = 10^8$ M$_\odot$. Deep VLA observations of Abell 2670 have revealed H I in approximately 15 member galaxies, the majority more than 1 Mpc from the cluster center (van Gorkom 1996). No H I has been found in the inner 250 kpc of the cluster.

Mori & Burkert (2000) study the influence of the hot ICM on the extended diffuse gas component of dwarf galaxies, both analytically and by simulations. Their calculations show that dwarf galaxies accreted by rich clusters will completely lose the hot gas component in typically less than one Gyr by ram-pressure stripping. Using their equation (32) and substituting the x-ray properties of Abell 2218 we find that the critical dark halo core mass for effective ram pressure stripping is 4.4×10^{12} M$_\odot$. This compares to a circular rotational velocity of approximately 500 km s^{-1} which implies that even giant galaxies accreting onto Abell 2218 will lose their diffuse gas component very efficiently in less than one Gyr. The cold H I component of the accreting galaxies is not yet taken into account in these calculations.

Two recent papers have addressed the interaction between the hot ICM and the cool gas of spiral galaxies being accreted onto the cluster. Abadi et al. (1999) employ 3-dimensional SPH simulations and find that approximately 75% of the H I disk of a spiral galaxies is removed after it has passed through the cluster core. The gas mass loss is found to depend strongly on the orientation of the infalling galaxy, where face-on interactions are most dramatic. However, the H I disk is never completely removed and hence star formation can still continue on a low level in galaxies that have followed a trajectory through the dense hot cluster gas. This is difficult to reconcile with the requirement that

galaxies undergo a rapid transition from spiral to S0 (Poggianti et al. 1999; van Dokkum et al. 1999). A refinement of the modeling is discussed by Quilis et al. (2000) who replace the smooth gas layer in the galaxies with a complex multi-phase structure. This increases the efficiency of gas removal significantly as it is found that spiral galaxies lose all their cool gas in 1×10^8 yr. In this latter case, the gas stripping is almost independent of the angle between the gas disk and the trajectory of the infalling galaxy.

The galaxy A2218-H1 does not show clear indications of the influence of ram-pressure stripping: the peak of the H I distribution is nicely coincident with the stellar disk. This is not surprising given its position just outside the outer edge of the hot ICM. The small radial velocity difference between the cluster center and the galaxy, in combination with the large projected distance suggests that the galaxy is currently infalling onto the cluster with a high tangential acceleration. If the galaxy is on a trajectory towards the cluster core, it will probably enter the ICM in roughly 2×10^8 yr. The abovementioned simulations by Quilis et al. (2000) predict that the H I disk will be stripped completely less than 1 Myr after that moment.

It is interesting that the most prominent H I signal in Abell 2218 does not originate in a regular star forming spiral galaxy, but in a system that could be interpreted as a quiescent merger system. Nearby mergers in the field at $z = 0$ generally show high star formation rates (Liu & Kennicutt 1992), probably because the gas experiences shocks during the interaction (Mihos & Hernquist 1996). The high gas content of galaxy A2218-H1 indicates that the truncation of star formation is, in this case, not caused by an exhausted fuel supply. Apparently star formation is inhibited, even though all the conditions for a strong star burst seem to be met: sufficient fuel and an interaction to trigger the burst. Interestingly, galaxy A2218-H1 resembles the red, quiescent mergers seen in the cluster MS1054-03 at $z = 0.83$ (van Dokkum et al. 1999). MS1054-03 also has a very high x-ray temperature, and its optically selected mergers are also located in the outskirts of the cluster.

8.6 Concluding remarks

A significant improvement in sensitivity and imaging capabilities of radio synthesis arrays can be expected in the future (Giant Metrewave Radio Telescope, VLA upgrade, Square Kilometer Array). One the main science drivers for these projects is to chart the H I content of the Universe over cosmic time. Optical studies have been successful in giving insight into galaxy evolution, but the field would be revolutionized if H I measurements are linked with these optical studies. Here we have shown that with present technology the first step can already be taken.

We have presented the first detection of H I 21cm emission at cosmological distance. This signal was revealed in a deep H I survey of Abell 2218 at a redshift of $z = 0.18$ and originates in an optical galaxy in the outskirts of the cluster. Its H I mass is modest, $M_{HI} = (2.3 \pm 0.8) \times 10^9 \, h_{100}^{-2} \, M_\odot$.

We demonstrated that a technique of stacking H I spectra of optically identified galaxies with known redshift can be applied to determine the average H I mass of cluster galaxies. This same technique can be performed to determine a statistical measure of the H I content of higher redshift galaxies. It will be particularly interesting to study the relation between damped Lyα systems, which dominate the cosmic H I content at $z \approx 3$, and Lyman break galaxies, which appear to be the dominant galaxy population at $z \approx 3$. It will be a crucial test for hierarchical galaxy formation scenarios to determine whether the Lyman

break galaxies contain the bulk of the H I, or whether the H I is distributed over many protogalactic clumps.

A more complete analysis of the H I data of Abell 2218 in combination with multi band imaging and spectroscopy of the field around Abell 2218 is in progress.

Acknowledgments

We thank the WSRT staff, in particular R. Vermeulen, for help with the data taking and we are grateful to the PATT for generous allocation of telescope time. T. Galama and A. Diercks are acknowledged for obtaining the Keck image.

References

Abadi, M. G., Moore, B., & Bower, R. G. 1999
Abell, G. O., Corwin, H. G., Jr., & Olowin, R. P. 1989, ApJS, 70, 1
Abraham, R. G., Smecker-Hane, T. A., Hutchings, J. B., Carlberg, R. G., Yee, H. K. C., Ellingson, E., Morris, S., Oke, J. B., & Rigler, M. 1996, ApJ, 471, 69
Bothun, G. D., Impey, C. D., Malin, D. F., Mould, J. R. 1987, AJ, 94, 23
Bravo-Alfaro, H., Cayatte, V., van Gorkom, J. H., & Balkowski, C. 2000, AJ, 119, 580
Butcher, H. & Oemler, A. 1984, ApJ, 285, 426
Cayatte, V., Balkowski, C., van Gorkom, J. H., & Kotanyi, C. 1990, AJ, 100, 604
Couch, W. J., Barger, A. J., Smail, I., Ellis, R. S., & Sharples, R. M. 1998, ApJ, 497, 188
Dressler, 1980, ApJ, 236, 351
Dressler, A. et al. 1997, ApJ, 490, 577
Gunn, J. E., & Gott, J. R. 1972, ApJ, 176, 1
Frenk, C. S., Evrard, A. E., White, S. D. M., & Summers, F. J. 1996, ApJ, 472, 460
Kneib, J.-P., Ellis, R. S., Smail, I., Couch, W. J., & Sharples, R. M. 1996, ApJ, 471, 643
Lane, W. M., Ph.D. Thesis, University of Groningen
Lavery, R. J. & Henry, J. P. 1988, ApJ, 330, 596
Le Borgne, J. F., Pelló, P., & Sanahuja, B. 1992, A&AS, 95, 87
Liu, C. T. & Kennicutt, R.C., Jr. 1995, ApJ, 450, 547
Mihos, J. C. & Hernquist, L. 1996, ApJ, 464, 641
Moore, B., Katz, N., Lake, G., Dressler, A., & Oemler, A., Jr. 1996, Nature, 379, 613
Mori, M. & Burkert, A. 2000, ApJ, 538, 559
Natarajan. P. & Pettini, M. 1997, MNRAS, 291, L28
Nulsen, P. E. J. 1982, MNRAS, 198, 1007
Oke, J. B., et al. 1995, PASP, 107, 375
Poggianti, B. M., Smail, I., Dressler, A., Couch, W. J., Barger, A. J., Butcher, H., Ellis, R. S., & Oemler, A. J. 1999, ApJ, 518, 576
Quilis, V.; Moore, B.; Bower, R. 2000, Science, 288, 1617
Rao, S. M. & Turnshek, D. A. 1999, astro-ph/9909164
Squires, G., Kaiser, N., Babul, A., Fahlman, G., Woods, D., Neumann, D. M., & Boehringer, H. 1996, ApJ, 461, 572
van Dokkum, P. G., Franx, M., Kelson, D. D., Illingworth, G. D. I., Fisher, D., & Fabricant, D. 1998, ApJ, 500, 714
van Dokkum, P. G., Franx, M., Fabricant, D., Kelson, D. D., & Illingworth, G. D. 1999, ApJ, 520, L95
van Dokkum, P. G., Franx, M., Fabricant, D., Illingworth, G. D., & Kelson, D. D. 2000, astro-ph/0002507
van Gorkom, J. H. 1996, in 'The Minnesota Lectures on Extragalactic Neutral Hydrogen' ed. E. D. Skillman
Zwaan, M. A., Briggs, F. H., Sprayberry, D., & Sorar, E. 1997, ApJ, 490, 173 **[Chapter 3]**

9

Summary and Conclusions

ABSTRACT — A deep H I survey of the extragalactic sky shows that the universe seen in the 21cm line is essentially the same universe as the one charted by optical surveys. H I selected galaxies have no properties that set them apart from optically identified galaxies. The H I mass function (HIMF) of galaxies is flat ($\alpha = -1.2$) and in good agreement with previous determinations based on optical redshift surveys. The mass density of H I is found to be $\Omega_{\rm HI}(z=0) = (2.1 \pm 0.4) \times 10^{-4} h_{100}^{-1}$, approximately a factor five lower than that at $z = 3$. $\Omega_{\rm HI}(z=0)$ is dominated by luminous, high surface brightness galaxies with high H I masses. The contribution of gas rich LSB galaxies (> 23.0 mag arcsec^{-2}) to the local cosmological H I and luminosity density is modest (18% and 5%). A $z = 0$ anchor point to the column density distribution function $f(N_{\rm HI})$ for damped Lyα systems is determined from 21cm synthesis observations of spiral galaxies. The $f(N_{\rm HI})$ has changed significantly from high z to the present and the change is greatest for the highest column densities. High velocity clouds play no significant part in the faint end of the HIMF. The hypothesis that Galactic high velocity clouds are Local Group satellites with H I masses of $\sim 10^7$ M$_\odot$ is highly inconsistent with the results from 21cm surveys. Finally, we have presented the first detection of 21cm emission in a galaxy in the outskirts of the cluster Abell 2218 at $z = 0.18$. This illustrates that H I observations at intermediate redshifts are feasible with present-day technology.

9.1 Summary

Properties of H I selected galaxies

The first half of this thesis presents the analysis of the Arecibo H I Strip Survey (AHISS), a blind extragalactic survey in the 21cm line. This survey covered two strips of sky at constant declination out to a redshift of $cz = 7400$ km s^{-1} and reached a column density limit of $\sim 10^{18}$ cm^{-2}, which makes it the deepest blind H I survey to date. The survey yielded 66 significant detections, which were followed up at 21cm with the VLA and in the optical *B*-band with the INT. All detections could be identified with optical galaxies, approximately 50% with galaxies listed in existing optical catalogs. No free floating H I clouds without stars were found. The uncataloged galaxies have higher gas fractions, lower luminosities, lower optical surface brightnesses and smaller exponential disk scale lengths than their cataloged counterparts. However, the predominance of gas rich dwarf galaxies is a natural result of the survey technique. The new galaxies are not anomalously gas rich for their intrinsic luminosity and they follow the same Tully-Fisher relation as optically identified galaxies. H I selected galaxies are not special.

Space density of H I selected galaxies

For models of galaxy evolution, it is essential that the space density of galaxies in the local Universe be well-determined over as large a dynamic range in galaxy properties as possible. A concern in optical redshift surveys is the existence of the surface brightness selection bias. An H I survey is ideal for measuring the space density of extragalactic objects free from this bias. From the AHISS sample the H I mass function (HIMF, Fig. 3.5) and optical luminosity function (LF, Fig. 4.1) for galaxies are constructed. Both have shallow faint end slopes ($\alpha \approx -1.2$ for the HIMF and $\alpha \approx -1.0$ for the LF) and are consistent with earlier estimates computed for the population of optically selected gas rich galaxies. This implies that there is not a large population of gas rich low luminosity or low surface brightness galaxies that has gone unnoticed by optical surveys.

The local H I and luminosity density

At high redshifts the cosmological mass density of H I is measured through damped Lyα systems: high column density absorbers seen in the spectra of background QSOs. A low redshift anchor point was determined from the AHISS sample. We found that $\Omega_{\rm HI}(z = 0) = (2.1 \pm 0.4) \times 10^{-4} h^{-1}$, approximately a factor 5 lower than what is derived at $z = 3$. The local H I density is dominated by late-type, luminous, high surface brightness galaxies (Fig. 3.8 and 4.3). The *B*-band luminosity density of gas rich galaxies is $\rho_{L_B} = (3.4 \pm 0.7) \times 10^{19} h_{100}^{-2}$ W Hz^{-1} Mpc^{-3}, approximately 50% of the integral luminosity density of the local Universe.

Cosmological significance of LSB galaxies

There is a longstanding debate on the question if LSB galaxies contribute significantly to the baryonic and total cosmic mass density. The results from the AHISS indicate a negative answer to this question. Galaxies with extrapolated central disk surface brightness $\mu_{0_I} > 23.0$ mag arcsec^{-2} account for only 18% of the H I density and 5% of the luminosity density. Their contribution to $\Omega_{\rm matter}$ is less certain, but probably $< 11\%$.

We determine lower limits to the average column densities $\langle N_{\rm HI} \rangle$ of the galaxies detected in the survey and find that none of the galaxies have $\langle N_{\rm HI} \rangle < 10^{19.7}$cm^{-2}, although

there are no observational selection criteria against finding lower density systems. This limit is good agreement with theoretical predictions of the ionization of gas layers by the extragalactic UV background. This H I cutoff is accompanied by a similar cutoff in the optical surface brightnesses of the H I selected galaxies: no galaxies have been found with $\mu_B > 24.0$ mag arcsec^{-2}. Even dimmer galaxies have been detected in deep CCD surveys. It is suggestive these ultra LSB systems have a fading stellar population and that their gas reservoir is either ionized or dislodged by supernova-driven winds from a first generation of stars.

The column density distribution at $z = 0$

A more specific comparison between damped Lyα systems at high z and the local H I is made by constructing the $z = 0$ column density distribution function $f(N_{\rm HI})$. Several observational effects conspire to make the determination of $f(N_{\rm HI})$ through QSO absorption lines difficult. Therefore, we have used 21cm maps of nearby spiral galaxies to estimate $f(N_{\rm HI})$ at $z = 0$. It is shown that $f(N_{\rm HI})$ undergoes strong redshift evolution from $z \sim 2.5$ to the present, especially at the high column densities (Fig. 5.2). The strong evolution of the higher column densities can be understood if gas consumption by star formation occurs most rapidly in regions of high neutral gas density. The measurements indicate that LSB galaxies make a minor contribution to the cross section for H I, especially for $N_{\rm HI} > 10^{21}$ cm $^{-2}$ (Fig. 5.3).

Intragroup H I clouds and the relation to HVCs

Hierarchical clustering scenarios explain the formation of galaxies by many generations of mergers of cold dark matter dominated smaller masses. Large numbers of satellites might survive to the present day if the mergers are not fully efficient. However, only about one in ten of the predicted sub- halos have been found in the Local Group. Recently, Galactic high velocity clouds have been suggested as being long lived, massive dark matter dominated clouds of primordial composition distributed throughout the Local Group. In this picture each HVC would contain a few $\times 10^7$ $M_\odot$ of H I and would be at a distance of a few hundred kpc to 1.5 Mpc from the Local Group barycenter. We have shown that this hypothesis is not in agreement with the results of the AHISS. This survey passes through the halos of ~ 14 external groups and ~ 300 galaxies. Several instances of intragroup H I clouds should have been detected in this survey if these groups and galaxies would have a distribution of H I clouds similar to what is proposed for the Local Group (Fig. 6.2 and Table 6.1). However, none were found.

Similar conclusions can be drawn from a targeted survey for intragroup H I clouds in five selected galaxy groups with properties similar to that of the Local Group. No significant detections have been made that could not unambiguously attributed to optical galaxies. This null result leads to the conclusion that the total H I mass of intragroup clouds must be less than 10% of the total H I mass of galaxy groups and less than 0.05% of the dynamical mass (Fig. 7.3 and 7.4). We conclude that HVCs are deployed at typical distances of $\leq$200 kpc from the galaxies or group barycenters. If each cloud is in gravitationally bound, virial equilibrium, their average dark matter fraction must be 98% or higher.

H I in the not so very local universe

The main part of this thesis concentrated on H I in the very local universe. Chapter 8 is the exception. There, the first results are presented of an H I survey in the direction of galaxy cluster Abell 2218 at intermediate redshift $z = 0.2$. The aim of this program is to study the gas content of galaxies in and around clusters as a function of distance from the cluster center, velocity, color, luminosity and morphology, and compare these to measurements at $z = 0$. A preliminary analysis of the data resulted in first detection of H I 21cm emission at $z \sim 0.2$. Optical imaging and spectroscopy with the Keck Telescope showed that the H I signal is associated with an interacting pair of galaxies, at a projected distance of approximately 1.5 Mpc from the cluster core.

9.2 The future of H I surveys

Toward smaller H I masses

The work in this thesis shows that the space density of objects more massive in H I than $10^{7.5}$M$_\odot$ has been determined accurately now; the results agree well with that of different teams. In group environments the HIMF is also flat down to $\sim 5 \times 10^6$ M$_\odot$, below that limit the space density is practically unconstrained. In field regions, where the overall density density is much lower, the HIMF is only measured reliably to H I masses of $M_{\rm HI} < 10^{7.5}$M$_\odot$. Recent large H I surveys (HIPASS, ADBS) are not be able to probe much below that. Optical luminosity functions suffer from the same observational limits. They loose much of their credibility below $M_B \sim -15$, where the estimates of different teams start to diverge dramatically (see also Fig. 4.2).

The introductory Chapter 1 stresses why measuring the space density of objects below $M_{\rm HI} = 10^7$ M$_\odot$ is essential. In short: 1) a significant fraction of $\Omega_{\rm HI}$ might still be hiding in H I masses $< 10^7$ M$_\odot$ if the faint tail of the HIMF rises to $\alpha \leq -2$ or higher, 2) the faint-end slope is a crucial test for galaxy formation scenarios.

Synthesis instruments like the WSRT, VLA, ATCA and GMRT may be the most useful for constraining the faint end. Thanks to their smaller dishes, these instruments sample larger volumes per single pointing than single dish instruments. Under the assumption that the shape of the HIMF does not vary with environment, local overdensities (galaxy groups) are most appealing to survey, because of the higher detection efficiency. Even so, in order to reach interesting H I mass limits and survey sufficient volume, several days of observing time are required. Typical crossing times in groups like Sculptor or Centaurus A are in the order of a Hubble time, which indicates that they are dynamically unevolved and might therefore be excellent places to study the faint end of the HIMF to the lowest measurable limits. However, if it is found that the flatness of the HIMF in groups persists down to very low H I masses this does not guarantee a flat field HIMF. Biased galaxy formation models predict that low mass galaxies preferentially inhabit the lower density regions. Instruments like the Square Kilometer Array are needed for good statistics of the HIMF below $M_{\rm HI} < 10^{6.5}$.

To higher redshifts

The detection of a galaxy near Abell 2218 at $z = 0.18$ (Chapter 8) shows that H I 21cm emission line surveys at $z > 0.1$ are feasible with present-day technology. Clusters are interesting sites to study from an astrophysical point of view, but also because the probability of making a detection are likely to be higher in the direction of these clear overden-

sities. 21cm surveys are now possible with the VLA and WSRT out to redshifts of $z = 0.2$ and with the GMRT to $z \approx 0.4$.

Field surveys at redshifts $z > 0.1$ can give valuable insight in the evolution of $\Omega_{\rm HI}$. At present, our knowledge of the $\Omega_{\rm HI}$ at $z = 0$ and at higher z relies on completely different observational strategies. At $z = 0$, the total 21cm emission line flux of galaxies is integrated to calculate $\Omega_{\rm HI}$ (Chapter 3). At high z, $\Omega_{\rm HI}$ is evaluated through the statistics of Lyα or 21cm absorbing systems. These latter studies only chart the evolution of $\Omega_{\rm HI}$ for $z > 0.5$. Assuming $q_0 = 0.5$ ($q_0 = 0$), the evolution of $\Omega_{\rm HI}$ over the most recent 50% (33%) of the history of the universe is unconstrained. Blind 21cm surveys like the one discussed in this thesis could be extended to higher z to measure the evolution of $\Omega_{\rm HI}$ directly. These measurements will provide strong constraints to galaxy evolution models, and will for the first time make a direct connection between damped Lyα statistics and the 21cm view of the local universe. With current radio telescopes it is possible to probe the high H I mass end of the HIMF to redshifts of $z = 0.2$. If it turns out that $\Omega_{\rm HI}$ evolves strongly, as indicated by the damped Lyα observations, these studies can be extended to $z \approx 0.4$ with the GMRT.

A concern in these extensive H I projects is the data reduction. Especially 21cm surveys at higher redshift, which imply observing outside the protected bands for radio astronomy, will be severely disturbed by man-made interfering signals. Projects as extensive as the survey discussed in Chapter 8 require an huge investment in time from the observer to inspect all baselines and all channels for unwanted signals. For performing future large H I surveys it is essential that more sophisticated RFI excision techniques be developed.

Nederlandse Samenvatting

WATERSTOF IS HET simpelste en meest voorkomende element in de natuur. Van alle materie in het heelal bestaat ongeveer driekwart uit waterstof. Een groot gedeelte zit opgesloten in sterren die de waterstof omzetten in zwaardere elementen en uit dit proces hun energie putten om het licht uit te zenden dat we 's nacht kunnen waarnemen. Dit proefschrift gaat echter over waterstof die zich niet *in* de sterren, maar *tussen* de sterren bevindt.

De ruimte tussen de sterren is namelijk niet leeg; hier bevindt zich de zogenaamde interstellaire materie. Deze materie is een mix van stof en gas. Het stof bestaat uit kleine zand-achtige deeltjes die het sterlicht absorberen en vertrooien. De aanwezigheid hiervan wordt verraden door de donkere vlekken die (voornamelijk op het zuidelijk halfrond) zichtbaar zijn in de witte band van sterren aan de hemel. De andere component, het waterstofgas, is echter onzichtbaar voor onze ogen. Ook met optische telescopen kunnen we deze koude, ijle wolken van waterstof niet waarnemen.

Het was de Nederlandse sterrenkundige Van de Hulst die in 1944 voor het eerst uitrekende hoe we dit waterstofgas wel zouden kunnen opsporen. De radiosterrenkunde was op dat moment in ontwikkeling en Van de Hulst onderzocht of er mogelijkheden waren om radio-technieken te gebruiken voor de bestudering van waterstof. Hij voorspelde dat waterstof elektromagnetische straling uitzendt met een zeer specifieke golflengte van 21.1 cm. Het mechanisme dat verantwoordelijk is voor deze straling is de zogenaamde hyperfijn overgang die optreedt als het elektron in een waterstof atoom spontaan van rotatierichting verandert. Bedenk dat zich in een melkwegstelsel ongeveer één waterstof atoom per kubieke centimeter bevindt en dat de hyperfijn overgang zo eens per 10 miljoen jaar plaatsvindt, en het is eenvoudig in te zien dat de 21cm straling zeer zwak en moeilijk waarneembaar is.

De 21cm straling werd zeven jaar na de theoretische voorspelling voor het eerst gedetecteerd. Een team uit Harvard was het eerste dat zijn apparatuur op orde kreeg en de straling afkomstig uit de gaswolken van onze Melkweg kon waarnemen. Slechts enkele weken later slaagden daarin ook Nederlandse en Australische teams en reeds in 1954 werd een eerste kaart van waterstofgas in ons Melkwegstelsel gepubliceerd. Eén van de belangrijkste toepassingen van waterstof is de bestudering van de massaverdeling en donkere materie in melkwegstelsels. Dit is een belangrijke industrie geworden die met name in Groningen floreerde.

Veel apparaten op Aarde werken op ongeveer dezelfde golflengte als waterstof. Mobiele telefoons communiceren in Nederland op een golflengte van 16 en 33 cm, televisiestations werken op een iets langere en magnetrons op een iets kortere golflengte. Dit hele gebied van het elektromagnetisch spectrum wordt radiostraling genoemd. Helaas zijn de aardse signalen doorgaans vele malen sterker dan die van de waterstofatomen in de ruimte. Radioastronomen moeten daarom vaak het onderste uit de kan halen om uit de warboel van opgevangen signalen de interessante er uit te pikken. Wat het meest interessant is, is natuurlijk uiterst subjectief: een telefoongesprek, een televisie uitzending, een warme maaltijd, of... de geheimen van het universum?

De motivatie

Het voornaamste doel van dit proefschrift is het inventariseren van waterstofgas in het nabije heelal. Uit de inleiding blijkt wellicht dat alle waterstof is opgesloten in de interstellaire materie in melkwegstelsels, maar dit is een ongefundeerde conclusie zonder dat men op ieder mogelijke plek in het universum naar waterstof heeft gezocht. De meeste 21cm studies zijn namelijk gericht op de ons bekende melkwegstelsels. Er bestaan catalogi van duizenden stelsels die gevonden zijn op fotografische platen en dus puur geselecteerd zijn op de aanwezigheid van sterren. Vervolgens wordt juist in deze stelsels het waterstofgas bestudeerd. Als we deze strategie blijven volgen bestaat de mogelijkheid dat we een zeer onvolledig beeld krijgen van de waterstof verdeling in het heelal. Misschien bestaan er grote reservoirs van waterstof in de ruimte *tussen* de melkwegstelsels die nog nooit door iemand zijn opgemerkt.

Een 'blinde' speurtocht naar waterstofgas kan veel duidelijkheid verschaffen en ons veel leren over de evolutie van het heelal en de melkwegstelsels daarin. Het jeugdige heelal bestond bijna uitsluitend uit waterstof en donkere materie. De eerste melkwegstelsels ontstonden op de plekken waar het gas en de donkere materie begonnen samen te klonteren. Daar waar de dichtheid erg groot werd, konden de eerste sterren ontstaan. In de loop van de tijd is er steeds meer gas omgezet in sterren. De hoeveelheid waterstofgas in het heelal neemt dus af en de hoeveelheid sterren neemt toe. Door precies te meten hoeveel gas er op elk moment in het heelal is, kunnen we bijvoorbeeld leren hoe efficïent melkwegstelsels zijn in hun verbruik van waterstofgas. In dit proefschrift wordt een lokaal ijkpunt bepaald: hoeveel waterstofgas is er op dit moment in het heelal.

Een andere reden om een dergelijke speurtocht uit te voeren is het krijgen van een volledig beeld van de populatie van melkwegstelsels in onze omgeving. Als we melkwegstelsels puur selecteren op de aanwezigheid van sterren, bestaat de kans dat we de schemerige stelsels missen. Deze schemerige stelsels worden met de onwelluidende naam 'lage-oppervlaktehelderheids-melkwegstelsels' aangeduid (low surface brightness of LSB in het Engels). Ondanks hun lage contrast met de achtergrond, kunnen deze LSBs toch veel waterstofgas bevatten en een grote massa[1] hebben. Als er veel van deze LSBs zijn, zouden ze kosmologisch gezien dus erg belangrijk kunnen zijn. Behalve deze schemerige stelsels, zouden er ook geheel donkere stelsels kunnen bestaan die alleen maar uit gas en donkere materie zijn opgebouwd. Met optische telescopen zoeken naar deze species heeft geen zin. Alleen met radiotelescopen kunnen we de donkerste melkwegstelsels vinden.

[1] In het dagelijkse gebruik wordt vaak abusievelijk het woord 'gewicht' gebruikt in plaats van 'massa'.

De Arecibo speurtocht

Het eerste gedeelte van dit proefschrift (Hoofdstuk 2, 3 en 4) beschrijft de resultaten van een speurtocht naar waterstofgas in het nabije heelal. Met het nabije heelal wordt in dit geval bedoeld alles wat dichterbij is dan 300 miljoen lichtjaar[2]. Voor deze speurtocht is gebruik gemaakt van de Arecibo-telescoop op Puerto Rico, met een doorsnede van 300 meter de grootste telescoop op Aarde. De Arecibo-telescoop heeft als een zoeklicht dertig dagen achtereen dezelfde smalle strook aan de hemel bekeken. De uiteindelijke gevoeligheid van de speurtocht is ongeëvenaard; nog nooit eerder was het mogelijk op een systematische manier kleine hoeveelheden waterstofgas op zeer grote afstand te vinden. In totaal werden 66 signalen geregistreerd.

Al deze signalen werden vervolgens opnieuw bestudeerd met de Very Large Array (VLA) in New Mexico. De bedoeling hiervan was de posities aan de hemel nauwkeuriger te bepalen, de waterstofverdeling in groter detail in kaart te brengen en de totale hoeveelheid waterstof in elk signaal beter te meten. Alle signalen die door de Arecibo-telescoop werden geregisteerd, konden door de VLA waarnemingen worden bevestigd. Dit illustreert de grote stabiliteit van de zoekmethode.

Naast de VLA waarnemingen werden bijna alle signalen ook bekeken met de optische Isaac Newton Telescoop (INT) op La Palma. Deze telescoop is, in tegenstelling tot Arecibo en de VLA, gevoelig voor zichtbaar licht en kan dus het sterlicht in kaart brengen. Een opvallende conclusie is dat op nagenoeg alle plekken waar we waterstof gevonden hebben met de Arecibo-telescoop, ook sterlicht zagen met de INT. De enige uitzonderingen zijn op plaatsen waar het licht aan ons oog wordt onttrokken door stoffige gebieden in onze Melkweg. Overal waar er dus waterstofgas is, worden er ook sterren gevormd. De geheel donkere melkwegstelsels blijken niet te bestaan.

Ongeveer de helft van de stelsels die werden gevonden kwam al voor in bestaande catalogi, die gebaseerd zijn op fotografische platen. De andere helft bestaat uit nieuwe melkwegstelsels. In Hoofdstuk 2 wordt gekeken of er een verschil bestaat tussen deze oude bekende en de nieuwe. Op het eerste gezicht zou de conclusie getrokken kunnen worden dat de nieuwe melkwegstelsels veel kleiner en schemeriger zijn en een relatief grotere hoeveelheid gas herbergen. Betekent dit dat we een nieuwe klasse van melkwegstelsels hebben ontdekt die onopgemerkt is gebleven in de catalogi van optisch geïdentificeerde melkwegstelsels? Het antwoord is iets subtieler. Reeds bekende verbanden tussen de gasinhoud, omvang en lichtsterkte van melkwegstelsels garanderen dat de waterstof-geselecteerde stelsels de waargenomen eigenschappen hebben. We laten zien dat een eerlijke vergelijking tussen beide klassen van stelsels leert dat we dezelfde soort objecten oppikken als die al voorkomen in de optische catalogi.

In Hoofdstuk 3 wordt bepaald hoeveel melkwegstelsels er voorkomen met een bepaalde massa aan waterstofgas. Dit lijkt een eenvoudige opgave. We kunnen de stelsels sorteren op hun hoeveelheid gas, verdelen in verschillende klassen en tellen hoeveel er zijn in elke klasse. De werkelijkheid is (helaas) complexer, omdat niet elk type melkwegstelsel even gemakkelijk kan worden gevonden door de Arecibo-telescoop. Er wordt daarom uitgebreid ingegaan op de manier waarop moet worden verdisconteerd dat grote, gas-rijke stelsels tot op grotere afstand kunnen worden gezien dan kleine, gas-arme. Na deze correctie toe te passen, blijkt dat er van elke gasmassa ongeveer evenveel stelsels

[2]Een lichtjaar is de afstand die het licht in één jaar aflegt en komt overeen met ongeveer 10.000.000.000.000 km.

zijn. Alleen van melkwegstelsels met heel grote gasmassa's zijn er erg weinig. Aan de hand van deze waarnemingen kunnen we ook bepalen dat de totale dichtheid van waterstof in het nabije heelal ongeveer één atoom per 700 kubieke meter is. Dit is ongeveer zes keer lager dan op het moment waarop het heelal nog maar een kwart van zijn huidige leeftijd had.

In Hoofdstuk 4 richt de aandacht zich meer op het sterlicht in de melkwegstelsels die gevonden zijn in de Arecibo speurtocht. Een opvallende conclusie hier is dat we binnen onze verzameling gasrijke stelsels geen extreem schemerige melkwegstelsels aantreffen. Voorbeelden van deze extreem schemerige stelsels zijn wel door anderen aangetroffen in optische speurtochten. De implicatie is dus dat de melkwegstelsels die zeer schemerig zijn, zonder gas zitten. Waarschijnlijk hebben deze al hun oorspronkelijke gas al omgezet in sterren en resteert er nu niets dan een langzaam dovende massa aan sterren. Ook bepalen we in dit hoofdstuk precies welk percentage de LSB stelsels bijdragen aan het waterstofgas, het licht en de totale materie in het nabije heelal. In tegenstelling tot eerdere enthousiaste speculaties, concluderen we dat de LSBs weinig in de melk te brokkelen hebben: van al het waterstofgas in het nabije heelal bevindt zich minder dan 20% in LSBs. Voor de sterren is dit 5%, voor de totale materie 10%.

Kolomdichtheidsverdeling

Met het soort speurwerk zoals beschreven in de vorige paragrafen, kan slechts iets geleerd worden over de toestand van het waterstofgas over de laatste 10% van de leeftijd van het heelal. Geheel andere technieken worden gebruikt om kennis te vergaren over het jongere heelal. Sterrenkundigen kijken terug in de tijd door naar objecten te kijken die op zeer grote afstand staan. Als het licht van deze objecten gedeeltelijk wordt uitgedoofd kan hieruit worden opgemaakt dat ergens tussen ons en het object zich waterstofgas bevindt. Dit is dus een indirecte methode, terwijl we voor het huidige heelal op een directe manier de 21cm straling van waterstofgas kunnen waarnemen.

In Hoofdstuk 5 wordt een direct verband gelegd tussen waterstofgas in het vroege en het huidige heelal, en tussen de twee methoden. Waterstofgas in het jeugdige heelal wordt vaak beschreven met behulp van de 'kolomdichtheidsverdeling'. Deze beschrijft de kans op het aantreffen van een bepaalde hoeveelheid waterstofgas als iemand in een willekeurige richting (maar in een rechte lijn) door het universum zou reizen. In dit hoofdstuk hebben we deze verdeling dichtbij gemeten aan de hand van 21cm waarnemingen afkomstig van de Westerbork telescoop. We vinden dat de verdeling in het nabije heelal goed te voorspellen valt met behulp van eenvoudige wiskundige modellen van melkwegstelsels. We zien ook dat het verschil tussen het huidige en het vroegere heelal vooral zit in de hoogste dichtheden: vroeger hield een veel groter deel van het gas zich op in gebieden met hoge dichtheden. Dit is consistent met het idee dat in deze gebieden het eerst sterren worden gevormd en het gas dus het eerst wordt opgegeten.

Wolken met hoge snelheid

In de jaren zestig van de vorige eeuw stuitten atronomen op waterstof wolken die niet participeren in de algemene rotatie van ons Melkwegstelsel, maar met schijnbaar zeer hoge snelheden bewegen. Nu, vier decennia later, is er nog steeds geen sluitende theorie die de oorsprong van deze hoge-snelheidswolken kan verklaren. Het grootste probleem bij de interpretatie is dat de afstanden tot deze wolken zeer moeilijk te bepalen zijn. Tot

melkwegstelsels of groepen van sterren kunnen afstanden worden bepaald door van individuele sterren de lichtkracht te bepalen en deze te vergelijken met sterren waarvan we de afstand kennen. In hoge-snelheidswolken is dit niet mogelijk, omdat sterren daar schitteren door afwezigheid.

Er zijn twee gangbare theorieën voor de hoge-snelheidswolken. Eén theorie, die sinds enkele jaren opgeld doet, stelt dat de wolken overgebleven zijn van de vorming van de Lokale Groep, een groepje van melkwegstelsels waarvan onze Melkweg en de Andromedanevel de belangrijkste leden zijn. Volgens deze 'Lokale Groep theorie' zijn de wolken verspreid door de Lokale Groep en is de typische hoeveelheid gas in een wolk vergelijkbaar met die in een klein melkwegstelsel. De theorie is aantrekkelijk omdat zij de verdeling van de wolken aan de hemel kan verklaren en tegelijkertijd een oplossing biedt voor het probleem van de vermiste leden van de Lokale Groep, die worden voorspeld in theoretische modellen maar niet worden gevonden. Een concurrerende theorie is de 'fontein theorie'. Deze zegt dat waterstofgas door ontploffende sterren in de Melkweg naar buiten wordt gestuwd. Eenmaal buiten de schijf van de Melkweg koelt het gas af, condenseert, en valt als regen weer terug. Dit is net als de water-cyclus op Aarde een constant proces, zodat er op elk moment wolken hangen boven de Melkweg. Volgens de fontein theorie zijn de wolken vele malen kleiner en staan veel dichterbij dan volgens de Lokale Groep theorie.

Huidig onderzoek aan hoge-snelheidswolken concentreert zich met name op het testen van beide theorieën. In Hoofdstukken 6 en 7 wordt een bijgedrage geleverd aan deze discussie. In Hoofdstuk 6 wordt getoond dat de verdeling van gasmassa's van de wolken, zoals voorspeld door de Lokale Groep theorie, niet overeenkomt met wat we meten. Door aan te nemen dat de Lokale Groep niet uniek is, maar dat alle groepen van melkwegstelsels grofweg dezelfde inhoud zouden moeten hebben, kunnen we precieze uitspraken doen over de theorie. We maken wederom gebruik van de speurtocht die is beschreven in Hoofdstuk 2, 3 en 4. De strook aan de hemel die door deze speurtocht wordt bedekt, passeert ruim honderd groepen op kleine afstand. Als de Lokale Groep theorie zou kloppen, zouden we enkele tientallen wolken hebben moeten vinden. We vonden er geen.

Hoofdstuk 7 is een variatie op hetzelfde thema. Er worden waarnemingen besproken die er specifiek op zijn gericht de voorspelde wolken te vinden. We gebruiken wederom de Arecibo-telescoop en richten hem deze keer op de omgeving van vijf groepen van melkwegstelsels. Ook deze keer wordt er geen enkele wolk gevonden. We kunnen dus met zeer grote waarschijnlijkheid zeggen dat de Lokale Groep theorie niet in overeenstemming is met de werkelijkheid. De meest bevredigende verklaring voor de wolken is dat ze een mix vormen van verschillende objecten. Sommige zijn wellicht oerwolken, overgebleven uit het jonge heelal, andere zijn misschien deel van de beschreven gasfontein. Het definitieve antwoord zal wellicht geleverd kunnen worden door onderzoek met supergrote radiotelescopen die in de toekomst gebouwd zullen worden.

Een record

Het afsluitende Hoofdstuk 8 beschrijft beknopt een excursie naar waterstofgas op zeer grote afstand. De Westerbork telescoop is ingezet om waterstof te vinden in, of in de omgeving van, een omvangrijk cluster van melkwegstelsels die op een afstand van twee miljard lichtjaar staat. Het sterkste signaal dat wordt gevonden blijkt afkomstig te zijn van een melkwegstelsel in de buitengebieden van de cluster, dat waarschijnlijk bezig is

de cluster binnen te dringen. Nog nooit eerder is het mogelijk geweest een afbeelding te maken van waterstofgas op een dergelijke afstand. De hoeveelheid energie die de 21cm straling met zich meedraagt is namelijk duizenden malen zwakker dan dat van het licht van de sterren. Het is daarom vrij eenvoudig de sterren te zien in een melkwegstelsel op miljarden lichtjaren afstand, maar voor het waterstofgas waren we totvoorkort gelimiteerd tot het zeer nabije heelal. De metingen laten zien dat het met de nieuwste techniek en een flinke investering in tijd, mogelijk is 21cm studies uit te breiden naar zeer grote afstanden. Omdat we terug kijken in de tijd als we naar grote afstanden kijken, stellen deze nieuwe technieken ons dus in staat een direct beeld te krijgen van waterstofgas in het jongere heelal.

Dankwoord

Toen ik vijf jaar geleden aan dit onderzoek begon, had ik geen idee waar het zou eindigen. Mijn begeleider Frank Briggs evenmin, maar dat was geloof ik zijn bedoeling. Dat dit proefschrift tot voltooing is gekomen dank ik aan Frank's goede advies, geduld, relativering en goede zorgen. Hij heeft me aangemoedigd mijn eigen weg te zoeken, maar was een bijna onuitputtelijke bron van inspiratie.

Natuurlijk dank ik alle bewoners van het Kapteyn Instituut voor de goede, en vaak inspirerende sfeer de afgelopen vijf jaar. Vooral veel (ex)collega-aio's hebben geholpen het leven in en buiten het instituut aangenaam te maken. Kamergenoten zijn erg bepalend voor de werksfeer. Hans is in dit opzicht natuurlijk onvervangbaar.

Met Peter is de samenwerking begonnen bij Sterrenkunde 1 en 10 jaar later uitgemond in Hoofdstuk 9 van dit proefschrift. Maar de ondernemingen en vriendschap hebben zich niet beperkt tot de sterrenkunde. Met Marc heb ik met veel plezier samengewerkt aan twee hoofdstukken en Marc en Marti's veelvuldige gastvrijheid in Socorro heb ik zeer gewaardeerd.

De leden van de beoordelingscommissie, Koen Kuijken, Bob Sanders en Renzo Sancisi waren gelukkig bereid op het laatst mogelijke moment het manuscript te lezen. Dank hiervoor.

I am grateful to David Sprayberry for his help with the optical follow-up on the AHISS project, which forms a significant part of the first two chapters of this thesis.

Mede door de financiele ondersteuning door het Leids Kerkhoven-Bosscha Fonds en het Kapteyn Instituut, heb ik verre reizen kunnen maken naar conferenties en observatoria en dit proefschrift kunnen laten drukken.

Mijn ouders ben ik vooral dankbaar dat ze me mijn eigen gang hebben laten gaan, maar wel hebben gesteund, onafhankelijk van mijn keuzes.

De meeste dank ben ik natuurlijk verschuldigd aan Jolanda. Zonder haar was dit proefschrift er ook wel was gekomen, maar met haar was het een stuk leuker. Bedankt voor je onvoorwaardelijke steun, de opoffereringen, je kritische houding jegens de sterrenkunde en vooral voor de al erg veel mooie jaren.

Martin Zwaan
Groningen, September 2000

ISBN: 90-367-1305-6